LBL-37650
UC-210

# Lawrence Berkeley Laboratory

UNIVERSITY OF CALIFORNIA

## ENERGY & ENVIRONMENT DIVISION

**Design and Simulation of Lithium Rechargeable Batteries**

C.M. Doyle
(Ph.D. Thesis)

August 1995

ENERGY
AND ENVIRONMENT
DIVISION



**Prepared for the U.S. Department of Energy under Contract Number DE-AC03-76SF00098**

LBL-37650
UC-210

# Design and Simulation of Lithium Rechargeable Batteries

C. Marc Doyle

Department of Chemical Engineering
University of California, Berkeley

and

Energy and Environment Division
Lawrence Berkeley National Laboratory
University of California
Berkeley, California 94720

August 1995

This work was supported by the Assistant Secretary for Energy Efficiency and Renewable Energy, Office of Transportation Technologies, Electric and Hybrid Propulsion Division, of the U.S. Department of Energy under Contract No. DE-AC03-76SF00098.

## Abstract

**Design and Simulation of Lithium Rechargeable Batteries**

by

Christopher Marc Doyle

Doctor of Philosophy in Chemical Engineering

University of California at Berkeley

Professor John Newman, Chair

Lithium-based rechargeable batteries that utilize insertion electrodes are being considered for electric-vehicle applications because of their high energy density and inherent reversibility. General mathematical models are developed that apply to a wide range of lithium-based systems, including the recently commercialized lithium-ion cell. The modeling approach is macroscopic, using porous electrode theory to treat the composite insertion electrodes and concentrated solution theory to describe the transport processes in the solution phase. The insertion process itself is treated with a charge-transfer process at the surface obeying Butler-Volmer kinetics, followed by diffusion of the lithium ion into the host structure. These models are used to explore the phenomena that occur inside of lithium cells under conditions of discharge, charge, and during periods of relaxation.

Also, in order to understand the phenomena that limit the high-rate discharge of these systems, we focus on the modeling of a particular system with well-characterized material properties and system parameters. The system chosen is a lithium-ion cell produced by Bellcore in Red Bank, NJ, consisting of a lithium-carbon negative electrode, a plasticized polymer electro-

lyte, and a lithium-manganese-oxide spinel positive electrode. This battery is being marketed for consumer electronic applications. The system is characterized experimentally in terms of its transport and thermodynamic properties, followed by detailed comparisons of simulation results with experimental discharge curves. Next, the optimization of this system for particular applications is explored based on Ragone plots of the specific energy *versus* average specific power provided by various designs.

Due to a lack of data in the literature on transport properties in polymer electrolytes, this subject is explored in some detail experimentally. A complete set of transport properties for sodium trifluoromethanesulfonate in poly(ethylene oxide) over a wide range of compositions (0.1 to 2.6 M) at 85°C is measured. The transport properties measured include the conductivity, the salt diffusion coefficient, and the sodium ion transference number. The mean molar activity coefficient of the salt is also determined. The conductivity is measured using the standard ac-impedance method. The salt diffusion coefficient is found by using the method of restricted diffusion.

The transference number and thermodynamic factor are found by combining concentration-cell data with the results of galvanostatic polarization experiments. This novel method of measuring the transference number is straightforward to perform experimentally and yet does not require that the solution be either dilute or ideal. A theoretical analysis of the experimental method based on concentrated-solution theory is given. The transference numbers found for the sodium ion are much lower than those reported for the lithium ion, especially in the concentrated solutions. The transference number of the sodium ion is negative in the more concentrated solutions and levels off at its maximum value of 0.31 in the dilute-concentration range.

# Table of Contents

## Acknowledgements

I would first and foremost like to thank Professor John Newman. I have no doubt that I could not have found a better advisor for myself at any other school. His availability for discussions and willingness to work on problems, technical or otherwise, whenever I have needed him has been greatly appreciated. In addition, his integrity, work ethic, and standards of conduct set an excellent example for others to follow. For his encouragement and advice, and his support for my abilities, I thank him.

I would also like to thank the people that I collaborated with during my time at Berkeley. This begins with Dr. Tom Fuller, who I worked with during my first two years as a graduate student. I learned a tremendous amount from Tom of both a technical nature and also on the most effective method of doing research. I should also like to thank my collaborators in the lithium battery area in Vancouver, Canada, including Dr. Jan Reimers and Dr. Ulrich von Sacken at Moli Energy and Dr. Jeff Dahn at Simon Frazer University. Next, I want to give a special thanks to Yanping Ma of the De Jonghe laboratory in the Department of Materials Science and Mineral Engineering at Berkeley. Her diligence and perseverance in our experimental work on transport property measurements was responsible for the success of this project. Last, I would like to thank my collaborators at Bellcore in Red Bank, NJ, including Dr. Tony Gozdz, Dr. Carolyn Schmutz, and Dr. Jean-Marie Tarascon. They have been very helpful in introducing me to many practical considerations involved in battery research and development. The quality of my collaborators is certainly responsible for much of my success during these last few years.

I am also indebted to the friends and family that have helped me at every step. This includes the past and present members of the Newman research group: Vince, Tom, Mei-Hui, Bava, Ben, Doug, Kathy, Carolyn, Blaine, Jeremy, Bob, Lin, Andy, and Rob. I am also very thankful to my wonderful and supportive girlfriend, Lucy, for helping me survive the final year. I hope that I can do the same for her in the coming months. I would last like to thank Dr. Elton J. Cairns and Dr. Lutgard C. De Jonghe for serving on my dissertation committee.

# Chapter 1

# Introduction

## 1.1 Rechargeable batteries

The worldwide market for electrochemical devices and processes was estimated to be thirty billion dollars in 1987.[1] This includes several extensive areas such as metal winning, chemical and semiconductor production by electrochemical processes, electroplating, corrosion, and batteries and fuel cells. Energy conversion and storage continues to be an important application for electrochemical systems. Batteries, in particular, accounted for over four billion dollars in worldwide sales in 1987, a number that is expected to grow to over eight billion in the current decade.[1] This market is roughly split between primary and rechargeable batteries. Much of the rechargeable battery market is for lead-acid batteries for SLI (starting, lighting, and ignition) automotive applications. However, there is also a sizeable market for rechargeable batteries for consumer applications.

The consumer electronics market accounts for a growing portion of rechargeable battery sales. With the ongoing miniaturization of electronic devices comes the desire to increase the capacity density and also the specific capacity of current battery systems. It is also increasingly important for a battery system to have inherent in its structure some amount of design flexibility so that modern electronic devices will not be compromised by the battery's shape. An example of an electronic device to which each of these criteria apply is the laptop computer. In this market, the desire for ever smaller devices has led to the battery module comprising a substantial portion of the system volume and mass. Newer laptop computers that are very thin (around 3 cm) are ideal for a thin-film battery system. Since the system's usefulness is inherently limited by the capacity of the battery, there is always the desire to increase the battery's capacity

per unit volume.

In addition, as environmental regulations become more strict, novel areas are being explored for battery technology, such as the recent resurgence of interest in a battery-powered automobile. This interest has been driven primarily by legislation instituted in the state of California by the California Air Resources Board (CARB). This legislation mandates that a certain percentage of new automobiles sold in the state of California be zero-emmision vehicles. Presently, the only zero-emmision vehicles available are battery powered. The legislation set targets of 2.0% of all vehicles under 1700 kg sold in 1998, increasing to 10.0% in 2003. This mandate applies only to automobile manufacturers that sell more than a certain number of vehicles in the state per year. The CARB legislation has catalyzed a major research effort in electric-vehicle batteries in order to produce a zero-emmision vehicle that can compete successfully in the automobile market.[2] However, to this day, within four years of the first CARB target date, there are still major problems to be overcome before a zero-emmision vehicle that will be competitive in cost and performance with current automobiles can be produced. The major demands for an electric-vehicle battery can be stated in terms of its cost, performance, and life.

In order to meet the CARB mandate, the Big Three automobile manufacturers (Chrysler, Ford, and General Motors) joined together with the Department of Energy, and the Electric Power Research Institute to form the United States Advanced Battery Consortium (USABC). The USABC has quantified the demands for an electric-vehicle battery by setting mid-term and long-term performance goals. These goals are given in Table 1.1. The demands on the USABC electric-vehicle battery are quite rigorous, including specific energy and specific power values that have not been met by any developed battery technology, as well as the desire to have a

long cycle life, low cost, maintanence-free operation, and inherent safety. The most stringent criteria can probably be considered the specific energy long-term goal of 200 Wh/kg. For comparison, the traditional lead-acid SLI battery can provide a specific energy of at most 40 Wh/kg, and its theoretical specific energy is only 170.4 Wh/kg. This goal in effect eliminates from consideration a wide range of emerging battery technologies such as most zinc-based systems and the nickel-metal hydride system.

At the same time, environmental concerns have impacted the battery industry; the disposal of batteries containing toxic materials such as cadmium or lead has increasingly become an ecological hazard. As an example, the use of mercury as an additive in $Zn/MnO_2$ cells has been all but eliminated over the last decade.[3] Issues surrounding the recyclability of battery raw materials are being addressed more frequently.[4] These concerns have fueled research into battery chemistries that are more environmentally friendly.

**Table 1.1.** US ABC battery criteria.

| Characteristic | Mid-Term | Long-Term |
|---|---|---|
| Specific energy (Wh/kg) | 80 | 200 |
| Specific power (W/kg) | 150 | 400 |
| Power density (W/l) | 250 | 600 |
| Lifetime (yr) | 5 | 10 |
| Cycle life | 600 | 1000 |
| Recharge time (hr) | <6 | 3 to 6 |
| Cost ($/kWh) | <150 | <100 |

## 1.2 Lithium batteries

One class of systems that has the potential to meet all of the goals addressed above is lithium-based rechargeable batteries. The advent of nonaqueous solvents brought about the development of lithium primary batteries beginning over three decades ago.[5] The most common of these are the high-specific-energy systems such as lithium-sulfur dioxide ($Li/SO_2$) and lithium-thionyl chloride (Li/SOCl) used for military applications. Lithium batteries generally have a high specific energy, caused by the low equivalent weight and reactivity of lithium metal. They also have a wide operating temperature range, good life, and a high unit cell voltage.[6]

Because of the tremendous reducing power of lithium metal ($U^{\theta}$=-3.045 V *vs.* NHE), the electrolytic solution in the lithium cell must use a nonaqueous solvent. Several have been developed for this purpose, including many carbonate-based liquids such as propylene carbonate (PC), ethylene carbonate (EC), and dimethyl carbonate (DMC). However, these solutions will usually have a lower ionic conductivity than aqueous-based solutions; this motivates the use of very thin cells to reduce ohmic drop in the solution phase. Also, even in the most stable of these solvents, lithium metal will react to some extent. In a successful system, the reaction of the solvent with lithium will only proceed until passivation of the lithium metal surface occurs.

A rechargeable lithium battery needs to incorporate a highly reversible cell reaction while retaining the large specific energy of the lithium systems. Reversibility immediately becomes a problem due to the poor cycling efficiency of lithium metal.[7] This is usually explained as being caused by a continual reaction of freshly-deposited lithium metal with the solution during charging. A possible advantage of solid polymer electrolytes in these cells is the potential to

develop more stable polymers with better lithium plating/stripping efficiencies. This has been achieved to some extent with poly(ethylene oxide), but many of the more-recently developed polymer electrolytes react with lithium in the same manner as the nonaqueous liquids.

The reaction between lithium metal and the electrolytic solution can also be a safety hazard. One type of rechargeable battery put on the cellular phone market in Japan by Moli Energy in 1988[8] had to be recalled due to several incidents of flaming while in use. This cell used the system:

$$\mathrm{Li} \mid \mathrm{PC/DME,\ LiAsF_6} \mid \mathrm{LiMoS_2}\,.$$

Moli believed that they had solved the problem of the low cycling efficiency of the lithium surface by applying large pressures to the cell stack.[9,10] This suppressed dendritic growth and minimized shape change, but still led to a large increase in surface area of the lithium metal as a highly porous, sponge-like deposit developed over the life of the cell. The increase in surface area meant more sites for the exothermic side reaction, which eventually became autocatalytic and caused the cell to vent with flame.[11] Unfortunately, cells near the end of their life after many low-rate cycles were most suceptible to this problem.[12-14] In constrast, safety testing of new cells is usually done with fresh cells and high charge/discharge rates.

The positive electrodes favored in most rechargeable lithium cells use a lithium insertion reaction. Consider the "Moli Cell" described above, which uses molybdenum disulfide at the positive side. On discharge, the stoichiometry of the electrode changes continuously from $MoS_2$ to $LiMoS_2$ as lithium ions are inserted into the crystal structure:

$$x\mathrm{Li}^+ + \mathrm{MoS_2} + x\mathrm{e}^- \rightleftarrows \mathrm{Li}_x\mathrm{MoS_2}\,.$$

Insertion reactions are inherently reversible because covalent bonds are neither formed nor broken during the insertion process. With $MoS_2$, for example, lithium atoms simply diffuse

between layers of sulfur atoms where they are stabilized by van der Waals forces; the host crystal structure is changed negligibly. Although the insertion process can be very energetic, it is usually possible to make it proceed in the reverse direction with a high degree of reversibility.

Thousands of materials that insert lithium ions reversibly have been identified[15,16] since their utility for lithium battery applications was realized in the early to mid 1970's.[17,18] Presently, the most popular insertion materials are transition metal oxides with very high free energies for the insertion process, such as $CoO_2$, $NiO_2$, and the spinel $Li_{0.2}Mn_2O_4$. These materials can attain large reversible specific capacities of around 100 to 200 mAh/g while charging up to potentials of 4.0 to 4.5 V *versus* lithium. This area is still a very popular research topic, as the goal of a high specific capacity (>200 mAh/g) at lower cost has not yet been met. Nearly all of the known stable oxides and sulfides have been tested for their lithium-insertion properties, and novel materials presently being developed are based on metastable low temperature synthesis routes[19] and doped or mixed-oxide materials.[20,21]

Over the last decade, insertion materials have been identified with energetics for the lithium insertion process spanning a range of potentials of almost five volts. Surprisingly enough, lithium insertion into carbon, with its poor energetics ($U^{\theta}$=1.5 to 0 V *vs.* Li), has had one of the biggest impacts on the field of lithium rechargeable batteries. An early solution to the poor cyclability of lithium metal attempted to make use of lithium alloys such as LiAl, $Li_3Sb$, $Li_{4.4}Si$, *etc.*[22-24] One such cell was even briefly made commercially available by Exxon as a coin cell for electronic watches.[25,26] However, as very high potential positive electrode materials had not yet been synthesized, this battery had only a moderate specific energy. Obviously, alloying the lithium metal negative electrode with any other material represents a loss of specific energy; although this may not be too substantial when one consid-

ers that the lithium foil used will necessarily include at least three times excess capacity.

Once materials were identified that had poor energetics for the insertion process, such as $Li_2TiS_2$, $LiWO_3$, $Li_6Fe_2O_3$, and $LiMoO_2$, it was recognized that these could potentially be cycled against other insertion materials to provide a similar solution to problems with metallic lithium. This was apparently first attempted by Murphy and Carides,[27] and then quickly elaborated on by Lazzari and Scrosati.[28,29] From the beginning, this concept was quite successful, as the use of insertion compounds presents several advantages over traditional lithium alloys due to enhanced cyclability and mechanical properties. This concept was dubbed the "rocking-chair" cell,[30] as lithium ions are "rocked" between the two insertion materials during cycling. However, the specific energy of these early lithium-ion cells was modest.[31,32] A schematic representation of the concept of the "rocking-chair" or dual lithium-ion insertion cell is given in figure 1-1.

The position of lithium-ion cells improved dramatically upon the development of carbon negative electrodes based on graphite and petroleum coke. These materials combine all of the necessary features of low cost, reversibility, and high lithium insertion capacity desired in an insertion electrode. A large number of carbon materials has been synthesized from various precursor materials and shown to insert lithium ions reversibly; the energetics for the insertion process relate critically to the structure of the carbon and thus to the processing route.[33] However, in general, lithium inserts up to the stoichiometry of $LiC_6$ (372 mAh/g) with a final open-circuit potential of nearly 0 V *vs.* lithium. When used beside high voltage transition metal oxides, the carbon/$MO_x$ couple still provides a high cell potential and a high specific energy.

The feasibility of lithium insertion into graphite was recognized early on,[34,35] but the concept was not exploited in batteries due to severe electrolyte decomposition[36] and solvent

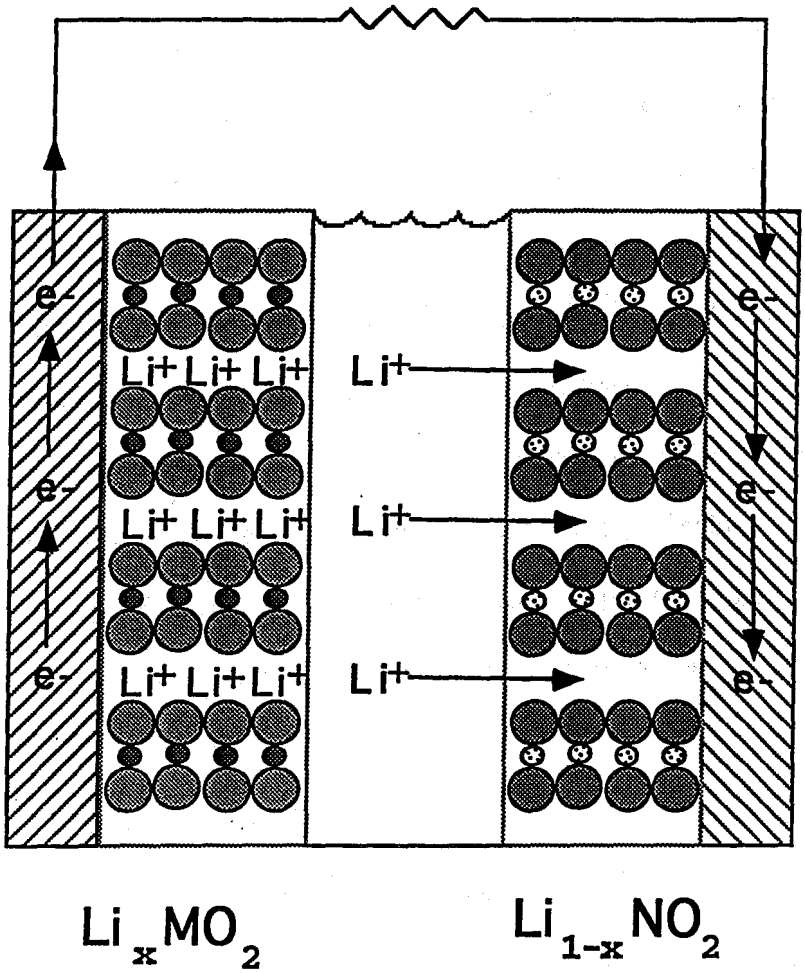


Figure 1-1. Schematic representation of the dual lithium-ion insertion cell.

cointercalation leading to graphite exfoliation.[35] Then, in the late 1980's, a research program instituted in Japan demonstrated that successful lithium intercalation with good reversibility into carbons having low crystallinity could be accomplished.[37-39] Disordered carbons generally have lower capacities for lithium insertion, on the order of one lithium per 12 carbons or about 180 mAh/g, but they maintain high reversibilities in a large number of electrolytes. Later, in 1990, the use of ethylene carbonate (EC) as a cosolvent to PC was shown to promote the formation of a passive layer on graphite that allowed reversible intercalation on subsequent cycles.[40] This opened up the use of higher capacity graphitic carbons for practical battery applications.

After being a hot research topic during the mid-1980's, the lithium-ion battery based on a carbon negative electrode and a cobalt dioxide positive electrode was finally commercialized in 1990 by Sony Corporation for cellular phone applications.[41] This first generation battery achieved a specific energy of about 80 Wh/kg and over 600 cycles, with 110 Wh/kg and 1200 cycles claimed for more recent designs using graphitic carbon.[42] This easily exceeds the performance of the Cd-NiOOH, Pb-acid, and metal hydride-NiOOH battery systems. Since Sony's commercialization of the lithium-ion battery, several other Japanese companies, including Sanyo, Matsushita, Fuji, Toshiba, and Japan Storage have released their own versions of the lithium-ion battery. Production of lithium-ion cells in Japan is estimated to be nearly one hundred million per year as of 1995. Although the use of lithium insertion compounds as battery electrodes and the lithium-ion concept were first demonstrated by Exxon[25] and AT&T Bell Labs[27] in the late 1970's, no American battery company has yet made available a lithium-ion battery on the market.

## 1.3 Mathematical modeling

The use of mathematical modeling in the design of batteries has a long history. Macroscopic models of the current and potential distribution in porous battery electrodes were first developed in the late 1950's.[43,44] Major strides towards understanding the behavior of porous electrodes were made in the early 1960's with the development of porous electrode theory,[45] which generalized earlier modeling efforts into a macrohomogeneous modeling framework that is still used in most models to this day. It was not until the early 1970's, when popular use was being made of numerical computation, that the scope of battery modeling increased from treating a single electrode to modeling the full-cell sandwich including two electrodes and the separator.[46,47] The full-cell sandwich modeling approach allowed the treatment of complicated interactions between a wide variety of phenomena that had previously been studied only separately under limiting conditions.

The lead-acid battery has been the subject of the most extensive mathematical modeling efforts to date.[48-54] Full-cell sandwich models of this system have been developed that include, in addition to the usual distributions of potential, reaction rate, and species concentration, also more detailed examinations of the cell behavior during charge and rest periods,[53] the precipitation of lead sulfate crystals,[54] and temperature effects.[50,52] Models have also been developed for the two-dimensional current distribution in current collecting grids for the lead-acid cell.[51,55] Many other battery systems have been the object of full-cell-sandwich models, including LiAl/FeS,[56] $Cd(OH)_2$/NiOOH,[57,58] Zn/$MnO_2$,[59] Li/$SOCl_2$,[60] and Li/PPy.[61]

The solid lithium and lithium-ion rechargeable batteries, which are just now beginning to be commercialized, are ideal systems to explore using mathematical modeling. At this point in the battery development process, once materials selection and preparation procedures have

been optimized, it is essential to proceed with detailed mathematical modeling of the full system if one is to produce the optimum cell design and configuration for a given application. Considering the large number of parameters which can be varied, it is prohibitive from both time and cost perspectives to develop the optimum design purely from experimental testing of cells. Mathematical modeling allows the battery designer to explore a wide variety of system parameters with a minimum expenditure of time and materials. This requires a certain amount of confidence in the ability of the battery model to describe properly the behavior of the true system. However, in any case, the optimum design that is identified in the modeling effort can be built and tested and used as a first approximation to a truly optimized design.

The ability of the battery model to perform this task depends on the knowledge of the experimental data that are input to the model. If much of the transport and thermodynamic data needed in the model are unknown, then it is unlikely that the model will give good results, especially when extrapolating outside the ranges of explored behavior. With a well-characterized system, on the other hand, the predictive power of the battery model will be at its best.

There have been a few previous attempts to model processes occurring in lithium-ion insertion based cells. The earliest are the mathematical models of rate limitations in the composite insertion electrode developed by West *et al.* in the 1980's.[62-65] The most detailed of these models is the pseudo-two-dimensional model of a single porous insertion electrode accounting for transport in the solution phase for a binary electrolyte with constant physical properties and diffusion of lithium ions into the assumed cylindrical electrode particles.[63] More recently, White *et al.* have produced a similar model to this one with the addition of a separator adjacent to the porous insertion electrode.[66]

The limitation of the model of West *et al.* is that it covers only a single porous electrode; thus, it does not have the advantages of a full-cell-sandwich model for the treatment of complex, interacting phenomena between the cell layers and utility for design purposes. In both cases these previous models confine themselves to treating insertion into $TiS_2$ with the kinetics for the insertion process assumed to be infinitely fast. This may well be a good assumption for many insertion materials; however, it is best to formulate the model to be as general as possible, including kinetic expressions at each electrode and an arbitrary choice of electrode materials. Also, both of these models treat the electrolyte as an ideal, dilute solution, which should be invalid for the concentrated solutions typically used in lithium batteries.

Another drawback of these models is the pseudo-two dimensional approach taken to describe the solid-state diffusion problem. This approach has the advantage of being able to treat variable diffusion coefficients, although the authors neglect to use it for this purpose. However, the increase in computational effort for this approach (by over an order of magnitude) may not justify the effort needed. A more subtle, yet much more facile, approach to solving the diffusion problem in the solid phase will be demonstrated in the present work.

### 1.4 Scope of thesis

We will focus here on the mathematical modeling of lithium cells that use at least one insertion electrode. This includes a wide range of rechargable battery systems that have been considered in the literature, including the lithium/polymer battery, lithium-ion batteries, and lithium-based electrochromic devices. The models are developed to be as general as possible; instead of being confined to one particular electrolytic solution or insertion electrode, the equations are developed for any choice of materials. The equations used in the mathematical models will first be outlined in chapter two. Here we will find it most convenient to separate

the models into two classes, depending on whether a single insertion electrode (FOIL) or two insertion electrodes (DUAL) are being used.

Next, in chapter three, the use of the simulation package DUAL is demonstrated by application to a particular lithium-ion cell being developed at Bellcore in Red Bank, NJ. This system has the advantage of being well-characterized experimentally and having very reproducible cell behavior. Thus, the comparisons between computer simulations and experimental discharge curves for cells with various designs should present an excellent test of the mathematical model. Also, we will use this system to demonstrate the use of the mathematical model for design purposes.

The last chapter will address the measurement of transport properties in solid polymer electrolytes commonly used in lithium batteries. These data are essential to the modeling effort; yet one finds in the literature much confusion regarding the measurement of transference numbers and diffusion coefficients in these systems. We shall consider one particular system, $NaCF_3SO_3$ in poly(ethylene oxide) at 85°C, and attempt to measure a complete set of transport properties over a wide range of salt concentrations. The polymer electrolyte solution will be treated as nonideal and concentrated, and issues surrounding speciation and ionic complexation and their effect on the macroscopic transport and thermodynamic property measurements will be discussed. We will also compare and critique various methods that can be found in the literature to measure the transference number in solid polymer electrolytes.

## References

[1] R. C. Alkire and S. M. Wolf, "New Horizons in Electrochemical Science and Technology," *J. of Metals,* February 1987, pp. 28-32.

[2] E. J. Cairns, "A New Opportunity for Electrochemical Energy Conversion," *Interface,* **1**, 38-39 (1992).

[3] N. C. Cahoon, in *The Primary Battery,* N. C. Cahoon and G. W. Heise, Eds., v. 2, John Wiley & Sons, New York (1976).

[4] K. G. McColl, "Regulatory Trends in the Battery Industry," *J. Power Sources,* **48**, 29-36 (1994).

[5] J.-P. Gabano, Ed., *Lithium Batteries,* Academic Press, New York, N. Y. (1983).

[6] R. J. Brodd, A. Kozawa, and K. V. Kordesch, "Primary Batteries 1951-1976," *J. Electrochem. Soc.,* **125**, 271C-283C (1978).

[7] R. Selim and P. Bro, "Some Observations on Rechargeable Lithium Electrodes in a Propylene Carbonate Electrolyte," *J. Electrochem. Soc.,* **121**, 1457-1459 (1974).

[8] Moli Energy's New Product Data Sheet, *JEC Battery Newsletter,* No. 6, p. 15 (Nov-Dec, 1988).

[9] J. Stiles and K. Brandt, Canadian Patent 1,190,279 (1985).

[10] F. C. Laman and K. Brandt, "Effect of Discharge Current on Cycle Life of a Rechargeable Lithium Battery," *J. Power Sources,* **24**, 195-206 (1988).

[11] K. Brandt, "Historical Development of Secondary Lithium Batteries," *S. S. Ionics,* **69**, 173-183 (1994).

[12] K. Brandt, D. Fouchard, and J. A. R. Stiles, in *Proc. 31st Power Sources Symp.,* p. 104 (1984).

[13] D. P. Wilkinson, J. Dahn, and U. von Sacken, in *Ext. Abstr. ECS Fall Meeting,* Seattle, WA, Oct. 14-19, 1990.

[14] U. von Sacken, E. Nodwell, A. Sundher, and J. R. Dahn, "Comparative Thermal Stability of Carbon Intercalation Anodes and Lithium Metal Anodes for Rechargeable Lithium Batteries," *S. S. Ionics,* **69**, 284-290 (1994).

[15] J. Desilvestro and O. Haas, "Metal Oxide Cathode Materials for Electrochemical Energy Storage: A Review," *J. Electrochem. Soc.,* **137**, 5C-22C (1990).

[16] A. M. Chippindale, P. G. Dickens, and A. V. Powell, "Insertion Compounds of Transition-Metal and Uranium Oxides," *Prog. Solid St. Chem.,* **21**, 133-198 (1991).

[17] M. S. Whittingham, "The Role of Ternary Phases in Cathode Reactions," *J. Electrochem. Soc.,* **123**, 315-320 (1976).

[18] D. W. Murphy and F. A. Trumbore, "The Chemistry of $TiS_3$ and $NbSe_3$ Cathodes," *J. Electrochem. Soc.,* **123**, 960-964 (1976).

[19] R. J. Gummow and M. M. Thackeray, "An Investigation of Spinel-Related and Orthorhombic $LiMnO_2$ Cathodes for Rechargeable Lithium Batteries," *J. Electrochem. Soc.,* **141**, 1178-1182 (1994).

[20] H. S. Wroblowa and N. Gupta, "Rechargeable Manganese Oxide Electrodes II. Physically Modified Materials," *J. Electroanal. Chem.,* **238**, 93-102 (1987).

[21] N. Kumagai, T. Fujiwara, K. Tanno, and T. Horiba, "Thermodynamic and Kinetic Studies of Electrochemical Lithium Insertion into Quaternary Li-Mn-V-O Spinel as Positive Materials for Rechargeable Lithium Batteries," *J. Electrochem. Soc.,* **140**, 3194-3199 (1993).

[22] C. J. Wen, B. A. Boukamp, R. A. Huggins, and W. Weppner, "Thermodynamic and Mass Transport Properties of LiAl," *J. Electrochem. Soc.*, **126**, 2258-2266 (1979).

[23] W. Weppner and R. A. Huggins, "Determination of the Kinetic Parameters of Mixed-Conducting Electrodes and Application to the System $Li_3Sb$," *J. Electrochem. Soc.*, **124**, 1569-1578 (1977).

[24] C. J. Wen and R. A. Huggins, "Chemical Diffusion in Intermediate Phases in the Lithum-Silicon System," *J. Solid State Chem.*, **37**, 271-278 (1981).

[25] M. S. Whittingham, "Electrical Energy Storage and Intercalation Chemistry," *Science*, **192**, 1126-1127 (1976).

[26] B. M. L. Rao, R. W. Francis, and H. A. Christopher, "Lithium-Aluminum Electrode," *J. Electrochem. Soc.*, **124**, 1490-1492 (1977).

[27] D. W. Murphy and J. N. Carides, "Low Voltage Behavior of Lithium/Metal Dichalcogenide Topochemical Cells," *J. Electrochem. Soc.*, **126**, 349-351 (1979).

[28] M. Lazzari and B. Scrosati, "A Cyclable Lithium Organic Electrolyte Cell Based on Two Intercalation Electrodes," *J. Electrochem. Soc.*, **127**, 773 (1980).

[29] Bruno Scrosati, "Lithium Rocking Chair Batteries: An Old Concept?" *J. Electrochem. Soc.*, **139**, 2776-2781 (1992).

[30] M. Armand, in *Materials for Advanced Batteries,* D. W. Murphy, J. Broadhead, and B. C. H. Steele, Eds., p. 145, Plenum Press, New York (1980).

[31] J. J. Auborn and Y. L. Barberio, "Lithium Intercalation Cells without Metallic Lithium," *J. Electrochem. Soc.*, **134**, 638-641 (1987).

[32] K. W. Semkow and A. F. Sammells, "Secondary Solid-State SPE Cells," *J. Electrochem. Soc.*, **134**, 766-767 (1987).

[33] J. R. Dahn, A. K. Sleigh, H. Shi, J. N. Reimers, Q. Zhong, and B. M. Way, "Dependence of the Electrochemical Intercalation of Lithium in Carbons on the Crystal Structure of the Carbon," *Electrochim. Acta,* **38**, 1179-1191 (1993).

[34] J. O. Besenhard, "The Electrochemical Preparation and Properties of Ionic Alkali Metal and $NR_4$-Graphite Intercalation Compounds in Organic Electrolytes," *Carbon,* **14**, 111-115 (1976).

[35] S. Basu, U. S. Patent 4,423,125 (1983).

[36] A. N. Dey and B. P. Sullivan, "The Electrochemical Decomposition of Propylene Carbonate on Graphite," *J. Electrochem. Soc.*, **117**, 222-224 (1970).

[37] A. Yoshino, K. Sanechika, and T. Nakajima, U. S. Patent 4,668,595 (1988).

[38] M. Mohri, N. Yanagisawa, T. Tajima, H. Tanaka, T. Mitate, S. Nakajima, M. Yoshida, Y. Yoshimoto, T. Suzuki, and H. Wada, "Rechargeable Lithium Battery Based on Pyrolytic Carbon as a Negative Electrode," *J. Power Sources,* **26**, 545-551 (1989).

[39] K. Inada, D. Ikeda, and Y. Sato, in *Proc. Symp. Electrochem. Soc., 88-6,* p. 530 (1988).

[40] R. Fong, U. von Sacken, and J. R. Dahn, "Studies of Lithium Intercalation into Carbons Using Nonaqueous Electrochemical Cells," *J. Electrochem. Soc.*, **137**, 2009-2013 (1990).

[41] T. Nagaura and K. Tozawa, *Prog. Batts. Sol. Cells,* **9**, 209 (1990).

[42] K. Ozawa, "Lithium-ion Rechargeable Batteries with $LiCoO_2$ and Carbon Electrodes: The $LiCoO_2$/C System," *S. S. Ionics,* **69**, 212-221 (1994).

[43] O. S. Ksenzhek and V. V. Stender, "Opredelenie udel'noĭ poverkhnosti poristykh elektrodov metodami izmereniya emkosti," *Doklady Akademii Nauk SSSR,* **106**, 487-490 (1956).

[44] J. Euler and W. Nonnenmacher, "Stromverteilung in porösen Elektroden," *Electrochim. Acta,* **2**, 268-286 (1960).

[45] J. S. Newman and C. W. Tobias, "Theoretical Analysis of Current Distribution in Porous Electrodes," *J. Electrochem. Soc.,* **109**, 1183-1191 (1962).

[46] J. Newman and W. Tiedemann, "Porous-Electrode Theory with Battery Applications," *AIChE J.,* **21**, 25-41 (1975).

[47] J. Newman, *Electrochemical Systems,* Prentice-Hall, Englewood Cliffs, New Jersey (1991).

[48] D. Simonsson, "A Mathematical Model for the Porous Lead Dioxide Electrode," *J. Appl. Electrochem.,* **3**, 261-270 (1973).

[49] K. Micka and I. Rousar, "Theory of Porous Electrodes-XI. The Positive Plate of the Lead-Acid Battery," *Electrochim. Acta,* **18**, 629-633 (1973).

[50] W. H. Tiedemann and J. Newman, "Mathematical Modeling of the Lead-Acid Cell," in *Proceedings of the Symposium in Battery Design and Optimization,* S. Gross, Ed., The Electrochemical Society, Inc., Princeton, NJ (1979) pp. 23-38.

[51] W. H. Tiedemann and J. Newman, "Current and Potential Distribution in Lead-Acid Battery Plates," in *Proceedings of the Symposium in Battery Design and Optimization,* S. Gross, Ed., The Electrochemical Society, Inc., Princeton, NJ (1979) pp. 39-49.

[52] W. H. Tiedemann and J. Newman, "Mathematical Modeling of Phenomena Contributing to Thermal Rise in Lead-Acid Batteries Used in Electric Vehicles," in *Proceedings of the Symposium on Advances in Lead-Acid Batteries,* The Electrochemical Society, Inc., Pennington, NJ (1984) pp. 360-377.

[53] H. Gu, T. V. Nguyen, and R. E. White, "A Mathematical Model of a Lead-Acid Cell," *J. Electrochem. Soc.,* **134**, 2953-2960 (1987).

[54] D. M. Bernardi, "Nucleation of Lead Sulfate in Porous Lead-Dioxide Electrodes," *J. Electrochem. Soc.,* **137**, 1670-1681 (1990).

[55] W. G. Sunu and B. W. Burrows, "Mathematical Model for Design of Battery Electrodes," *J. Electrochem. Soc.,* **129**, 688-695 (1982).

[56] R. Pollard and J. Newman, "Mathematical Modeling of the Lithium-Aluminum, Iron Sulfide Battery," *J. Electrochem. Soc.,* **128**, 491-502 (1981).

[57] D. Fan and R. E. White, "A Mathematical Model of a Sealed Nickel-Cadmium Battery," *J. Electrochem. Soc.,* **138**, 17-25 (1991).

[58] D. Fan and R. E. White, "Mathematical Modeling of a Nickel-Cadmium Battery," *J. Electrochem. Soc.,* **138**, 2952-2960 (1991).

[59] J.-S. Chen and H. Y. Cheh, "Modeling of Cylindrical Alkaline Cells III. Mixed-Reaction Model for the Anode," *J. Electrochem. Soc.,* **140**, 1205-1218 (1993).

[60] K.-C. Tsaur and R. Pollard, "Mathematical Modeling of the Lithium, Thionyl Chloride Static Cell," *J. Electrochem. Soc.*, **131**, 975-990 (1984).

[61] T. Yeu and R. E. White, "Mathematical Model of a Lithium/Polypyrrole Cell," *J. Electrochem. Soc.*, **137**, 1327-1336 (1990).

[62] S. Atlung, K. West, and T. Jacobsen, "Dynamic Aspects of Solid Solution Cathodes for Electrochemical Power Sources," *J. Electrochem. Soc.*, **126**, 1311-1321 (1979).

[63] K. West, T. Jacobsen, and S. Atlung, "Modeling of Porous Insertion Electrodes with Liquid Electrolytes," *J. Electrochem. Soc.*, **129**, 1480-1485 (1982).

[64] S. Atlung, B. Z.-Christiansen, K. West, and T. Jacobsen, "The Composite Insertion Electrode," *J. Electrochem. Soc.*, **131**, 1200-1207 (1984).

[65] B. C. Knutz, K. West, B. Z.-Christiansen, and S. Atlung, "Discharge Performance of Composite Insertion Electrodes. Analysis of Discharges of 50 vol.% $Li_3N/TiS_2$ Electrodes," *J. Power Sources,* **43-44**, 733-741 (1993).

[66] Z. Mao and R. E. White, "A Model for the Deliverable Capacity of the $TiS_2$ Electrode in a $Li/TiS_2$ Cell," *J. Power Sources,* **43-44**, 181-191 (1993).

# Chapter 2

## Development of Model Equations

### 2.1 Modeling approach

In this chapter, we develop the equations to describe the isothermal discharge of several types of lithium batteries. One must keep in mind that a very large number of different lithium-based systems have been considered in the literature, many using different electrode reactions, electrode configurations, or electrolyte phases.[1-10] The models that we develop here are intended to be sufficiently general to apply to many of the different specific systems that follow the assumptions set forth below. In particular, we consider lithium batteries that have at least one electrode which uses an insertion-type reaction. Thus, we can consider two main classes of lithium cells based on whether a single insertion reaction is employed, with solid lithium as the other electrode, *versus* a cell using two different insertion reactions, the so-called dual lithium-ion insertion cell or "rocking-chair" cell. These two classes of systems are modeled separately and refered to as the "foil" model and the "dual" model, respectively. For the insertion electrodes, we can also consider whether the system uses a porous-electrode geometry *versus* a flat, nonporous geometry, which will also affect the governing equations.

The two main classes of systems considered here are pictured in figure 2-1. The negative electrode, on the left, is either a solid lithium foil (2-1a) or an insertion-type electrode (2-1b). The positive electrode, on the right, is in both cases an insertion-type electrode. Nearly all of the insertion electrodes are configured as porous electrodes; we will reserve the consideration of nonporous electrodes for later (section 2.7). The electrolyte is assumed to consist of a single salt in a single solvent in both cases. The analysis of more complex solutions, such as those containing two salts or two or more solvents, follows directly from the present work. The

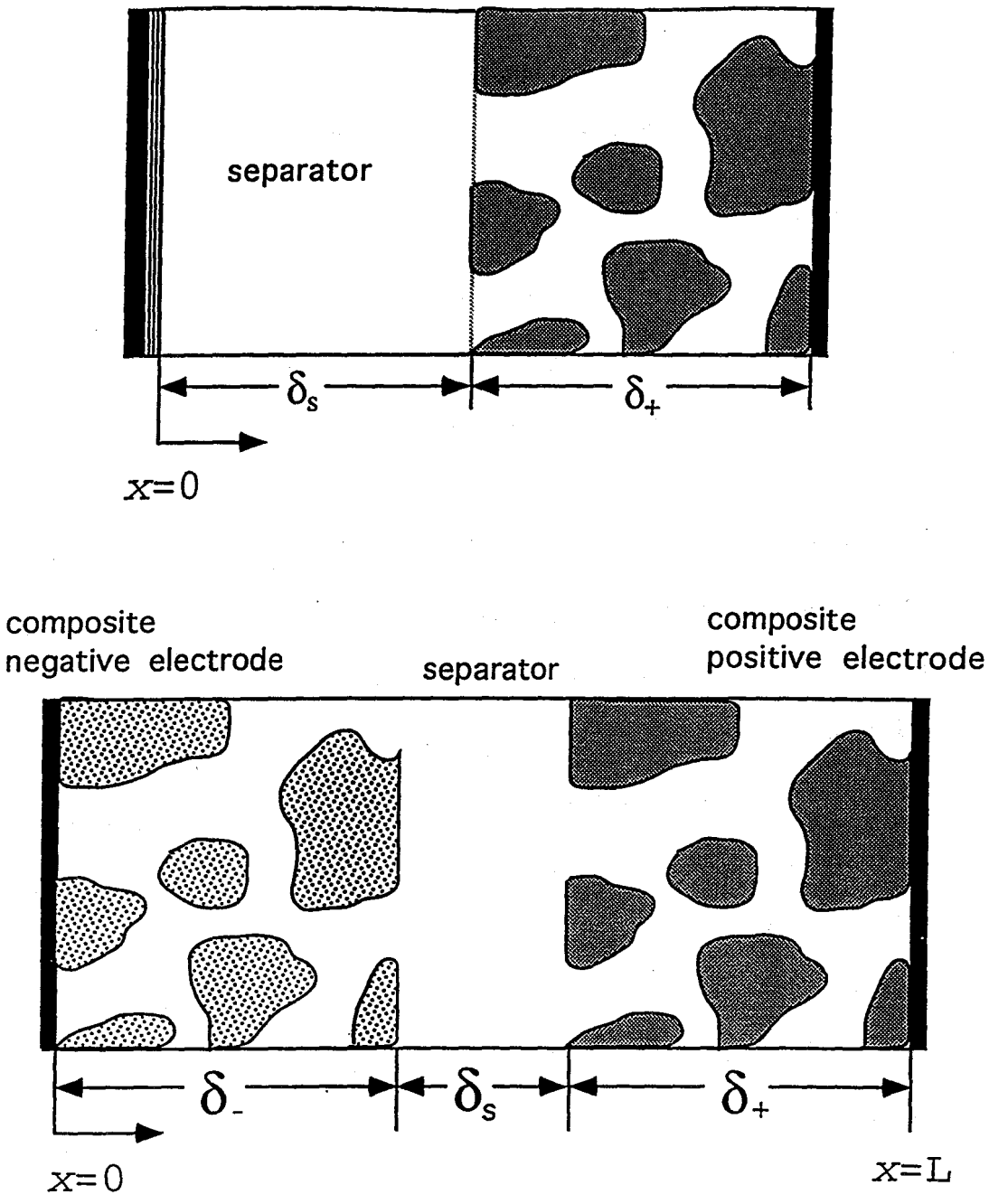


Figure 2-1. Lithium insertion cells. (a) Upper cell contains a lithium foil negative electrode. (b) The lower cell ("rocking-chair" type) uses an insertion-type negative electrode.

solvent can either be a nonaqueous liquid or a solid polymer; the treatment is identical.

The full-cell sandwich approach to battery modeling is necessarily a multi-region problem involving coupled differential equations. In all of the battery models to be considered here, the cell can be divided into three regions: the negative electrode, separator, and positive electrode. No external or interior solution reservoirs are considered, and current collectors are assumed to have infinite conductivity. The models to follow are also all one-dimensional; this is most adequate for the thin-film configuration used extensively with lithium-based systems.

## 2.2 Concentrated solution theory

As for most battery systems, the salt concentrations used in lithium batteries are generally large ($c$>1 M). Thus, transport of the electrolyte should be treated rigorously by using concentrated solution theory. In concentrated solution theory, the driving force for mass transfer at constant temperature and pressure is the gradient of the electrochemical potential for an ionic species. This driving force for the $i$th species is related to the fluxes of each of the other species through the multicomponent diffusion equation,[11]

$$c_i \nabla \mu_i = RT \sum_j \frac{c_i c_j}{c_T \mathcal{D}_{ij}} \left( \mathbf{v}_j - \mathbf{v}_i \right) . \qquad (2\text{-}1)$$

Here the $\mathcal{D}_{ij}$ are diffusion coefficients describing the interactions between the $i$th and $j$th species. By the Onsager reciprocal relationship, $\mathcal{D}_{ij}$=$\mathcal{D}_{ji}$. Since $\mathcal{D}_{ii}$ are not defined, we find that an $n$-component solution is described by $\frac{1}{2}n(n-1)$ independent transport properties. For a mixture of $n$ species, there are $(n-1)$ independent relationships of the form 2-1, as can be shown easily by summing 2-1 over all species and using the Gibbs-Duhem relation.

As equation 2-1 gives the driving force for mass transfer in terms of the species fluxes, we must invert these equations to obtain the flux in terms of the driving forces for use in a material balance equation. At this point we will limit ourselves to a binary electrolyte, and we will take the solvent velocity to be the reference velocity. This choice becomes particularly useful for treating polymer electrolytes, for which $\mathbf{v}_0 = 0$ can usually be assumed. Substitution of the definition of the current density

$$\mathbf{i} = F \sum_i z_i \mathbf{N}_i , \tag{2-2}$$

gives the following flux expressions

$$\mathbf{N}_+ = -\frac{\nu_+ \mathcal{D}}{\nu RT} \frac{c_T}{c_0} c \nabla \mu_e + \frac{\mathbf{i} t_+^0}{z_+ F} + c_+ \mathbf{v}_0 , \tag{2-3}$$

$$\mathbf{N}_- = -\frac{\nu_- \mathcal{D}}{\nu RT} \frac{c_T}{c_0} c \nabla \mu_e + \frac{\mathbf{i} t_-^0}{z_- F} + c_- \mathbf{v}_0 , \tag{2-4}$$

and

$$\mathbf{N}_0 = c_0 \mathbf{v}_0 . \tag{2-5}$$

We would prefer to relate these fluxes to a concentration driving force rather than a thermodynamic one,

$$\mathbf{N}_i = -\nu_i \left[ 1 - \frac{d \ln c_0}{d \ln c} \right] D \nabla c + \frac{\mathbf{i} t_i^0}{z_i F} + c_i \mathbf{v}_0 . \tag{2-6}$$

Here the salt diffusion coefficient $D$ is the property that is commonly measured; this is related

to the diffusion coefficient based on a thermodynamic driving force through[11]

$$D = \mathcal{D}\frac{c_T}{c_0}\left[1 + \frac{d\ln \gamma_{\pm}}{d\ln m}\right]. \tag{2-7}$$

Next, we substitute the flux expression into a general material balance for species $i$ of the form

$$\frac{\partial c_i}{\partial t} = -\nabla\cdot\mathbf{N}_i + R_i\,. \tag{2-8}$$

Inserting the flux equations 2-3 to 2-5 into this material balance, rearranging, and using electroneutrality, we find the following conservation relationships hold

$$\frac{\partial c}{\partial t} + \nabla\cdot\left[c\,\mathbf{v}_0\right] = \nabla\cdot\left[D\left[1 - \frac{d\ln c_0}{d\ln c}\right]\nabla c\right] - \frac{\mathrm{i}\,\nabla t_+^0}{z_+\nu_+ F}\,, \tag{2-9}$$

and

$$\frac{\partial c_0}{\partial t} = -\nabla\cdot\left[c_0\,\mathbf{v}_0\right]. \tag{2-10}$$

Equation 2-9 is a material balance on the salt, whereas equation 2-10 can be regarded as a continuity equation for the solvent velocity. In equation 2-9 we have assumed that the separator region is nonporous ($\varepsilon_s = 1$). At this point, we will assume that the solvent velocity is sufficiently small to be neglected, *i.e.*, $\mathbf{v}_0 = 0$, an assumption that will be returned to later in section 4.3. With this assumption, equation 2-9 has the final one-dimensional form,

$$\frac{\partial c}{\partial t} = \frac{\partial}{\partial x}\left[D\left[1 - \frac{d\ln c_0}{d\ln c}\right]\frac{\partial c}{\partial x}\right] - \frac{i_x}{z_+\nu_+ F}\frac{\partial t_+^0}{\partial x}. \qquad (2\text{-}11)$$

Notice that we have allowed the transport properties $D$ and $t_+^0$ to be arbitrary functions of the salt concentration in equation 2-11.

The variation of electrical state in the solution is to be defined with respect to a lithium reference electrode in solution. This leads to the following expression for the potential in solution[11]

$$\nabla\Phi = -\frac{\mathbf{i}}{\kappa} + \frac{RT}{F}\left[1 + \frac{d\ln f_A}{d\ln c}\right]\left[1 - t_+^0\right]\nabla\ln c\,, \qquad (2\text{-}12)$$

where the activity coefficient of the salt, $f_A$, is defined according to

$$\mu_e = RT\ln\left[cf_A a_A^\theta\right]. \qquad (2\text{-}13)$$

This can be contrasted with an expression employing the mean molar activity coefficient of the salt, $f_\pm$,

$$\nabla\Phi = -\frac{\mathbf{i}}{\kappa} + \frac{2RT}{F}\left[1 + \frac{d\ln f_\pm}{d\ln c}\right]\left[1 - t_+^0\right]\nabla\ln c\,, \qquad (2\text{-}14)$$

which will be used later (section 4.2) in connection with measurements of the transport properties in these solutions. The use of equation 2-12 over 2-14 can be viewed as an arbitrary assumption regarding the state of dissociation of the salt at infinite dilution.

Equations 2-11 and 2-12 define the three independent, measurable transport properties for a binary electrolyte: $\kappa$, $t_+^0$, and $D$. These can be related to the three pairwise interaction parameters $\mathcal{D}_{ij}$ through complicated expressions.[11] This situation can be contrasted with the

dilute-solution theory treatment of a binary electrolyte, which gives only two independent transport properties. For most battery applications, where large salt concentrations are used, it is essential to use the more rigorous concentrated solution theory. It has been shown that the assumptions of dilute-solution theory are particularly poor for the polymer electrolytes commonly used in lithium systems.[12]

## 2.3 Porous electrode theory

The porous electrode is the preferred configuration for battery applications because of the large interfacial area that it provides for the electrode reaction as well as the reduction in the distance between reactants and the surface. The theory of the macroscopic description of porous electrodes is described by Newman.[11,13] The porous electrode is treated as a superposition of continuous electrode and solution phases, each of known volume fraction. Thus, we do not consider the detailed pore geometry but, instead, describe the porous electrode by its specific interfacial area, $a$, and volume fractions of each phase, $\varepsilon$. As there exists interface between the two phases at each point in the volume of the electrode, the electrochemical reaction at the surface becomes a homogeneous reaction term in the species material balance. Following convention, we refer to properties of the electrode phase with a subscript 1 and those of the solution phase with a 2.

We consider the solution phase first, still taking the reference velocity to be the solvent velocity as above. In the absence of homogeneous chemical reactions, a material balance on the salt in the pores of the electrode gives

$$\varepsilon\frac{\partial c}{\partial t} + \mathbf{v}_0\cdot\nabla c = \nabla\cdot\left[\varepsilon D\left[1-\frac{d\ln c_0}{d\ln c}\right]\nabla c\right] + \left[1-t_+^0\right]\frac{aj_{+n}}{\nu_+} + \left[1-t_+^0\right]\frac{aj_{-n}}{\nu_-} - \frac{\mathbf{i}\,\nabla t_+^0}{z_+\nu_+F} - c\left[\frac{\partial\varepsilon}{\partial t} + \nabla\cdot\mathbf{v}_0\right]. \tag{2-15}$$

Similarly, a material balance on the solvent is

$$c_0\left[\frac{\partial\varepsilon}{\partial t} + \nabla\cdot\mathbf{v}_0\right] = -\varepsilon\frac{\partial c_0}{\partial t} - \mathbf{v}_0\cdot\nabla c_0 + aj_{0n}, \tag{2-16}$$

which can also be viewed as a conservation of pore volume. This equation, along with the following relationship:[11]

$$\frac{\partial\varepsilon}{\partial t} = \sum_j\left[\frac{s_jM_j}{\rho_j nF}\right]\nabla\cdot\mathbf{i}_2,\ j = \text{solid phases}, \tag{2-17}$$

can be used to account for solvent flow and changes in the porosity of the electrode due to the electrochemical reaction. The $s_j$ in equation 2-17 are the stoichiometric coefficients for the electrochemical reaction. We will neglect these effects for the present models. If experimental data demonstrate their importance, these phenomena can be added to the models in the future. For example, we may wish to use equation 2-17 to account for expansion or contraction of the electrode during the lithium ion insertion process.

For the present models, only the lithium ion participates in the electrochemical reaction, and thus $j_{-n} = j_{0n} = 0$. We will also assume that $\varepsilon$ is constant. With the additional assumption made earlier that $\mathbf{v}_0 = 0$, the material balance on the salt becomes, in one dimension,

$$\varepsilon\frac{\partial c}{\partial t} = \frac{\partial}{\partial x}\left[D_{\text{eff}}\left[1-\frac{d\ln c_0}{d\ln c}\right]\frac{\partial c}{\partial x}\right] + \left[1-t_+^0\right]\frac{aj_{+n}}{\nu_+} - \frac{i_{2,x}}{z_+\nu_+F}\frac{\partial t_+^0}{\partial x}. \tag{2-18}$$

The potential in the solution phase of the porous electrode, still defined with respect to a lithium reference electrode in solution, is given by

$$\nabla\Phi_2 = -\frac{\mathbf{i}_2}{\kappa_{\text{eff}}} + \frac{RT}{F}\left[1 + \frac{d\ln f_A}{d\ln c}\right]\left[1 - t_+^0\right]\nabla\ln c\,. \tag{2-19}$$

For a single electrode reaction of the form,

$$\sum_i s_i \mathrm{M}_i^{z_i} \rightleftarrows n\mathrm{e}^-$$

the pore-wall flux can be related to the divergence of the superficial current density in the solution phase

$$aj_{+n} = -\frac{s_+}{nF}\frac{\partial i_{2,x}}{\partial x}\,. \tag{2-20}$$

The potential in the electrode phase follows Ohm's law,

$$\nabla\Phi_1 = -\frac{\mathbf{i}_1}{\sigma_{\text{eff}}}\,, \tag{2-21}$$

where $\sigma_{\text{eff}}$ is an effective conductivity for the porous electrode. It is common to add an inert, conducting phase to the porous electrode mixture, such as carbon black. This is essentially treated as dead volume, but the value of $\sigma_{\text{eff}}$ used above is assumed to be that measured for the porous electrode in the presence of the additive. The superficial current density in the two phases is conserved through a charge balance, which leads to

$$I = \mathbf{i}_1 + \mathbf{i}_2\,, \tag{2-22}$$

with $I$ being the cell current density. This equation can be used to eliminate $i_1$ from all of the governing equations.

All of the transport properties in the porous medium are modified to account for the porosity by using effective values. It is common to express these in terms of a correction for the reduced volume of the conducting phase and a correction for the increase in path length brought about by the tortuosity of the porous material:[14]

$$\kappa_{eff} = \frac{\varepsilon\kappa_\infty}{\tau} \quad \text{or} \quad \kappa_{eff} = \frac{\varepsilon\kappa_\infty}{\gamma^2}. \tag{2-23}$$

The tortuosity factor, $\tau$ or $\gamma$, is then usually related to the porosity[15]

$$\tau = \varepsilon^{-\frac{1}{2}}. \tag{2-24}$$

This naturally leads to the standard Bruggeman correction, which takes the form:[16]

$$\kappa_{eff} = \varepsilon^{1.5}\kappa_\infty. \tag{2-25}$$

We will simply use the Bruggeman form to convert the transport properties, including $\kappa$, $D$, and $\sigma$, to their effective values. Note that our convention is in contrast to the usual procedure for the effective diffusion coefficient of using the exponent 0.5 in equation 2-25 and treating the porosity correction separately.[11]

### 2.4 Boundary conditions

We will construct the model based on a galvanostatic charge/discharge mode. A potentiostatic charge or discharge is simulated by iterating the cell current density and solving the galvanostatic equations until the desired cell potential is achieved. The boundary condition on

the salt concentration at the lithium electrode (figure 2-1a) is found by setting the anion flux to zero,

$$\nabla c = -\frac{I\left[1 - t_+^0\right]}{FD} \quad \text{at} \quad x = 0 . \tag{2-26}$$

At the positive electrode/current collector boundary, the flux of ions is equal to zero, and all of the current is carried by electrons. This leads to boundary conditions on the salt concentration and solution-phase current density,

$$\nabla c = 0 \quad \text{at} \quad x = \delta_s + \delta_+ , \tag{2-27}$$

and

$$\mathbf{i}_2 = 0 \quad \text{at} \quad x = \delta_s + \delta_+ . \tag{2-28}$$

This latter condition can also be viewed as a condition on the solid-phase potential gradient,

$$\nabla \Phi_1 = -\frac{I}{\sigma} \quad \text{at} \quad x = \delta_s + \delta_+ . \tag{2-29}$$

For the dual lithium-ion insertion cell (figure 2-1b), the boundary conditions on the negative electrode/current collector boundary are analogous to those on the positive electrode/current collector boundary,

$$\nabla c = 0 \quad \text{at} \quad x = 0 , \tag{2-30}$$

and

$$\mathbf{i}_2 = 0 \text{ at } x = 0. \tag{2-31}$$

We can also arbitrarily set $\Phi_2 = 0$ at any point in the domain, as only potential differences are measurable. For the lithium foil model, it is most convenient to have $\Phi_2 = 0$ at $x = 0$; for the dual insertion model, we let $\Phi_2 = 0$ at $x = L$.

The internal boundaries include $x = \delta_s$ for figure 2-1a and $x = \delta_- $ and $x = \delta_- + \delta_s$ for figure 2-1b. At these boundaries, all of the variables, as well as the flux of salt, must be continuous. The current density at these points is equal to the applied cell current density,

$$\mathbf{i}_2 = I. \tag{2-32}$$

The following condition should be obeyed by the solid-phase potential at either boundary,

$$\nabla\Phi_1 = 0. \tag{2-33}$$

## 2.5 Solid-state diffusion

The slowest step in the lithium insertion process has long been thought to be the diffusion of lithium into the oxide lattice.[17] Hence, this diffusion process cannot be ignored in the battery models. For this purpose, we can imagine that the solid phase of the porous electrode consists of spherical particles of a given average diameter. Taking the direction normal to the surface of the particles to be the $r$-direction, a material balance on lithium gives

$$\frac{\partial c_s}{\partial t} = D_s \left[ \frac{\partial^2 c_s}{\partial r^2} + \frac{2}{r} \frac{\partial c_s}{\partial r} \right], \tag{2-34}$$

where $c_s$ represents the concentration of lithium in the solid electrode particle and $D_s$ is assumed to be constant. The following boundary condition results from symmetry

$$\frac{\partial c_s}{\partial r} = 0 \text{ at } r = 0. \tag{2-35}$$

A second boundary condition on this equation is provided by relating the pore-wall flux across the interface with the rate of transport of lithium ions into the solid phase,

$$j_n = -D_s \frac{\partial c_s}{\partial r} \text{ at } r = R_s. \tag{2-36}$$

Under this model of the diffusion process, the superficial area per unit volume of the porous electrode is related to the sphere's radius through:

$$a = \frac{3(1-\varepsilon)}{R_s}. \tag{2-37}$$

As we have assumed that the diffusion coefficient in the solid, $D_s$, does not depend on concentration, this problem is linear and can be solved by the method of superposition.[18]

Using Duhamel's superposition integral, the flux into a particle can be expressed as

$$\frac{\partial c_s}{\partial r}(R_s, t) = \int_0^t \frac{\partial c_s}{\partial t}(R_s, \delta) \frac{\partial \bar{c}_s}{\partial r}(R_s, t-\delta)\, d\delta, \tag{2-38}$$

where $\bar{c}_s$ represents the solution to equation 2-34 for a unit step change in concentration at the surface. Equation 2-38 is a Volterra, or initial-value type, integral equation. Thus, it can be calculated numerically using the method suggested by Wagner[19] and by Acrivos and Chambré.[20] Whence,

$$\frac{\partial c_s}{\partial r}(R_s,t) = \sum_{k=0}^{n-2} \frac{\left[c_{s,k+1} - c_{s,k}\right]}{\Delta t} A_{n-k} + \frac{\left[c_{s,n} - c_{s,n-1}\right]}{\Delta t} A_1, \tag{2-39}$$

where

$$A_{n-k} = a[(n-k)\Delta t] - a[(n-k-1)\Delta t] \tag{2-40}$$

and

$$a(t) = \int_0^t \frac{\partial \bar{c}_s}{\partial r}(R_s, \zeta) d\zeta. \tag{2-41}$$

Additional details on this approach can be found in the work of Matlosz[21] and Shain.[22]

By means of Laplace transforms, two expressions for the dimensionless $a(t)$ were developed: at long times,

$$a(\tau) = \frac{2}{\pi^2} \sum_{n=1}^{\infty} \frac{1}{n^2} \left[1 - \exp\left[-n^2\pi^2\tau\right]\right], \tag{2-42}$$

and for short times

$$a(\tau) = -\tau + 2\left[\frac{\tau}{\pi}\right]^{1/2} \left[1 + 2\sum_{n=1}^{\infty} \exp\left[\frac{-n^2}{\tau}\right] - n\left[\frac{\pi}{\tau}\right]^{1/2} \operatorname{erfc}\left[\frac{n}{\sqrt{\tau}}\right]\right]. \tag{2-43}$$

$\tau$ is the dimensionless time, defined as $\tau = tD_s/R_s^2$. These expressions are each uniformly valid; however, the latter expression converges much more quickly with fewer terms at very short times. The values of $a(\tau)$ and $A_{n-k}$ can be calculated separately and used whenever equation 2-39 needs to be evaluated. This approach, applicable only to diffusion with a constant diffusion coefficient, is much more efficient than solving the pseudo two-dimensional transport problem directly.[23] The numerical solution provides the relationship between two important quantities for the battery model, which are the values of the lithium flux and solid-phase concentration at the surface of the particle. Detailed internal profiles can be derived from these

results if desired.

An analogous approach can be taken to treat diffusion into either planar or cylindrical particles. This might be interesting, for example, if the insertion material has a preferred crystallographic orientation for the diffusion process. For the planar geometry, the expressions for $a(\tau)$ at long and short times, repectively, are

$$a(\tau) = \frac{2}{\pi^2} \sum_{n=1}^{\infty} \frac{(-1)^n}{(2n+1)^2} \left[1 - \exp\left[-(2n+1)^2 \pi^2 \tau\right]\right], \tag{2-44}$$

$$a(\tau) = 2\left[\frac{\tau}{\pi}\right]^{1/2} \left[1 + 2\sum_{n=1}^{\infty} (-1)^n \left[\exp\left[-\frac{n^2}{\tau}\right] - \frac{\pi^{1/2} n}{\tau^{1/2}} \operatorname{erfc}\left[\frac{n}{\tau^{1/2}}\right]\right]\right]. \tag{2-45}$$

For the cylindrical geometry, these are

$$a(\tau) = 2 \sum_{n=1}^{\infty} \frac{1}{\lambda_n^2} \left[1 - \exp\left[-\lambda_n^2 \tau\right]\right], \tag{2-46}$$

$$a(\tau) = 2\left[\frac{\tau}{\pi}\right]^{1/2} - \frac{\tau}{4} - \frac{5\tau^{3/2}}{96\pi^{1/2}} - \frac{31\tau^2}{2048} + O(\tau^{5/2}), \tag{2-47}$$

where in equation 2-46 the eigenvalues, $\lambda_n$, are given by $J_0(\lambda_n) = 0$. Equation 2-47 for the cylindrical short-time solution is not valid at long times.

The optimum time to switch between the long and short-time solutions above must be determined by examining the accuracy of each solution as a function of the number of terms employed and the dimensionless time.[22] In general, one wants to have the largest possible accuracy while evaluating a minimum number of terms from each expression. This can be satisfied by comparing the errors involved in evaluating the solution for $a(\tau)$ using increasing numbers of terms in the long and short-time series solutions (for example 2-42 and 2-43). As a

basis for comparison, we take the long-time solution evaluated out to one hundred terms. To assure sufficient accuracy, we demand that the log of the relative error should be less than -8. In this way the error is made to be much less than this at both long and short times (*i.e.*, the maximum relative error is $10^{-8}$). For the spherical case, we find that evaluating 3 terms of the short-time solution and 5 terms of the long-time solution is satisfactory. The long-time solution is used to calculate $a(\tau)$ unless $\tau$ is less than 0.06.

### 2.6 Electrode kinetics

For cells using a lithium negative electrode, we assume that the charge-transfer reaction in a liquid electrolyte has the form

$$\mathrm{Li} \rightleftarrows \mathrm{Li}^{+} + \mathrm{e}^{-}.$$

The kinetics of this process is described by the Butler-Volmer relation,

$$I = i_{0,1}\left[\exp\left[\frac{\alpha_{a,1} F \eta_{s,1}}{RT}\right] - \exp\left[-\frac{\alpha_{c,1} F \eta_{s,1}}{RT}\right]\right]. \tag{2-48}$$

This equation applies at $x = 0$ in figure 2-1a. The local value of the surface overpotential is defined by

$$\eta_{s,1} = \Phi_1 - \Phi_2 - U_1\,, \tag{2-49}$$

and, in addition, $U_1 = 0$ because we are measuring the potential with repect to a lithium reference electrode in solution at the same local concentration. The exchange-current density for this reaction has the form

$$i_{0,1} = F(k_{a,1})^{\alpha_{c,1}}(k_{c,1})^{\alpha_{a,1}}c^{\alpha_{a,1}} . \qquad (2\text{-}50)$$

For the commonly used polymer electrolyte, poly(ethylene oxide) (PEO), there is experimental evidence for a charge-transfer process of the form[24]

$$\mathrm{Li} + \Theta_p \rightleftarrows \mathrm{Li}^+ - \Theta_p + \mathrm{e}^- ,$$

where $\Theta_p$ represents a site in the polymer lattice. This corresponds to an equilibrium between occupied and unoccupied lithium sites in the solid-polymer electrolyte. In this case, an identical kinetic expression will hold, but the exchange-current density is defined as

$$i_{0,1} = F(k_{a,1})^{\alpha_{c,1}}(k_{c,1})^{\alpha_{a,1}}(c_{\max} - c)^{\alpha_{c,1}}(c)^{\alpha_{a,1}} , \qquad (2\text{-}51)$$

where $c_{\max}$ is the maximum salt concentration permissible in the PEO.

A general lithium ion insertion process is described by a charge-transfer reaction of the form

$$\mathrm{Li}^+ + \Theta_s + \mathrm{e}^- \rightleftarrows \mathrm{Li} - \Theta_s ,$$

with $\Theta_s$ representing a site in the solid lattice. This could, for example, represent lithium insertion in the lithium-manganese-oxide spinel

$$\mathrm{Li}^+ + \mathrm{Mn_2O_4} + \mathrm{e}^- \rightleftarrows \mathrm{LiMn_2O_4} .$$

The kinetics of this reaction is also described by the Butler-Volmer equation,

$$i_n = i_{0,2}\left[\exp\left[\frac{\alpha_{a,2}F\eta_{s,2}}{RT}\right] - \exp\left[-\frac{\alpha_{c,2}F\eta_{s,2}}{RT}\right]\right] , \qquad (2\text{-}52)$$

where the normal component of the current density is related to the pore-wall flux by $i_n = Fj_{+n}$. The exchange-current density now has the form

$$i_{0,2} = F(k_{a,2})^{\alpha_{c,2}}(k_{c,2})^{\alpha_{a,2}}(c_t - c_s)^{\alpha_{a,2}}(c_s)^{\alpha_{c,2}}(c)^{\alpha_{a,2}} . \qquad (2\text{-}53)$$

The solid-phase lithium concentration, $c_s$, which appears in these expressions is that evaluated at the surface of the particle, determined previously from the internal diffusion problem. The surface overpotential is defined as

$$\eta_{s,2} = \Phi_1 - \Phi_2 - U(c_s, T) , \qquad (2\text{-}54)$$

and the open-circuit potential of the insertion process, $U$, is allowed to be a general function of the amount of lithium inserted and the temperature:

$$U = U^{\theta} + f(c_s, T) .$$

For example, the open-circuit potential for lithium insertion into titanium disulfide has the form[17]

$$U = 2.17 + \frac{RT}{F}\left[\ln\left[\frac{c_t - c_s}{c_s}\right] + \beta c_s + \zeta\right] ,$$

where $c_t$ = 29.0 mol/dm$^3$, $\beta$=-0.558 dm$^3$/mol, and $\zeta$=8.10. Any differentiable function can be used for $U$ in the computer programs. Appendix 2-A gives several additional examples of functional fits to open-circuit potential data for insertion electrode materials (including $Mn_2O_4$, $CoO_2$, $NiO_2$, $V_2O_5$, $WO_3$, $C_6$, and $NaCoO_2$).

## 2.7 Nonporous insertion electrodes

Lithium rechargeable batteries based on a flat, nonporous configuration for the insertion electrode have been considered for very low-rate discharge applications and all-solid-state devices.[25,26] Thin-film microbatteries based on successive deposition of lithium, a solid electrolyte, and an insertion compound layer will allow integration of a backup power source with the electronic circuit board.[27] These systems generally use cell components that are very thin, on the order of ten μm or less, so that diffusion limitations in the insertion electrode are not too severe and ohmic drop through the poorly conducting solid electrolyte is not excessive. A diagram of the cell under consideration is given as figure 2-2. We will only consider this geometry with a single insertion electrode, as the generalization to a dual insertion electrode cell is trivial. This configuration is also interesting from the perspective of materials characterization, as a cell of this form may be used to measure properties of the insertion material such as kinetic or transport parameters. Thus, this model could be useful for the interpretation of experimental data.

The mathematical model of this configuration is just a simplification of the previous models. Identical equations apply in the separator (equations 2-11 and 2-12) and at the surface of the lithium electrode (equation 2-48). However, in the positive-electrode region ($\delta_s<x<\delta_s+\delta_+$), we can simplify the previous treatment. At the separator/positive electrode boundary ($x=\delta_s$), a charge-transfer reaction with the following kinetic expression occurs

$$I = i_{0,2}\left[\exp\left[\frac{\alpha_{a,2}F\eta_{s,2}}{RT}\right] - \exp\left[-\frac{\alpha_{c,2}F\eta_{s,2}}{RT}\right]\right], \qquad (2\text{-}55)$$

with $i_{0,2}$ and $\eta_{s,2}$ defined identically as earlier. The solid-phase concentration appearing in $i_{0,2}$ is just that evaluated at the surface, $c_s=c_s(x=\delta_s)$. Also, the boundary condition for the diffusion

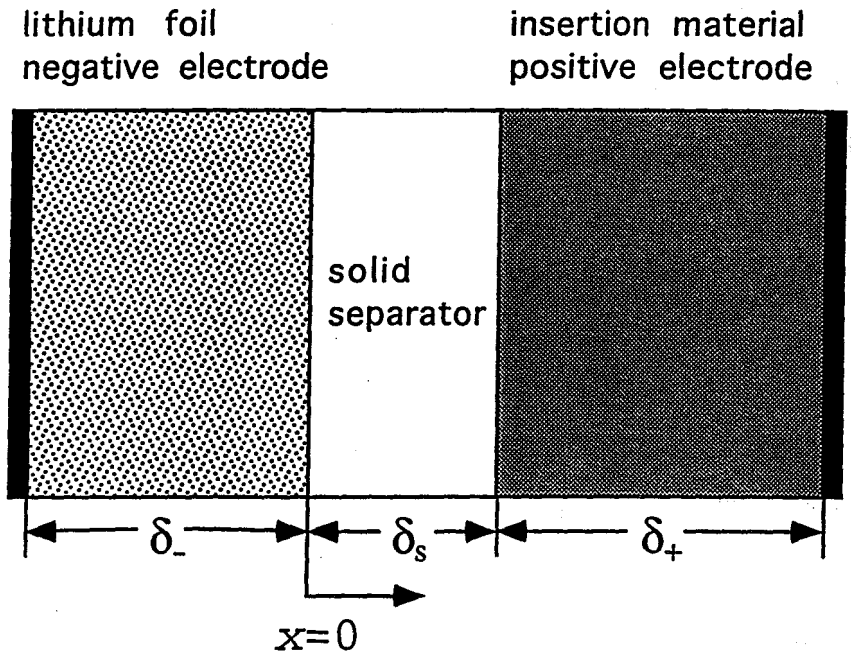


Figure 2-2. Lithium-based cell sandwich consisting of lithium foil negative electrode, solid electrolyte, and nonporous insertion material positive electrode.

problem in the solid phase is now (compare with equation 2-36)

$$\frac{I}{F} = -D_s \frac{\partial c_s}{\partial x} \text{ at } x=\delta_s . \tag{2-56}$$

The diffusion process into the positive electrode is best viewed as a planar problem, and no longer needs to be solved by using a superposition integral as before. For a galvanostatic discharge, the boundary condition equation 2-56 is now a constant, so we can solve the diffusion problem exactly. The diffusion problem is:

$$\frac{\partial c_s}{\partial t} = D_s \frac{\partial^2 c_s}{\partial x^2} , \tag{2-57}$$

with boundary conditions:

$$\frac{\partial c_s}{\partial x}(x=\delta_s, t) = -\frac{I}{FD_s} , \tag{2-58}$$

$$\frac{\partial c_s}{\partial x}(x=\delta_s + \delta_+, t) = 0 , \tag{2-59}$$

and

$$c_s(x, t=0) = c_s^0 . \tag{2-60}$$

The solution to this problem can be found[28]

$$c_s(x,\,t) = c_s^0 + \frac{\delta_+ I}{FD_s}\left[\frac{D_s t}{\delta_+^2} + \frac{3\left[x-(\delta_s+\delta_+)\right]^2 - \delta_+^2}{6\delta_+^2}\right] - \frac{\delta_+ I}{FD_s}\left[\frac{2}{\pi^2}\sum_{n=1}^{\infty}\frac{(-1)^n}{n^2}\exp\left[-\frac{D_s n^2\pi^2 t}{\delta_+^2}\right]\cos\left[\frac{n\pi}{\delta_+}\left[(\delta_s+\delta_+)-x\right]\right]\right]. \tag{2-61}$$

As was the case earlier, at short times it is easiest to use a different solution for the concentration rather then have to evaluate many terms of the above series. Using a variable transformation from the concentration to the flux, one finds that the above problem reduces to a more familiar one involving an error function solution. At short times, the back of the insertion electrode is taken to be infinitely far away and the concentration profiles have the form:

$$c_s(x,\,t) \approx c_s^0 + \frac{2It^{1/2}}{FD_s^{1/2}}\,\mathrm{ierfc}\left[\frac{x-\delta_s}{2(D_s t)^{1/2}}\right]. \tag{2-62}$$

This is just a simplification of the full solution:

$$c_s(x,\,t) = c_s^0 + \frac{2It^{1/2}}{FD_s^{1/2}}\sum_{n=0}^{\infty}\mathrm{ierfc}\left[\frac{(2n+1)\delta_+ - (\delta_+ + \delta_s - x)}{2(D_s t)^{1/2}}\right] + \frac{2It^{1/2}}{FD_s^{1/2}}\sum_{n=0}^{\infty}\mathrm{ierfc}\left[\frac{(2n+1)\delta_+ + (\delta_+ + \delta_s - x)}{2(D_s t)^{1/2}}\right]. \tag{2-63}$$

The most important quantity to extract from the diffusion problem is the surface value of the solid-phase lithium concentration, which is needed to evaluate both the exchange-current density and the open-circuit potential in the kinetic expression. This quantity is easy to extract from the latter short-time solution, giving:

$$c_s(x=0,\,t) = c_s^0 + \frac{2It^{1/2}}{F\pi^{1/2}D_s^{1/2}}. \tag{2-64}$$

Otherwise, a long-time approximation to the surface concentration may be used:

$$c_s(x=0,\, t) = c_s^0 + \frac{\delta_+ I}{F D_s}\left[\frac{D_s t}{\delta_+^2} + \frac{1}{3} - \frac{2}{\pi^2}\exp\left[-\frac{D_s \pi^2 t}{\delta_+^2}\right]\right]. \qquad (2\text{-}65)$$

The surface concentration cannot exceed its maximum value, $c_t$, and still provide the constant current that is being drawn from the cell. If we wish to obtain detailed solid-phase concentration profiles, they can be evaluated from either equation 2-61 or 2-63, whichever is more convenient.

Equation 2-64 or 2-65 for the surface concentration should be substituted directly into the Butler-Volmer equation 2-55. Then, for a constant electronic conductivity, we recognize that Ohm's law in the solid phase can be integrated directly, giving:

$$\Phi_1(x=\delta_s + \delta_+) - \Phi_1(x=\delta_s) = -\frac{I\delta_+}{\sigma}. \qquad (2\text{-}66)$$

The value of $\Phi_1$ needed in the Butler-Volmer equation can then be substituted directly into equation 2-55. This eliminates the nonporous electrode region completely from the coupled differential equations in the separator.

Considering the simplicity of this model, we may wish to consider adding more complexity by treating the solid-phase diffusion coefficient and electronic conductivity as functions of the electrode's state of charge. This is possible for the nonporous insertion electrode with little added difficulty. The electrode region would then need to be discretized, and the diffusion equation and Ohm's law solved simultaneously with known forms for $D_s=D_s(c_s)$ and $\sigma=\sigma(c_s)$. The diffusion equation to be solved is:

$$\frac{\partial c_s}{\partial t} = \frac{\partial}{\partial x}\left[D_s \frac{\partial c_s}{\partial x}\right], \tag{2-67}$$

where we have not assumed that $D_s$ is a constant. In addition, for generality, we should like to relax the assumption of a constant current density in equation 2-56 and instead allow the current density to be any known function of time. This would allow, for example, the ability to simulate cycling and driving profiles that are commonly used in electric-vehicle applications. This could be accomplished by making use of the superposition-integral framework already in place.

## 2.8 Summary of model equations

In summary, the equations to be solved for the lithium foil model (figure 2-1a) are given below. The model can be divided into the separator and porous positive electrode regions. In the solution phase of the positive electrode the equations are

$$\varepsilon \frac{\partial c}{\partial t} = \frac{\partial}{\partial x}\left[D_{\text{eff}}\left[1 - \frac{d\ln c_0}{d\ln c}\right]\frac{\partial c}{\partial x}\right] + \left[1 - t_+^0\right] a j_{+n} - \frac{i_{2,x}}{F}\frac{\partial t_+^0}{\partial x}, \tag{2-68}$$

$$\frac{\partial \Phi_2}{\partial x} = -\frac{i_{2,x}}{\kappa_{\text{eff}}} + \frac{RT}{F}\left[1 + \frac{\partial \ln f_A}{\partial \ln c}\right]\left[1 - t_+^0\right]\frac{\partial \ln c}{\partial x}, \tag{2-69}$$

$$a j_n = \frac{1}{F}\frac{\partial i_{2,x}}{\partial x}. \tag{2-70}$$

In the solid phase of the positive electrode

$$\frac{\partial \Phi_1}{\partial x} = -\frac{I - i_{2,x}}{\sigma_{\text{eff}}} . \tag{2-71}$$

The solid-phase diffusion problem

$$\frac{\partial c_s}{\partial t} = D_s \left[ \frac{\partial^2 c_s}{\partial r^2} + \frac{2}{r} \frac{\partial c_s}{\partial r} \right] , \tag{2-72}$$

is solved and relegated to a surface integral equation leading to:

$$j_{+n} = -D_s \left[ \sum_{k=0}^{n-2} \frac{\left( c_{s,k+1} - c_{s,k} \right)}{\Delta t} A_{n-k} + \frac{\left( c_{s,n} - c_{s,n-1} \right)}{\Delta t} A_1 \right] . \tag{2-73}$$

The two phases are also related through the Butler-Volmer kinetic expression,

$$j_{+n} = \frac{i_{0,2}}{F} \left[ \exp \left[ \frac{\alpha_{a,2} F \eta_{s,2}}{RT} \right] - \exp \left[ -\frac{\alpha_{c,2} F \eta_{s,2}}{RT} \right] \right] . \tag{2-74}$$

If we now combine equations 2-69 and 2-71, we find that the variables $\Phi_1$ and $\Phi_2$ always appear in the combination $\Phi_1 - \Phi_2$; thus we define $\eta = \Phi_1 - \Phi_2$ and instead solve the equation,

$$\frac{\partial \eta}{\partial x} = -\frac{I}{\sigma_{\text{eff}}} + i_{2,x} \left[ \frac{1}{\sigma_{\text{eff}}} + \frac{1}{\kappa_{\text{eff}}} \right] - \frac{RT}{F} \left[ 1 + \frac{\partial \ln f_A}{\partial \ln c} \right] \left[ 1 - t_+^0 \right] \frac{\partial \ln c}{\partial x} . \tag{2-75}$$

In the separator region, the first two equations apply with $j_{+n}$=0 and $\varepsilon$=1.0. We have two independent variables ($x$ and $t$) and five dependent variables ($c$, $\eta$, $c_s$, $i_{2,x}$, and $j_{+n}$).

For the dual insertion electrode model (figure 2-1b), the equations are similar to the above set; however, the cell now has three regions. We still have the same two equations (2-11 and 2-12) in the separator. In either porous electrode, we have the six equations above (2-68 to 2-

71, 2-73, and 2-74), but with different electrode properties in each region. We do not use the combined variable $\eta$ in the dual model because different values of $\Phi_1$ apply in each electrode and this would cause $\eta$ to be discontinuous. Thus, in this model we have two independent variables ($x$ and $t$) and six dependent variables ($c$, $\Phi_2$, $c_s$, $i_{2,x}$, $j_{+n}$, and $\Phi_1$).

The above sets of equations are solved simultaneously at each time step according to the procedure detailed in section 2.9. A quantity of primary interest is the cell potential, which can be calculated after each time step by taking the difference in solid-phase potentials between the two current collectors. For example, for the dual lithium-ion insertion cell model,

$$V = \Phi_1(x = L) - \Phi_1(x = 0). \tag{2-76}$$

This quantity is next used to calculate average values of the specific energy and power that the cell has provided from

$$E = \frac{1}{M}\int_0^t IV\,\mathrm{d}t \tag{2-77}$$

and

$$P = \frac{E}{t}. \tag{2-78}$$

Here $M$ is the mass per unit area of the cell, in units of kg/m$^2$; this can be calculated for the dual lithium-ion insertion cell, for example, from

$$\begin{aligned} M = {} & \rho_{-}\delta_{-}(1 - \varepsilon_{-} - \varepsilon_{f,-}) + \rho_e\delta_{-}\varepsilon_{-} + \rho_f\delta_{-}\varepsilon_{f,-} + \rho_e\delta_s \\ & + \rho_{+}\delta_{+}(1 - \varepsilon_{+} - \varepsilon_{f,+}) + \rho_e\delta_{+}\varepsilon_{+} + \rho_f\delta_{+}\varepsilon_{f,+}. \end{aligned} \tag{2-79}$$

This mass includes the two composite electrodes and separator, but not current collectors or residual masses. The instantaneous cell temperature can also be calculated at each time step

from an energy balance of the form[11]

$$M\hat{C}_p\frac{dT}{dt} = I\left[U(T^0) - V - T^0\frac{dU}{dT}\right] + h_0\left[T_{amb} - T\right], \qquad (2\text{-}80)$$

where $T^0$ is the initial temperature and $T_{amb}$ is the ambient temperature. However, we shall generally refrain from discussing nonisothermal simulation results, as this has been covered elsewhere.[29-31]

## 2.9 Numerical solution procedure

The method used here to solve the above sets of coupled, nonlinear differential and algebraic equations has been summarized previously, and we will only touch on the most important points.[11] First, the nonlinear equations must be linearized about a trial solution. The solution to these linear equations is then used as the next trial solution, and this process is iterated until the desired degree of convergence is achieved. The variable physical properties are treated as known functions of the salt concentration, which are expanded in Taylor series about a trial value. For example, a term involving the gradient of the transference number (such as in equation 2-11) would become

$$\frac{dt_+^0}{dx} = \frac{dt_+^0}{dc}\frac{\partial c}{\partial x} = \left[\left.\frac{dt_+^0}{dc}\right|_{c=c^0} + \left.\frac{d^2t_+^0}{dc^2}\right|_{c=c^0}\left[c - c^0\right]\right]\frac{\partial c}{\partial x}, \qquad (2\text{-}81)$$

where $c^0$ represents the trial solution. Notice that not only is $t_+^0 = t_+^0(c)$ required, but also the first and second derivatives of this function are needed.

The linearized differential equations are cast into finite-difference form accurate to O ($h^2$) for solution by the subroutine BAND.[11] The central-difference form is used for second-order

differential equations such as the salt material balance, while either the forward or backward-difference form is used for first-order differential equations. For a first-order differential equation, the choice of whether to use the forward or backward-difference form depends on the position of the boundary condition. Time derivatives are approximated using the Crank-Nicolson implicit method, which consists of weighting solutions at the old and new time steps equally.

We should take a moment to discuss the application of boundary conditions at an internal boundary. In order to ensure the desired O ($h^2$) accuracy for the second-order differential equations, it is necessary to perform a local material balance about the boundary region. This necessity arises because the matrices that are solved with the subroutines BAND and MATINV must be tridiagonal. There exist different methods for dealing with internal boundaries in multiple-region problems like this one.[32,33]

The boundary material balance can be formulated as the sum of material balances applied at either side of the boundary. For example, at the separator/positive electrode boundary in the foil model ($x=\delta_s$), we can perform material balances around the half-node points on either side of the boundary (node $j$) to find the following two expressions:

$$\varepsilon_s \left[ \frac{3c(j) + c(j-1) - 3\bar{c}(j) - \bar{c}(j-1)}{4\Delta t} \right] = \frac{N_+(j-\tfrac{1}{2}) - N_+(j)}{h_s} + \frac{\bar{N}_+(j-\tfrac{1}{2}) - \bar{N}_+(j)}{h_s}, \tag{2-82}$$

$$\varepsilon_p \left[ \frac{3c(j) + c(j+1) - 3\bar{c}(j) - \bar{c}(j+1)}{4\Delta t} \right] = \frac{N_+(j) - N_+(j+\tfrac{1}{2})}{h} + \frac{\bar{N}_+(j) - \bar{N}_+(j+\tfrac{1}{2})}{h} + \frac{a}{8}\left[3j_n(j) + j_n(j+1)\right] + \frac{a}{8}\left[3\bar{j}_n(j) + \bar{j}_n(j+1)\right], \tag{2-83}$$

where $\bar{x}(j)$ is the value of $x(j)$ at the previous time step and $h_s$ and $h$ are the mesh spacings in the two regions. Multiplying by the mesh spacings, adding these together, canceling the fluxes $N_+(j)$ which are identical by the continuity condition, and using properly averaged flux expressions such as

$$N_+(j-½) = -\varepsilon_s D(j-½)\left[\frac{c(j)-c(j-1)}{h_s}\right] + \frac{t_+^0(j-½)}{F}\left[\frac{I(j-1)+I(j)}{2}\right] \qquad (2\text{-}84)$$

gives a difference expression for the boundary node.

This procedure for deriving difference equations, called the control-volume method,[34-36] can also be used to formulate the material balance across the whole cell. The equations at the two external boundary nodes ($j=0$ and $j=nj$) are simply derived from material balances around the points $j=½$ and $j=nj-½$ using the boundary conditions at $j=0$ and $j=nj$. An advantage of this technique is that the total amount of salt contained in the cell will be rigorously equal to a constant. It has not been proven that this method will be accurate to O ($h^2$), but it does appear to be.[36] The computer programs DUAL and FOIL given in Appendix 2-C, and also the computer program CHECK given in Appendix 4-A, have been programmed using the control-volume method.

## 2.10 Computer programs

Two primary computer programs have been written for full-cell simulation of lithium systems. The lithium foil model (figure 2-1a) is solved in FOIL; the dual lithium-ion insertion model (figure 2-1b) is solved by DUAL. The data files for these programs are given in Appendix 2-B; both of these computer programs are written in FORTRAN and are given in Appendix 2-C. We shall only briefly discuss the capabilities of the computer programs here; the code is

well documented already and is also easy to use because of its extensive use and upgrading by industrial and academic collaborators.

There are several choices of modes in which one can discharge or charge the cell using the models. In the galvanostatic mode, one may choose to discharge for a set amount of time or until the cell reaches a prescribed cutoff potential. One also has the option to discharge in the potentiostatic mode for a set amount of time. In addition, one may perform any number (up to 50 with the dimensions given) of these options successively in a single run, including, if desired, relaxation periods of arbitrary lengths in between. This feature allows one to simulate potentiostatic taper charging[37] and signature curve discharges,[38] for example. The flexibility of the code allows the user to simulate a large variety of experimental conditions to which batteries are exposed, a point that will be explored in some detail in the next chapter.

The standard output that both codes provide includes values of the following quantities at each time step: utilization of positive electrode material, cell potential (V), material balance check, and time (min). The utilization is given in terms of the stoichiometric coefficient of lithium in the insertion electrode, which can be calculated from the average state of charge,

$$y = \frac{<c_s>}{c_t}.$$

The material balance calculates the amount of salt in the solution phase divided by the initial amount of salt and should always be equal to unity. At the end of the discharge, one is also given the values of the average specific energy and power and the mass per unit area of the cell. This set of information is referred to as the "short" output option from the input file.

The "long" output option includes all of the above information, as well as detailed profiles of all of the variables across the cell at specified time steps. One is able to choose the

frequency of nodes and time steps at which all of the profiles are given. Thus, for example, one could request the values of each variable at every other node point and every fifth time step.

In addition to these standard output choices, there are a handful of more specialized output modes that arise for specific applications. For instance, with nonisothermal modeling, one can obtain information on either the adiabatic cell temperature as a function of time or the cell temperature during a nonisothermal discharge using a given heat-transfer coefficient with the exterior. Also, one has the option of calling either one of two specialized subroutines: SOL and PEAK. The subroutine SOL provides concentration profiles of lithium in the solid electrode particles at specified positions in either electrode and at specified times into the discharge.

Subroutine PEAK, on the other hand, interrupts the discharge at a given point and ramps the current until a maximum in the specific power is reached. The ramp involves passing increasing values of the current for a thirty-second period, each from the same initial condition. The peak power obtained thus represents the average value over a thirty-second current pulse. The output from this subroutine includes the values of the cell potential, current density, and power density during the current ramp. The power density should go through a maximum if the current is ramped out to a sufficiently large value. Occasionally numerical problems can prevent the power from going through this maximum. This occurs because the power output from a battery as a function of discharge rate drops off very quickly after going through its maximum value.[39]

A substantial number of parameters is required to simulate the full-cell sandwich. The complete list of the necessary parameters, as well as a brief description of how each can be obtained experimentally, is available.[40] These parameters can be classified according to whether they are design-adjustable parameters or material properties. The material properties

can be further broken down into thermodynamic and transport properties. In general, the design-adjustable parameters, such as for example electrode thicknesses and porosities, are entered in the input file. Many of the material properties, on the other hand, are installed into the main body of the codes FOIL or DUAL. These properties are entered into one of two subroutines, subroutine EKIN and subroutine PROP. These two subroutines represent the only sections of the code that the user needs to access.

Subroutine EKIN generates the Butler-Volmer kinetics expression for each insertion electrode (for DUAL) or for the single insertion electrode (for FOIL). The user may enter into EKIN the open-circuit potential for each insertion electrode being used. Currently, the user is able to select one of the many options for materials of interest whose open-circuit potentials have been previously fit to functional forms and used in past simulations. These materials and the open-circuit potential functions are given in Appendix 2-A.

The transport properties for the binary electrolyte are entered into subroutine PROP. This includes the concentration-dependent values of $\kappa$, $t_+^0$, and $D$. Also, the thermodynamic factor for the salt is entered into this subroutine. This parameter is input in the form:

$$\frac{\mathrm{d}\ln f_A}{\mathrm{d}c}, \quad \frac{\mathrm{d}^2\ln f_A}{\mathrm{d}c^2}.$$

As stated earlier, not only is a functional fit to the concentration dependence of each of these properties required, but also the first derivative with respect to concentration is needed (and the second derivative of the thermodynamic factor in the form shown above). If desired, of course, constant values of each of these properties can be used. This will be the case in some of the simulation results to follow, where the concentration dependence of many of the properties is not available.

## Appendix 2-A Open-circuit potential functional fits

The open-circuit potential data given below generally correspond to the potential of the insertion material *versus* a lithium reference electrode in solution during a very-low-rate discharge at 25°C, often referred to as a coulometric titration curve. Each of the curve fits given below is provided in figures 2-3 to 2-11.

1. Disordered carbon (Conoco petroleum coke):[41] $Li_xC_6$ ($0<x<0.7$)

$$U = -0.132056 + 1.40854 \exp(-3.52312x). \tag{A-1}$$

2. Tungsten oxide:[42] $Li_xWO_3$ ($0<x<0.67$)

$$U = 2.8767 - 0.9046x + 0.76679x^2 - 0.15975 \exp\left[100.0(x - 0.671)\right]. \tag{A-2}$$

3. Titanium disulfide:[17] $Li_yTiS_2$ ($0<y<1$)

$$U = 2.17 + \frac{RT}{F}\left[\left[\log\frac{1-y}{y}\right] - 16.2y + 8.1\right]. \tag{A-3}$$

4. Cobalt dioxide:[43] $Li_yCoO_2$ ($0.3<y<0.9$)

$$U = 4.82551 - 0.950237 \exp\left[-\left[\frac{y - 0.913511}{0.600492}\right]^{2.0}\right]. \tag{A-4}$$

5. Sodium cobalt dioxide (P2 phase):[44] $Na_yCoO_2$ ($0.3<y<0.92$)

$$\begin{aligned} U = {} & 4.4108 - 2.086y + 0.10465 \tanh\left[-133.42y + 89.825\right] \\ & + 0.16284 \tanh\left[-145.01y + 71.92\right] + 0.01 \exp\left[-200.0(y - 0.30)\right] \\ & - 0.01 \exp\left[200(y - 0.885)\right]. \end{aligned} \tag{A-5}$$

6. Manganese dioxide (lower plateau):[45] $Li_{1+y}MnO_2$ ($0<y<0.8$)

$$U = 2.06307 - 0.869705 \tanh\left[8.65375(y - 0.981258)\right] . \quad \text{(A-6)}$$

7. Lithium-manganese-oxide spinel:[46] $Li_yMn_2O_4$ ($0.19<y<1$)

$$\begin{aligned} U = {} & 4.06279 + 0.0677504 \tanh[-21.8502y + 12.8268] \\ & -0.105734\left[(1.00167-y)^{-0.379571} - 1.575994\right] \\ & - 0.045 \exp(-71.69y^8) + 0.01\exp[-200(y-0.19)] . \end{aligned} \quad \text{(A-7)}$$

8. Nickel dioxide:[47] $Li_yNiO_2$ ($0.45<y<1$)

$$\begin{aligned} U = {} & 6.515 + 2.3192y - 5.3342y^{1/2} + 0.41082 \exp[200(0.44-y)] \\ & - 0.24247 \exp[60.0(y-0.99)] . \end{aligned} \quad \text{(A-8)}$$

9. Vanadium oxide:[48] $Li_yV_2O_5$ ($0<y<0.96$)

$$\begin{aligned} U = {} & 3.3059 + 0.092769 \tanh\left[-14.362y + 6.6874\right] - \\ & 0.034252 \exp[100(y-0.96)] + 0.00724 \exp[80.0(0.01-y)] . \end{aligned} \quad \text{(A-9)}$$

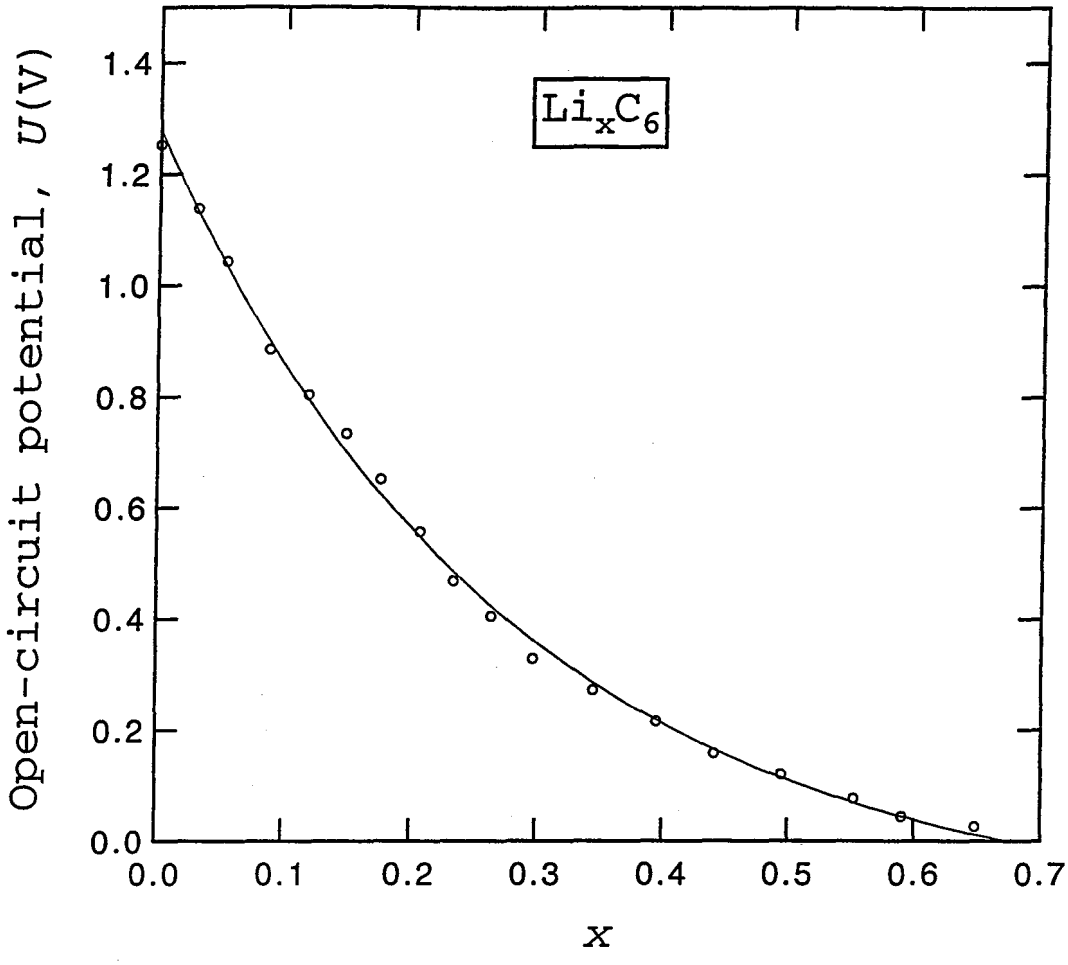


Figure 2-3. The open-circuit potential of carbon (petroleum coke) as a function of state of charge relative to the potential of solid lithium at the same electrolyte concentration.

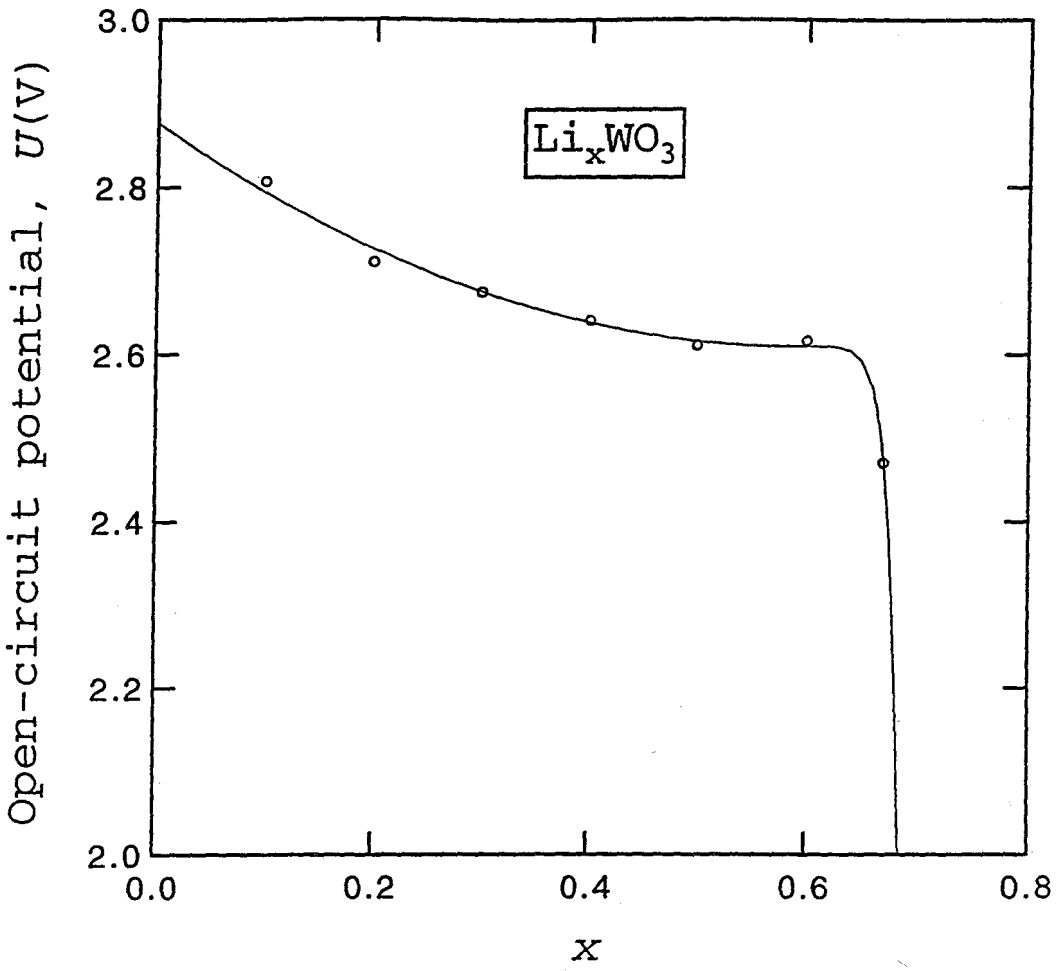


Figure 2-4. The open-circuit potential of tungsten trioxide ($Li_xWO_3$) as a function of state of charge relative to the potential of solid lithium at the same electrolyte concentration.

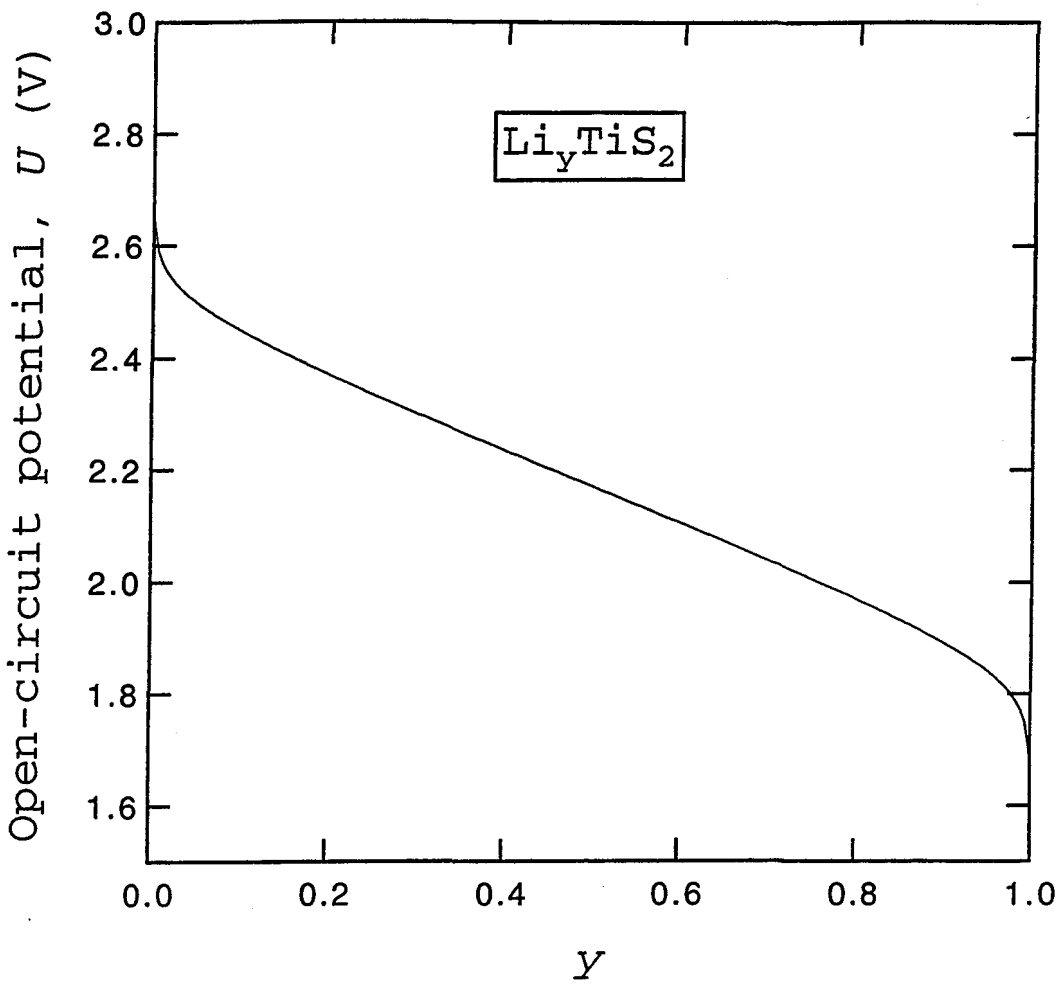


Figure 2-5. The open-circuit potential of titanium disulfide ($Li_yTiS_2$) as a function of state of charge relative to the potential of solid lithium at the same electrolyte composition.

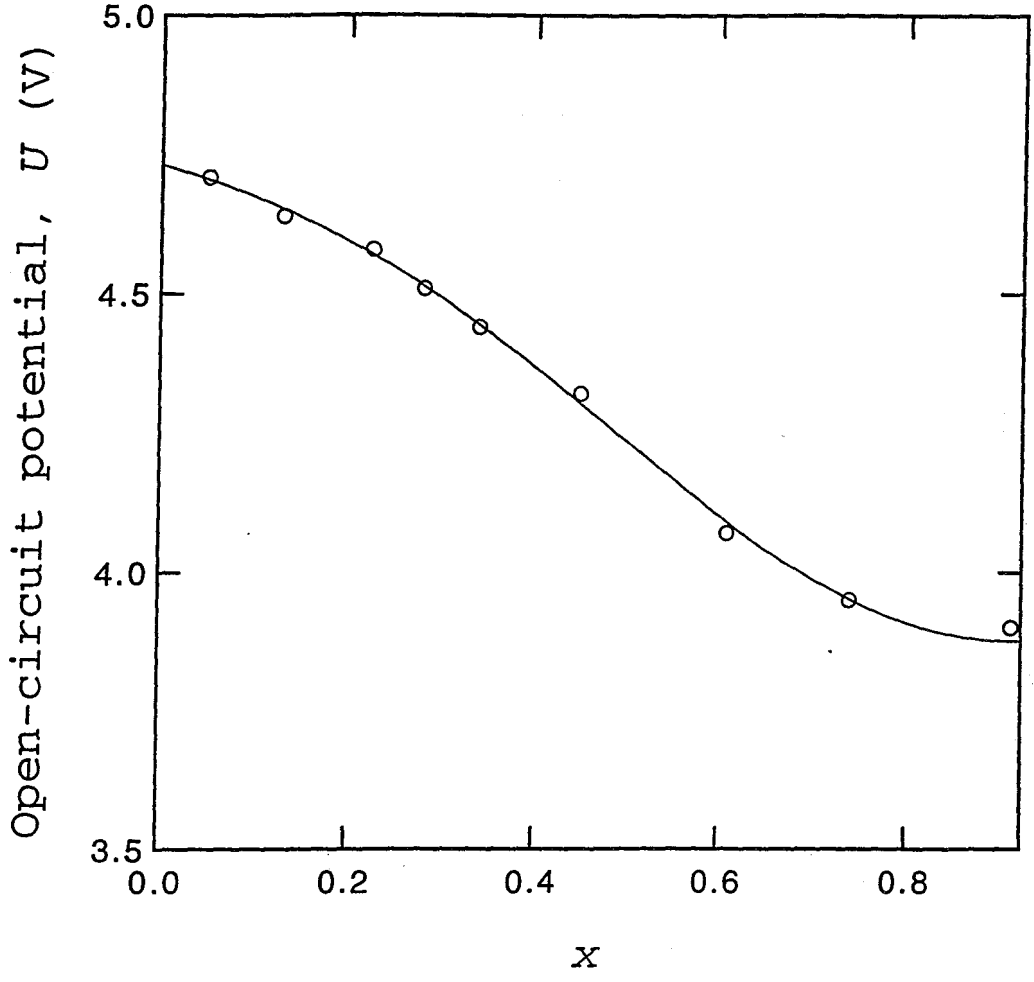


Figure 2-6. The open-circuit potential of cobalt dioxide ($Li_yCoO_2$) as a function of state of charge relative to the potential of solid lithium at the same electrolyte concentration.

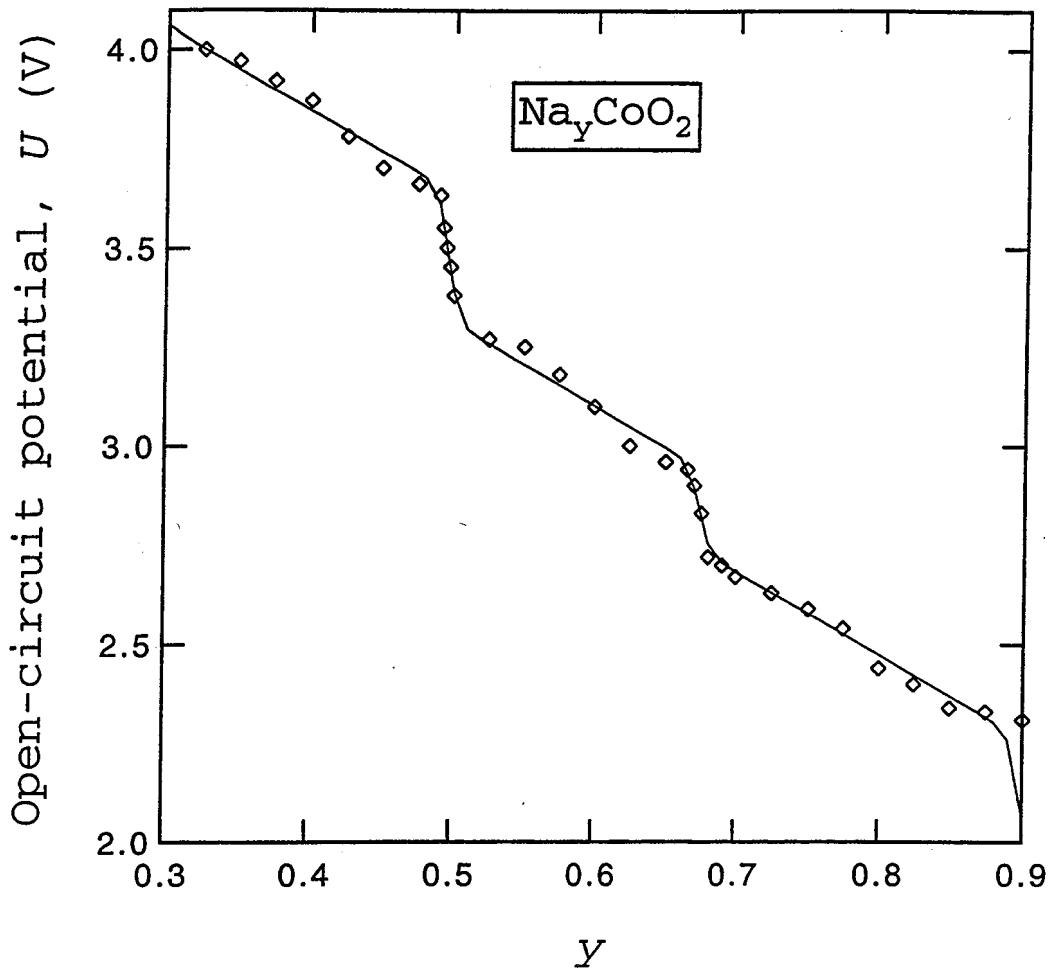


Figure 2-7. The open-circuit potential of sodium cobalt oxide ($Na_yCoO_2$, P2 phase) as a function of the state of charge relative to the potential of solid sodium at the same electrolyte concentration.

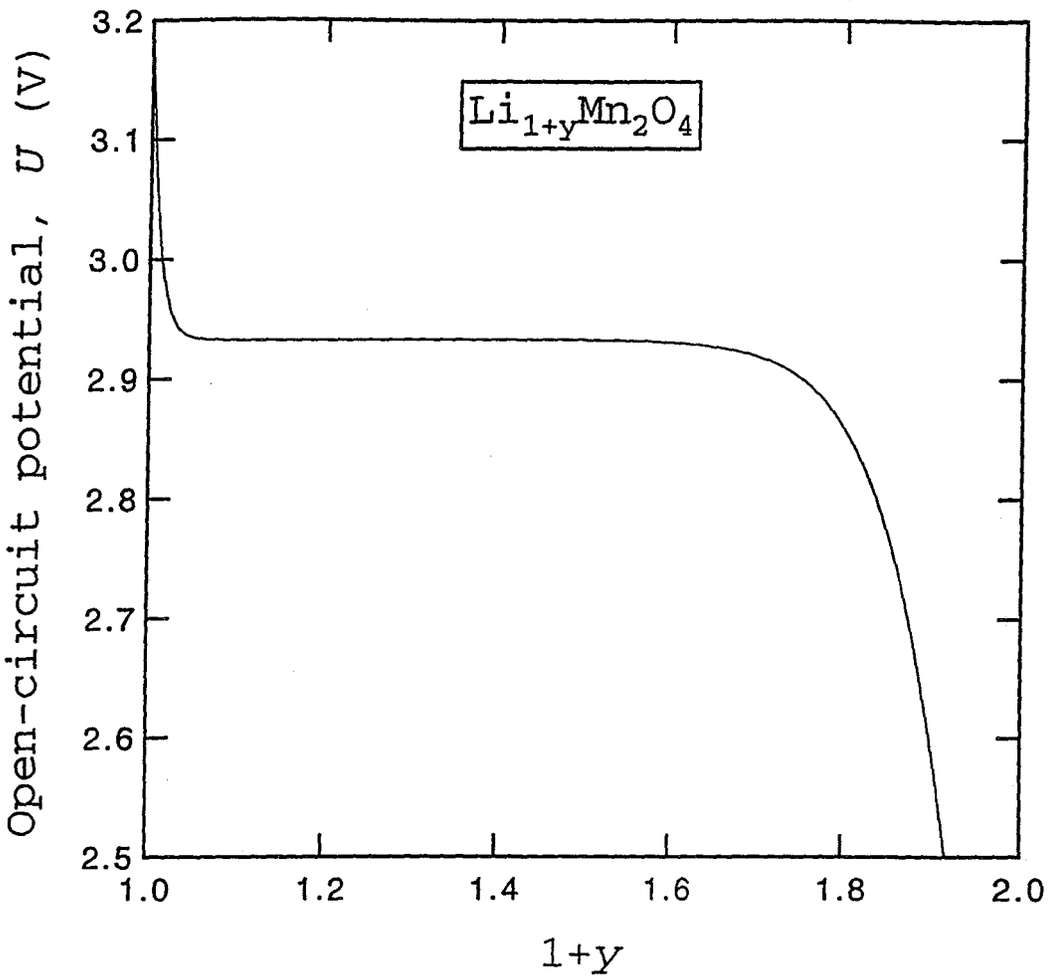


Figure 2-8. The open-circuit potential of manganese dioxide ($Li_{1+y}Mn_2O_4$) as a function of state of charge relative to the potential of solid lithium at the same electrolyte concentration.

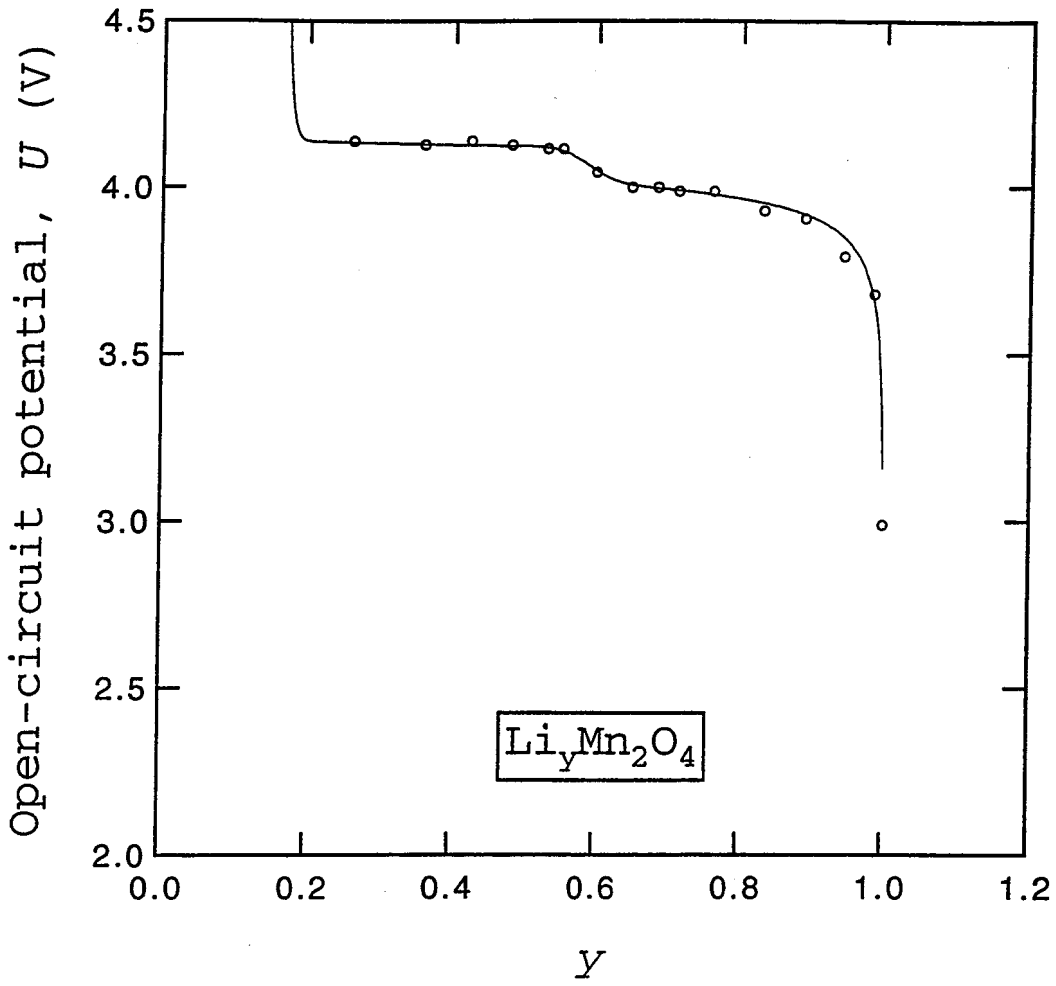


Figure 2-9. The open-circuit potential of manganese dioxide ($Li_yMn_2O_4$, spinel phase) as a function of state of charge relative to the potential of solid lithium at the same electrolyte concentration.

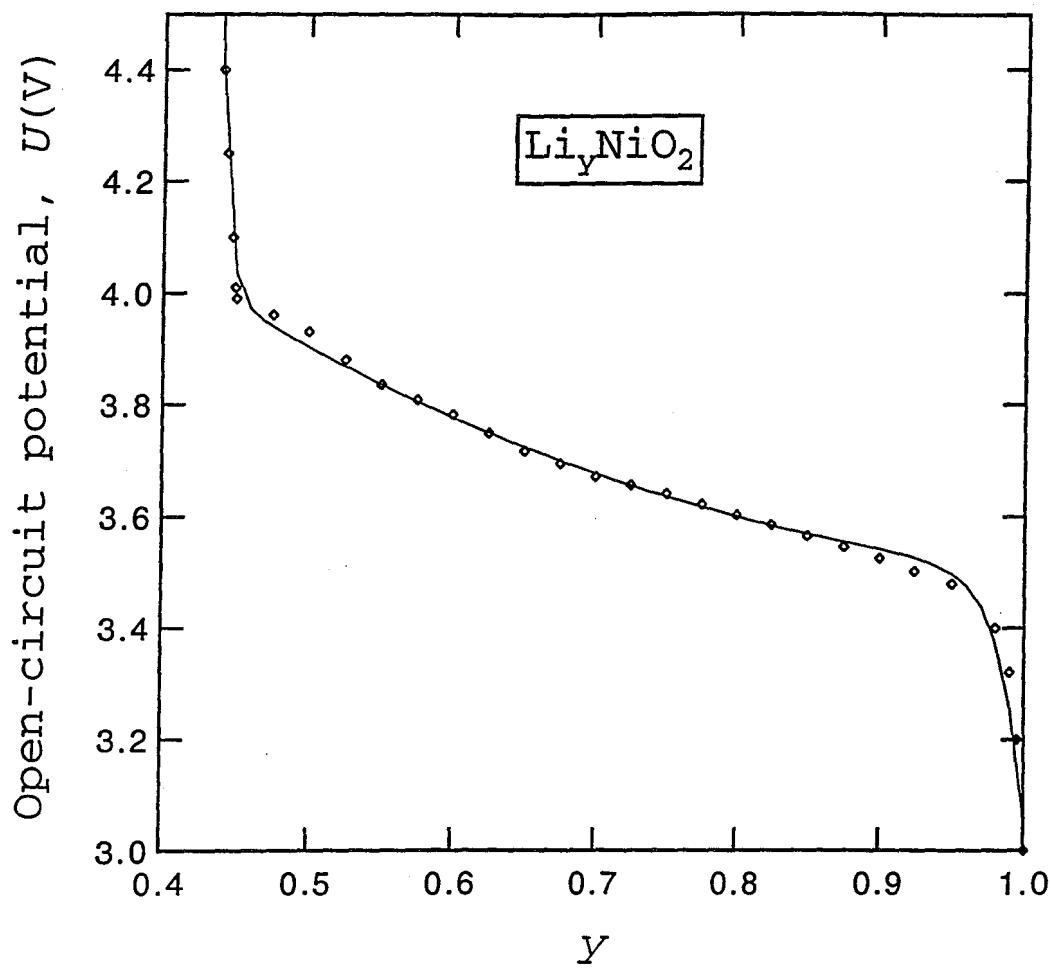


Figure 2-10. The open-circuit potential of nickel dioxide ($Li_yNiO_2$) as a function of state of charge relative to the potential of solid lithium at the same electrolyte concentration.

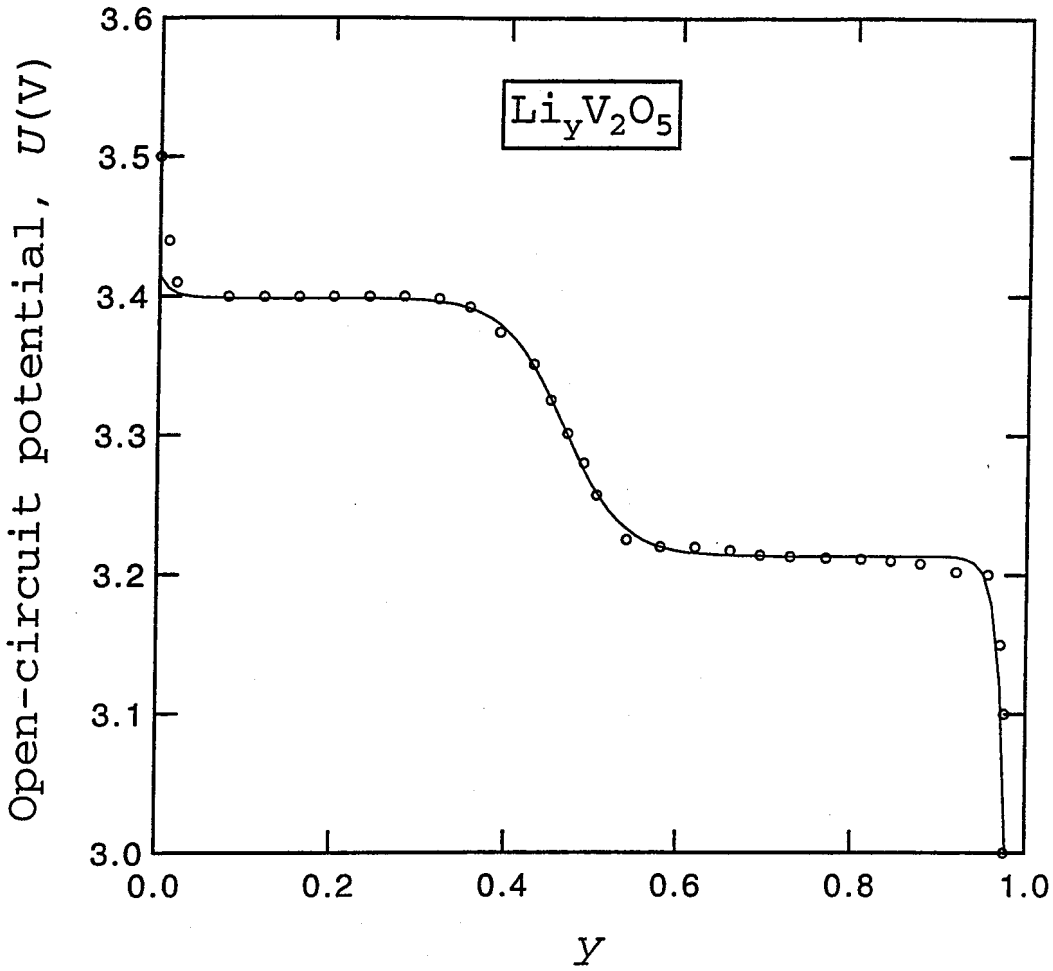


Figure 2-11. The open-circuit potential of vanadium oxide bronze ($Li_yV_2O_5$) as a function of state of charge relative to the potential of solid lithium at the same electrolyte concentration.

## Appendix 2-B Data files for DUAL and FOIL

DUAL data file

```
20          ! lim, limit on number of iterations
240.d-06    ! h1, thickness of negative electrode (m)
25.d-06     ! h2, thickness of separator (m)
190.d-06    ! h3, thickness of positive electrode (m)
0.0         ! hcn, thickness of negative electrode current collector (m)
0.0         ! hcp, thickness of positive electrode current collector (m)
80          ! n1, number of nodes in negative electrode
40          ! n2, number of nodes in separator
80          ! n3, number of nodes in positive electrode
298.15      ! T, temperature (K)
1000.       ! xi(1,1), initial concentration (mol/m3)
0.6440      ! csx, initial stoichiometric parameter for carbon
0.0366      ! csy, initial stoichiometric parameter for positive
120.0       ! tmmax, maximum time step size (s)
.00         ! vcut, cutoff potential
5.0d-13     ! dfs1, diffusion coefficient in negative solid (m2/s)
5.0d-13     ! dfs3, diffusion coefficient in positive solid (m2/s)
1.0d-06     ! Rad1, radius of negative particles (m)
1.0d-06     ! Rad3, radius of positive particles (m)
0.36        ! ep1, volume fraction of electrolyte in negative electrode
0.00        ! epp1, volume fraction of polymer phase in negative electrode
0.117       ! epf1, volume fraction of inert filler in negative electrode
0.38        ! ep2, volume fraction of electrolyte in separator
0.00        ! epp2, volume fraction of polymer phase in separator
0.26        ! ep3, volume fraction of electrolyte in positive electrode
0.00        ! epp3, volume fraction of polymer phase in positive electrode
0.04        ! epf3, volume fraction of inert filler in positive electrode
10.         ! sig1, conductivity of negative matrix (S/m)
10.         ! sig3, conductivity of positive matrix (S/m)
1.0d-11     ! rka1, reaction rate constant for negative reaction
1.0d-11     ! rka3, reaction rate constant for positive reaction
0.0         ! ranode, anode film resistance (ohm-m2)
0.0         ! rcathde, cathode film resistance (ohm-m2)
324.2d0     ! cot1, coulombic capacity of negative material (mAh/g)
332.8d0     ! cot3, coulombic capacity of positive material (mAh/g)
1204.       ! re, density of electrolyte (kg/m3)
```

```
2000.                   ! rs1, density of negative insertion material (kg/m3)
4400.                   ! rs3, density of positive insertion material (kg/m3)
2000.                   ! rf,  density of inert filler (kg/m3)
2200.                   ! rpl, density of polymer phase (kg/m3)
2200.                   ! rc,  density of separator material (kg/m3)
0.0                     ! rcn, density of negative current collector (kg/m3)
0.0                     ! rcp, density of positive current collector (kg/m3)
6.0                     ! htc, heat transfer coefficient at ends of cell stack (W/m2K)
0.0                     ! dUdT, temperature coefficient of open circuit potential (V/K)
2000.0                  ! Cp,   heat capacity of system (J/kg-K)
298.0                   ! Tam,  ambient air temperature (K)
1                       ! ncell, number of cells in a cell stack
2                       ! lht,  0 uses htc, 1 calculates htc, 2 isothermal
0                       ! il1,  1 for long print-out 0 for short print-out
2                       ! il2,  prints every il2 th node in long print-out
1                       ! il3,  prints every il3 th time step in long print-out
1                       ! lflag, 0 for electrolyte in separator only, 1 for uniform
0                       ! lpow   0 for no power peaks, 1 for power peaks
0                       ! jsol   calculate solid profiles if 1 < jsol < nj
2                       ! nneg   see below
4                       ! nprop  see below
6                       ! npos   see below
2                       ! lcurs, number of current changes
10.00d0     5.0d0       1
-10.00d0    5.0d0       1
0.00d00     30.0d0      1
0.0001d0    15.0d0      1
5.00d0      2.0d0       2
0.0001d0    15.0d0      1
17.50d0     2.5d0       2
0.0001d0    15.0d0      1
8.75d0      2.5d0       2
0.0001d0    15.0d0      1
4.40d0      2.5d0       2
0.0001d0    15.0d0      1
2.20d0      2.5d0       2
0.0001d0    15.0d0      1
1.25d0      2.5d0       2
```

DUAL data file comments

line 34,35: cot1,cot3

cot1 coulombic capacity of negative electrode (mAh/g)
when x=1 in LixC6

cot3 coulombic capacity of positive electrode (mAh/g)
when y=1 in LiyCoO2 (332.8), Li1+yMn2O4(144.50)

lines 50 to 52: il1,il2,il3
il1 0 gives short print-out no matter if a run converges or not
1 gives long print-out no matter if a run converges or not
The long print-out stops at t(noncovergence).
2 gives short print-out if a run converges but a long
print-out if the run does not converge.
il2 1/il2 = fraction of nodes in long print-out
il3 1/il3 = fraction of time steps in long print-out

line 59: lcurs, number of current changes

line 60 onward: cu(i), tt(i), mc(i)
cu(i) The ith value of the current (A/m2) or potential (V) of
the discharge
tt(i) The ith value of the time (min) or cutoff potential (V)
of the discharge
mc(i) The mode of discharge; 0 for potentiostatic, 1 for galvanostatic
for a given time, 2 for galvanostatic to a cutoff potential

nneg:
1 ! Li foil (not active)
2 ! Carbon (petroleum coke)
3 ! MCMB 2510 carbon (Bellcore)
4 ! TiS2
5 ! Tungsten oxide (LixWO3 with 0<x<0.67)
6 ! Lonza KS-6 graphite (Bellcore)

nprop:
1 ! AsF6 in methyl acetate
2 ! Perchlorate in PEO
3 ! Sodium Triflate in PEO
4 ! LiPF6 in PC (Sony cell simulation)
5 ! Perchlorate in PC (West simulation)
6 ! Triflate in PEO
7 ! LiPF6 in EC/DMC and p(VdF-HFP) (Bellcore)

npos:
1 ! TiS2
2 ! Spinel Mn2O4 (lower plateau)
3 ! NaCoO2: Sodium cobalt oxide
4 ! Spinel Mn2O4 (upper plateau)
5 ! Tungsten oxide (LixWO3 with 0<x<0.67)
6 ! CoO2 (Cobalt dioxide)
7 ! V2O5 (Vanadium oxide)
8 ! NiO2 (Nickel dioxide)
9 ! Spinel Mn2O4 (Bellcore)

FOIL data file

```
40          ! lim  limit on number of iterations
50.d-6      ! h1   thickness of separator (m)
200.d-6     ! h2   thickness of positive electrode (m)
25.d-6      ! hcn  thickness of negative electrode current collector (m)
25.d-6      ! hcp  thickness of positive electrode current collector (m)
80          ! n1   number of nodes in separator
80          ! n2   number of nodes in positive electrode
398.15      ! T    temperature (K)
1200.       ! xi(1,1) initial concentration (mol/m3)
0.38        ! y    initial stoichiometric parameter for electrode
120.0       ! tmmax maximum time step size (s)
0.0         ! vcut  cutoff potential
1.0d-13     ! dfs  diffusion coefficient in solid (m2/s)
1.0d-05     ! Rad  radius of particles (m)
0.300       ! ep   volume fraction of electrolyte in composite electrode
0.100       ! epf  volume fraction of inert filler in composite electrode
0.000       ! epp  volume fraction of polymer phase in composite electrode
0.38        ! eps  volume fraction of electrolyte in separator
0.00        ! epps  volume fraction of polymer phase in separator
100.        ! sig  conductivity of solid matrix (S/m)
148.0       ! capt  coulombic capacity of insertion material (mAh/g)
8.5d03      ! cmax maximum concentration in electrolyte
1.0d-11     ! rka  reaction rate constant for insertion reaction
0.03750     ! rkf  exchange current density for lithium foil
1           ! il4  1 for polymer, 0 for liquid electrolyte
1.2041d3    ! re  density of electrolyte (kg/m3)
4.210d3     ! rs  density of insertion material (kg/m3)
2.0d3       ! rf  density of inert filler (kg/m3)
2.2d3       ! rp  density of polymer phase (kg/m3)
2.0d3       ! rc  density of separator material (kg/m3)
4.0         ! ef  excess capacity of lithium foil
8.93d3      ! rcn  density of negative current collector (kg/m3)
2.70d3      ! rcp  density of positive current collector (kg/m3)
0.0         ! ranode  anode film resistance (ohm-m2)
0.0         ! rcathde  cathode film resistance (ohm-m2)
2.0         ! htc  heat transfer coefficient with external medium (W/m2K)
0.0         ! dUdT  temperature coefficient of EMF (V/K)
2000.0      ! Cp   heat capacity of cell (J/kg-K)
333.1       ! Tam  ambient temperature (K)
1           ! ncell number of cells in a cell stack
```

```
2                   ! lht  0 uses htc, 1 calculates htc, 2 isothermal
0                   ! il1  1 for long print-out  0 for short print-out
2                   ! il2  prints every il2 th node in long print-out
5                   ! il3  prints every il3 th time step in long print-out
4                   ! nprop (see below)
6                   ! npos  (see below)
1                   ! lcurs number of current changes
1.00d01     1.0d0
-7.0d0      4.0d0
0.001d0     60
7.0d0       120
-0.001d0    60
7.0d0       180
0.001d0     60
-3.50d0     360
-0.001d0    60
```

FOIL data file comments

line 48 onward: cu(i)  tt(i)
cu(i) operating current density (A/m2)
tt(i)  time (min)

nprop:
1 ! LiAsF6 in methyl acetate
2 ! Li Perchlorate in PEO
3 ! Sodium triflate in PEO
4 ! LiPF6 in PC (Sony cell simulation)
5 ! Li Perchlorate in PC (West simulation)
6 ! Li Triflate in PEO

npos:
1 ! TiS2
2 ! Spinel Mn2O4 (lower plateau)
3 ! NaCoO2:  Sodium cobalt oxide
4 ! Spinel Mn2O4 (upper plateau)
5 ! Tungsten oxide (LixWO3 with 0<x<0.67)
6 ! CoO2 (Cobalt dioxide)
7 ! V2O5 (Vanadium oxide)
8 ! NiO2 (Nickel dioxide)

## Appendix 2-C Computer programs DUAL and FOIL

### DUAL program

```
**********************************************************************
c
c     dual.f  (version 2.0)  July 20, 1995
c     Dual lithium ion insertion cell
c
c  Note: For lflag=0, the model works only for initially zero current.
c
c**********************************************************************
      implicit real*8(a-h,o-z)
      parameter(maxt=900)
      common /n/ nx,nt,n1,n2,nj,n3,tmmax
      common /calc/ ai(maxt),ai2(maxt),u(223,maxt),ts(maxt),
     1h,h1,h2,h3,hcn,hcp,rr,rrmax
      common/const/ fc,r,t,frt,cur,ep3,ep2,pi,nneg,nprop,npos,
     1ep1,epf3,epf1,epp1,epp2,epp3,shape3,shape1
      common/power/ ed,Vold,ranode,rcathde
      common/ssblock/ xp0(6),xx0(6,221),term(221),fj(221)
      common/var/ xp(10),xx(6,221),xi(6,221),xt(6,221,maxt)
      common/cprop/ sig3,area,rka3,ct3,dfs3,Rad3,
     1sig1,area2,rka1,ct1,dfs1,Rad1,tw
      common/tprop/df(221),cd(221),tm(221),
     1ddf(221),dcd(221),dtm(221),dfu(221),d2fu(221)
      common/temp/ thk,htc,dudt,Cp,dens,tam,g0,ncell,lht
      dimension tt(50),cu(50),mc(50),tot(50)
   44 format(/'            mass  = ',f7.4,' kg/m2')
   45 format(' specific energy  = ',f8.2,' W-h/kg')
   46 format(' specific power   = ',f8.2,' W/kg')
c
c     n is number of equations
      n=6
      lim2=20
      data fc/96487.0d0/, r/8.314d0/, pi/3.141592653589d0/
c
c**********************************************************
c     read in parameters and boundary conditions
c
      read *, lim !limit on number of iterations
      read *, h1  !thickness of negative electrode (m)
      read *, h2  !thickness of separator (m)
      read *, h3  !thickness of positive electrode (m)
      read *, hcn !thickness of negative electrode current collector(m)
```

```
      read *, hcp !thickness of positive electrode current collector(m)
      thk=h1+h2+h3
      read *, n1  !number of nodes in negative electrode
      read *, n2  !number of nodes in separator
      read *, n3  !number of nodes in positive electrode
      read *, t   !temperature (K)
      print 1101, lim,1.d6*h1,1.d6*h2,1.d6*h3,1.d6*hcn,1.d6*hcp
     &,n1,n2,n3,t
c     n1=n1+1       ! from foil
c     nj = n1 + n2 ! from foil
      n2=n2+1
      nj=n1+n2+n3
c
      read *, xi(1,n1+2)!initial concentration (mol/m3)
c     guess for PHI2
      xi(2,1)=0.05d0
      xi(2,nj)=0.0d0
      read *,csx   !initial stochiometric parameter for negative
      read *,csy   !initial stochiometric parameter for positive
      read *, tmmax!maximum time step size (s)
      read *, vcut !cutoff potential
      read *, dfs1 !diffusion coefficient in negative solid (m2/s)
      read *, dfs3 !diffusion coefficient in positive solid (m2/s)
      read *, Rad1 !radius of negative particles (m)
      read *, Rad3 !radius of positive particles (m)
      print 1102, xi(1,n1+2),csx,csy,tmmax,vcut,dfs1,dfs3,1.d6*Rad1
     &,1.d6*Rad3
      read *, ep1 !volume fraction of electrolyte in neg. electrode
      read *, epp1!volume fraction of polymer phase in neg. electrode
      read *, epf1!volume fraction of inert filler in neg. electrode
      read *, ep2 !volume fraction of electrolyte in separator
      read *, epp2!volume fraction of polymer phase in separator
      read *, ep3 !volume fraction of electrolyte in pos. electrode
      read *, epp3!volume fraction of polymer phase in pos. electrode
      read *, epf3!volume fraction of inert filler in pos. electrode
      read *, sig1!conductivity of solid negative matrix (S/m)
      read *, sig3!conductivity of solid positive matrix (S/m)
c     read *, cmax!maximum concentration in electrolyte     (mol/m3)
      read *, rka1!reaction rate constant for negative reaction
      read *, rka3!reaction rate constant for positive reaction
      read *, ranode  !anode film resistance (out of place)
      read *, rcathde !cathode film resistance (out of place)
c     read *, il4 !1 for polymer, 0 for liquid electrolyte
      read *, cot1 !coulombic capacity of negative material (mAh/g)
      read *, cot3 !coulombic capacity of positive material (mAh/g)
      print 1103, ep1,epp1,epf1,ep2,epp2,ep3,epp3,epf3,sig1,sig3,cot1
```

```
     &,cot3,cmax,rka1,rka3,il4
      read *, re  ! density of electrolyte (kg/m3)
      read *, rs1 ! density of negative insertion material (kg/m3)
      read *, rs3 ! density of positive insertion material (kg/m3)
      read *, rf  ! density of inert filler (kg/m3)
      read *, rpl ! density of polymer phase (kg/m3)
      read *, rc  ! density of separator material (kg/m3)
      read *, rcn ! density of negative current collector (kg/m3)
      read *, rcp ! density of positive current collector (kg/m3)
      print 1104, re,rs1,rs3,rf,rpl,rc,rcn,rcp
      read *, htc  !heat transfer coeff. with external medium (W/m2K)
      read *, dUdT !temperature coefficient of EMF (V/K)
      read *, Cp   !heat capacity of cell (J/kgK)
      read *, Tam  !ambient temperature (K)
      read *, ncell!number of cells in a cell stack
      read *, lht  !0 uses htc, 1 calcs htc, 2 isothermal
      print 1105, ranode,rcathde,htc,dudt,Cp,tam,ncell,lht
      read *, il1   !1 for long print-out 0 for short print-out
      read *, il2   !1/il2 = fraction of nodes in long print-out
      read *, il3   !1/il3 = fraction of time steps in long print-out
      read *, lflag ! 0 for electrolyte in sep. only, 1 for uniform
      read *, lpow  ! 0 for no power peaks, 1 for power peaks
      read *, jsol  ! calculate solid profiles if 1<jsol<nj
      read *, nneg  ! designates negative electrode system
      read *, nprop ! designates electrolyte system
      read *, npos  ! designates positive electrode system
      read *, lcurs ! number of current changes
      print 1106, il1,il2,il3,lflag,lcurs
c
      read *,(cu(i),tt(i),mc(i),i=1,lcurs)
c     read *,(cu(i),tt(i), i=1,lcurs) ! from foil
c     cu(i)  operating current density (A/m2)
c     tt(i)       time (min)
c
 1101 format (i7,'  lim, limit on number of iterations'
     &/1x,f6.2,'  h1,  thickness of negative electrode (microns)'
     &/1x,f6.2,'  h2,  thickness of separator (microns)'
     &/1x,f6.2,'  h3,  thickness of positive electrode (microns)'
     &/1x,f6.2,'  hcn, ',
     &'thickness of negative electrode current collector (microns)'
     &/1x,f6.2,'  hcp, thickness of positive electrode current'
     &,' collector (microns)'
     &/i7,'  n1,  number of nodes in negative electrode'
     &/i7,'  n2,  number of nodes in separator'
     &/i7,'  n3,  number of nodes in positive electrode'
     &/1x,f6.2, '  T,   temperature (K)')
```

```
1102 format (/1x,f6.1,'  xi(1,n1+2), initial concentration (mol/m3)'
    &/1x,f6.4,'  csx,   initial stoichiometric parameter for negative'
    &/1x,f6.4,'  csy,   initial stoichiometric parameter for positive'
    &/1x,f6.1,'  tmmax, maximum time step size (s)'
    &/1x,f6.2,'  vcut,  cutoff potential'
    &/1x,e6.1,'  dfs1,  diffusion coefficient in negative solid (m2/s)'
    &/1x,e6.1,'  dfs3,  diffusion coefficient in positive solid (m2/s)'
    &/1x,f6.2,'  Rad1,  radius of negative particles (microns)'
    &/1x,f6.2,'  Rad3,  radius of positive particles (microns)')
1103 format (/1x,f6.3,'  ep1,'
    &,'   volume fraction of electrolyte in negative electrode'
    &/1x,f6.3,'  epp1,'
    &,'  volume fraction of polymer phase in negative electrode'
    &/1x,f6.3,'  epf1,'
    &,'  volume fraction of inert filler in negative electrode'
    &/1x,f6.3,'  ep2,   volume fraction of electrolyte in separator'
    &/1x,f6.3,'  epp2,  volume fraction of polymer phase in separator'
    &/1x,f6.3,'  ep3,'
    &,'   volume fraction of electrolyte in positive electrode'
    &/1x,f6.3,'  epp3,'
    &,'  volume fraction of polymer phase in positive electrode'
    &/1x,f6.3,'  epf3,'
    &,'  volume fraction of inert filler in positive electrode'
    &/1x,f7.2,'  sig1,  conductivity of negative matrix (S/m)'
    &/1x,f7.2,'  sig3,  conductivity of positive matrix (S/m)'
    &/1x,f6.2,'  cot1,  coulombic capacity of negative material'
    &,' (mAh/g)'
    &/1x,f6.2,'  cot3,  coulombic capacity of positive material'
    &,' (mAh/g)'
    &/1x,f6.0,'  cmax,  maximum concentration in electrolyte (mol/m3)'
    &/1x,e6.1,'  rka1,  reaction rate constant for negative reaction '
    &/1x,e6.1,'  rka3,  reaction rate constant for positive reaction '
    &/i7,'  il4,  1 for polymer, 0 for liquid electrolyte')
1104 format (/1x,f6.1,'  re,   density of electrolyte (kg/m3)'
    &/1x,f6.1,'  rs1,  density of negative insertion material (kg/m3)'
    &/1x,f6.1,'  rs3,  density of positive insertion material (kg/m3)'
    &/1x,f6.1,'  rf,   density of inert filler (kg/m3)'
    &/1x,f6.1,'  rpl,  density of polymer phase (kg/m3)'
    &/1x,f6.1,'  rc,   density of separator material (kg/m3)'
    &/1x,f6.1,'  rcn,  density of negative current collector (kg/m3)'
    &/1x,f6.1,'  rcp,  density of positive current collector (kg/m3)')
1105 format (/1x,f6.1,'  ranode,   anode film resistance (ohm-m2)'
    &/1x,f6.1,'  rcathde,  cathode film resistance (ohm-m2)'
    &/1x,f6.2,'  htc,   heat transfer coefficient with'
    &,' external medium (W/m2K)'
    &/1x,f6.2,'  dUdT,  temperature coefficient of EMF (V/K)'
```

```
     &/1x,f6.1,'  Cp,     heat capacity of cell (J/kg-K)'
     &/1x,f6.2,'  Tam,    ambient temperature (K)'
     &/i7,'  ncell, number of cells in a cell stack'
     &/i7,'  lht,    0 uses htc,  1 calcs htc,  2 isothermal')
1106 format (/i7,'  il1, 1 for long print-out  0 for short print-out'
     &/i7,'  il2,    prints every il2 th node in long print-out'
     &/i7,'  il3,    prints every il3 th time step in long print-out'
     &/i7,'  lflag, 0 for electrolyte in separator only, 1 for uniform'
     &/i7,'  lcurs, number of current changes')
      go to (111,112,113,114,115,116),nneg
      print*,' '
 111  print *,  'Li foil'
      go to 117
 112  print *,  'Carbon (petroleum coke)'
      go to 117
 113  print *,  'MCMB 2510 Carbon (Bellcore)'
      go to 117
 114  print *,  'TiS2'
      go to 117
 115  print *,  'Tungsten oxide (LixWO3 with 0<x<0.67)'
      go to 117
 116  print *,  'Lonza KS-6 graphite (Bellcore)'
 117  go to (101,102,103,104,105,106,107),nprop
 101  print *, 'AsF6 in methyl acetate'
      go to 200
 102  print *, 'Perchlorate in PEO'
      go to 200
 103  print *, 'Sodium Triflate in PEO'
      go to 200
 104  print *, 'LiPF6 in PC (Sony cell simulation)'
      go to 200
 105  print *, 'Perchlorate in PC (West simulation)'
      go to 200
 106  print *, 'Triflate in PEO'
      go to 200
 107  print *, 'LiPF6 in EC/DMC and p(VdF-HFP)'
      go to 200
 200  go to (201,202,203,204,205,206,207,208,209),npos
 201  print *, 'TiS2'
      go to 300
 202  print *, 'Spinel Mn2O4 (lower plateau)'
      go to 300
 203  print *, 'NaCoO2:  Sodium Cobalt Oxide'
      go to 300
 204  print *, 'Spinel Mn2O4 (upper plateau)'
      go to 300
```

```
  205 print *, 'Tungsten oxide (LixWO3 with 0<x<0.67)'
      go to 300
  206 print *, 'CoO2 (Cobalt dioxide)'
      go to 300
  207 print *, 'V2O5 (Vanadium oxide)'
      go to 300
  208 print *, 'NiO2 (Nickel dioxide)'
      go to 300
  209 print *, 'Spinel Mn2O4 (Bellcore)'
      go to 300
  300 continue
c
c     Convert coulombic capacity to total concentrations:
      ct1=3.6d03*cot1*rs1/fc
      ct3=3.6d03*cot3*rs3/fc
      xi(3,1)=ct1*csx
      xi(3,n1+1)=xi(3,1)
      xi(3,n2+n1)=ct3*csy
      xi(3,nj)=xi(3,n2+n1)
c
      shape1=3.0d0
      shape3=3.0d0
c     assume current density linear in electrodes
      cur=cu(1)
      xi(4,1)=0.0d0
      xi(4,n1+1)=cur
      xi(4,n2+n1)=cur
      xi(4,nj)=0.0d0
c
c     Convert times to seconds and sum up times of mode changes
      if (mc(1).lt.2) then
      tot(1)=6.0d01*tt(1)
      else
      tot(1)=0.0d0
      end if
      do 51 i=2,lcurs
      if (mc(i).lt.2) then
      tot(i)=tot(i-1)+6.0d01*tt(i)
      else
      tot(i)=tot(i-1)
      end if
   51 continue
c
c     specific area calculated from geometry
      area=shape3*(1.0d0-ep3-epf3-epp3)/Rad3
      area2=shape1*(1.0d0-ep1-epf1-epp1)/Rad1
```

```
c
c     assume uniform rate of insertion in electrodes
      xi(5,1)=cur/fc/h1/area2
      xi(5,n1+1)=cur/fc/h1/area2
      xi(5,n2+n1)=-cur/fc/h3/area
      xi(5,nj)=-cur/fc/h3/area
c
      sig3=sig3*((1.0d0-ep3-epp3)**(1.5d0))
      sig1=sig1*((1.0d0-ep1-epp1)**(1.5d0))
c
      h2=h2/(n2-1)
      h3=h3/n3
      h1=h1/n1
      h=h2
      frt=fc/(r*t)
c
c     Find initial solid phase potential guesses
c     from initial solid concentrations:
      call ekin(1,kk,1,csx)
      xi(6,1)=g0
      xi(6,n1+1)=xi(6,1)
      call ekin(nj,kk,1,csy)
      xi(6,nj)=g0
      xi(6,n2+n1)=xi(6,nj)
c
c     fj is flag to cut off parts of the electrode when c=0
c     Not currently active (10/1/94-CMD)
c     do 52 j=1,nj
c  52 fj(j)=0
c
      print*,' '
      print*,'     DUAL INSERTION CELL VERSION 2.0'
      print*,' '
      if (lht.eq.2) then
      print*,'  util    cell pot    material     time         cur'
      print*,'    y       (V)       balance      (min)      A/m2'
      else if (lht.eq.0) then
      print*,' util  ','   cell pot  ',' temp  ','     time  ',
     1'    U ocp     cur'
      print*,'   y   ','     (V)     ','  (C)  ','     (min)  ',
     1'    (V)  '
      else if (lht.eq.1) then
      print*,' util  ','   cell pot ','  htcoeff ','   time  ',
     1'    U ocp     cur'
      print*,'   y   ','     (V)    ','  (W/m2K) ','   (min) ',
     1'     (V)  '
```

```
      end if
      print*,' '
c
c*****************************************************************
c
c     initialize time counting variables
      k=1
      time=0.0d0
      time2=0.0d0
      rr=0.0d0
      ts(1)=0.0d0
c
c     Must activate lpow=1 in data file if you want peak powers:
      kkflag=0
      nflag=0
      call guess(1flag)
c     calculate mass (kg/m2) of the cell
      call mass(re,rs3,rs1,rf,rpl,rc,rcn,rcp)
      dens=tw/thk
c
      call comp(n,lim,k,rr,0,nflag,0,jcount)
      call cellpot(k,vv,1,0,lflag)
c
c     rr is the size of a time step.
c     initial time step is 1 second
      rr=1.0d0
c
      iflag=0
      L=0
   53 L=L+1
c     do 53 l=1,lcurs
  123 k=k+1
      nt=k-1
c
c     adjust time step to match time of change in current
      time=ts(k-1)+rr
      if(time .ge. tot(l) .and. mc(l).lt.2) then
      rr=tot(l)-ts(k-1)
      time=tot(l)
      iflag=1
      end if
c
  129 ts(k)=ts(k-1)+rr
      call calca(k)
c
      if(mc(l) .gt. 0) then
```

```
c     mc is 1 or 2 so run galvanostatically
      dtnow=rr
      call comp(n,lim,k,rr,0,nflag,0,jcount)
      if(rr.lt.0.9999*dtnow) iflag=0
      if(mc(l).lt.2) call cellpot(k,vv,1,0,lflag)
      if(mc(l).eq.2) call cellpot(k,vv,0,0,lflag)
      frt=fc/r/t
c
      else
c     mc is 0 so run potentiostatically
c
      jc2=0
      f1=1.0d0
      cur1=cur
      cp1=vv
c
  609 jc2=jc2+1
      cur=cur1 + (cu(l)-cp1)/f1
      rr=10.d0
      ts(k)=ts(k-1)+rr
      call calca(k)
      call comp(n,lim,k,rr,0,nflag,0,jcount)
      call cellpot(k,vv,0,0,lflag)
      frt=fc/r/t
      if (dabs(vv-cu(l)) .gt. dabs(1.0d-05*cu(l))) then
      if (jc2 .gt. lim2) then
      print*, 'this run did not converge'
      stop
      else
      f1=(vv-cp1)/(cur-cur1)
      cp1=vv
      cur1=cur
      go to 609
      end if
c
      else
      call cellpot(k,vv,1,0,lflag)
      frt=fc/r/t
      end if
c
      end if
c
      IF(VV.LT.VCUT) GO TO 100
c     check to see if cutoff potential is exceeded if mc is 2
      if (mc(l).eq.2) then
      IF ((VV.LT.TT(L) .AND. CU(L).GT.0.0) .OR.
```

```
     &(VV.GT.TT(L) .AND. CU(L).LT.0.0)) THEN
      if (dabs(vv-tt(l)) .gt. 1.0d-04) then
c     print*,'not quite right yet ',vv,rr
      rr=rr/2.0d0
      iflag=1
      go to 129
      else
      time2=time2+rr
      call cellpot(k,vv,1,0,lflag)
      frt=fc/r/t
      iflag=1
      end if
      else
      iflag=0
      time2=time2+rr
      call cellpot(k,vv,1,0,lflag)
      frt=fc/r/t
      end if
      end if
c
c     Increasing time steps:
      rrmax=tmmax
      if(k.le.20) rrmax=10.0d0
      if(jcount.lt.5 .and. k.gt.2 .and. rr.lt.rrmax .and.
     1iflag.eq.0) then
      rr=rr*2.0d0
c     print*,'next time step increased to ', rr,' (s)'
      end if
c
      if(k.GE.maxt-1) then
        print*,'kmax=',k,' a larger matrix needed for xt'
        go to 100
      endif
      if (k.GE.501) then ! trim stored solid concentrations
c     should we have been printing long output as we go along?
      do 92 kk=3,401,2
      kput=(KK+1)/2
      ts(kput)=ts(kk)
      do 92 j=1,nj
      do 92 i=1,n
   92 xt(i,j,kput)=xt(i,j,kk)
      do 93 kk=402,K
      ts(kk-200)=ts(kk)
      do 93 j=1,nj
      do 93 i=1,n
   93 xt(i,j,kk-200)=xt(i,j,kk)
```

```
      k=k-200
      endif
c
      if (iflag .eq. 0) go to 123
      iflag=0
      if (mc(1).eq.2) then
      do 124 m=1,lcurs
  124 tot(m)=tot(m)+time2
      time2=0.0d0
      end if
      IF(L.EQ.LCURS .AND. LCURS.GE.10) THEN
      L=0
      tot(1)=TOT(LCURS)
      if (mc(1).lt.2) TOT(1)=TOT(1)+60.0D0*TT(1)
      do 403 i=2,lcurs
      if (mc(i).lt.2) then
      tot(i)=tot(i-1)+6.0d01*tt(i)
      else
      tot(i)=tot(i-1)
      end if
  403 continue
      ENDIF
      if(mc(l+1) .gt. 0) cur=cu(l+1)
c     calculate zero time solution for change in current
      if(mc(l+1) .gt. 0) then
      k=k+1
      ts(k)=ts(k-1)
      rr=0.0
      call comp(n,lim,k,rr,0,nflag,0,jcount)
      call cellpot(k,vv,1,0,lflag)
      endif
      rr=2.0d0
      IF(L.LT.LCURS) GO TO 53
c
c%%%%%%%%%%%%%%%%%%%%%%%%%%%%%%%%%%%%%%%%%%%%%%%%%%%%%%%%%%%%%%%%%%%%%%%
c     Additional features section:
c     Old method of calculating utilization:
c     call util
c
c     peak-power subroutine:
      if(lpow.eq.1) then
      il1=0
      call peak(n,lim,cu(1))
      endif
c
c     Solid-phase concentration profiles at given time and position
```

```
      if(jsol.gt.0 .and. jsol.lt.nj) call sol(85,jsol)
c
c     print detailed information if requested
  100 if(il1 .eq. 1) call nucamb(il2,il3)
c
c     calculate average energy and power:
      ed=ed/tw/3.6d03
      pow=3.6d03*ed/ts(nt+1)
      print44,tw
      print45,ed
      print46,pow
c
      end
c
c*********************************************************************
      subroutine comp(n,lim,kk,tau,kkflag,nflag,lpow,jcount)
      implicit real*8(a-h,o-z)
      parameter(maxt=900)
      common /n/ nx,nt,n1,n2,nj,n3,tmmax
      common /calc/ ai(maxt),ai2(maxt),u(223,maxt),ts(maxt),
     1h,h1,h2,h3,hcn,hcp,rr,rrmax
      common/const/ fc,r,t,frt,cur,ep3,ep2,pi,nneg,nprop,npos,
     1ep1,epf3,epf1,epp1,epp2,epp3,shape3,shape1
      common/power/ ed,Vold,ranode,rcathde
      common/ssblock/ xp0(6),xx0(6,221),term(221),fj(221)
      common/var/ xp(10),xx(6,221),xi(6,221),xt(6,221,maxt)
      common/cprop/ sig3,area,rka3,ct3,dfs3,Rad3,
     1sig1,area2,rka1,ct1,dfs2,Rad1,tw
      common/tprop/df(221),cd(221),tm(221),
     1ddf(221),dcd(221),dtm(221),dfu(221),d2fu(221)
      common/mat/ b,d
      common/bnd/ a,c,g,x,y
      dimension b(10,10),d(10,21),termn(221)
      dimension a(10,10),c(10,221),g(10),x(10,10),y(10,10)
   99 format (1h ,//5x,'this run just did not converge'//)
      nx=n
c
  666 kadd=0
      if(rr.eq.0 .and. lpow.eq.1) kadd=1
      do 1 j=1,nj
      do 1 i=1,n
      c(i,j)=xt(i,j,kk-1+kadd)
    1 xx(i,j)=xt(i,j,kk-1+kadd)
c     sets first guess to last time-step values
c
c     initialize variables to begin each iteration
```

```
c      (jcount is iteration #)
       jcount=0
       do 4 i=1,n
     4 xp(i)=0.0d0
c
     8 j=0
       jcount=jcount+1
c      calculate physical properties
       call prop(nj,n2,n1)
c
c      initialize x and y for iteration
       do 9 i=1,n
       do 9 k=1,n
       x(i,k)=0.0d0
     9 y(i,k)=0.0d0
c
c      store previous iteration of  (xp in xp0)  &  (xx in xx0)
       do 6 i=1,n
       xp0(i)=xp(i)
       xx0(i,n1-10)=xx(i,n1-10)
     6 xx0(i,n1+n2+10)=xx(i,n1+n2+10)
c
c      for a given iteration, set up governing equations and bc's
c      start at the left interface and move across polymer
c      initialize a,b,d,g arrays for each node
c
    10 j=j+1
c
       do 11 i=1,n
       g(i)=0.0d0
       xx(i,j)=c(i,j)
       do 11 k=1,n
       a(i,k)=0.0d0
       b(i,k)=0.0d0
    11 d(i,k)=0.0d0
c
       if(rr.le.0.0) then ! treat as a zero time step
       b(1,1)=1.0d0
       g(1)=xt(1,j,kk-1)-c(1,j) ! fix electrolyte concentration
       b(4,3)=1.0d0
       g(4)=xt(3,j,kk-1)-c(3,j) ! fix solid concentration
       go to 112
       endif
c      ------------------------------------------------------
c      Equation 1, mass balance.
c
```

```
 termn(j)=0.
 fac=1.
 if(j.eq.n1+2) fac=((ep2+epp2)/(ep1+epp1))**1.5
 if(j.eq.n1+n2+1) fac=((ep3+epp3)/(ep2+epp2))**1.5
 epn=ep1+epp1
 hn=h1
 if(j.gt.n1+1) then
 epn=ep2+epp2
 hn=h2
 endif
 if (j.gt.n1+n2) then
 epn=ep3+epp3
 hn=h3
 endif
 if(j.ne.1) then ! deal with box to left of point.
 termn(j)=-(df(j)+fac*df(j-1))*(c(1,j)-c(1,j-1))/hn/2.
&-(1.-0.5*(tm(j)+tm(j-1)))*(c(4,j)+c(4,j-1))/2./fc
 a(1,1)=epn*hn*0.125/rr
&-(df(j)+fac*df(j-1))/hn/4.+fac*ddf(j-1)*(c(1,j)-c(1,j-1))/hn/4.
&-dtm(j-1)*(c(4,j)+c(4,j-1))/8./fc
 b(1,1)=epn*hn*0.375/rr
&+(df(j)+fac*df(j-1))/hn/4.+ddf(j)*(c(1,j)-c(1,j-1))/hn/4.
&-dtm(j)*(c(4,j)+c(4,j-1))/8./fc
 a(1,4)=(1.-0.5*(tm(j)+tm(j-1)))/4./fc
 b(1,4)=(1.-0.5*(tm(j)+tm(j-1)))/4./fc
 g(1)=-epn*hn*(0.375*(c(1,j)-xt(1,j,kk-1))
&+0.125*(c(1,j-1)-xt(1,j-1,kk-1)))/rr
 endif
 fac=1.
 if(j.eq.n1+1) then
 fac=((ep2+epp2)/(ep1+epp1))**1.5
 epn=ep2+epp2
 hn=h2
 else if(j.eq.n1+n2) then
 fac=((ep3+epp3)/(ep2+epp2))**1.5
 epn=ep3+epp3
 hn=h3
 endif
 if(j.ne.nj) then ! deal with box to right of point.
 termn(j)=termn(j)-(fac*df(j)+df(j+1))*(c(1,j)-c(1,j+1))/hn/2.
&+(1.-0.5*(tm(j)+tm(j+1)))*(c(4,j)+c(4,j+1))/2./fc
 d(1,1)=epn*hn*0.125/rr
&-(fac*df(j)+df(j+1))/hn/4.+ddf(j+1)*(c(1,j)-c(1,j+1))/hn/4.
&+dtm(j+1)*(c(4,j)+c(4,j+1))/8./fc
 b(1,1)=b(1,1)+epn*hn*0.375/rr
&+(fac*df(j)+df(j+1))/hn/4.+fac*ddf(j)*(c(1,j)-c(1,j+1))/hn/4.
```

```
     &+dtm(j)*(c(4,j)+c(4,j+1))/8./fc
      d(1,4)=-(1.-0.5*(tm(j)+tm(j+1)))/4./fc
      b(1,4)=b(1,4)-(1.-0.5*(tm(j)+tm(j+1)))/4./fc
      g(1)=g(1)-epn*hn*(0.375*(c(1,j)-xt(1,j,kk-1))
     &+0.125*(c(1,j+1)-xt(1,j+1,kk-1)))/rr
      endif
      g(1)=g(1)+(termn(j)+term(j))/2.
c     ------------------------------------------------------
c     Equation 4, material balance in solid insertion material.
c
      sum=0.0d0
      if(j.le.n1+1) then
      if (kk .gt. 2) then
      do 54 i=1, kk-2
   54 if(ts(i+1)-ts(i).ne.0.0)
     &sum=sum + (xt(3,j,i+1) - xt(3,j,i))*ai2(kk-i)/(ts(i+1)-ts(i))
      end if
      b(4,3)=ai2(1)/rr
      b(4,5)=1.0d0/Rad1
      g(4)=ai2(1)*xt(3,j,kk-1)/rr - sum -ai2(1)/rr*c(3,j)-c(5,j)/Rad1
      else if(j.ge.n1+n2) then
      if (kk .gt. 2) then
      do 95 i=1, kk-2
   95 if(ts(i+1)-ts(i).ne.0.0)
     &sum=sum + (xt(3,j,i+1) - xt(3,j,i))*ai(kk-i)/(ts(i+1)-ts(i))
      end if
      b(4,3)=ai(1)/rr
      b(4,5)=1.0d0/Rad3
      g(4)=ai(1)*xt(3,j,kk-1)/rr - sum -c(3,j)*ai(1)/rr-c(5,j)/Rad3
      else
      b(4,3)=1.0d0
      g(4)=-c(3,j)
      endif
c     ------------------------------------------------------
c     Equation 2, Ohm's law.
c
  112 if(j.le.n1) then
      h=h1
      else if(j.lt.n1+n2) then
      h=h2
      else
      h=h3
      endif
      fac=1.0
      if(j.eq.n1+1 .and. nprop.ne.7)
     1fac=((ep2+epp2)/(ep1+epp1))**1.5
```

```
      if(j.eq.n1+n2 .and. nprop.ne.7)
     1fac=((ep3+epp3)/(ep2+epp2))**1.5
      if(j.eq.n1+1 .and. nprop.eq.7)
     1fac=((ep2+epp2)/(ep1+epp1))**4.2
      if(j.eq.n1+n2 .and. nprop.eq.7)
     1fac=((ep3+epp3)/(ep2+epp2))**4.2
c
      if(j.eq.nj .or. fj(j).ne.0.0) then
      b(2,2)=1.0d0
      g(2)=-c(2,j)
      go to 12
      endif
      dcf=(xx(1,j+1)-xx(1,j))/h
      r1=(xx(1,j+1)+xx(1,j))/2.0d0
      r4=(xx(4,j+1)+xx(4,j))/2.0d0
      p1=(tm(j)+tm(j+1))/2.0d0
      p2=(fac*cd(j)+cd(j+1))/2.0d0
      p4=(dfu(j)+dfu(j+1))/2.0d0
      d(2,1)=(1.0d0-p1)*(1.0d0/r1+p4)/h
      b(2,1)=-d(2,1)+((1.0d0-p1)*(d2fu(j)-1.0d0/r1/r1)*dcf
     1-(1.0d0/r1+p4)*dcf*dtm(j)+frt*r4*fac*dcd(j)/p2/p2)/2.0d0
      d(2,1)=d(2,1)+((1.0d0-p1)*(d2fu(j+1)-1.0d0/r1/r1)*dcf
     1-(1.0d0/r1+p4)*dcf*dtm(j+1)+frt*r4*dcd(j+1)/p2/p2)/2.0d0
      d(2,2)=-frt/h
      b(2,2)=frt/h
      b(2,4)=-frt/p2/2.0d0
      d(2,4)=-frt/p2/2.0d0
      g(2)=-(1.0d0-p1)*(1.0d0/r1+p4)*dcf+frt*(c(2,j+1)-c(2,j))/h
     &+frt/p2*(c(4,j)+c(4,j+1))/2.0d0
c     ------------------------------------------------------
c     Equation 3, Butler-Volmer kinetics
c
   12 if((j.gt.n1+1 .and. j.lt.n1+n2) .or. fj(j).ne.0.0) then
      b(3,5)=1.0d0
      g(3)=-c(5,j)
      else
      call ekin(j,kk,0,0)
      endif
c
c     ------------------------------------------------------
c
      if(j.ne.1) go to 13
c     ------------------------------------------------------
c
c     specify boundary conditions at left interface (j=1)
c     anode/current collector
```

```
c
      h=h1
c
      b(5,4)=1.0d0/h
      d(5,4)=-1.0d0/h
      b(5,5)=area2*fc/2.0d0
      d(5,5)=area2*fc/2.0d0
      g(5)=(c(4,j+1)-c(4,j))/h-area2*fc/2.0d0*(c(5,j+1)+c(5,j))
c
      b(6,4)=1.0d0
      g(6)=-c(4,j)
c
c     do 501 i=3,3
      call band(j)
      go to 10
c
c     ------------------------------------------------------
c     specify governing equations in composite anode [1<j<n1+1]
  13  if (j .ge. (n1+1)) go to 110
c
      b(5,4)=1.0d0/h
      d(5,4)=-1.0d0/h
      b(5,5)=area2*fc/2.0d0
      d(5,5)=area2*fc/2.0d0
      g(5)=(c(4,j+1)-c(4,j))/h-area2*fc/2.0d0*(c(5,j+1)+c(5,j))
c
      b(6,6)=1.0d0/h
      a(6,6)=-1.0d0/h
      b(6,4)=-0.5d0/sig1
      a(6,4)=-0.5d0/sig1
      g(6)=-cur/sig1+0.5/sig1*(c(4,j-1)+c(4,j))+(c(6,j-1)-c(6,j))/h
c
c     do 502 i=3,3
      call band(j)
      go to 10
c     ------------------------------------------------------
  110 if (j .ne. (n1+1)) go to 120
c
c     Now for the boundary between anode and separator(j=n1+1)
c
      b(5,4)=1.0d0
      g(5)=cur-c(4,j)
c
      b(6,6)=1.0d0/h1
      a(6,6)=-1.0d0/h1
      b(6,4)=-0.5d0/sig1
```

```
      a(6,4)=-0.5d0/sig1
      g(6)=-cur/sig1+0.5/sig1*(c(4,j-1)+c(4,j))+(c(6,j-1)-c(6,j))/h1
c
c     do 503 i=3,3
      call band(j)
      go to 10
c     ------------------------------------------------------
  120 if(j .ge. (n1+n2)) go to 130
c     specify governing equations [ n1 < j < n2+n1 ]
c     in separator
c
      h=h2
c
      b(5,4)=1.0d0
      g(5)=cur-c(4,j)
c
      b(6,6)=1.0d0
      g(6)=-c(6,j)
c
c     do 504 i=3,3
      call band(j)
      go to 10
c     ------------------------------------------------------
  130 if (j .ne. (n2+n1)) go to 140
c     Boundary between positive and separator(j=n2+n1):
c
      b(5,4)=1.0d0
      g(5)=cur-c(4,j)
c
      d(6,6)=1.0d0/h3
      b(6,6)=-1.0d0/h3
      d(6,4)=-0.5d0/sig3
      b(6,4)=-0.5d0/sig3
      g(6)=-cur/sig3+0.5/sig3*(c(4,j+1)+c(4,j))-(c(6,j+1)-c(6,j))/h3
c
c     do 505 i=3,3
      call band(j)
      go to 10
c     ------------------------------------------------------
  140 if (j .eq. nj) go to 16
c
c     specify governing equations [ n2+n1 < j < nj ]
c     composite cathode
c
      h=h3
c
```

```
      b(5,4)=-1.0d0/h
      a(5,4)=1.0d0/h
      b(5,5)=area*fc/2.0d0
      a(5,5)=area*fc/2.0d0
      g(5)=(c(4,j)-c(4,j-1))/h-area*fc/2.0d0*(c(5,j-1)+c(5,j))
c
      d(6,6)=1.0d0/h
      b(6,6)=-1.0d0/h
      d(6,4)=-0.5d0/sig3
      b(6,4)=-0.5d0/sig3
      g(6)=-cur/sig3+0.5/sig3*(c(4,j+1)+c(4,j))-(c(6,j+1)-c(6,j))/h
c
c     do 506 i=3,3
      call band(j)
      go to 10
c
c     ------------------------------------------------------
c
   16 continue
c     specify boundary conditions at right interface(j=nj)
c
      b(5,4)=-1.0d0/h
      a(5,4)=1.0d0/h
      b(5,5)=area*fc/2.0d0
      a(5,5)=area*fc/2.0d0
      g(5)=(c(4,j)-c(4,j-1))/h-area*fc/2.0d0*(c(5,j-1)+c(5,j))
c
      b(6,4)=1.0d0
      g(6)=-c(4,j)
c
c     do 507 i=3,3
      call band(j)
      do 607 jj=1,nj
      do 607 i=1,n
  607 c(i,jj)=xx(i,jj)+c(i,jj)
c     ------------------------------------------------------
c
c     check for convergence
c
      do 56 i=1,n
   56 xp(i)=(4.0d0*c(i,2)-3.0d0*c(i,1)-c(i,3))/2.0d0/h1
c
      nerr=0
      do 25 j=1,nj
c
c%%%%%%%%%%%%%%%%%%%%%%%%%%%%%%%%%%%%%%%%%%%%%%%%%%%%%%%%%%%%%%%%%%%%%%%%%%%
```

```
c     shoe horns:
      if(c(1,j).lt.xx(1,j)/100.) c(1,j)=xx(1,j)/100.
      if (c(2,j).lt.(xx(2,j)-0.02)) c(2,j)=xx(2,j)-0.02
      if (c(2,j).gt.(xx(2,j)+0.02)) c(2,j)=xx(2,j)+0.02
      if (c(6,j).lt.(xx(6,j)-0.02)) c(6,j)=xx(6,j)-0.02
      if (c(6,j).gt.(xx(6,j)+0.02)) c(6,j)=xx(6,j)+0.02
      if (c(2,j).gt. 9.9) c(2,j)= 9.9
      if (c(2,j).lt.-9.9) c(2,j)=-9.9
      if (c(6,j).gt. 9.9) c(6,j)= 9.9
      if (c(6,j).lt.-9.9) c(6,j)=-9.9
c
      if (j .ge. n1+n2) then
      if(c(3,j).lt.xx(3,j)/100.) nerr=nerr+1
      if(c(3,j).lt.xx(3,j)/100.) c(3,j)=xx(3,j)/100. ! use cs min
      if(ct3-c(3,j).le.(ct3-xx(3,j))/100.) nerr=nerr+1
      if(ct3-c(3,j).le.(ct3-xx(3,j))/100.)
     1c(3,j)=ct3-(ct3-xx(3,j))/100.
      if(c(3,j).ge.ct3) c(3,j)=0.999999*ct3
      if(c(3,j).lt.1.0d-12) c(3,j)=1.0d-12
c
      else if (j .le. n1+1) then
      if(c(3,j).lt.xx(3,j)/100.) nerr=nerr+1
      if(c(3,j).lt.xx(3,j)/100.) c(3,j)=xx(3,j)/100. ! use cs min
      if(ct1-c(3,j).le.(ct1-xx(3,j))/100.) nerr=nerr+1
      if(ct1-c(3,j).le.(ct1-xx(3,j))/100.)
     1c(3,j)=ct1-(ct1-xx(3,j))/100.
      if(c(3,j).ge.ct1) c(3,j)=0.999999*ct1
      if(c(3,j).lt.1.0d-12) c(3,j)=1.0d-12
      endif
c     to avoid underflow or overflow:
      if(c(1,j).lt.1.0d-12) c(1,j)=1.0d-12
      if(c(1,j).lt.1.0d-10) c(5,j)=0.0
c
c%%%%%%%%%%%%%%%%%%%%%%%%%%%%%%%%%%%%%%%%%%%%%%%%%%%%%%%%%%%%%%%%%%%%%%%%
c
      do 25 i=1,n
   25 xx(i,j)=c(i,j)
c
      if (jcount .gt. 3*lim .and. rr.eq.0.0d0) then
      print 99
      stop
      endif
c     ------------------------------------------------------------
c
c     Decreasing time steps:
      if (jcount .gt. lim .and. rr.gt.0.0d0) then
```

```
      tau=tau/2.0d0
      rr=tau
      ts(kk)=ts(kk-1)+tau
      print*,'time step reduced to ', tau, ts(kk)
      if (tau.lt.1.0d-4) then
      if (lpow.eq.1) then  !peak power activated
      nflag=1
      go to 66
      endif
      nt=nt-1
      ed=ed/tw/3.6d03
      pow=3.6d03*ed/ts(nt+1)
      print*,'mass is ',tw
      print*,'energy is ',ed
      print*,'power is ',pow
      print*,kk-1,' this time step did not converge'
      call nucamb(1,5)
      stop
      else
      iflag=0
      call calca(kk)
      go to 666
      end if
c
      else
c
      if(nerr.ne.0) go to 8
      do 55 ii=1,n
      errlim=1.d-10
      if(ii.eq.5) errlim=1.d-16
      dxp=dabs( xp(ii)-xp0(ii) )
      dxx=dabs( xx(ii,n1-10)-xx0(ii,n1-10) )
      dxx2=dabs( xx(ii,n1+n2+10)-xx0(ii,n1+n2+10) )
      if(dxx.gt.1.d-9*dabs(xx(ii,n1-10)).and.dxx.gt.errlim) go to 8
      if(dxx2.gt.1.d-9*dabs(xx(ii,n1+n2+10)).and.dxx2.gt.errlim)
     1go to 8
c     if(dxp.gt.1.d-7*dabs(xp(ii)) .and. dxp.gt.errlim) go to 8
   55 continue
c
c     ------------------------------------------------------
c
      if(lpow.ne.1) print*,jcount,' iterations required'
c
      do 60 ll=1, nj  ! save present time results in xt()
      do 60 lk=1,n
   60 xt(lk,ll,kk)=xx(lk,ll)
```

```
c
c     do 57 j=1,nj
c     if(xx(1,j) .lt. 1.0d-03) fj(j)=1
c  57 if(xx(1,j) .gt. 1.0d-01) fj(j)=0
c
c- - - - - - - - - - - - - - - - - - - - - - - - - - - - - - - - - - -
      if(rr.ne.0.0d0) then
      do 58 j=1,nj  ! fix to calculate here for zero time step
   58 term(j)=termn(j)
      else
      do 65 j=1,nj
      term(j)=0.
      fac=1.
      if(j.eq.n1+2) fac=((ep2+epp2)/(ep1+epp1))**1.5
      if(j.eq.n1+n2+1) fac=((ep3+epp3)/(ep2+epp2))**1.5
      epn=ep1+epp1
      hn=h1
      if(j.gt.n1+1) then
      epn=ep2+epp2
      hn=h2
      endif
      if (j.gt.n1+n2) then
      epn=ep3+epp3
      hn=h3
      endif
      if(j.ne.1) term(j)=
     &-(df(j)+fac*df(j-1))*(c(1,j)-c(1,j-1))/hn/2.
     &-(1.-0.5*(tm(j)+tm(j-1)))*(c(4,j)+c(4,j-1))/2./fc
      fac=1.
      if(j.eq.n1+1) then
      fac=((ep2+epp2)/(ep1+epp1))**1.5
      epn=ep2+epp2
      hn=h2
      else if(j.eq.n1+n2) then
      fac=((ep3+epp3)/(ep2+epp2))**1.5
      epn=ep3+epp3
      hn=h3
      endif
   65 if(j.ne.nj) term(j)=term(j)
     &-(fac*df(j)+df(j+1))*(c(1,j)-c(1,j+1))/hn/2.
     &+(1.-0.5*(tm(j)+tm(j+1)))*(c(4,j)+c(4,j+1))/2./fc
      endif
c- - - - - - - - - - - - - - - - - - - - - - - - - - - - - - - - - - -
c
      end if
c
```

```
   66 continue
      return
      end
c
c*********************************************************************
      subroutine calca(kk)
      implicit real*8(a-h,o-z)
      parameter(maxt=900)
      common /n/ nx,nt,n1,n2,nj,n3,tmmax
      common /calc/ ai(maxt),ai2(maxt),u(223,maxt),ts(maxt),
     1h,h1,h2,h3,hcn,hcp,rr,rrmax
      common/const/ fc,r,t,frt,cur,ep3,ep2,pi,nneg,nprop,npos,
     1ep1,epf3,epf1,epp1,epp2,epp3,shape3,shape1
      common/cprop/ sig3,area,rka3,ct3,dfs3,Rad3,
     1sig1,area2,rka1,ct1,dfs1,Rad1,tw
      dimension ar(4,maxt),bz(6)
c
      do 319 l=1,nt
      ai2(l)=0.0d0
  319 ai(l)=0.0d0
c
      do 70 i=1,kk-1
      ar(1,i)=dfs3*(ts(kk)-ts(i))/Rad3/Rad3
      ar(2,i)=dfs3*(ts(kk)-ts(i+1))/Rad3/Rad3
      ar(3,i)=dfs1*(ts(kk)-ts(i))/Rad1/Rad1
      ar(4,i)=dfs1*(ts(kk)-ts(i+1))/Rad1/Rad1
c
      do 69 m=1,2
      t1=ar(m,i)
      t2=ar((m+2),i)
c
      a1=0.0d0
      a12=0.0d0
c
      s=1.644934066848d0
c
c     Bessel's function zeros:
      bz(1)=2.4048255577d0
      bz(2)=5.5200781103d0
      bz(3)=8.6537281103d0
      bz(4)=11.7915344391d0
      bz(5)=14.9309177086d0
c
      if (shape3.gt.2.0d0) then
c     spherical particles:
      if (t1 .gt. 0.06d0) then
```

```
c
      do 59 j=1,5
      y1=j*j*pi*pi*t1
   59 if (y1 .le. 1.5d02) a1=a1+(expf(-y1))/j/j
      a1=2.0d0*(s-a1)/pi/pi
c
      else
c
      if (t1.LE.0.0d0) then
      a1=0.0d0
      else
      do 60 j=1,3
      z=j/dsqrt(t1)
      call erfc(z,e)
      y2=j*j/t1
      if(y2 .ge. 1.5d02) then
      da=-j*dsqrt(pi/t1)*e
      else
      da=expf(-y2)-j*dsqrt(pi/t1)*e
      end if
   60 a1=a1+da
      a1=-t1 + 2.0d0*dsqrt(t1/pi)*(1.0d0+2.0d0*a1)
      end if
c
      end if
      else
c
      if (shape3.lt.2.0d0) then
c     planar particles:
      if(t1 .gt. 0.06d0) then
c
      do 61 j=1,5
      da=((-1.0d0)**(j))*(1.0d0 - expf(-(2.0d0*j+1.0d0)*
     1(2.0d0*j+1.0d0)*pi*pi*t1))/(2.0d0*j+1.0d0)/(2.0d0*j+1.0d0)
   61 a1=a1+da
      a1=4.0d0*a1/pi/pi
c
      else
c
      do 62 j=1,3
      z=j/2.0d0/dsqrt(t1)
      call erfc(z,e)
      da=((-1.0d0)**(j))*(expf(-j*j/4.0d0/t1)-j/2.0d0*dsqrt(pi/t1)*e)
   62 a1=a1+da
      a1=2.0d0*dsqrt(t1/pi)*(1.0d0+2.0d0*a1)
c
```

```
      end if
      else
c     cylindrical particles:
      if (t1.gt.0.06d0) then
c
      do 63 j=1,5
      da=(1.0d0-expf(-bz(j)*bz(j)*t1))/bz(j)/bz(j)
   63 a1=a1+da
      a1=2.0d0*a1
c
      else
c
      a1=2.0d0*dsqrt(t1/pi)-t1/4.0d0-5.0d0*(t1**1.5d0)/96.0d0
     1/dsqrt(pi)-31.0d0*t1*t1/2048.0d0
c
      end if
      end if
      end if
c
      if (shape1.gt.2.0d0) then
c     spherical particles:
      if(t2 .gt. 0.06d0) then
c
      do 64 j=1,5
      y2=j*j*pi*pi*t2
   64 if(y2 .le. 1.5d02) a12=a12+(expf(-y2))/j/j
      a12=2.0d0*(s-a12)/pi/pi
c
      else
c
      if (t2.eq.0.0d0) then
      a12=0.0d0
      else
      do 65 j=1,3
      z=j/dsqrt(t2)
      call erfc(z,e)
      y2=j*j/t2
      if(y2 .gt. 1.5d02) then
      da=-j*dsqrt(pi/t2)*e
      else
      da=expf(-y2)-j*dsqrt(pi/t2)*e
      end if
   65 a12=a12+da
      a12=-t2 + 2.0d0*dsqrt(t2/pi)*(1.0d0+2.0d0*a12)
      end if
      end if
```

```
c
      else
      if (shape1.lt.2.0d0) then
c     planar particles:
      if(t2 .gt. 0.06d0) then
c
      do 66 j=1,5
      da=((-1.0d0)**(j))*(1.0d0 - expf(-(2.0d0*j+1.0d0)*
     1(2.0d0*j+1.0d0)*pi*pi*t2))/(2.0d0*j+1.0d0)/(2.0d0*j+1.0d0)
   66 a12=a12+da
      a12=4.0d0*a12/pi/pi
c
      else
c
      do 67 j=1,3
      z=j/2.0d0/dsqrt(t2)
      call erfc(z,e)
      da=((-1.0d0)**(j))*(expf(-j*j/4.0d0/t2)-j/2.0d0*dsqrt(pi/t2)*e)
   67 a12=a12+da
      a12=2.0d0*dsqrt(t2/pi)*(1.0d0+2.0d0*a12)
c
      end if
      else
c     cylindrical particles:
      if (t2.gt.0.06d0) then
c
      do 68 j=1,5
      da=(1.0d0-expf(-bz(j)*bz(j)*t2))/bz(j)/bz(j)
   68 a12=a12+da
      a12=2.0d0*a12
c
      else
c
      a12=2.0d0*dsqrt(t2/pi)-t2/4.0d0-5.0d0*(t2**1.5d0)/
     196.0d0/dsqrt(pi)-31.0d0*t2*t2/2048.0d0
c
      end if
      end if
      end if
c
      ar(m,i)=a1
   69 ar((m+2),i)=a12
c
      ai(kk-i)=ar(1,i)-ar(2,i)
   70 ai2(kk-i)=ar(3,i)-ar(4,i)
c
```

```
      return
      end
c*********************************************************************
      subroutine erfc(z,e)
      implicit real*8(a-h,o-z)
      common/const/ fc,r,t,frt,cur,ep3,ep2,pi,nneg,nprop,npos,
     1ep1,epf3,epf1,epp1,epp2,epp3,shape3,shape1
c
      a1=0.254829592d0
      a2=-0.284496736d0
      a3=1.421413741d0
      a4=-1.453152027d0
      a5=1.061405429d0
      if(z .lt. 2.747192d0) then
      t3=1.0d0/(1.0d0+0.3275911d0*z)
      e=(a1*t3+a2*t3*t3+a3*(t3**3.0d0)+a4*(t3**4.0d0)
     1+a5*(t3**5.0d0))*expf(-z*z)
      else
c
      if(z .gt. 25.0d0) then
      e=0.0d0
      else
c
      sum=0.0d0
      max=z*z + 0.5
      fac=-0.5d0/z/z
      sum=fac
      tl=fac
      n=1
  10  n=n+1
      if(n .gt. max) go to 15
      tn=tl*(2.0d0*n-1.0d0)*fac
      sum=sum + tn
      if(tn .lt. 1.0d-06) go to 15
      tl=tn
      go to 10
   15 e=(expf(-z*z))*(1.0d0+sum)/dsqrt(pi)/z
      end if
      end if
c
      return
      end
c*********************************************************************
      subroutine band(j)
      implicit real*8(a-h,o-z)
      common /n/ nx,nt,n1,n2,nj,n3,tmmax
```

```
      common/mat/ b,d
      common/bnd/ a,c,g,x,y
      dimension b(10,10),d(10,21)
      dimension a(10,10),c(10,221),g(10),x(10,10),y(10,10)
      dimension e(10,11,221)
  101 format (15h determ=0 at j=,i4)
      n=nx
      if (j-2)  1,6,8
    1 np1= n + 1
      do 2 i=1,n
      d(i,2*n+1)= g(i)
      do 2 l=1,n
      lpn= l + n
    2 d(i,lpn)= x(i,l)
      call matinv(n,2*n+1,determ)
      if (determ)  4,3,4
    3 print 101, j
    4 do 5 k=1,n
      e(k,np1,1)= d(k,2*n+1)
      do 5 l=1,n
      e(k,l,1)= - d(k,l)
      lpn= l + n
    5 x(k,l)= - d(k,lpn)
      return
    6 do 7 i=1,n
      do 7 k=1,n
      do 7 l=1,n
    7 d(i,k)= d(i,k) + a(i,l)*x(l,k)
    8 if (j-nj)  11,9,9
    9 do 10 i=1,n
      do 10 l=1,n
      g(i)= g(i) - y(i,l)*e(l,np1,j-2)
      do 10 m=1,n
   10 a(i,l)= a(i,l) + y(i,m)*e(m,l,j-2)
   11 do 12 i=1,n
      d(i,np1)= - g(i)
      do 12 l=1,n
      d(i,np1)= d(i,np1) + a(i,l)*e(l,np1,j-1)
      do 12 k=1,n
   12 b(i,k)= b(i,k) + a(i,l)*e(l,k,j-1)
      call matinv(n,np1,determ)
      if (determ)  14,13,14
   13 print 101, j
   14 do 15 k=1,n
      do 15 m=1,np1
   15 e(k,m,j)= - d(k,m)
```

```
      if (j-nj)  20,16,16
   16 do 17 k=1,n
   17 c(k,j)= e(k,np1,j)
      do 18 jj=2,nj
      m= nj - jj + 1
      do 18 k=1,n
      c(k,m)= e(k,np1,m)
      do 18 l=1,n
   18 c(k,m)= c(k,m) + e(k,l,m)*c(l,m+1)
      do 19 l=1,n
      do 19 k=1,n
   19 c(k,1)= c(k,1) + x(k,l)*c(l,3)
   20 return
      end
c*********************************************************************
      subroutine matinv(n,m,determ)
      implicit real*8(a-h,o-z)
      common/mat/ b,d
      dimension b(10,10),d(10,21)
      dimension id(10)
      determ=1.0
      do 1 i=1,n
    1 id(i)=0
      do 18 nn=1,n
      bmax=1.1
      do 6 i=1,n
      if(id(i).ne.0) go to 6
      bnext=0.0
      btry=0.0
      do 5 j=1,n
      if(id(j).ne.0) go to 5
      if(dabs(b(i,j)).le.bnext) go to 5
      bnext=dabs(b(i,j))
      if(bnext.le.btry) go to 5
      bnext=btry
      btry=dabs(b(i,j))
      jc=j
    5 continue
      if(bnext.ge.bmax*btry) go to 6
      bmax=bnext/btry
      irow=i
      jcol=jc
    6 continue
      if(id(jc).eq.0) go to 8
      determ=0.0
      return
```

```
    8 id(jcol)=1
      if(jcol.eq.irow) go to 12
      do 10 j=1,n
      save=b(irow,j)
      b(irow,j)=b(jcol,j)
   10 b(jcol,j)=save
      do 11 k=1,m
      save=d(irow,k)
      d(irow,k)=d(jcol,k)
   11 d(jcol,k)=save
   12 f=1.0/b(jcol,jcol)
      do 13 j=1,n
   13 b(jcol,j)=b(jcol,j)*f
      do 14 k=1,m
   14 d(jcol,k)=d(jcol,k)*f
      do 18 i=1,n
      if(i.eq.jcol) go to 18
      f=b(i,jcol)
      do 16 j=1,n
   16 b(i,j)=b(i,j)-f*b(jcol,j)
      do 17 k=1,m
   17 d(i,k)=d(i,k)-f*d(jcol,k)
   18 continue
      return
      end
c*********************************************************************
      subroutine nucamb(il2,il3)
      implicit real*8(a-h,o-z)
      parameter(maxt=900)
      common /n/ nx,nt,n1,n2,nj,n3,tmmax
      common /calc/ ai(maxt),ai2(maxt),u(223,maxt),ts(maxt),
     1h,h1,h2,h3,hcn,hcp,rr,rrmax
      common/const/ fc,r,t,frt,cur,ep3,ep2,pi,nneg,nprop,npos,
     1ep1,epf3,epf1,epp1,epp2,epp3,shape3,shape1
      common/var/ xp(10),xx(6,221),xi(6,221),xt(6,221,maxt)
      common/cprop/ sig3,area,rka3,ct3,dfs3,Rad3,
     1sig1,area2,rka1,ct1,dfs1,Rad1,tw
      common/tprop/df(221),cd(221),tm(221),
     1ddf(221),dcd(221),dtm(221),dfu(221),d2fu(221)
      dimension zz(221)
  109 format(f6.1,', ',f7.1,', ',f7.4,', 'g10.4,', ',f6.2
     1,', ',g10.4,', ',g10.4)
  309 format(f8.5,', ',f8.5)
   44 format(' t = ',f12.6,' min')
c
      do 5 i=1,n1+1
```

```
      w=i-1
    5 zz(i) = w*h1*1.0d06
      do 71 i=n1+2,n2+n1
      w=i-(n1+1)
   71 zz(i)=zz(n1+1)+w*h2*1.0d06
      do 72 i=n1+n2+1,nj
      w=i-(n1+n2)
   72 zz(i)=zz(n2+n1)+w*h3*1.0d06
c
      do 11 l=1,nt+1
      if (l.lt.nt-5 .and. mod(l-1,il3).ne.0) go to 11
      print*,' '
      print*,'distance concen    PHI2    c solid',
     1'    current      j       PHI1'
      print*,'microns  (mol/m3)   (V)    x or y ',
     1'     (A/m2)   (A/m3)      (V)'
      print44,ts(l)/60.0d0
c
      do 10 j=1,nj,il2
      if (j .le. n1+1) then
      csol=ct1
      else
      csol=ct3
      end if
      if(j.le.n1+1) then
      curden=area*fc*xt(5,j,l)
      else if(j.ge.n1+n2) then
      curden=area2*fc*xt(5,j,l)
      else
      curden=0.0
      endif
   10 print109,zz(j),xt(1,j,l),xt(2,j,l),xt(3,j,l)/csol,xt(4,j,l)
     1,curden,xt(6,j,l)
   11 continue
c
      return
      end
c*********************************************************************
      subroutine guess(lflag)
      implicit real*8(a-h,o-z)
      parameter(maxt=900)
      common /n/ nx,nt,n1,n2,nj,n3,tmmax
      common /calc/ ai(maxt),ai2(maxt),u(223,maxt),ts(maxt),
     1h,h1,h2,h3,hcn,hcp,rr,rrmax
      common/const/ fc,r,t,frt,cur,ep3,ep2,pi,nneg,nprop,npos,
     1ep1,epf3,epf1,epp1,epp2,epp3,shape3,shape1
```

```
      common/var/ xp(10),xx(6,221),xi(6,221),xt(6,221,maxt)
      common/cprop/ sig3,area,rka3,ct3,dfs3,Rad3,
     1sig1,area2,rka1,ct1,dfs1,Rad1,tw
      common/tprop/df(221),cd(221),tm(221),
     1ddf(221),dcd(221),dtm(221),dfu(221),d2fu(221)
      dimension del(6)
c
      del(2)=cur*h/2.5
      del(3)=cur/(n1)
      del(4)=cur/(n3)
      del(5)=(xi(5,nj)-xi(5,1))/(nj-1)
c
      do 73 i=1,(n1+1)
      xi(2,i)=xi(2,1)*(nj-i)/nj
      xi(3,i)=xi(3,1)
      xi(4,i)=xi(4,1)+del(3)*(i-1)
      xi(5,i)=xi(5,1)
   73 xi(6,i)=xi(6,1)
c
      do 74 i=(n1+2),(n2+n1-1)
c     xi(2,i)=xi(2,1)-del(2)*(i-n1-2)
      xi(2,i)=xi(2,1)*(nj-i)/nj
      xi(3,i)=0.0d0
      xi(4,i)=cur
      xi(5,i)=0.0d0
   74 xi(6,i)=0.0d0
c
      do 75 i=(n2+n1),nj
      xi(2,i)=xi(2,1)*(nj-i)/nj
      xi(3,i)=xi(3,nj)
      xi(4,i)=xi(4,n2+n1)-del(4)*(i-n1-n2)
      xi(5,i)=xi(5,n2+n1)
   75 xi(6,i)=xi(6,nj)
c
      do 15 i=1,nj
      xt(6,i,1)=xi(6,i)
      xt(5,i,1)=xi(5,i)
      xt(4,i,1)=xi(4,i)
      xt(3,i,1)=xi(3,i)
   15 xt(2,i,1)=xi(2,i)
c
      do 16 i=1,nj
      xi(1,i)=xi(1,n1+2)
c     Uniform initial concentration if lflag=1
c     Step function initial concentration if lflag=0
      if(lflag.eq.0 .and. (i.le.n1+1 .or. i.ge.n1+n2))
```

```
      &xi(1,i)=1.0d-01
   16 xt(1,i,1)=xi(1,i)
      return
      end
c*********************************************************************
      subroutine util
      implicit real*8(a-h,o-z)
      parameter(maxt=900)
      common /n/ nx,nt,n1,n2,nj,n3,tmmax
      common /calc/ ai(maxt),ai2(maxt),u(223,maxt),ts(maxt),
     1h,h1,h2,h3,hcn,hcp,rr,rrmax
      common/const/ fc,r,t,frt,cur,ep3,ep2,pi,nneg,nprop,npos,
     1ep1,epf3,epf1,epp1,epp2,epp3,shape3,shape1
      common/var/ xp(10),xx(6,221),xi(6,221),xt(6,221,maxt)
      common/cprop/ sig3,area,rka3,ct3,dfs3,Rad3,
     1sig1,area2,rka1,ct1,dfs1,Rad1,tw
c
      do 10 j=(n2+n1),nj
      u(j,1)=0.0d0
      do 76 k=2,nt+1
   76 u(j,k)=u(j,k-1)-1.5d0*(xt(5,j,k)+xt(5,j,k-1))*
     1(ts(k)-ts(k-1))/Rad3
      do 77 k=2,nt+1
   77 u(j,k)=(u(j,k)+xt(3,j,1))/ct3
      u(j,1)=xt(3,j,1)/ct3
   10 continue
c
      do 20 j=1,n1
      u(j,1)=0.0d0
      do 78 k=2,nt+1
   78 u(j,k)=u(j,k-1)-1.5d0*(xt(5,j,k)+xt(5,j,k-1))*
     1(ts(k)-ts(k-1))/Rad1
      do 79 k=2,nt+1
   79 u(j,k)=(u(j,k)+xt(3,j,1))/ct1
      u(j,1)=xt(3,j,1)/ct1
   20 continue
c
c     calculate average utilization in cathode:
      do 81 k=1,nt+1
      u(nj+1,k)=0.0d0
      do 80 j=n2+n1+1,nj-1
   80 u(nj+1,k)=u(nj+1,k)+u(j,k)
      u(nj+1,k)=u(nj+1,k)+0.5d0*(u(n2+n1,k)+u(nj,k))
   81 u(nj+1,k)=u(nj+1,k)/(nj-n2-n1)
c
c     calculate average utilization in anode:
```

```
      do 83 k=1,nt+1
      u(nj+2,k)=0.0d0
      do 82 j=2,n1-1
   82 u(nj+2,k)=u(nj+2,k)+u(j,k)
      u(nj+2,k)=u(nj+2,k)+0.5d0*(u(1,k)+u(n1,k))
   83 u(nj+2,k)=u(nj+2,k)/n1
c
      return
      end
c*********************************************************************
      subroutine peak(n,lim,curr)
      implicit real*8(a-h,o-z)
      parameter(maxt=900)
      common /n/ nx,nt,n1,n2,nj,n3,tmmax
      common /calc/ ai(maxt),ai2(maxt),u(223,maxt),ts(maxt),
     1h,h1,h2,h3,hcn,hcp,rr,rrmax
      common/const/ fc,r,t,frt,cur,ep3,ep2,pi,nneg,nprop,npos,
     1ep1,epf3,epf1,epp1,epp2,epp3,shape3,shape1
      common/var/ xp(10),xx(6,221),xi(6,221),xt(6,221,maxt)
      common/cprop/ sig3,area,rka3,ct3,dfs3,Rad3,
     1sig1,area2,rka1,ct1,dfs1,Rad1,tw
  311 format(f8.5,', ',f7.3,', ',f7.2)
c
c     Peak power current ramp section:
      print*,' '
      print*,'    PEAK POWER '
      print*,' '
      print*,'cell pot  ',' current','   power'
      print*,'  (V)  ','    (A/m2)','   (W/m2)'
c
c     Duration of current pulse is 30 seconds.
c
      kcount=0
      fact=20.0d0
      rrmax=30.0d0
  127 k=nt+2
      do 126 j=1,nj
      do 126 i=1,n
  126 xt(i,j,k)=xt(i,j,k-1)
      ppow=0.0
      opow=ppow
      ii=0
      mflag=1
      curinit=curr
      cur=curr
c     Ramp current:
```

```
c
  128 continue
      if (ppow.ge.opow.and.ii.lt.200) then
c
      opow=ppow
      ocur=cur
      energ=0.0
      ii=ii+1
      cur=cur+fact
      kkflag=0
      iflag=0
      nflag=0
      k=nt+2
      timpk=0.0d0
      rr=0.0d0
      ts(k)=ts(k-1)
      call comp(n,lim,k,rr,kkflag,nflag,1,jcount)
      call cellpot(k,vv,0,1,lflag)
      vlast=vv
      rr=0.2d0
  129 kkflag=kkflag+1
      k=k+1
      ts(k)=ts(k-1)+rr
      call calca(k)
c
      call comp(n,lim,k,rr,kkflag,nflag,1,jcount)
c
      if (nflag.eq.1.and.kcount.lt.20) then
      cur=cur-2.0*fact
      fact=fact/2.
      kcount=kcount+1
      print*,'Peak current decreased',kcount,fact
      go to 128
      endif
      if (kcount.ge.10) return
c
      call cellpot(k,vv,0,1,lflag)
      energ=energ+(vlast+vv)*(ts(k)-ts(k-1))*cur/2.0d0
c
      timpk=timpk+rr
      if (dabs(timpk-30.0d0).gt.0.1) then
c
      if (timpk.lt.30.0) then
      vlast=vv
c     Increasing time steps:
      if(jcount.lt.6 .and. kkflag.gt.5 .and. (2.0d0*rr
```

```
     1+timpk).lt.30.0d0 .and. iflag.eq.0) then
         rr=rr*2.0d0
c        print*,'next time step increased to ', rr,'(s)'
      end if
      if(timpk+rr.gt.30.0) iflag=1
      if(timpk+rr.gt.30.0) rr=30.0d0-timpk
      go to 129
      end if
c
      end if
      ppow=energ/30.0d0
      print 311, ppow/cur,cur,ppow
      go to 128
c
      else
      if (kcount.ne.0) mflag=0
      if (ii.gt.2.and.mflag.eq.0) print 311, opow/ocur,ocur,opow
      if (mflag.eq.1) then
      opow=0.0d0
      ppow=opow
      cur=cur-2.0*fact
      fact=1.0d0
      mflag=0
      go to 128
      end if
c
      end if
      if (ii.le.2) then
      curr=curinit/2.0
      go to 127
      end if
c
      return
      end
c**********************************************************************
      subroutine cellpot(kk,v,li,lpow,lflag)
      implicit real*8(a-h,o-z)
      parameter(maxt=900)
      common /n/ nx,nt,n1,n2,nj,n3,tmmax
      common /calc/ ai(maxt),ai2(maxt),u(223,maxt),ts(maxt),
     1h,h1,h2,h3,hcn,hcp,rr,rrmax
      common/const/ fc,r,t,frt,cur,ep3,ep2,pi,nneg,nprop,npos,
     1ep1,epf3,epf1,epp1,epp2,epp3,shape3,shape1
      common/power/ ed,Vold,ranode,rcathde
      common/var/ xp(10),xx(6,221),xi(6,221),xt(6,221,maxt)
      common/cprop/ sig3,area,rka3,ct3,dfs3,Rad3,
```

```
     1sig1,area2,rka1,ct1,dfs1,Rad1,tw
      common/temp/ thk,htc,dudt,Cp,dens,tam,g0,ncell,lht
  309 format(f8.5,', ',f8.5,', ',f8.3,', ',f8.3,',',' ',f7.3
     1,', ',f7.3)
  307 format(f8.5,', ',f8.5,', ',f9.5,', ',f11.6,',',' ',f7.3,',',i3)
c
c     Material balance criteria:
      sum=0.0d0
      do 85 j=2,n1
   85 sum=sum+xt(1,j,kk)*(ep1+epp1)*h1
      sum=sum+(xt(1,1,kk)+xt(1,n1+1,kk))*(ep1+epp1)*h1/2.0d0
      do 86 j=n1+2,n2+n1-1
   86 sum=sum+xt(1,j,kk)*(ep2+epp2)*h2
      sum=sum+(xt(1,n1+1,kk)+xt(1,n2+n1,kk))*(ep2+epp2)*h2/2.0d0
      do 87 j=n2+n1+1,nj-1
   87 sum=sum+xt(1,j,kk)*(ep3+epp3)*h3
      sum=sum+(xt(1,n1+n2,kk)+xt(1,nj,kk))*h3*(ep3+epp3)/2.0d0
c     calculate total salt in cell from initial profile:
      w=xt(1,n1+2,1)*((n2-1)*(ep2+epp2)*h2+n1*(ep1+epp1)*h1
     1+n3*(ep3+epp3)*h3)
      if(lflag.eq.0) w=w-(xt(1,n1+2,1)-xt(1,1,1))*(n1*(ep1+epp1)*h1
     1+n3*(ep3+epp3)*h3)
      if(lflag.eq.0) w=w-(xt(1,n1+2,1)-xt(1,1,1))*(ep2+epp2)*h2
c     material balance parameter should be ca=1.00
      ca=sum/w
c
      if (kk.eq.1) then
      ut=xt(3,nj,1)/ct3
      ut2=xt(3,1,1)/ct1
      end if
c
c     Calculate cell potential from dif of solid phase potentials:
      v=xt(6,nj,kk)-xt(6,1,kk)
c
c     Calculate util. of two electrodes based on coulombs passed:
      if(li.eq.1) then
c     Calculate energy density by running sum of currentxvoltage:
      ed=ed+(Vold+v)*(ts(kk)-ts(kk-1))*cur/2.0d0
      Vold=v
      ut=cur*(ts(kk)-ts(kk-1))/fc/(1.0d0-ep3-epf3-epp3)/n3/h3/ct3+ut
      ut2=ut2-cur*rr/fc/(1.0d0-ep1-epf1-epp1)/n1/h1/(ct1)
      th=ts(kk)/6.0d01
c
      if(lht.ne.2) call temperature(kk,v,q,ut,ut2,Uoc)
      tprint=t-273.15
      if(lpow.ne.0) then
```

```
c     ! isothermal peak power output:
      print309,v,ca,cur,v*cur
      else
      if (lht.eq.0) then ! T varies, uses htc:
      print309,ut,v,tprint,th,Uoc,cur
      else if (lht.eq.1) then ! calculated htc:
      print309,ut,v,htc,th,Uoc,cur
      else if (lht.eq.2) then ! isothermal output:
      print307,ut,v,ca,th,cur,kk
      endif
      endif
      endif
c
      return
      end
c*********************************************************************
      subroutine sol(nmax,jj)
      implicit real*8(a-h,o-z)
c     Calculate the solid phase concentration profiles.
      parameter(maxt=900)
      common /calc/ ai(maxt),ai2(maxt),u(223,maxt),ts(maxt),
     1h,h1,h2,h3,hcn,hcp,rr,rrmax
      common/var/ xp(10),xx(6,221),xi(6,221),xt(6,221,maxt)
      common/const/ fc,r,t,frt,cur,ep3,ep2,pi,nneg,nprop,npos,
     1ep1,epf3,epf1,epp1,epp2,epp3,shape3,shape1
      common/cprop/ sig3,area,rka3,ct3,dfs3,Rad3,
     1sig1,area2,rka1,ct1,dfs1,Rad1,tw
      dimension cs(50)
c
c     set initial value of solid concentration
      do 88 i=1, 50
c     cs(i)=0.0d0
   88 cs(i)=xt(3,jj,1)
c
c     complete calculations for 50 points along radius of particle
      do 10 i=1,50
      y2=2.0d-02*i
c
      sum1=0.0d0
      do 20 kk=1,nmax
      k=nmax+1-kk
c
      t1=(ts(nmax+1)-ts(k))*dfs1/Rad1/Rad1
      sum2=sum1
c
c     calculate c bar (r,t1)
```

```
      sum1=0.0d0
      r1=1.0d0
c
      do 89 j=1,15
      r1=-r1
      y1=j*j*pi*pi*t1
      y3=j*pi*y2
      if (y1 .gt. 1.50d02) then
      da=0.0d0
      else
      da=expf(-y1)
      end if
   89 sum1=sum1-2.0d0*r1*da*dsin(y3)/j/pi/y2
      sum1=1.0d0-sum1
c
c     perform superposition
c
      cs(i)=cs(i)+(xt(3,jj,k+1)+xt(3,jj,k)-2.0d0*xt(3,jj,1)
     1)*(sum1-sum2)/2.0d0
   20 continue
c
   10 continue
c
      print*,' '
      print*,'time is ',ts(nmax)
      print*,' '
      do 90 i=1, 50, 1
   90 print*,.02*i,' ',cs(i)
c
      return
      end
c**********************************************************************
      subroutine mass(re,rs3,rs1,rf,rpl,rc,rcn,rcp)
      implicit real*8(a-h,o-z)
      parameter(maxt=900)
      common /n/ nx,nt,n1,n2,nj,n3,tmmax
      common /calc/ ai(maxt),ai2(maxt),u(223,maxt),ts(maxt),
     1h,h1,h2,h3,hcn,hcp,rr,rrmax
      common/const/ fc,r,t,frt,cur,ep3,ep2,pi,nneg,nprop,npos,
     1ep1,epf3,epf1,epp1,epp2,epp3,shape3,shape1
      common/var/ xp(10),xx(6,221),xi(6,221),xt(6,221,maxt)
      common/cprop/ sig3,area,rka3,ct3,dfs3,Rad3,
     1sig1,area2,rka1,ct1,dfs1,Rad1,tw
c
c     mass of positive electrode
      c1=h3*n3*(re*ep3+rpl*epp3+rs3*(1.0d0-ep3-epf3-epp3)+rf*epf3)
```

```
c
c     mass of separator
      s=(re*ep2+rpl*epp2+rc*(1-ep2-epp2))*h2*(n2-1)
c
c     mass of negative electrode
      a1=h1*n1*(re*ep1+rpl*epp1+rs1*(1.0d0-ep1-epf1-epp1)+rf*epf1)
c
c     mass of current collectors
      cc1=rcn*hcn+rcp*hcp
c
      tw=c1+s+a1+cc1
c
      return
      end
c*********************************************************************
      subroutine temperature(kk,v,q,ut,ut2,Uoc)
      implicit real*8(a-h,o-z)
      parameter(maxt=900)
      common /n/ nx,nt,n1,n2,nj,n3,tmmax
      common /calc/ ai(maxt),ai2(maxt),u(223,maxt),ts(maxt),
     1h,h1,h2,h3,hcn,hcp,rr,rrmax
      common/const/ fc,r,t,frt,cur,ep3,ep2,pi,nneg,nprop,npos,
     1ep1,epf3,epf1,epp1,epp2,epp3,shape3,shape1
      common/cprop/ sig3,area,rka3,ct3,dfs3,Rad3,
     1sig1,area2,rka1,ct1,dfs1,Rad1,tw
      common/temp/ thk,htc,dudt,Cp,dens,tam,g0,ncell,lht
c
c     calculate open-circuit potential of cell at current state
c     of charge:
      call ekin(1,kk,1,ut2)
      Ua=g0
      call ekin(n1+n2,kk,1,ut)
      Uc=g0
      Uoc=Uc-Ua
c
c     if (kk.eq.2) print*,htc,dudt,ncell,cur,tam-273.15
c     per cell heat generation
      q=cur*(Uoc-v-t*dudt)
c     The heat transfer coefficient is for heat transferred out of
c     one side of the cell; it is defined based on cell area.
c     htcc is a per-cell heat transfer coefficient.
      if (lht.eq.0) then
      htcc=htc/Ncell
      t=(dens*Cp*thk*t+rr*(Uoc-v)*cur + rr*htcc*tam)
     &/(dens*Cp*thk+rr*dudt*cur + rr*htcc)
      else
```

```
c*********Calculate htc instead of Temp **********************
c     For this case the temperature is assumed constant, and the
c     heat transfer coefficient required to keep it constant is
c     calculated as a function of time.  The heat transfer coef.
c     is calculated for heat transferred out of one side of the
c     cell stack.  Htcc is defined as a per-cell heat transfer
c     coefficient.
         if (t.ne.tam) then
           htc=cur*Ncell*(Uoc-v-t*dudt)/(t-tam)
         else
           htc=0
         endif
         htcc=htc/Ncell
c*************************************************************
       endif
c
       return
       end
c*****************************************************************************
      double precision function expf(x)
      implicit real*8 (a-h,o-z)
      expf=0.d0
      if(x.gt.-700.d0) expf=dexp(x)
      return
      end
c*****************************************************************************
      subroutine ekin(j,kk,lag,utz)
      implicit real*8(a-h,o-z)
c     This subroutine evaluates the Butler-Volmer equations.
      parameter(maxt=900)
      common /n/ nx,nt,n1,n2,nj,n3,tmmax
      common/const/ fc,r,t,frt,cur,ep3,ep2,pi,nneg,nprop,npos,
     1ep1,epf3,epf1,epp1,epp2,epp3,shape3,shape1
      common/power/ ed,Vold,ranode,rcathde
      common/var/ xp(10),xx(6,221),xi(6,221),xt(6,221,maxt)
      common/cprop/ sig3,area,rka3,ct3,dfs3,Rad3,
     1sig1,area2,rka1,ct1,dfs1,Rad1,tw
      common/temp/ thk,htc,dudt,Cp,dens,tam,g0,ncell,lht
      common/mat/ b,d
      common/bnd/ a,c,g,x,y
      dimension b(10,10),d(10,21)
      dimension a(10,10),c(10,221),g(10),x(10,10),y(10,10)
c
c     Calculate average open-circuit potential in either
c     electrode if lag=1, otherwise lag=0
c
```

```
c%%%%%%%%%%%%%%%%%%%%%%%%%%%%%%%%%%%%%%%%%%%%%%%%%%%%%%%%%%%%%%%%%%%%%%%%%%%
c
c     OPEN-CIRCUIT POTENTIAL FUNCTIONS:
c
c     g0 is the open-circuit potential in terms of the solid
c     concentration, xx(3,j),
c     g1 is the derivative of the open-circuit potential wrt
c     the solid concentration
c
c  &&&&&&&&&&&&&&&&&&&&&&&&&&&&&&&&&&&&&&&&&&&&&&&&&&&&&&&&&&&&&&&&&&&&&&&
c
c     FOR THE NEGATIVE ELECTRODE
c
      if (j .le. n1+1) then
c
      if (lag.eq.1) xx(3,j)=utz*ct1
c
c  &&&&&&&&&&&&&&&&&&&&&&&&&&&&&&&&&&&&&&&&&&&&
c
      go to (11,12,13,14,15,16),nneg
   11 go to 111  ! Li foil
   12 go to 112  ! Carbon (petroleum coke)
   13 go to 113  ! MCMB 2510 Carbon (Bellcore)
   14 go to 114  ! TiS2
   15 go to 115  ! Tungsten oxide (LixWO3 with 0<x<0.67)
   16 go to 116  ! Lonza KS-6 graphite (Bellcore)
c
c  &&&&&&&&&&&&&&&&&&&&&&&&&&&&&&&&&&&&&&&&&&&&
  111 stop ! save space for Li foil
c  &&&&&&&&&&&&&&&&&&&&&&&&&&&&&&&&&&&&&&&&&&&&
c     Carbon (petroleum coke):
c
  112 c1=-0.132056d0
      c2=1.40854d0
      c3=-3.52312d0
      g0=c1+c2*expf(c3*xx(3,j)/ct1)
      g1=c2*c3*expf(c3*xx(3,j)/ct1)/ct1
      go to 97
c  &&&&&&&&&&&&&&&&&&&&&&&&&&&&&&&&&&&&&&&&&&&&
c     MCMB 2510 carbon (Bellcore)
c
  113 c1=-0.160d0
      c2=1.32d0
      c3=-3.0d0
      g0=c1+c2*expf(c3*xx(3,j)/ct1)
      g1=c2*c3*expf(c3*xx(3,j)/ct1)/ct1
```

```
      go to 97
c  &&&&&&&&&&&&&&&&&&&&&&&&&&&&&&&&&&&&
c     TiS2
c
  114 delt=-5.58d-04
      zeta=8.1d0
c     ct1=2.9d04
      g0=2.17+(dlog((ct1-xx(3,j))/xx(3,j))+delt*xx(3,j)+zeta)/frt
      g1=(delt-ct1/xx(3,j)/(ct1-xx(3,j)))/frt
      go to 97
c  &&&&&&&&&&&&&&&&&&&&&&&&&&&&&&&&&&&&
c     Tungsten oxide (LixWO3 with 0<x<0.67):
c     literature data from Whittingham
c
  115 c1=2.8767d0
      c2=-0.9046d0
      c3=0.76679d0
      c4=-0.15975d0
      c5=0.671d0
      g0=c1+c2*xx(3,j)/ct1+c3*xx(3,j)*xx(3,j)/ct1/ct1+
     1c4*expf(100.0d0*(xx(3,j)/ct1-0.671))
      g1=c2/ct1+2.0d0*c3*xx(3,j)/ct1/ct1+
     1c4*100.0d0*expf(100.0d0*(xx(3,j)/ct1-0.671))/ct1
      go to 97
c  &&&&&&&&&&&&&&&&&&&&&&&&&&&&&&&&&&&&
c     Bellcore graphite (Lonza KS-6)
c
  116 c1=0.7222d0
      c2=0.13868d0
      c3=0.028952d0
      c4=0.017189d0
      c5=0.0019144d0
      c6=0.28082d0
      c7=0.79844d0
      c8=0.44649d0
      xtem=xx(3,j)/ct1
      g0=c1+c2*xtem+c3*(xtem**0.5d0)-c4*(xtem**-1.0d0)
     1+c5*(xtem**-1.5d0)+c6*expf(15.0d0*(0.06d0-xtem))-c7*
     1expf(c8*(xtem-0.92d0))
      g1=c2/ct1+c3*0.5d0*(ct1**-0.5d0)*(xx(3,j)**-0.5d0)+
     1c4*ct1*(xx(3,j)**-2.0d0)-c5*1.5d0*(ct1**1.5d0)*
     1(xx(3,j)**-2.5d0)-c6*15.0d0/ct1*expf(15.0d0*(0.06d0-xtem))
     1-c7*c8/ct1*expf(c8*(xtem-0.92d0))
      go to 97
c  &&&&&&&&&&&&&&&&&&&&&&&&&&&&&&&&&&&&&&&&&&&&&&&&&&&&&&&&&&&&&&&&
c
```

```
c      KINETIC EXPRESSIONS FOR NEGATIVE ELECTRODE
c
c      h0 is the exchange current density (A/m2)
c      h1 is the derivative of io wrt solid concentration, xx(3,j)
c      h2 is the derivative of io wrt electrolyte concen., xx(1,j)
c
c  &&&&&&&&&&&&&&&&&&&&&&&&&&&&&&&&
c
c      NONAQUEOUS LIQUIDS
c
   97 if (lag.eq.1) go to 99
      alpha=0.5d0
      alphc=0.5d0
      h0=rka1*dsqrt(xx(1,j))*dsqrt(ct1-xx(3,j))*dsqrt(xx(3,j))
      h1=-rka1*dsqrt(xx(1,j))*dsqrt(ct1-xx(3,j))*dsqrt(xx(3,j))*
     1(1.0d0/(ct1-xx(3,j))-1.0d0/xx(3,j))/2.0d0
      h2=rka1*dsqrt(ct1-xx(3,j))*dsqrt(xx(3,j))/dsqrt(xx(1,j))/2.0d0
c
c  &&&&&&&&&&&&&&&&&&&&&&&&&&&&&&&&
c
c      POLYMER
c
c      cmax=3.92d03
c      alpha=0.5d0
c      alphc=0.5d0
c      h0=rka1*dsqrt(xx(1,j))*dsqrt(cmax-xx(1,j))*dsqrt(ct1-xx(3,j))
c     1*dsqrt(xx(3,j))
c      h1=-rka1*dsqrt(xx(1,j))*dsqrt(cmax-xx(1,j))*dsqrt(ct1-xx(3,j))
c     1*dsqrt(xx(3,j))*(1.0d0/(ct1-xx(3,j))-1.0d0/xx(3,j))/2.0d0
c      h2=-rka1*dsqrt(xx(3,j))*dsqrt(ct1-xx(3,j))*dsqrt(cmax-xx(1,j))
c     1*dsqrt(xx(1,j))*(1.0d0/(cmax-xx(1,j))-1.0d0/xx(1,j))/2.0d0
c
c  &&&&&&&&&&&&&&&&&&&&&&&&&&&&&&&&
c
      end if
c
c  &&&&&&&&&&&&&&&&&&&&&&&&&&&&&&&&&&&&&&&&&&&&&&&&&&&&&&&&&&&&&&&&&&&
c
c      FOR THE POSITIVE ELECTRODE
c
      if (j .ge. n1+n2) then
c
c  &&&&&&&&&&&&&&&&&&&&&&&&&&&&&&&&
c
      if (lag.eq.1) xx(3,j)=utz*ct3
      go to (1,2,3,4,5,6,7,8,9),npos
```

```
     1 go to 101  ! TiS2
     2 go to 102  ! Spinel Mn2O4 (lower plateau)
     3 go to 103  ! NaCoO2:  Sodium cobalt oxide
     4 go to 104  ! Spinel Mn2O4 (upper plateau)
     5 go to 105  ! Tungsten oxide (LixWO3 with 0<x<0.67)
     6 go to 106  ! CoO2 (Cobalt dioxide)
     7 go to 107  ! V2O5 (Vanadium oxide)
     8 go to 108  ! NiO2 (Nickel dioxide)
     9 go to 109  ! Spinel Mn2O4 (Bellcore)
c
c  &&&&&&&&&&&&&&&&&&&&&&&&&&&&&&&&&&&
c      TiS2
c
  101 delt=-5.58d-04
      zeta=8.1d0
      g0=2.17+(dlog((ct3-xx(3,j))/xx(3,j))+delt*xx(3,j)+zeta)/frt
      g1=(delt-ct3/xx(3,j)/(ct3-xx(3,j)))/frt
      go to 98
c  &&&&&&&&&&&&&&&&&&&&&&&&&&&&&&&&&&&
c      Spinel Mn2O4 (lower plateau)
c
  102 c1=2.06307d0
      c2=-0.869705d0
      c3=8.65375d0
      c4=0.981258d0
      a1=c3*(xx(3,j)/ct3-c4)
      g0=c1+c2*(dtanh(a1))
      g1=c2*c3/ct3/(dcosh(a1))/(dcosh(a1))
      go to 98
c  &&&&&&&&&&&&&&&&&&&&&&&&&&&&&&&&&&&
c      NaCoO2:  Sodium Cobalt Oxide (P2 phase, 0.3<y<0.92)
c
  103 c1=4.4108d0
      c2=-2.086d0
      c3=0.10465d0
      c4=133.42d0
      c5=89.825d0
      c6=0.16284d0
      c7=145.01d0
      c8=71.92d0
      c9=0.01d0
      c10=200.0d0
      c11=0.3d0
      c12=0.885d0
      a1=xx(3,j)/ct3
      g0=c1+c2*a1+c3*dtanh(-c4*a1+c5)+c6*dtanh(-c7*a1+c8)+c9*
```

```
     1expf(-c10*(a1-c11))-c9*expf(c10*(a1-c12))
      g1=c2/ct3-c3*c4/dcosh(-c4*a1+c5)/dcosh(-c4*a1+c5)/ct3-c6*c7
     1/dcosh(-c7*a1+c8)/dcosh(-c7*a1+c8)/ct3-c9*c10*
     1expf(-c10*(a1-c11))/ct3-c9*c10*expf(c10*(a1-c12))/ct3
      go to 98
c  &&&&&&&&&&&&&&&&&&&&&&&&&&&&&&&&&&&&
c     Spinel Mn2O4 (upper plateau 0.2<y<1.0)
c     Literature version
c
  104 a1=4.06279d0
      a2=0.0677504d0
      a3=21.8502d0
      a4=12.8268d0
      a5=0.105734d0
      a6=1.00167d0
      a7=-0.379571d0
      a8=1.575994d0
      a9=0.045d0
      a10=71.69d0
      a11=0.01d0
      a12=200.0d0
      a13=0.19d0
      g0=a1+a2*dtanh(-a3*xx(3,j)/ct3+a4)-a5*((a6-xx(3,j)/ct3)**a7-
     1a8)-a9*expf(-a10*((xx(3,j)/ct3)**8.0d0))+a11
     1*expf(-a12*(xx(3,j)/ct3-a13))
      g1=(1.0d0/ct3)*(-a2*a3/dcosh(-a3*xx(3,j)/ct3+a4)/dcosh(-a3
     1*xx(3,j)/ct3+a4)+a5*a7*(a6-xx(3,j)/ct3)**(-1.0d0+a7)+
     1a9*a10*8.0d0*((xx(3,j)/ct3)**7.0d0)*expf(-a10*
     1(xx(3,j)/ct3)**8.0d0))-a11*a12/ct3*
     1expf(-a12*(xx(3,j)/ct3-a13))
c
      if (g0.gt.4.5) then
      g0=4.5d0
      g1=0.0d0
c     print*,'U theta overflow - positive'
      else if (g0.lt.3.0) then
      g0=3.0d0
      g1=0.0d0
c     print*,'U theta underflow - positive'
      end if
      go to 98
c  &&&&&&&&&&&&&&&&&&&&&&&&&&&&&&&&&&&&
c     Tungsten oxide (LixWO3 with 0<x<0.67)
c     literature data from Whittingham
c
  105 c1=2.8767d0
```

```
      c2=-0.9046d0
      c3=0.76679d0
      c4=-0.15975d0
      c5=0.671d0
      g0=c1+c2*xx(3,j)/ct3+c3*xx(3,j)*xx(3,j)/ct3/ct3+
     1c4*expf(100.0d0*(xx(3,j)/ct3-0.671))
      g1=c2/ct3+2.0d0*c3*xx(3,j)/ct3/ct3+
     1c4*100.0d0*expf(100.0d0*(xx(3,j)/ct3-0.671))/ct3
      go to 98
c  &&&&&&&&&&&&&&&&&&&&&&&&&&&&&&&&&&&
c     CoO2 (Cobalt dioxide)
c
  106 r1=4.825510
      r2=0.950237
      r3=0.913511
      r4=0.600492
      g0=r1-r2*expf(-((xx(3,j)/ct3-r3)/r4)**2.0d0)
      g1=2.0d0*r2*(xx(3,j)/ct3-r3)*expf(-((xx(3,j)/ct3
     1-r3)/r4)**2.0d0)/r4/r4/ct3
      go to 98
c  &&&&&&&&&&&&&&&&&&&&&&&&&&&&&&&&&&&
c     V2O5 (Vanadium oxide 0<y<0.95)
c
  107 r1=3.3059d0
      r2=0.092769d0
      r3=14.362d0
      r4=6.6874d0
      r5=0.034252d0
      r6=100.0d0
      r7=0.96d0
      r8=0.00724d0
      r9=80.0d0
      r10=0.01d0
      a2=xx(3,j)/ct3
      g0=r1+r2*dtanh(-r3*a2+r4)-r5*expf(r6*(a2-r7))+r8*expf(r9*
     1(r10-a2))
      g1=-r2*r3/dcosh(-r3*a2+r4)/dcosh(-r3*a2-r4)/ct3-r5*r6*expf(r6*
     1(a2-r7))/ct3-r8*r9*expf(r9*(r10-a2))/ct3
      go to 98
c  &&&&&&&&&&&&&&&&&&&&&&&&&&&&&&&&&&&
c     NiO2 (Nickel dioxide 0.45<y<1.0)
c
  108 r1=6.515d0
      r2=2.3192d0
      r3=5.3342d0
      r4=0.41082d0
```

```
      r5=200.0d0
      r6=0.44d0
      r7=0.24247d0
      r8=60.0d0
      r9=0.99d0
      a3=xx(3,j)/ct3
      g0=r1+r2*a3-r3*a3**0.5d0+r4*expf(r5*(r6-a3))-
     1r7*expf(r8*(a3-r9))
      g1=r2/ct3-0.5d0*r3*(xx(3,j)**-0.5d0)/ct3**0.5d0
     1-r4*r5*expf(r5*(r6-a3))/ct3-r7*r8*expf(r8*(a3-r9))/ct3
      go to 98
c  &&&&&&&&&&&&&&&&&&&&&&&&&&&&&&&&
c     Spinel Mn2O4 (Bellcore 0.17<y<1.0)
c
  109 a1=4.19829d0
      a2=0.0565661d0
      a3=14.5546d0
      a4=8.60942d0
      a5=0.0275479d0
      a6=0.998432d0
      a7=-0.492465d0
      a8=1.901110d0
      a9=0.157123d0
      a10=0.04738d0
      a11=0.810239d0
      a12=40.0d0
      a13=0.133875d0
      g0=a1+a2*dtanh(-a3*xx(3,j)/ct3+a4)-a5*((a6-xx(3,j)/ct3)**a7-
     1a8)-a9*expf(-a10*((xx(3,j)/ct3)**8.0d0))+a11
     1*expf(-a12*(xx(3,j)/ct3-a13))
      g1=(1.0d0/ct3)*(-a2*a3/dcosh(-a3*xx(3,j)/ct3+a4)/dcosh(-a3
     1*xx(3,j)/ct3+a4)+a5*a7*(a6-xx(3,j)/ct3)**(-1.0d0+a7)+
     1a9*a10*8.0d0*((xx(3,j)/ct3)**7.0d0)*expf(-a10*
     1(xx(3,j)/ct3)**8.0d0))-a11*a12/ct3*
     1expf(-a12*(xx(3,j)/ct3-a13))
c
      if (g0.gt.4.5) then
      g0=4.5d0
      g1=0.0d0
c     print*,'U theta overflow - positive'
      else if (g0.lt.3.0) then
      g0=3.0d0
      g1=0.0d0
c     print*,'U theta underflow - positive'
      end if
      go to 98
```

```
c%%%%%%%%%%%%%%%%%%%%%%%%%%%%%%%%%%%%%%%%%%%%%%%%%%%%%%%%%%%%%%%%%%%%%%%%%%%%
c
c     KINETIC EXPRESSIONS FOR THE POSITIVE ELECTRODE
c
c     h0 is the exchange current density (A/m2)
c     h1 is the derivative of io wrt solid concentration, xx(3,j)
c     h2 is the derivative of io wrt electrolyte concen., xx(1,j)
c
c  &&&&&&&&&&&&&&&&&&&&&&&&&&&&&&&&&&&&
c
c     NONAQUEOUS LIQUIDS
c
   98 if (lag.eq.1) go to 99
      alpha=0.5d0
      alphc=0.5d0
      h0=rka3*dsqrt(xx(1,j))*dsqrt(ct3-xx(3,j))*dsqrt(xx(3,j))
      h1=-rka3*dsqrt(xx(1,j))*dsqrt(ct3-xx(3,j))*dsqrt(xx(3,j))
     1*(1.0d0/(ct3-xx(3,j))-1.0d0/xx(3,j))/2.0d0
      h2=rka3*dsqrt(ct3-xx(3,j))*dsqrt(xx(3,j))/dsqrt(xx(1,j))/2.0d0
c
c  &&&&&&&&&&&&&&&&&&&&&&&&&&&&&&&&&&&&
c
c     POLYMER
c
c     alpha=0.5d0
c     alphc=0.5d0
c     h0=rka3*dsqrt(xx(1,j))*dsqrt(cmax-xx(1,j))*dsqrt(ct3-xx(3,j))
c    1*dsqrt(xx(3,j))
c     h1=-rka3*dsqrt(xx(1,j))*dsqrt(cmax-xx(1,j))*dsqrt(ct3-xx(3,j))
c    1*dsqrt(xx(3,j))*(1.0d0/(ct3-xx(3,j))-1.0d0/xx(3,j))/2.0d0
c     h2=-rka3*dsqrt(xx(3,j))*dsqrt(ct3-xx(3,j))*dsqrt(cmax-xx(1,j))
c    1*dsqrt(xx(1,j))*(1.0d0/(cmax-xx(1,j))-1.0d0/xx(1,j))/2.0d0
c
c  &&&&&&&&&&&&&&&&&&&&&&&&&&&&&&&&&&&&
c
      end if
c%%%%%%%%%%%%%%%%%%%%%%%%%%%%%%%%%%%%%%%%%%%%%%%%%%%%%%%%%%%%%%%%%%%%%%%%%%%%
      if (lag.eq.1) go to 99
c
      r1=alpha*frt
      if(j.le.n1+1) then
           an1=1.0d0
           an2=0.0d0
         else
           an1=0.0d0
           an2=1.0d0
```

```
      endif

      r2=r1*(xx(6,j)-xx(2,j)-g0-fc*xx(5,j)*(an1*ranode+an2*rcathde))
c
      de=-2.d0*r2-r2**3/3.d0
      if(dabs(r2).gt.1.0d-7) de=expf(-r2)-expf(r2)
      pe=expf(-r2)+expf(r2)
      b(3,1)=h2*de
      b(3,2)=h0*r1*pe
      b(3,6)=-b(3,2)
      b(3,3)=h1*de+h0*r1*g1*pe
      b(3,5)=1.0d0+fc*b(3,2)*(an1*ranode+an2*rcathde)
      g(3)=-h0*de+b(3,1)*xx(1,j)+b(3,2)*xx(2,j)+
     1b(3,3)*xx(3,j)+b(3,6)*xx(6,j)+(b(3,5)-1.0d0)*xx(5,j)
     &-b(3,1)*c(1,j)-b(3,2)*c(2,j)-b(3,6)*c(6,j)-b(3,3)*c(3,j)
     &-b(3,5)*c(5,j)
c
   99 return
      end
c**********************************************************************
      subroutine prop(nj,n2,n1)
      implicit real*8(a-h,o-z)
      parameter(maxt=900)
      common/const/ fc,r,t,frt,cur,ep3,ep2,pi,nneg,nprop,npos,
     1ep1,epf3,epf1,epp1,epp2,epp3,shape3,shape1
      common/var/ xp(10),xx(6,221),xi(6,221),xt(6,221,maxt)
      common/tprop/df(221),cd(221),tm(221),
     1ddf(221),dcd(221),dtm(221),dfu(221),d2fu(221)
      common/temp/ thk,htc,dudt,Cp,dens,tam,g0,ncell,lht
c
      do 99 j=1,nj
      ee=ep2+epp2
      if(j .lt. n1+2) ee=ep1+epp1
      if(j .gt. n2+n1) ee=ep3+epp3
      go to (1,2,3,4,5,6,7),nprop
    1 go to 101  ! AsF6 in methyl acetate
    2 go to 102  ! Perchlorate in PEO
    3 go to 103  ! Sodium Triflate in PEO
    4 go to 104  ! LiPF6 in PC (Sony cell simulation)
    5 go to 105  ! Perchlorate in PC (West's simulation)
    6 go to 106  ! Triflate in PEO
    7 go to 107  ! LiPF6 in EC/DMC and p(VdF-HFP) (Bellcore)
c
c  &&&&&&&&&&&&&&&&&&&&&&&&&&&&&&&&&&
c     AsF6 in methyl acetate
c
```

```
c     diffusion coefficient of the salt (m2/s)
  101 df(j)=(ee**1.5d0)*1.54d-09
      ddf(j)=0.0d0
c     conductivity of the salt (S/m)
      cd(j)=2.5d0*(ee**(1.5d0))
      dcd(j)=0.0d0
c     transference number of lithium
      tm(j)=0.20d0
      dtm(j)=0.0d0
c     activity factor for the salt
      dfu(j)=0.0d0
      d2fu(j)=0.0d0
      go to 99
c  &&&&&&&&&&&&&&&&&&&&&&&&&&&&&&&&
c     Perchlorate in PEO
c
c     diffusion coefficient of the salt (m2/s)
  102 df(j)=(ee**1.5d0)*1.78d-12
      ddf(j)=0.0d0
c     conductivity of the salt (S/m)
      cd(j)=1.6d-02*ee**(1.5d0)
      dcd(j)=0.0d0
c     transference number of lithium
      tm(j)=0.10d0
      dtm(j)=0.0d0
c     activity factor for the salt
      dfu(j)=0.0d0
      d2fu(j)=0.0d0
      go to 99
c  &&&&&&&&&&&&&&&&&&&&&&&&&&&&&&&&
c     Sodium Triflate in PEO
c
  103 r0=1.3041d-07
      r1=4.4978d-07
      r2=-3.1248d-07
      r3=-2.2383d-07
      r4=8.9264d-09
c
c     diffusion coefficient of the salt (m2/s)
      df(j)=0.0001d0*(ee**1.5d0)*(r0+r1*xx(1,j)/1000+
     1r2*((xx(1,j)/1000)**0.5d0) + r3*((xx(1,j)/1000)**1.5d0)
     1+ r4*((xx(1,j)/1000)**3.0d0))
      ddf(j)=0.0001d0*(ee**1.5d0)*(r1/1000d0 +
     10.5d0*r2*(xx(1,j)**(-0.5d0))/(1000.0d0**0.5d0)
     1+ 1.5d0*r3*(xx(1,j)**0.5d0)/1000d0**1.5d0 +
     13.0d0*r4*(xx(1,j)**2.0d0)/1000d0**3.0d0)
```

```
      if (xx(1,j).ge.3.0d03) then
      df(j)=(ee**1.5d0)*1.6477d-12
      ddf(j)=0.0d0
      end if
c     conductivity of the salt (S/m)
      r7=4.32d-05
      r8=0.00017d0
      r9=0.000153d0
      r10=3.73d-05
c
      cd(j)=100*(ee**(1.5d0))*(r7+r8*xx(1,j)/1000+r9*xx(1,j)*xx(1,j)
     1/1000000+r10*xx(1,j)*xx(1,j)*xx(1,j)/1000000000)
      dcd(j)=100*(ee**(1.5d0))*(r8/1000+2.0*r9*xx(1,j)/1000000+
     13.0*r10*xx(1,j)*xx(1,j)/1000000000)
c
c     transference number of lithium
c
      if(xx(1,j).lt.0.3d03) then
      r5=0.32141d0
      r6=2.5768d0
      r11=71.369d0
      r12=643.63d0
      r13=1983.7d0
      r14=2008.d0
      r15=287.46d0
      tm(j)=r5-r6*xx(1,j)/1000.+r11*xx(1,j)*xx(1,j)/1000000.
     1-r12*((xx(1,j)/1000.)**(3.0d0))+r13*((xx(1,j)/1000.)**4.0d0)
     1-r14*((xx(1,j)/1000.)**(5.0d0))+r15*((xx(1,j)/1000.)**6.0d0)
      dtm(j)=-r6/1000.+2.0d0*r11*xx(1,j)/1000000.-
     13.0d0*r12*(xx(1,j)**2.0d0)/(1000.**3.0d0) +
     14.0d0*r13*(xx(1,j)**3.0d0)/(1000.**4.0d0) -
     15.0d0*r14*(xx(1,j)**4.0d0)/(1000.**5.0d0) +
     16.0d0*r15*(xx(1,j)**5.0d0)/(1000.**6.0d0)
      else
      tm(j)=0.0d0
      dtm(j)=0.0d0
      end if
c
      if(xx(1,j).ge.0.70d03) then
      r5=4.5679d0
      r6=4.506d0
      r11=0.60173d0
      r12=1.0698d0
      tm(j)=-r5+r6*expf(-((xx(1,j)/1000.-r11)/r12)**2.)
      dtm(j)=-r6*(xx(1,j)/1000.-r11)*2.
     1*expf(-((xx(1,j)/1000.-r11)/r12)**2.)/r12/r12/1000.
```

```
      end if
c
      if(xx(1,j).ge.2.58d03) then
      tm(j)=-4.4204d0
      dtm(j)=0.0d0
      end if
c
c     activity factor for the salt:  (dlnf/dc) and (d2lnf/dc2)
c
      if(xx(1,j).gt.0.45d03) then
      r17=0.98249d0
      r18=1.3527d0
      r19=0.71498d0
      r20=0.16715d0
      r21=0.014511d0
      thermf=r17-r18*xx(1,j)/1000.+r19*xx(1,j)*xx(1,j)/1000000.-
     1r20*xx(1,j)*xx(1,j)*xx(1,j)/1000000000.+r21*xx(1,j)*xx(1,j)
     1*xx(1,j)*xx(1,j)/1000000000000.
      dthermf=-r18/1000.+2.*r19*xx(1,j)/1000000.-
     13.*r20*xx(1,j)*xx(1,j)/1000000000.+4.*r21*xx(1,j)*xx(1,j)
     1*xx(1,j)/1000000000000.
      end if
c
      if(xx(1,j).le.0.45d03) then
      r23=0.99161d0
      r24=0.17804d0
      r25=55.653d0
      r26=303.57d0
      r27=590.97d0
      r28=400.21d0
      thermf=r23-r24*xx(1,j)/1000.-r25*xx(1,j)*xx(1,j)/1000000.+
     1r26*xx(1,j)*xx(1,j)*xx(1,j)/1000000000.-r27*xx(1,j)*xx(1,j)
     1*xx(1,j)*xx(1,j)/1000000000000.+r28*xx(1,j)*xx(1,j)*xx(1,j)
     1*xx(1,j)*xx(1,j)/1000000000000000.
      dthermf=-r24/1000.-2.*r25*xx(1,j)/1000000.+
     13.*r26*xx(1,j)*xx(1,j)/1000000000.-4.*r27*xx(1,j)
     1*xx(1,j)*xx(1,j)/1000000000000.+5.*r28*xx(1,j)*xx(1,j)
     1*xx(1,j)*xx(1,j)/1000000000000000.
      end if
c
      dfu(j)=(-1.+2.*thermf)/xx(1,j)
      d2fu(j)=1./xx(1,j)/xx(1,j)-2.*thermf/xx(1,j)/xx(1,j)+
     12.*dthermf/xx(1,j)
c
      if(xx(1,j).ge.3.00d03) then
      dfu(j)=-0.9520/xx(1,j)
```

```
      d2fu(j)=0.9520/xx(1,j)/xx(1,j)
      end if
      go to 99
c  &&&&&&&&&&&&&&&&&&&&&&&&&&&&&&&&&&&&
c     LiPF6 in PC (Sony cell simulation)
c
c     this is actually the diff coeff for perchlorate
c     diffusion coefficient of the salt (m2/s)
  104 df(j)=(ee**1.5d0)*2.58d-10
      ddf(j)=0.0d0
c     conductivity of the salt (S/m)
c     pmax=0.5409
      pmax=0.035d0
      pu=0.857d0
      aa=1.093
      bb=0.04d0
      rho=1.2041d03
      fun=pmax*((1.0d0/rho/pu)**aa)*expf(bb*((xx(1,j)/rho-pu)**2.0)
     1-(aa/pu)*(xx(1,j)/rho-pu))
      fun2=2.0d0*(bb/rho)*(xx(1,j)/rho-pu)-aa/pu/rho
      cd(j)=0.0001+(ee**1.5d0)*((xx(1,j))**aa)*fun
      dcd(j)=(ee**1.5d0)*fun*(aa*(xx(1,j)**(aa-1.0d0))+(xx(1,j)**aa)
     1*fun2)
c     transference number of lithium
      tm(j)=0.20d0
      dtm(j)=0.0d0
c
c     activity factor for the salt (dlnf/dc and d2lnf/dc2)
      dfu(j)=0.0d0
      d2fu(j)=0.0d0
      go to 99
c  &&&&&&&&&&&&&&&&&&&&&&&&&&&&&&&&&&&&
c     Perchlorate in PC (West's simulation)
c
c     diffusion coefficient of the salt (m2/s)
  105 df(j)=(ee**1.5d0)*2.58d-10
      ddf(j)=0.0d0
c     conductivity of the salt (S/m)
      pmax=0.542d0
      pu=0.6616d0
      aa=0.855d0
      bb=-0.08d0
      rho=1.2041d03
      fun=pmax*((1.0d0/rho/pu)**aa)*expf(bb*((xx(1,j)/rho-pu)**2.0)
     1-(aa/pu)*(xx(1,j)/rho-pu))
      fun2=2.0d0*(bb/rho)*(xx(1,j)/rho-pu)-aa/pu/rho
```

```
      cd(j)=0.0001+(ee**1.5d0)*((xx(1,j))**aa)*fun
      dcd(j)=(ee**1.5d0)*fun*(aa*(xx(1,j)**(aa-1.0d0))+
     1(xx(1,j)**aa)*fun2)
c     transference number of lithium
      tm(j)=0.20d0
      dtm(j)=0.0d0
c     activity factor for the salt
      dfu(j)=0.0d0
      d2fu(j)=0.0d0
      go to 99
c  &&&&&&&&&&&&&&&&&&&&&&&&&&&&&&&&&&
c     Triflate in PEO
c
  106 r0=-5.0891863844d-05
      r1=8.38645199394d-07
      r2=-5.19747901855d-10
      r3=8.0832709407d-14
c     diffusion coefficient of the salt (m2/s)
      df(j)=(ee**1.5d0)*7.5d-12
      ddf(j)=0.0d0
c     conductivity of the salt (S/m)
      cd(j)=(ee**(1.5d0))*100.0d0*(r0 + r1*xx(1,j)
     1+r2*xx(1,j)*xx(1,j)+r3*xx(1,j)*xx(1,j)*xx(1,j))
      dcd(j)=(ee**1.5d0)*100.0d0*(r1 + 2.0d0*r2*xx(1,j) +
     13.0d0*r3*xx(1,j)**2.0d0)
c     transference number of lithium
c     rough conc. dependence of t+ - highly suspect
      tm(j)=0.0107907d0 + 1.48837d-04*xx(1,j)
      dtm(j)=1.48837d-04
c     activity factor for the salt
      dfu(j)=0.0d0
      d2fu(j)=0.0d0
      go to 99
c  &&&&&&&&&&&&&&&&&&&&&&&&&&&&&&&&&&
c     LiPF6 in EC/DMC and p(VdF-HFP) (Bellcore)
c     D and t+ given below were fit from discharge curves
c
c     diffusion coefficient of the salt (m2/s)
  107 df(j)=(ee**1.5d0)*9.00d-11
      ddf(j)=0.0d0
c
c     conductivity of the salt (S/m)
c     This is the conductivity of the liquid + salt only (no polymer)
c
c     kappa (c) for EC/DMC 2:1 with LiPF6 at 25 deg C
c     cd(j)=(ee**1.5d0)*(0.0911+1.9101*xx(1,j)/1000-1.052*xx(1,j)*
```

```
c     1xx(1,j)/1000/1000+0.1554*(xx(1,j)/1000)**3.0d0)
c      derivative of kappa (c) for EC/DMC 2:1 at 25 deg C
c      dcd(j)=(ee**1.5d0)*(1.9101/1000-2.0*1.052*xx(1,j)/1000/1000
c     1+3.0*0.1554/1000*(xx(1,j)/1000)**2.0d0)
c
c      kappa (c) for EC/DMC 1:2 w/ LiPF6 at 25 deg C
c      Note Bruggeman exponent should be adjusted to account for
c      polymer phase - this also affects "fac" parameter in Ohm's law
       r1=0.00010793d0
       r2=0.0067461d0
       r3=0.0052245d0
       r4=0.0013605d0
       r5=0.00011724d0
       cd(j)=(ee**4.2d0)*(r1+r2*xx(1,j)/1000
      1-r3*xx(1,j)*xx(1,j)/1000000
      1+r4*(xx(1,j)/1000)**3.0d0-r5*(xx(1,j)/1000)**4.0d0)*100
       dcd(j)=(ee**4.2d0)*(r2/10-r3*2.0d0*xx(1,j)/10000
      1+3.0d0*r4*xx(1,j)*xx(1,j)/10000000
      1-0.4d0*r5*(xx(1,j)/1000)**3.0d0)
c
c      transference number of lithium
       tm(j)=0.363d0
       dtm(j)=0.0d0
c
c      activity factor for the salt (dlnf/dc and d2lnf/dc2)
       dfu(j)=0.0d0
       d2fu(j)=0.0d0
       go to 99
c   &&&&&&&&&&&&&&&&&&&&&&&&&&&&&&&&&
c
    99 continue
c
       return
       end
c*********************************************************************
c      That's All Folks!
c*********************************************************************
```

# FOIL program

```
**********************************************************************
c
c     foil.f  (foil version 2.0) January 15, 1995
c     Model for li/polymer/insertion cell
c
c     Significant revisions:
c  1. The input file is new and should be easier to read.
c  2. Film resistance is added in both electrodes.
c  3. Driving profiles are added (see input file).
c  4. Power pulses are added but are not generally activated.
c  5. Concentration profiles in the solid versus time can be
c     obtained, but are not generally activated.
c  6. Temperature rise and the use of a heat-transfer
c     coefficient have been added (see input file).
c  7. Material balances in the electrolyte have been modified
c     to give an absolute overall balance.
c  8. Ekin and prop (the user subroutines) have been modified
c     to make them easier to change from case to case and to see
c     what is valid and what is obsolete.  (See npos and nprop.)
c  9. Some robustness has been incorporated to make it easier
c     to avoid underflows and concentrations (solid or
c     electrolyte) less than zero or greater than saturation.
c     Change variables (Electrochemical Systems, pp. 549-550)
c     have been incorporated.
c**********************************************************************
c  Power pulses should be activated as follows:
c     Call subroutine peak should be uncommented - 15-second current
c     pulses of increasing size are applied until the power goes
c     through a maximum.  This is performed at the end of any
c     previously requested discharge or charge steps.
c     Note that the use of power pulses can be tricky because
c     the solution may be impossible to obtain at a current
c     which gives a power less than the previous current.
c
c  Solid-phase concentration profile is activated as follows:
c     Call subroutine sol with a given time step # and node #.  Must
c     be careful that the requested node # is inside the positive
c     electrode.  The lithium concentration in the solid is printed
c     versus radius into the particle at the requested time and
c     position.
c
c**********************************************************************
      implicit real*8(a-h,o-z)
      parameter(maxt=900)
```

```
      common /n/ nx,nt,n1,n2,nj
      common /calc/ ai(maxt),u(222,900),ts(maxt),h,h1,h2,hcp,
     1hcn,rr
      common/const/ fc,r,t,frt,cur,ep,epf,eps,epp,epps,pi,nneg,
     1nprop,npos
      common/power/ ed,Vold,ranode,rcathde
      common/ssblock/ xp0(5),xx0(5,221),term(221)
      common/var/ xp(10),xx(5,221),xi(5,221),xt(5,221,maxt)
      common/cprop/ sig,area,ct,dfs,Rad,cmax,rka,rkf,tmmax,g01
      common/temp/thk,htc,dudt,Cp,dens,tam,ncell,tin,lht
      common/tprop/df(221),cd(221),tm(221),
     1ddf(221),dcd(221),dtm(221),dfu(221),d2fu(221)
      dimension tt(16),cu(16)
   44 format(/'           mass  = ',f7.4,' kg/m2')
   45 format('specific energy  = ',f8.2,' W-h/kg')
   46 format('specific power   = ',f8.2,' W/kg')
c
      n=5
c     n is number of equations
      data fc/96487.0d0/, r/8.314d0/, pi/3.141592653589d0/
      rr=1.0  ! initial time step is 1 s.
c
c*************************************************************
      print*,'    FOIL VERSION 2.0'
c     Read in and Print out Parameters
c
      read *, lim !limit on number of iterations
      read *, h1  !thickness of separator (m)
      read *, h2  !thickness of positive electrode (m)
      read *, hcn !thickness of neg. electrode current collector (m)
      read *, hcp !thickness of pos. electrode current collector (m)
      read *, n1  !number of nodes in separator
      read *, n2  !number of nodes in positive electrode
      read *, t   !temperature (K)
 1101 format (i7,'  lim, limit on number of iterations'
     &/1x,f6.2,'  h1,  thickness of separator (microns)'
     &/1x,f6.2,'  h2,  thickness of positive electrode (microns)'
     &/1x,f6.2,'  hcn, ',
     &'thickness of neg. electrode current collector (microns)'
     &/1x,f6.2,'  hcp, thickness of pos. electrode current'
     &,' collector (microns)'
     &/i7,'  n1,  number of nodes in separator'
     &/i7,'  n2,  number of nodes in positive electrode'
     &/1x,f6.2, '  T,   temperature (K)')
      print 1101, lim,1.d6*h1,1.d6*h2,1.d6*hcn,1.d6*hcp,n1,n2,t
      n1=n1+1
```

```
      nj = n1 + n2
      read *, xi(1,1)!initial concentration (mol/m3)
      read *,csy   !initial stochiometric parameter for electrode
      read *, tmmax!maximum time step size (s)
      read *, vcut !cutoff potential
      read *, dfs !diffusion coefficient in solid (m2/s)
      read *, Rad !radius of particles (m)
 1102 format (/1x,f6.1,'  xi(1,1), initial concentration (mol/m3)'
     &/1x,f6.2,'  csy, initial stoichiometric parameter for electrode'
     &/1x,f6.1,'  tmmax, maximum time step size (s)'
     &/1x,f6.2,'  vcut,  cutoff potential'
     &/1x,e6.1,'  dfs, diffusion coefficient in solid (m2/s)'
     &/1x,f6.2,'  Rad, radius of particles (microns)')
      print 1102, xi(1,1),csy,tmmax,vcut,dfs,1.d6*Rad
      read *, ep  !vol. frac. of electrolyte in composite electrode
      read *, epf !vol. frac. of inert filler in composite electrode
      read *, epp !vol. frac. of polymer phase in composite electrode
      read *, eps !volume fraction of electrolyte in separator
      read *, epps !volume fraction of polymer phase in separator
      read *, sig !conductivity of solid matrix (S/m)
      read *, capt !coulombic capacity of insertion material (mAh/g)
      read *, cmax!maximum concentration in electrolyte      (mol/m3)
      read *, rka !reaction rate constant for insertion reaction
      read *, rkf !exchange current density for lithium foil
      read *, il4 !1 for polymer, 0 for liquid electrolyte
 1103 format (/1x,f6.2,'  ep,'
     &,'   volume fraction of electrolyte in composite electrode'
     &/1x,f6.2,'  epf,'
     &,'  volume fraction of inert filler in composite electrode'
     &/1x,f6.2,'  epp,'
     &,'  volume fraction of polymer phase in composite electrode'
     &/1x,f6.2,'  eps, vol. frac. of electrolyte in separator'
     &/1x,f6.2,'  epps, vol. frac. of polymer phase in separator'
     &/1x,f6.2,'  sig,  conductivity of solid matrix (S/m)'
     &/1x,f6.2,'  capt, coulombic capacity of insertion material'
     &,' (mAh/g)'
     &/1x,f6.0,'  cmax, maximum conc. in electrolyte (mol/m3)'
     &/1x,e6.1,'  rka, reaction rate constant for insertion reaction'
     &/1x,f6.4,'  rkf, exchange current density for lithium foil'
     &/i7,'  il4,  1 for polymer, 0 for liquid electrolyte')
      print 1103, ep,epf,epp,eps,epps,sig,capt,cmax,rka,rkf,il4
      read *, re !density of electrolyte (kg/m3)
      read *, rs !density of insertion material (kg/m3)
      read *, rf !density of inert filler (kg/m3)
      read *, rp !density of polymer phase (kg/m3)
      read *, rc !density of separator material (kg/m3)
```

```
      read *, ef !excess capacity of lithium foil
      read *, rcn !density of negative current collector (kg/m3)
      read *, rcp !density of positive current collector (kg/m3)
 1104 format (/1x,f6.1,'  re,   density of electrolyte (kg/m3)'
     &/1x,f6.1,'  rs,   density of insertion material (kg/m3)'
     &/1x,f6.1,'  rf,   density of inert filler (kg/m3)'
     &/1x,f6.1,'  rp,   density of polymer phase (kg/m3)'
     &/1x,f6.1,'  rc,   density of separator material (kg/m3)'
     &/1x,f6.3,'  ef,   excess capacity of lithium foil'
     &/1x,f6.1,'  rcn,  density of neg. current collector (kg/m3)'
     &/1x,f6.1,'  rcp,  density of pos. current collector (kg/m3)')
      print 1104, re,rs,rf,rp,rc,ef,rcn,rcp
      read *, ranode  !anode film resistance
      read *, rcathde !cathode film resistance
      read *, htc !heat transfer coeff. with external medium (W/m2K)
      read *, dudt !temperature coefficient of EMF (V/K)
      read *, Cp   !heat capacity of cell (J/kgK)
      read *, tam  !ambient temperature (K)
      read *, ncell!number of cells in a cell stack
      read *, lht  !0 temp varies, 1 uses htc, 2 isothermal
 1105 format (/1x,f6.1,'  ranode,   anode film resistance (ohm-m2)'
     &/1x,f6.1,'  rcathde,  cathode film resistance (ohm-m2)'
     &/1x,f6.2,'  htc,    heat transfer coefficient with'
     &,' external medium (W/m2K)'
     &/1x,f6.2,'  dUdT,  temperature coefficient of EMF (V/K)'
     &/1x,f6.1,'  Cp,     heat capacity of cell (J/kg-K)'
     &/1x,f6.2,'  Tam,    ambient temperature (K)'
     &/i7,'  ncell, number of cells in a cell stack'
     &/i7,'  lht,    0 adiabatic,  1 uses htc,  2 isothermal')
      print 1105, ranode,rcathde,htc,dudt,Cp,tam,ncell,lht
      read *, il1 !1 for long print-out 0 for short print-out
      read *, il2 !1/il2 = fraction of nodes in long print-out
      read *, il3 !1/il3 = fraction of time steps in long print-out
      read *, nprop ! designates electrolyte system
      read *, npos  ! designates positive electrode system
      read *, lcurs! number of current changes
 1106 format (/i7,' il1, 1 for long print-out  0 for short print-out'
     &/i7,'  il2,    prints every il2 th node in long print-out'
     &/i7,'  il3,    prints every il3 th time step in long print-out'
     &/i7,'  lcurs, number of current changes')
      print 1106, il1,il2,il3,lcurs
      go to (101,102,103,104,105,106),nprop
  101 print *, 'AsF6 in methyl acetate'
      go to 200
  102 print *, 'Perchlorate in PEO'
      go to 200
```

```
  103 print *, 'Sodium Triflate in PEO'
      go to 200
  104 print *, 'LiPF6 in PC (Sony cell simulation)'
      go to 200
  105 print *, 'Perchlorate in PC (West simulation)'
      go to 200
  106 print *, 'Triflate in PEO'
      go to 200
  200 go to (201,202,203,204,205,206,207,208),npos
  201 print *, 'TiS2'
      go to 300
  202 print *, 'Spinel Mn2O4 (lower plateau)'
      go to 300
  203 print *, 'NaCoO2:  Sodium cobalt oxide'
      go to 300
  204 print *, 'Spinel Mn2O4 (upper plateau)'
      go to 300
  205 print *, 'Tungsten oxide (LixWO3 with 0<x<0.67)'
      go to 300
  206 print *, 'CoO2 (Cobalt dioxide)'
      go to 300
  207 print *, 'V2O5 (Vanadium oxide)'
      go to 300
  208 print *, 'NiO2 (Nickel dioxide)'
      go to 300
  300 read *,(cu(i),tt(i), i=1,lcurs)
c    cu(i)  operating current density (A/m2)
c    tt(i)       time (min)
c
      xi(1,nj)=xi(1,1)
      ct=3.6d03*capt*rs/fc
      call ekin(1,1,csy,il4)
      xi(2,nj)=g01
      xi(2,1)=g01+0.05d0
c
c     Calculate thickness of lithium foil and full cell:
      hli=ef*(1.0d0-ep-epf-epp)*(ct)*(1.-csy)*h2*6.941
     1/1.0d03/542.0d0
      thk=h1+h2+hli+hcn+hcp
c     print*,'thicknesses are ',hcn,hli,h1,h2,hcp,thk
c
      xi(3,n1)=csy*ct
      xi(3,nj)=xi(3,n1)
c
      xi(4,1)=cu(1)
      xi(5,nj)=-1.0d-07
```

```
c
      tt(1)=6.0d01*tt(1)
      do 51 i=2,lcurs
   51 tt(i)=tt(i-1)+6.0d01*tt(i)
c
c     rr is the size of a time step and should equal dt times
c     the radius squared over dfs, nt the number of steps
      dt=rr*dfs/Rad/Rad
      ts(1)=0.0d0
c
      area=3.0d0*(1.0d0-ep-epf)/Rad
      sig=sig*((1.0d0-ep-epf-epp)**(1.5d0))
      h1=h1/dble(n1-1)
      h2=h2/dble(n2)
      frt=fc/(r*t)
c
      print*,' '
      if (lht.eq.2) then
      print*,' util  ',' cell pot  ',' material',' time ',
     1'  time step'
      print*,'   y   ','     (V)     ',' balance','     (min) '
      else
      if (lht.eq.0) then
      print*,' util  ',' cell pot  ',' temp  ',' heat gen',
     1'  time step'
      print*,'   y   ','     (V)     ','  (K)  ','      (J)  '
      else
      if (lht.eq.1) then
      print*,' util  ',' cell pot  ',' htcoeff ',' time  ',
     1'  time step'
      print*,'   y   ','     (V)     ',' (W/m2K) ',' (min)'
      else
      continue
      end if
      end if
      end if
c
c*************************************************************
c
      call guess(n)
      call mass(tw,re,rs,rf,rp,rc,ef,rcn,rcp)
      dens=tw/thk
c
c%%%%%%%%%%%%%%%%%%%%%%%%%%%%%%%%%%%%%%%%%%%%
c
      cur=cu(1)
```

```
      call zts(n,lim,2,dt,1,il4)
c     guess/zts set the initial guesses/zero-time-step values.
c
      k=1
      call cellpot(k,il4,vv,1)
c
      iflag=0
      do 53 l=1,lcurs
  123 k=k+1
      nt=k-1
c
c     adjust time step to match time of change in current
c
      if (time .gt. tt(l)) then
      dt=tt(l)*dfs/Rad/Rad-ts(k-1)
      rr=dt*Rad*Rad/dfs
      iflag=1
      endif
c
      ts(k)=ts(k-1)+dt
      call calca(k)
      dtnow=rr
      call comp(n,lim,k,dt,1,tw,il4,jcount)
      if (rr.lt.dtnow) iflag=0
c     sets values for time step k
c
      do 10 i=1,n
      do 10 j=1,nj
   10 xt(i,j,k)=xx(i,j)
c
      call cellpot(k,il4,vv,1)
      if (vv.lt.vcut) go to 100  ! cutoff potential exceeded:
c
c     Increasing time steps:
      if(jcount.lt.6 .and. k.gt.5 .and. 2.0d0*rr.lt.tmmax .and.
     1   iflag.eq.0) then
         dt=dt*2.0d0
         rr=rr*2.0d0
         print*,'next time step increased to ', rr,'(s)'
       end if

       if(k.eq.maxt) then
         print*,'kmax=',k,' a larger matrix needed for xt'
         go to 100
       endif
```

```
c     anticipate time at next time step
      time=(ts(k)+dt)*Rad*Rad/dfs
c
      if (iflag .eq. 0) go to 123
      cur=cu(l+1)
      iflag=0
c     calculate zero time solution for change in current
      if (l .lt. lcurs) then
      k=k+1
      ts(k)=ts(k-1)
      call zts(n,lim,k,dt,k,il4)
      call cellpot(k,il4,vv,1)
      endif
      rr=2.0d0
   53 dt=rr*dfs/Rad/Rad
c
c%%%%%%%%%%%%%%%%%%%%%%%%%%%%%%%%%%%%%%%%%%%%%%%%%%%%%%%%%%
c
  100 if(il1 .eq. 1) call nucamb(n,il2,il3)
c     call sol(10,81)
c     call sol(30,81)
c     call sol(60,81)
c     call sol(90,81)
      ed=ed/tw/3.6d03
      pow=3.6d03*dfs*ed/ts(k)/Rad/Rad
      print44,tw
      print45,ed
      print46,pow
c     call peak(n,lim,il4,cu(1))
      end
c
c*********************************************************************
      subroutine comp(n,lim,kk,tau,li,tw,il4,jcount)
      implicit real*8(a-h,o-z)
      parameter(maxt=900)
      common /n/ nx,nt,n1,n2,nj
      common /calc/ ai(maxt),u(222,900),ts(maxt),h,h1,h2,hcp,
     1hcn,rr
      common/const/ fc,r,t,frt,cur,ep,epf,eps,epp,epps,pi,nneg,
     1nprop,npos
      common/power/ ed,Vold,ranode,rcathde
      common/ssblock/ xp0(5),xx0(5,221),term(221)
      common/var/ xp(10),xx(5,221),xi(5,221),xt(5,221,maxt)
      common/cprop/ sig,area,ct,dfs,Rad,cmax,rka,rkf,tmmax,g01
      common/temp/thk,htc,dudt,Cp,dens,tam,ncell,tin,lht
      common/tprop/df(221),cd(221),tm(221),
```

```
      1ddf(221),dcd(221),dtm(221),dfu(221),d2fu(221)
       common/mat/ b,d
       common/bnd/ a,c,g,x,y
       dimension b(10,10),d(10,21),termn(221)
       dimension a(10,10),c(10,221),g(10),x(10,10),y(10,10)
c
       nx=n
c
  666 continue
       if (li .eq. 1) then
       do 1 j=1,nj
       do 1 i=1,n
            c(i,j)=xt(i,j,kk-1)
    1       xx(i,j)=xt(i,j,kk-1)
c      sets first guess to last time step values
       else
       do 81 j=1,nj
       do 81 i=1,n
            c(i,j)=xt(i,j,kk)
   81       xx(i,j)=xt(i,j,kk)
       endif
       jcount=0
       do 4 i=1,n
    4       xp(i)=0.0d0
c      initialize variables to begin each iteration
c      (jcount is iteration #)
    8 j=0
       jcount=jcount+1
       call prop(nj,n1)
c      obtains physical properties at this specific point
       do 9 i=1,n
       do 9 k=1,n
            x(i,k)=0.0d0
    9       y(i,k)=0.0d0
c
c      store previous iteration of  (xp in xp0)  &  (xx in xx0)
       do 6 i=1,n
            xp0(i)=xp(i)
    6       xx0(i,n1+10)=xx(i,n1+10)
c
c      for a given iteration, set up governing equations and bc's
c      start at the left interface and move across polymer
c
   10 j=j+1
c
       do 11 i=1,n
```

```
            g(i)=0.0d0
         do 11 k=1,n
               a(i,k)=0.0d0
               b(i,k)=0.0d0
   11          d(i,k)=0.0d0
c        clears all arrays before use
c
c        Equation 1, mass balance
c        Red alert.  if kk.ne.2 but we just changed the current,
c        we are in trouble.
c        Also, properties should be evaluated at old time step
c        (composition and temperature).
         if(kk.eq.2 .and. jcount.eq.1) then
         term(j)=0.
         epn=eps
         hn=h1
         if(j.gt.n1) epn=ep
         if(j.gt.n1) hn=h2
         fac=1.
         if(j.eq.n1+1) fac=(ep/eps)**1.5
         if(j.ne.1) term(j)=
        &-(df(j)+fac*df(j-1))*(c(1,j)-c(1,j-1))/hn/2.
        &-(1.-0.5*(tm(j)+tm(j-1)))*(c(4,j)+c(4,j-1))/2./fc
         if(j.eq.n1) epn=ep
         if(j.eq.n1) hn=h2
         fac=1.
         if(j.eq.n1) fac=(ep/eps)**1.5
         if(j.ne.nj) term(j)=term(j)+
        &-(fac*df(j)+df(j+1))*(c(1,j)-c(1,j+1))/hn/2.
        &+(1.-0.5*(tm(j)+tm(j+1)))*(c(4,j)+c(4,j+1))/2./fc
         endif

         termn(j)=0.
         fac=1.
         if(j.eq.n1+1) fac=(ep/eps)**1.5
         epn=eps
         hn=h1
         if(j.gt.n1) epn=ep
         if(j.gt.n1) hn=h2
         if(j.ne.1) then ! deal with box to left of point.
         termn(j)=-(df(j)+fac*df(j-1))*(c(1,j)-c(1,j-1))/hn/2.
        &-(1.-0.5*(tm(j)+tm(j-1)))*(c(4,j)+c(4,j-1))/2./fc
         a(1,1)=epn*hn*0.125/rr
        &-(df(j)+fac*df(j-1))/hn/4.+fac*ddf(j-1)*(c(1,j)-c(1,j-1))/hn/4.
        &-dtm(j-1)*(c(4,j)+c(4,j-1))/8./fc
         b(1,1)=epn*hn*0.375/rr
```

```
     &+(df(j)+fac*df(j-1))/hn/4.+ddf(j)*(c(1,j)-c(1,j-1))/hn/4.
     &-dtm(j)*(c(4,j)+c(4,j-1))/8./fc
      a(1,4)=(1.-0.5*(tm(j)+tm(j-1)))/4./fc
      b(1,4)=(1.-0.5*(tm(j)+tm(j-1)))/4./fc
      g(1)=-epn*hn*(0.375*(c(1,j)-xt(1,j,kk-1))
     &+0.125*(c(1,j-1)-xt(1,j-1,kk-1)))/rr
      endif
      fac=1.
      if(j.eq.n1) fac=(ep/eps)**1.5
      if(j.eq.n1) epn=ep
      if(j.eq.n1) hn=h2
      if(j.ne.nj) then ! deal with box to right of point.
      termn(j)=termn(j)-(fac*df(j)+df(j+1))*(c(1,j)-c(1,j+1))/hn/2.
     &+(1.-0.5*(tm(j)+tm(j+1)))*(c(4,j)+c(4,j+1))/2./fc
      d(1,1)=epn*hn*0.125/rr
     &-(fac*df(j)+df(j+1))/hn/4.+ddf(j+1)*(c(1,j)-c(1,j+1))/hn/4.
     &+dtm(j+1)*(c(4,j)+c(4,j+1))/8./fc
      b(1,1)=b(1,1)+epn*hn*0.375/rr
     &+(fac*df(j)+df(j+1))/hn/4.+fac*ddf(j)*(c(1,j)-c(1,j+1))/hn/4.
     &+dtm(j)*(c(4,j)+c(4,j+1))/8./fc
      d(1,4)=-(1.-0.5*(tm(j)+tm(j+1)))/4./fc
      b(1,4)=b(1,4)-(1.-0.5*(tm(j)+tm(j+1)))/4./fc
      g(1)=g(1)-epn*hn*(0.375*(c(1,j)-xt(1,j,kk-1))
     &+0.125*(c(1,j+1)-xt(1,j+1,kk-1)))/rr
      endif
      g(1)=g(1)+(termn(j)+term(j))/2.
c
c     ------------------------------------------------------
c
      if(j.ne.1) go to 13
c
c     specify boundary conditions at left interface (j=1)
c     boundary conditions at negative electrode
      h=h1
c
      dcf=(xx(1,j+1)-xx(1,j))/h
      r1=(xx(1,j+1)+xx(1,j))/2.0d0
      p1=(tm(j)+tm(j+1))/2.0d0
      p2=(cd(j)+cd(j+1))/2.0d0
      p3=(dtm(j)+dtm(j+1))/2.0d0
      p4=(dfu(j)+dfu(j+1))/2.0d0
      p6=(d2fu(j)+d2fu(j+1))/2.0d0
      d(2,1)=(1.0d0-p1)*(1.0d0/r1+p4)/h
      b(2,1)=-d(2,1)+((1.0d0-p1)*(p6-1.0d0/r1/r1)*dcf
     1       -(1.0d0/r1+p4)*dcf*p3)/2.0d0
      d(2,1)=d(2,1)+((1.0d0-p1)*(p6-1.0d0/r1/r1)*dcf
```

```
     1       -(1.0d0/r1+p4)*dcf*p3)/2.0d0
      d(2,2)=frt/h
      b(2,2)=-frt/h
      g(2)=frt*cur/p2+(1.0d0-p1)*(p6-1.0d0/r1/r1)*dcf*r1 -
     1     (1.0d0/r1+p4)*dcf*p3*r1
     &-((1.0d0-p1)*(1.0d0/r1+p4)/h)*(c(1,j+1)-c(1,j))
     &-(((1.0d0-p1)*(p6-1.0d0/r1/r1)*dcf
     1-(1.0d0/r1+p4)*dcf*p3)/2.0d0)*(c(1,j)+c(1,j+1))
     &+frt/h*(c(2,j)-c(2,j+1))
c
      b(3,5)=1.0d0
      g(3)=-c(5,j)
      b(4,3)=1.0d0
      g(4)=-c(3,j)
      b(5,4)=1.0d0
      g(5)=cur-c(4,j)
c
      call band(j)
      go to 10
c
c     ------------------------------------------------
c     specify governing equations in polymer separator
  13  if (j .ge. n1) go to 110
c
      dcf=(xx(1,j+1)-xx(1,j))/h
      r1=(xx(1,j+1)+xx(1,j))/2.0d0
      p1=(tm(j)+tm(j+1))/2.0d0
      p2=(cd(j)+cd(j+1))/2.0d0
      p3=(dtm(j)+dtm(j+1))/2.0d0
      p4=(dfu(j)+dfu(j+1))/2.0d0
      p5=(dcd(j)+dcd(j+1))/2.0d0
      p6=(d2fu(j)+d2fu(j+1))/2.0d0
      d(2,1)=(1.0d0-p1)*(1.0d0/r1+p4)/h
      b(2,1)=-d(2,1)+((1.0d0-p1)*(p6-1.0d0/r1/r1)*dcf
     1       -(1.0d0/r1+p4)*dcf*p3)/2.0d0
      d(2,1)=d(2,1)+((1.0d0-p1)*(p6-1.0d0/r1/r1)*dcf
     1       -(1.0d0/r1+p4)*dcf*p3)/2.0d0
      d(2,2)=frt/h
      b(2,2)=-frt/h
      g(2)=frt*cur/p2+(1.0d0-p1)*(p6-1.0d0/r1/r1)*dcf*r1 -
     1     (1.0d0/r1+p4)*dcf*p3*r1
     &-((1.0d0-p1)*(1.0d0/r1+p4)/h)*(c(1,j+1)-c(1,j))
     &-(((1.0d0-p1)*(p6-1.0d0/r1/r1)*dcf
     1-(1.0d0/r1+p4)*dcf*p3)/2.0d0)*(c(1,j)+c(1,j+1))
     &+frt/h*(c(2,j)-c(2,j+1))
c
```

```
      b(3,5)=1.0d0
      g(3)=-c(5,j)
      b(4,3)=1.0d0
      g(4)=-c(3,j)
      b(5,4)=1.0d0
      g(5)=cur-c(4,j)
      call band(j)
      go to 10
c     ------------------------------------------------------------
c     Now for the boundary between cathode and separator(j=n1):
  110 if (j .ne. n1) go to 120
      sum=0.0d0
      h=h2
c
      dcf=(xx(1,j+1)-xx(1,j))/h
      r1=(xx(1,j+1)+xx(1,j))/2.0d0
      r4=(xx(4,j+1)+xx(4,j))/2.0d0
      p1=(tm(j)+tm(j+1))/2.0d0
      p2=((ep**1.50d0)*cd(j)/(eps**1.5d0)+cd(j+1))/2.0d0
      p3=(dtm(j)+dtm(j+1))/2.0d0
      p4=(dfu(j)+dfu(j+1))/2.0d0
      p5=((ep**1.50d0)*dcd(j)/(eps**1.5d0)+dcd(j+1))/2.0d0
      p6=(d2fu(j)+d2fu(j+1))/2.0d0
      d(2,1)=(1.0d0-p1)*(1.0d0/r1+p4)/h
      b(2,1)=-d(2,1)+((1.0d0-p1)*(p6-1.0d0/r1/r1)*dcf
     1       -(1.0d0/r1+p4)*dcf*p3+frt*r4*p5/p2/p2)/2.0d0
      d(2,1)=d(2,1)+((1.0d0-p1)*(p6-1.0d0/r1/r1)*dcf
     1       -(1.0d0/r1+p4)*dcf*p3+frt*r4*p5/p2/p2)/2.0d0
      d(2,2)=frt/h
      b(2,2)=-frt/h
      b(2,4)=-frt*(1.0d0/p2+1.0d0/sig)/2.0d0
      d(2,4)=b(2,4)
      g(2)=-frt*cur/sig + (1.0d0-p1)*(p6-1.0d0/r1/r1)*dcf*r1
     1     -(1.0d0/r1+p4)*dcf*p3*r1+frt*r4*p5*r1/p2/p2
     1-((1.0d0-p1)*(1.0d0/r1+p4)/h)*(c(1,j+1)-c(1,j))
     1-(((1.0d0-p1)*(p6-1.0d0/r1/r1)*dcf
     1-(1.0d0/r1+p4)*dcf*p3+frt*r4*p5/p2/p2)/2.0d0)*(c(1,j)+c(1,j+1))
     1+frt/h*(c(2,j)-c(2,j+1))
     1+frt*(1.0d0/p2+1.0d0/sig)/2.0d0*(c(4,j)+c(4,j+1))
c
      call ekin(j,0,0,il4)
c
      if (kk .gt. 2) then
      sum=0.0d0
      do 54 i=1, kk-2
      if(ts(i+1)-ts(i).gt.0.0)
```

```
     1sum=sum + (xt(3,j,i+1)-xt(3,j,i))*ai(kk-i)/(ts(i+1)-ts(i))
   54 continue
      else sum=0.0d0
      end if
      b(4,3)=ai(1)/rr
      b(4,5)=1.0d0/Rad
      g(4)=ai(1)*(xt(3,j,kk-1)-c(3,j))/rr-sum*dfs/Rad/Rad-c(5,j)/Rad
      b(5,4)=1.0d0
      g(5)=cur-c(4,j)
c
      call band(j)
      go to 10
c     ------------------------------------------------------
  120 if (j .eq. nj) go to 16
c
c     specify governing equations [ n1+1 < j < nj ]
c     composite cathode
c
      sum=0.0d0
      h=h2
c
      dcf=(xx(1,j+1)-xx(1,j))/h
      r1=(xx(1,j+1)+xx(1,j))/2.0d0
      r4=(xx(4,j+1)+xx(4,j))/2.0d0
      p1=(tm(j)+tm(j+1))/2.0d0
      p2=(cd(j)+cd(j+1))/2.0d0
      p3=(dtm(j)+dtm(j+1))/2.0d0
      p4=(dfu(j)+dfu(j+1))/2.0d0
      p5=(dcd(j)+dcd(j+1))/2.0d0
      p6=(d2fu(j)+d2fu(j+1))/2.0d0
      d(2,1)=(1.0d0-p1)*(1.0d0/r1+p4)/h
      b(2,1)=-d(2,1)+((1.0d0-p1)*(p6-1.0d0/r1/r1)*dcf
     1       -(1.0d0/r1+p4)*dcf*p3+frt*r4*p5/p2/p2)/2.0d0
      d(2,1)=d(2,1)+((1.0d0-p1)*(p6-1.0d0/r1/r1)*dcf
     1       -(1.0d0/r1+p4)*dcf*p3+frt*r4*p5/p2/p2)/2.0d0
      d(2,2)=frt/h
      b(2,2)=-frt/h
      b(2,4)=-frt*(1.0d0/p2+1.0d0/sig)/2.0d0
      d(2,4)=-frt*(1.0d0/p2+1.0d0/sig)/2.0d0
      g(2)=-frt*cur/sig + (1.0d0-p1)*(p6-1.0d0/r1/r1)*dcf*r1 -
     1     (1.0d0/r1+p4)*dcf*p3*r1+frt*r4*p5*r1/p2/p2
     1-((1.0d0-p1)*(1.0d0/r1+p4)/h)*(c(1,j+1)-c(1,j))
     1-(((1.0d0-p1)*(p6-1.0d0/r1/r1)*dcf
     1-(1.0d0/r1+p4)*dcf*p3+frt*r4*p5/p2/p2)/2.0d0)*(c(1,j)
     1+c(1,j+1))+frt/h*(c(2,j)-c(2,j+1))
     1+frt*(1.0d0/p2+1.0d0/sig)/2.0d0*(c(4,j)+c(4,j+1))
```

```
c
      call ekin(j,0,0,il4)
c
      if (kk .gt. 2) then
      sum=0.0d0
      do 56 i=1, kk-2
      if(ts(i+1)-ts(i).gt.0.0)
     1sum=sum + (xt(3,j,i+1)-xt(3,j,i))*ai(kk-i)/(ts(i+1)-ts(i))
   56 continue
      else sum=0.0d0
      end if
      b(4,3)=ai(1)/rr
      b(4,5)=1.0d0/Rad
      g(4)=ai(1)*(xt(3,j,kk-1)-c(3,j))/rr-sum*dfs/Rad/Rad
     1-c(5,j)/Rad
c
      b(5,4)=-1.0d0/h
      a(5,4)=1.0d0/h
      b(5,5)=area*fc/2.0d0
      a(5,5)=area*fc/2.0d0
      g(5)=-area*fc/2.d0*(c(5,j)+c(5,j-1))+(c(4,j)-c(4,j-1))/h
c
      call band(j)
      go to 10
c
c     ------------------------------------------------
c
   16 continue
c     specify boundary conditions at right interface(j=nj)
c
      sum=0.0d0
c     the "irrefutable" boundary conditions:
c
      g(2)=-c(4,j)
      b(2,4)=1.0
c
      call ekin(j,0,0,il4)
c
      if (kk .gt. 2) then
      sum=0.0d0
      do 57 i=1, kk-2
      if(ts(i+1)-ts(i).gt.0.0)
     1sum=sum + (xt(3,j,i+1)-xt(3,j,i))*ai(kk-i)/(ts(i+1)-ts(i))
   57 continue
      else sum=0.0d0
      end if
```

```
      b(4,3)=ai(1)/rr
      b(4,5)=1.0d0/Rad
      g(4)=ai(1)*(xt(3,j,kk-1)-c(3,j))/rr-sum*dfs/Rad/Rad
     1-c(5,j)/Rad
c
      b(5,4)=-1.0d0/h
      a(5,4)=1.0d0/h
      b(5,5)=area*fc/2.0d0
      a(5,5)=area*fc/2.0d0
      g(5)=-area*fc/2.d0*(c(5,j)+c(5,j-1))+(c(4,j)-c(4,j-1))/h
c
      call band(j)
      do 605 jj=1,nj
      do 605 i=1,n
  605 c(i,jj)=xx(i,jj)+c(i,jj)
c     ------------------------------------------------
c
c     begin check for convergence
c
      nerr=0
      do 58 i=1,n
   58 xp(i)=(4.0d0*c(i,2)-3.0d0*c(i,1)-c(i,3))/2.0d0/h
      do 25 j=1,nj
c     shoe horns:
      if(c(1,j).lt.xx(1,j)/100.) c(1,j)=xx(1,j)/100.
      if(cmax-c(1,j).le.(cmax-xx(1,j))/100.)
     1c(1,j)=cmax-(cmax-xx(1,j))/100.
        if(c(1,j).ge.cmax) c(1,j)=0.999999*cmax
      if(c(2,j).lt.xx(2,j)-0.2) c(2,j)=xx(2,j)-0.2
      if(c(2,j).gt.xx(2,j)+0.2) c(2,j)=xx(2,j)+0.2
      if(c(3,j).lt.xx(3,j)/1.d2) c(3,j)=xx(3,j)/1.d2 ! use cs min
      if(ct-c(3,j).le.(ct-xx(3,j))/1.d2) then
          nerr = nerr+1
        c(3,j)=ct-(ct-xx(3,j))/1.d2
      endif
      if(c(3,j).ge.ct) c(3,j)=0.999999*ct
c     to avoid underflow or overflow:
      if(c(1,j).lt.1.0d-12) c(1,j)=1.0d-12
      if(c(1,j).lt.1.0d-04) c(5,j)=0.0d0
      do 25 i=1,n
 25   xx(i,j)=c(i,j)
c
      if (jcount .gt. lim ) then
      if (rr .lt. 1.d-2) then
      print*,kk, ' this time step did not converge'
      jc1=0
```

```
      jc3=0
      do 59 j=n1,nj
        if(c(1,j).le.1.0d-10) jc1=jc1+1
        if(c(3,j).ge.0.9999*ct) jc3=jc3+1
   59 continue
      if(jc1.gt.0) print*,'Depletion of Li occurs'
      if(jc3.gt.0) print*,'Saturation of Li occurs'
      nt=nt-1
      ed=ed/tw/3.6d03
      pow=3.6d03*dfs*ed/ts(nt+1)/Rad/Rad
      print*,'energy is ',ed
      print*,'power is ',pow
      call nucamb (n,2,30)
      stop
      else
      tau=tau/2.0d0
      rr=rr/2.0d0
      ts(kk)=ts(kk-1)+tau
      print*,' time step reduced to ', rr
      call calca(kk)
      go to 666
      end if
c
      else
          if(nerr.ne.0) go to 8
          do 55 ii=1,n
      errlim=1.d-10
      if(ii.eq.5) errlim=1.d-16
                dxp=dabs( xp(ii)-xp0(ii) )
                dxx=dabs( xx(ii,n1+10)-xx0(ii,n1+10) )
      if (dxx.gt.1.d-9*dabs(xx(ii,n1+10)).and.dxx.gt.errlim)
     1go to 8
      if (dxp.gt.1.d-7*dabs(xp(ii)).and.dxp.gt.errlim) go to 8
   55     continue
c
      print*,jcount,' iterations required'
c
c- - - - - - - - - - - - - - - - - - - - - - - - - - - - - - - -
      do 60 j=1,nj
   60 term(j)=termn(j)
c- - - - - - - - - - - - - - - - - - - - - - - - - - - - - - - -
c
      end if
c
      return
      end
```

```
c
c**********************************************************************
      subroutine calca(kk)
      implicit real*8(a-h,o-z)
      parameter(maxt=900)
      common /n/ nx,nt,n1,n2,nj
      common /calc/ ai(maxt),u(222,900),ts(maxt),h,h1,h2,hcp,
     1hcn,rr
      common/const/ fc,r,t,frt,cur,ep,epf,eps,epp,epps,pi,nneg,
     1nprop,npos
      dimension ar(2,maxt)
c
      s=1.644934066848d0
c
      do 64 i=1,kk-1
      ar(1,i)=ts(kk)-ts(i)
      ar(2,i)=ts(kk)-ts(i+1)
      do 63 m=1,2
      t1=ar(m,i)
      a1=0.0d0
c
      if(t1 .gt. 0.06d0) then
c
      do 61 j=1,5
      da=(expf(-dble(j*j)*pi*pi*t1))/j/j
   61 a1=a1+da
      a1=2.0d0*(s-a1)/pi/pi
c
      else
c
      if(t1 .eq. 0.0d0) then
      a1=0.0d0
      else
      do 62 j=1,3
      z=dble(j)/dsqrt(t1)
      call erfc(z,e)
      da=expf(-dble(j*j)/t1)-dble(j)*dsqrt(pi/t1)*e
   62 a1=a1+da
      a1=-t1 + 2.0d0*dsqrt(t1/pi)*(1.0d0+2.0d0*a1)
      end if
c
      end if
   63 ar(m,i)=a1
c
   64 ai(kk-i)=ar(1,i)-ar(2,i)
c
```

```
      return
      end
c*********************************************************************
      subroutine erfc(z,e)
      implicit real*8(a-h,o-z)
      common/const/ fc,r,t,frt,cur,ep,epf,eps,epp,epps,pi,nneg,
     1nprop,npos
      a1=0.254829592d0
      a2=-0.284496736d0
      a3=1.421413741d0
      a4=-1.453152027d0
      a5=1.061405429d0
      if(z .lt. 2.747192d0) then
      t2=1.0d0/(1.0d0+0.3275911d0*z)
      e=(a1*t2+a2*t2*t2+a3*t2**3.0d0+a4*t2**4.0d0
     1+a5*t2**5.0d0)*expf(-z*z)
      else
c
      if (z .gt. 25.0d0) then
      e=0.0d0
      else
c
      sum=0.0d0
      max=z*z + 0.5
      fac=-0.5d0/z/z
      sum=fac
      tl=fac
      n=1
  10  n=n+1
      if(n .gt. max) go to 15
      tn=tl*(2.0d0*n-1.0d0)*fac
      sum=sum + tn
      if(tn .lt. 1.0d-06) go to 15
      tl=tn
      go to 10
   15 e=(expf(-z*z))*(1.0d0+sum)/dsqrt(pi)/z
      end if
      end if
c
      return
      end
c*********************************************************************
      subroutine band(j)
      implicit real*8(a-h,o-z)
      common /n/ nx,nt,n1,n2,nj
      common/mat/ b,d
```

```
      common/bnd/ a,c,g,x,y
      dimension b(10,10),d(10,21)
      dimension a(10,10),c(10,221),g(10),x(10,10),y(10,10)
      dimension e(10,11,221)
  101 format (15h determ=0 at j=,i4)
      n=nx
      if (j-2)  1,6,8
    1 np1= n + 1
      do 2 i=1,n
      d(i,2*n+1)= g(i)
      do 2 l=1,n
      lpn= l + n
    2 d(i,lpn)= x(i,l)
      call matinv(n,2*n+1,determ)
      if (determ)  4,3,4
    3 print 101, j
    4 do 5 k=1,n
      e(k,np1,1)= d(k,2*n+1)
      do 5 l=1,n
      e(k,l,1)= - d(k,l)
      lpn= l + n
    5 x(k,l)= - d(k,lpn)
      return
    6 do 7 i=1,n
      do 7 k=1,n
      do 7 l=1,n
    7 d(i,k)= d(i,k) + a(i,l)*x(l,k)
    8 if (j-nj)  11,9,9
    9 do 10 i=1,n
      do 10 l=1,n
      g(i)= g(i) - y(i,l)*e(l,np1,j-2)
      do 10 m=1,n
   10 a(i,l)= a(i,l) + y(i,m)*e(m,l,j-2)
   11 do 12 i=1,n
      d(i,np1)= - g(i)
      do 12 l=1,n
      d(i,np1)= d(i,np1) + a(i,l)*e(l,np1,j-1)
      do 12 k=1,n
   12 b(i,k)= b(i,k) + a(i,l)*e(l,k,j-1)
      call matinv(n,np1,determ)
      if (determ)  14,13,14
   13 print 101, j
   14 do 15 k=1,n
      do 15 m=1,np1
   15 e(k,m,j)= - d(k,m)
      if (j-nj)  20,16,16
```

```
   16 do 17 k=1,n
   17 c(k,j)= e(k,np1,j)
      do 18 jj=2,nj
      m= nj - jj + 1
      do 18 k=1,n
      c(k,m)= e(k,np1,m)
      do 18 l=1,n
      if(e(k,l,m).ne.0.0 .and. c(l,m+1).ne.0.0) then
      if(dlog(dabs(e(k,l,m)))+dlog(dabs(c(l,m+1))).gt.-200.0)
     &c(k,m)= c(k,m) + e(k,l,m)*c(l,m+1)
      endif
   18 continue
      do 19 l=1,n
      do 19 k=1,n
   19 c(k,1)= c(k,1) + x(k,l)*c(l,3)
   20 return
      end
c*********************************************************************
      subroutine matinv(n,m,determ)
      implicit real*8(a-h,o-z)
      common/mat/ b,d
      dimension b(10,10),d(10,21)
      dimension id(10)
      determ=1.0
      do 1 i=1,n
   1  id(i)=0
      do 18 nn=1,n
      bmax=1.1
      do 6 i=1,n
      if(id(i).ne.0) go to 6
      bnext=0.0
      btry=0.0
      do 5 j=1,n
      if(id(j).ne.0) go to 5
      if(dabs(b(i,j)).le.bnext) go to 5
      bnext=dabs(b(i,j))
      if(bnext.le.btry) go to 5
      bnext=btry
      btry=dabs(b(i,j))
      jc=j
   5  continue
      if(bnext.ge.bmax*btry) go to 6
      bmax=bnext/btry
      irow=i
      jcol=jc
   6  continue
```

```
      if(id(jc).eq.0) go to 8
      determ=0.0
      return
    8 id(jcol)=1
      if(jcol.eq.irow) go to 12
      do 10 j=1,n
      save=b(irow,j)
      b(irow,j)=b(jcol,j)
   10 b(jcol,j)=save
      do 11 k=1,m
      save=d(irow,k)
      d(irow,k)=d(jcol,k)
   11 d(jcol,k)=save
   12 f=1.0/b(jcol,jcol)
      do 13 j=1,n
   13 b(jcol,j)=b(jcol,j)*f
      do 14 k=1,m
   14 d(jcol,k)=d(jcol,k)*f
      do 18 i=1,n
      if(i.eq.jcol) go to 18
      f=b(i,jcol)
      do 16 j=1,n
   16 b(i,j)=b(i,j)-f*b(jcol,j)
      do 17 k=1,m
   17 d(i,k)=d(i,k)-f*d(jcol,k)
   18 continue
      return
      end
c*********************************************************************
      subroutine nucamb(n,il2,il3)
      implicit real*8(a-h,o-z)
      parameter(maxt=900)
      common /n/ nx,nt,n1,n2,nj
      common /calc/ ai(maxt),u(222,900),ts(maxt),h,h1,h2,hcp,
     1hcn,rr
      common/const/ fc,r,t,frt,cur,ep,epf,eps,epp,epps,pi,nneg,
     1nprop,npos
      common/power/ ed,Vold,ranode,rcathde
      common/var/ xp(10),xx(5,221),xi(5,221),xt(5,221,maxt)
      common/cprop/ sig,area,ct,dfs,Rad,cmax,rka,rkf,tmmax,g01
      common/temp/thk,htc,dudt,Cp,dens,tam,ncell,tin,lht
      common/tprop/df(221),cd(221),tm(221),
     1ddf(221),dcd(221),dtm(221),dfu(221),d2fu(221)
      dimension zz(221)
c
  109 format(f7.1,', ',f7.1,', ',f7.4,', 'f12.8,', ',g12.4
```

```
     1,', ',g12.4)
  309 format(f8.5,', ',f8.5)
   44 format('t = ',f7.2,' min')
c
      do 5 i=1,n1
      w=i-1
   5  zz(i) = w*h1*1.0d06
      do 7 i=n1+1,nj
      w=i-n1
   7  zz(i) = zz(n1)+w*h2*1.0d06
c
      do 11 l=1,nt+1
      if (l.lt.nt-5.and.mod(l-1,il3).ne.0.and.l.ne.nt+1) go to 11
      print*,' '
      print*,'distance  concen  potential   y solid',
     1'     current             j'
      print*,'microns  (mol/m3)   (V)              ',
     1'     (A/m2)         (mol/m2-s)'
      print44,ts(l)*Rad*Rad/dfs/60.0d0
      do 10 j=1,nj,il2
  10  print109,zz(j),xt(1,j,l),xt(2,j,l),xt(3,j,l)/ct,xt(4,j,l),
     1xt(5,j,l)
  11  continue
c
      return
      end
c*********************************************************************
      subroutine guess(n)
      implicit real*8(a-h,o-z)
      parameter(maxt=900)
      common /n/ nx,nt,n1,n2,nj
      common /calc/ ai(maxt),u(222,900),ts(maxt),h,h1,h2,hcp,
     1hcn,rr
      common/const/ fc,r,t,frt,cur,ep,epf,eps,epp,epps,pi,nneg,
     1nprop,npos
      common/var/ xp(10),xx(5,221),xi(5,221),xt(5,221,maxt)
      common/cprop/ sig,area,ct,dfs,Rad,cmax,rka,rkf,tmmax,g01
      common/temp/thk,htc,dudt,Cp,dens,tam,ncell,tin,lht
      common/tprop/df(221),cd(221),tm(221),
     1ddf(221),dcd(221),dtm(221),dfu(221),d2fu(221)
      dimension del(5)
c
      del(2)=cur*h2/2.0d-02
      del(4)=cur/dble(n2)
      del(5)=(xi(5,nj))/dble(nj-1)
      xi(4,1)=cur
```

```
c
      do 71 i=1,n1-1
      xi(3,i)=0.0d0
      xi(4,i)=cur
   71 xi(5,i)=0.0d0
      do 72 i=n1,nj
      xi(3,i)=xi(3,n1)
      xi(4,i)=xi(4,1)-del(4)*(i-n1)
   72 xi(5,i)=xi(5,nj)
c
      do 15 i=1,nj
      xt(5,i,1)=xi(5,i)
      xt(4,i,1)=xi(4,i)
      xt(3,i,1)=xi(3,i)
c     xi(2,i)=xi(2,1)+del(2)*(i-1)
      xt(2,i,1)=xi(2,1)
      xi(1,i)=xi(1,1)
   15 xt(1,i,1)=xi(1,i)
c
      return
      end
c*********************************************************************
      subroutine util
      implicit real*8(a-h,o-z)
      parameter(maxt=900)
      common /n/ nx,nt,n1,n2,nj
      common /calc/ ai(maxt),u(222,900),ts(maxt),h,h1,h2,hcp,
     1hcn,rr
      common/const/ fc,r,t,frt,cur,ep,epf,eps,epp,epps,pi,nneg,
     1nprop,npos
      common/var/ xp(10),xx(5,221),xi(5,221),xt(5,221,maxt)
      common/cprop/ sig,area,ct,dfs,Rad,cmax,rka,rkf,tmmax,g01
c
      do 10 j=n1,nj
      u(j,1)=0.0d0
          do 76 k=2,nt+1
   76     u(j,k)=u(j,k-1)-1.5d0*(xt(5,j,k)+xt(5,j,k-1))*rr/Rad
      do 77 k=2,nt+1
   77 u(j,k)=(u(j,k)+xt(3,j,1))/ct
      u(j,1)=xt(3,j,1)/ct
   10 continue
      do 79 k=1,nt+1
      u(nj+1,k)=0.0d0
         do 78 j=n1+1,nj-1
   78    u(nj+1,k)=u(nj+1,k)+u(j,k)
         u(nj+1,k)=u(nj+1,k)+0.5d0*(u(n1,k)+u(nj,k))
```

```
   79 u(nj+1,k)=u(nj+1,k)/(nj-n1)
c
      return
      end
c*************************************************************
      subroutine peak(n,lim,il4,curr)
      implicit real*8(a-h,o-z)
      parameter(maxt=900)
      common /n/ nx,nt,n1,n2,nj
      common /calc/ ai(maxt),u(222,900),ts(maxt),h,h1,h2,hcp,
     1hcn,rr
      common/const/ fc,r,t,frt,cur,ep,epf,eps,epp,epps,pi,nneg,
     1nprop,npos
      common/power/ ed,Vold,ranode,rcathde
      common/var/ xp(10),xx(5,221),xi(5,221),xt(5,221,maxt)
      common/cprop/ sig,area,ct,dfs,Rad,cmax,rka,rkf,tmmax,g01
      common/temp/thk,htc,dudt,Cp,dens,tam,ncell,tin,lht
  311 format(f8.5,', ',f7.3,', ',f7.2)
c
c     Peak power current ramp section:
      print*,' '
      print*,'    PEAK POWER '
      print*,' '
      print*,'cell pot  ',' current','   power'
      print*,'  (V)  ','    (A/m2)','   (W/m2)'
c
c     Duration of current pulse is 30 seconds.
c
      li=0
      fact=5.0d0
  127 k=nt+2
      rr=0.2d0
      rrmax=30.0d0
      dt=dfs*rr/Rad/Rad
      ts(k)=ts(k-1)+rr*dfs/Rad/Rad
      call calca(k)
      opow=0.0
      ppow=0.0
      call cellpot(k-1,il4,vv,0)
      vlast=vv
      ii=0
      lflag=1
      curinit=curr
      cur=curr
c     Ramp current:
c
```

```
  128 continue
      if (ppow.ge.opow.and.ii.lt.200) then
c
      opow=ppow
      ocur=cur
      energ=0.0
      ii=ii+1
      cur=cur+fact
      kkflag=0
      iflag=0
      li=0
      k=nt+2
      timpk=0.0d0
      rr=0.2d0
      call zts(n,lim,k,dt,k,il4)
      call cellpot(k,il4,vv,0)
      vlast=vv
  129 kkflag=kkflag+1
      dt=dfs*rr/Rad/Rad
      ts(k)=ts(k-1)+rr*dfs/Rad/Rad
      call calca(k)
c
      call comp(n,lim,k,dt,1,tw,il4,jcount)
c
      do 40 i=1,n
      do 40 j=1,nj
   40 xt(i,j,k)=xx(i,j)
c
      call cellpot(k,il4,vv,0)
      energ=energ+(vlast+vv)*(ts(k)-ts(k-1))*cur*Rad*Rad/dfs/2.0d0
c
      timpk=timpk+rr
      if (dabs(timpk-30.0d0).gt.0.1) then

      if (timpk.lt.30.0) then
      k=k+1
      vlast=vv
c     Increasing time steps:
      if(jcount.lt.6 .and. kkflag.gt.5 .and. (2.0d0*rr
     1+timpk).lt.30.0d0 .and. iflag.eq.0) then
         dt=dt*2.0d0
         rr=rr*2.0d0
c        print*,'next time step increased to ', rr,'(s)'
       end if
      if(timpk+rr.gt.30.0) iflag=1
      if(timpk+rr.gt.30.0) rr=30.0d0-timpk
```

```
      go to 129
      end if
c
      end if
      ppow=energ/30.0d0
      print 311, ppow/cur,cur,ppow
      go to 128
c
      else
      if (ii.gt.2.and.lflag.eq.0) print 311, opow/ocur,ocur,opow
      if (lflag.eq.1) then
      opow=ppow
      cur=cur-2.0*fact
      fact=1.0d0
      lflag=0
      go to 128
      end if
c
      end if
      if (ii.le.2) then
      curr=curinit/2.0
      go to 127
      end if
c
      return
      end
c*********************************************************************
      subroutine cellpot(kk,il4,v,li)
      implicit real*8(a-h,o-z)
      parameter(maxt=900)
      common /n/ nx,nt,n1,n2,nj
      common /calc/ ai(maxt),u(222,900),ts(maxt),h,h1,h2,hcp,
     1hcn,rr
      common/const/ fc,r,t,frt,cur,ep,epf,eps,epp,epps,pi,nneg,
     1nprop,npos
      common/power/ ed,Vold,ranode,rcathde
      common/var/ xp(10),xx(5,221),xi(5,221),xt(5,221,maxt)
      common/cprop/ sig,area,ct,dfs,Rad,cmax,rka,rkf,tmmax,g01
      common/temp/thk,htc,dudt,Cp,dens,tam,ncell,tin,lht
  309 format(f8.5,', ',f8.5,', ',f7.3,', ',f8.3,',   ',i3)
  319 format(f8.5,', ',f7.3,', ',f7.2,',   ',f7.2,', ',f7.2)
      lim=20
c
      if (il4 .eq. 1 ) then
c     For polymer PEO elyte:
      x0=rkf*(dsqrt((cmax-xt(1,1,kk))*xt(1,1,kk)))
```

```
c
      else
c
c     For liquid PC elyte:
      x0=rkf*(dsqrt(xt(1,1,kk)))
      end if
c
      p20=-0.01d0
      p2=p20
      jcount=0
c
    8 jcount = jcount +1
      p20=p2
      a1=0.33d0*frt
      c1=0.67d0*frt
c
      p2=-cur/x0+(1.0d0+p20*a1)*expf(-p20*a1)
     1-(1.0d0-p20*c1)*expf(p20*c1)
      p2=p2/(a1*expf(-a1*p20)+c1*expf(c1*p20))
c
      if(jcount .gt. lim) then
c     print*,'jcount ',jcount
      stop
      else
      dx=dabs(p2-p20)
      if(dx .gt. dabs(1.0d-09*p2)) go to 8
      end if
c
      sum=0.0d0
c     print*,'overpotential is ',p2
      do 85 j=n1+1,nj-1
   85 sum=sum+xt(4,j,kk)*h2
      sum=sum-cur*h2*dble(nj-n1)+0.5*h2*(xt(4,n1,kk)+xt(4,nj,kk))
      v=xt(2,1,kk)  +p2-cur*ranode  +sum/sig
c
c     Material balance criteria:
      sum=0.0d0
      do 86 j=2,n1-1
   86 sum=sum+xt(1,j,kk)*h1*eps
      sum=sum+(xt(1,1,kk)+xt(1,n1,kk))*h1*eps/2.0d0
      do 87 j=n1+1,nj-1
   87 sum=sum+xt(1,j,kk)*ep*h2
      sum=sum+(xt(1,n1,kk)+xt(1,nj,kk))*h2*ep/2.0d0
      w=xt(1,1,1)*((n1-1)*h1*eps+n2*ep*h2)
      ca=sum/w
c
```

```
      th=ts(kk)*Rad*Rad/dfs/60.0
c     Volume fraction filler is epf:
      if(kk .le. 2) ut=xt(3,n1,1)/ct
      r4=0.0
      if(kk.gt.1)
     &r4=(ts(kk)-ts(kk-1))*Rad*Rad/dfs
      ut=ut + cur*r4/fc/(1.0d0-ep-epf)/dble(nj-n1)/h2/ct
      if (lht.ne.2) call temperature(kk,v,q,ut,Uoc,il4)
c     tprint is the uniform cell T in deg celsius
      tprint=t-273.15
c     print 309, 1.+ut,v,ca,th,kk  ! lower plateau for Mn2O4 only
      if(li.eq.1) then
      if (lht.eq.2) print 309, ut,v,ca,th,kk
      if (lht.eq.0) print 309, ut,v,tprint,q,kk
      if (lht.eq.1) print 309, ut,v,htc,q,kk
      endif
      if(kk.ge.maxt-2) print *, 'warning: k is approaching kmax!'
      if(kk .le. 2) ed=0.0d0
      if(kk.gt.1)
     &ed=ed+(Vold+v)*(ts(kk)-ts(kk-1))*cur*Rad*Rad/dfs/2.0d0
      Vold=v
      return
      end
c**********************************************************************
      subroutine sol(nmax,jj)
      implicit real*8(a-h,o-z)
      parameter(maxt=900)
      common /calc/ ai(maxt),u(222,900),ts(maxt),h,h1,h2,hcp,
     1hcn,rr
      common/var/ xp(10),xx(5,221),xi(5,221),xt(5,221,maxt)
      common/const/ fc,r,t,frt,cur,ep,epf,eps,epp,epps,pi,nneg,
     1nprop,npos
      common/cprop/ sig,area,ct,dfs,Rad,cmax,rka,rkf,tmmax,g01
      common/temp/thk,htc,dudt,Cp,dens,tam,ncell,tin,lht
      dimension cs(50)
c
c     set initial value of solid concentration
      do 88 i=1, 50
c     cs(i)=0.0d0
   88 cs(i)=xt(3,jj,1)
c
c     complete calculations for 50 points along radius of particle
      do 10 i=1,50
      y2=2.0d-02*i
c
c
```

```
      sum1=0.0d0
      do 20 kk=1,nmax
      k=nmax+1-kk
c
      t1=(ts(nmax+1)-ts(k))
c     print*,t1
      sum2=sum1
c
c     calculate c bar (r,t1)
c
      sum1=0.0d0
      r1=1.0d0
c
      do 89 j=1,15
      r1=-r1
      y1=j*j*pi*pi*t1
      y3=j*pi*y2
      if (y1 .gt. 1.50d02) then
      da=0.0d0
      else
      da=expf(-y1)
      end if
   89 sum1=sum1-2.0d0*r1*da*dsin(y3)/j/pi/y2
      sum1=1.0d0-sum1
c
c     perform superposition
c
      cs(i)=cs(i)+(xt(3,jj,k+1)+xt(3,jj,k)-2.0d0*xt(3,jj,1)
     1)*(sum1-sum2)/2.0d0
   20 continue
c
   10 continue
c
      print*,' '
      print*,ts(nmax)
      print*,' '
      do 90 i=1, 50, 1
   90 print*,.02*i,' ',cs(i)
      return
      end
c*********************************************************************
      subroutine mass(tw,re,rs,rf,rp,rc,ef,rcn,rcp)
      implicit real*8(a-h,o-z)
      parameter(maxt=900)
      common /n/ nx,nt,n1,n2,nj
      common /calc/ ai(maxt),u(222,900),ts(maxt),h,h1,h2,hcp,
```

```
     1hcn,rr
      common/const/ fc,r,t,frt,cur,ep,epf,eps,epp,epps,pi,nneg,
     1nprop,npos
      common/var/ xp(10),xx(5,221),xi(5,221),xt(5,221,maxt)
      common/cprop/ sig,area,ct,dfs,Rad,cmax,rka,rkf,tmmax,g01
      common/temp/thk,htc,dudt,Cp,dens,tam,ncell,tin,lht
  309 format(f8.5,', ',f8.5,', ',f8.5,', ',f8.5)
c
c     mass of positive electrode
      c1=h2*n2*(re*ep+rp*epp+rs*(1.0d0-ep-epf-epp)+rf*epf)
c
c     mass of separator
      s=(re*eps+rp*epps+rc*(1.0d0-eps-epps))*h1*(n1-1)
c
c     mass of negative electrode
      a1=ef*(1.0d0-ep-epf-epp)*(ct)*h2*(n2)*6.941/1.0d03
c     mass of current collectors
      cc1=hcn*rcn+hcp*rcp
      tw=c1+s+a1+cc1
c     print309,a1,s,c1,tw
c
      return
      end
c*********************************************************************
      subroutine zts(n,lim,kk,tau,li,il4)
      implicit real*8(a-h,o-z)
      parameter(maxt=900)
      common /n/ nx,nt,n1,n2,nj
      common /calc/ ai(maxt),u(222,900),ts(maxt),h,h1,h2,hcp,
     1hcn,rr
      common/const/ fc,r,t,frt,cur,ep,epf,eps,epp,epps,pi,nneg,
     1nprop,npos
      common/ssblock/ xp0(5),xx0(5,221),term(221)
      common/var/ xp(10),xx(5,221),xi(5,221),xt(5,221,maxt)
      common/cprop/ sig,area,ct,dfs,Rad,cmax,rka,rkf,tmmax,g01
      common/temp/thk,htc,dudt,Cp,dens,tam,ncell,tin,lht
      common/tprop/df(221),cd(221),tm(221),
     1ddf(221),dcd(221),dtm(221),dfu(221),d2fu(221)
      common/mat/ b,d
      common/bnd/ a,c,g,x,y
      dimension b(10,10),d(10,21)
      dimension a(10,10),c(10,221),g(10),x(10,10),y(10,10)
c
   99 format (1h ,//5x,'this run just did not converge'//)
      nx=n
c
```

```
      do 1 j=1,nj
      do 1 i=1,n
           c(i,j)=xt(i,j,kk-1)
    1      xx(i,j)=xt(i,j,kk-1)
c     sets first guess to last time step values
      jcount=0
      do 4 i=1,n
    4      xp(i)=0.0d0
c     initialize variables to begin each iteration
c     (jcount is iteration #)
    8 j=0
      jcount=jcount+1
      call prop(nj,n1)
c     obtains physical properties at this specific point
      do 9 i=1,n
      do 9 k=1,n
           x(i,k)=0.0d0
    9      y(i,k)=0.0d0
c
c     store previous iteration of  (xp in xp0)  &  (xx in xx0)
      do 6 i=1,n
           xp0(i)=xp(i)
    6      xx0(i,n1+10)=xx(i,n1+10)
c
c     for a given iteration, set up governing equations and bc's
c     start at the left interface and move across polymer
c
   10 j=j+1
c
      do 11 i=1,n
           g(i)=0.0d0
      do 11 k=1,n
           a(i,k)=0.0d0
           b(i,k)=0.0d0
   11      d(i,k)=0.0d0
c     clears all arrays before use
      if(j.ne.1) go to 13
c
c     ------------------------------------------------
c
c     specify boundary conditions at left interface (j=1)
c     boundary conditions at negative electrode
      h=h1
c
      b(1,1)=1.0d0
      g(1)=xt(1,j,kk-1)-c(1,j)
```

```
c
      dcf=(xx(1,j+1)-xx(1,j))/h
      r1=(xx(1,j+1)+xx(1,j))/2.0d0
      p1=(tm(j)+tm(j+1))/2.0d0
      p2=(cd(j)+cd(j+1))/2.0d0
      p3=(dtm(j)+dtm(j+1))/2.0d0
      p4=(dfu(j)+dfu(j+1))/2.0d0
      p6=(d2fu(j)+d2fu(j+1))/2.0d0
      d(2,1)=(1.0d0-p1)*(1.0d0/r1+p4)/h
      b(2,1)=-d(2,1)+((1.0d0-p1)*(p6-1.0d0/r1/r1)*dcf
     1       -(1.0d0/r1+p4)*dcf*p3)/2.0d0
      d(2,1)=d(2,1)+((1.0d0-p1)*(p6-1.0d0/r1/r1)*dcf
     1       -(1.0d0/r1+p4)*dcf*p3)/2.0d0
      d(2,2)=frt/h
      b(2,2)=-frt/h
      g(2)=frt*cur/p2+(1.0d0-p1)*(p6-1.0d0/r1/r1)*dcf*r1 -
     1     (1.0d0/r1+p4)*dcf*p3*r1
     1-((1.0d0-p1)*(1.0d0/r1+p4)/h)*(c(1,j+1)-c(1,j))
     1-(((1.0d0-p1)*(p6-1.0d0/r1/r1)*dcf
     1-(1.0d0/r1+p4)*dcf*p3)/2.0d0)*(c(1,j)+c(1,j+1))
     1+frt/h*(c(2,j)-c(2,j+1))
c
      b(3,5)=1.0d0
      g(3)=-c(5,j)
      b(4,3)=1.0d0
      g(4)=-c(3,j)
      b(5,4)=1.0d0
      g(5)=cur-c(4,j)
c
      call band(j)
      go to 10
c
c     ------------------------------------------------------
c     specify governing equations in polymer separator
  13  if (j .ge. n1) go to 110
c
      b(1,1)=1.0d0
      g(1)=xt(1,j,kk-1)-c(1,j)
c
      dcf=(xx(1,j+1)-xx(1,j))/h
      r1=(xx(1,j+1)+xx(1,j))/2.0d0
      p1=(tm(j)+tm(j+1))/2.0d0
      p2=(cd(j)+cd(j+1))/2.0d0
      p3=(dtm(j)+dtm(j+1))/2.0d0
      p4=(dfu(j)+dfu(j+1))/2.0d0
      p5=(dcd(j)+dcd(j+1))/2.0d0
```

```
      p6=(d2fu(j)+d2fu(j+1))/2.0d0
      d(2,1)=(1.0d0-p1)*(1.0d0/r1+p4)/h
      b(2,1)=-d(2,1)+((1.0d0-p1)*(p6-1.0d0/r1/r1)*dcf
     1       -(1.0d0/r1+p4)*dcf*p3)/2.0d0
      d(2,1)=d(2,1)+((1.0d0-p1)*(p6-1.0d0/r1/r1)*dcf
     1       -(1.0d0/r1+p4)*dcf*p3)/2.0d0
      d(2,2)=frt/h
      b(2,2)=-frt/h
      g(2)=frt*cur/p2+(1.0d0-p1)*(p6-1.0d0/r1/r1)*dcf*r1 -
     1     (1.0d0/r1+p4)*dcf*p3*r1
     1-((1.0d0-p1)*(1.0d0/r1+p4)/h)*(c(1,j+1)-c(1,j))
     1-(((1.0d0-p1)*(p6-1.0d0/r1/r1)*dcf
     1-(1.0d0/r1+p4)*dcf*p3)/2.0d0)*(c(1,j)+c(1,j+1))
     1+frt/h*(c(2,j)-c(2,j+1))
c
      b(3,5)=1.0d0
      g(3)=-c(5,j)
      b(4,3)=1.0d0
      g(4)=-c(3,j)
      b(5,4)=1.0d0
      g(5)=cur-c(4,j)
      call band(j)
      go to 10
c     ------------------------------------------------------
c     Now for the boundary between cathode and separator(j=n1):
  110 if (j .ne. n1) go to 120
      h=h2
c
      b(1,1)=1.0d0
      g(1)=xt(1,j,kk-1)-c(1,j)
c
      dcf=(xx(1,j+1)-xx(1,j))/h
      r1=(xx(1,j+1)+xx(1,j))/2.0d0
      r4=(xx(4,j+1)+xx(4,j))/2.0d0
      p1=(tm(j)+tm(j+1))/2.0d0
      p2=((ep**1.50d0)*cd(j)/(eps**1.5d0)+cd(j+1))/2.0d0
      p3=(dtm(j)+dtm(j+1))/2.0d0
      p4=(dfu(j)+dfu(j+1))/2.0d0
      p5=((ep**1.50d0)*dcd(j)/(eps**1.5d0)+dcd(j+1))/2.0d0
      p6=(d2fu(j)+d2fu(j+1))/2.0d0
      d(2,1)=(1.0d0-p1)*(1.0d0/r1+p4)/h
      b(2,1)=-d(2,1)+((1.0d0-p1)*(p6-1.0d0/r1/r1)*dcf
     1       -(1.0d0/r1+p4)*dcf*p3+frt*r4*p5/p2/p2)/2.0d0
      d(2,1)=d(2,1)+((1.0d0-p1)*(p6-1.0d0/r1/r1)*dcf
     1       -(1.0d0/r1+p4)*dcf*p3+frt*r4*p5/p2/p2)/2.0d0
      d(2,2)=frt/h
```

```
      b(2,2)=-frt/h
      b(2,4)=-frt*(1.0d0/p2+1.0d0/sig)/2.0d0
      d(2,4)=b(2,4)
      g(2)=-frt*cur/sig + (1.0d0-p1)*(p6-1.0d0/r1/r1)*dcf*r1
     1     -(1.0d0/r1+p4)*dcf*p3*r1+frt*r4*p5*r1/p2/p2
     1-((1.0d0-p1)*(1.0d0/r1+p4)/h)*(c(1,j+1)-c(1,j))
     1-(((1.0d0-p1)*(p6-1.0d0/r1/r1)*dcf
     1-(1.0d0/r1+p4)*dcf*p3+frt*r4*p5/p2/p2)/2.0d0)*(c(1,j)
     1+c(1,j+1))+frt/h*(c(2,j)-c(2,j+1))
     1+frt*(1.0d0/p2+1.0d0/sig)/2.0d0*(c(4,j)+c(4,j+1))
c
      call ekin(j,0,0,il4)
c
      b(4,3)=1.0d0
      g(4)=xt(3,j,kk-1)-c(3,j)
c
      b(5,4)=1.0d0
      g(5)=cur-c(4,j)
c
      call band(j)
      go to 10
c     ------------------------------------------------------
  120 if (j .eq. nj) go to 16
c
c     specify governing equations [ n1+1 < j < nj ]
c     composite cathode
      sum=0.0d0
      h=h2
c
      b(1,1)=1.0d0
      g(1)=xt(1,j,kk-1)-c(1,j)
c
      dcf=(xx(1,j+1)-xx(1,j))/h
      r1=(xx(1,j+1)+xx(1,j))/2.0d0
      r4=(xx(4,j+1)+xx(4,j))/2.0d0
      p1=(tm(j)+tm(j+1))/2.0d0
      p2=(cd(j)+cd(j+1))/2.0d0
      p3=(dtm(j)+dtm(j+1))/2.0d0
      p4=(dfu(j)+dfu(j+1))/2.0d0
      p5=(dcd(j)+dcd(j+1))/2.0d0
      p6=(d2fu(j)+d2fu(j+1))/2.0d0
      d(2,1)=(1.0d0-p1)*(1.0d0/r1+p4)/h
      b(2,1)=-d(2,1)+((1.0d0-p1)*(p6-1.0d0/r1/r1)*dcf
     1       -(1.0d0/r1+p4)*dcf*p3+frt*r4*p5/p2/p2)/2.0d0
      d(2,1)=d(2,1)+((1.0d0-p1)*(p6-1.0d0/r1/r1)*dcf
     1       -(1.0d0/r1+p4)*dcf*p3+frt*r4*p5/p2/p2)/2.0d0
```

```
      d(2,2)=frt/h
      b(2,2)=-frt/h
      b(2,4)=-frt*(1.0d0/p2+1.0d0/sig)/2.0d0
      d(2,4)=-frt*(1.0d0/p2+1.0d0/sig)/2.0d0
      g(2)=-frt*cur/sig + (1.0d0-p1)*(p6-1.0d0/r1/r1)*dcf*r1 -
     1     (1.0d0/r1+p4)*dcf*p3*r1+frt*r4*p5*r1/p2/p2
     1-((1.0d0-p1)*(1.0d0/r1+p4)/h)*(c(1,j+1)-c(1,j))
     1-(((1.0d0-p1)*(p6-1.0d0/r1/r1)*dcf
     1-(1.0d0/r1+p4)*dcf*p3+frt*r4*p5/p2/p2)/2.0d0)*(c(1,j)+c(1,j+1))
     1+frt/h*(c(2,j)-c(2,j+1))
     1+frt*(1.0d0/p2+1.0d0/sig)/2.0d0*(c(4,j)+c(4,j+1))
c
      call ekin(j,0,0,il4)
c
      b(4,3)=1.0d0
      g(4)=xt(3,j,kk-1)-c(3,j)
c
      b(5,4)=-1.0d0/h
      a(5,4)=1.0d0/h
      b(5,5)=area*fc/2.0d0
      a(5,5)=area*fc/2.0d0
      g(5)=-area*fc/2.d0*(c(5,j)+c(5,j-1))+(c(4,j)-c(4,j-1))/h
c
      call band(j)
      go to 10
c
c     ------------------------------------------------------
c
   16 continue
c     specify boundary conditions at right interface(j=nj)
c
      sum=0.0d0
c     the "irrefutable" boundary conditions:
      b(1,1)=1.0d0
      g(1)=xt(1,j,kk-1)-c(1,j)
c
      g(2)=-c(4,j)
      b(2,4)=1.0
c
      call ekin(j,0,0,il4)
c
      b(4,3)=1.0d0
      g(4)=xt(3,j,kk-1)-c(3,j)
c
      b(5,4)=-1.0d0/h
      a(5,4)=1.0d0/h
```

```
      b(5,5)=area*fc/2.0d0
      a(5,5)=area*fc/2.0d0
      g(5)=-area*fc/2.d0*(c(5,j)+c(5,j-1))+(c(4,j)-c(4,j-1))/h
c
      call band(j)
      do 610 jj=1,nj
      do 610 i=1,n
  610 c(i,jj)=xx(i,jj)+c(i,jj)
c     ------------------------------------------------------
c
c     begin check for convergence
c
      do 91 i=1,n
   91 xp(i)=(4.0d0*c(i,2)-3.0d0*c(i,1)-c(i,3))/2.0d0/h
      do 25 j=1,nj
      if(c(2,j).lt.xx(2,j)-0.3d0) c(2,j)=xx(2,j)-0.3d00
      if(c(2,j).gt.xx(2,j)+0.3d0) c(2,j)=xx(2,j)+0.3d00
      do 25 i=1,n
 25   xx(i,j)=c(i,j)
c
      if (jcount .gt. 3*lim ) then
      print99
      stop
c
      else
      do 55 ii=1,n
      errlim=1.d-10
      if(ii.eq.5) errlim=1.d-16
                dxp=dabs( xp(ii)-xp0(ii) )
                dxx=dabs( xx(ii,n1+10)-xx0(ii,n1+10) )
      if (dxx.gt.1.d-9*dabs(xx(ii,n1+10)).and.dxx.gt.errlim)
     1go to 8
      if (dxp.gt.1.d-7*dabs(xp(ii)).and.dxp.gt.errlim) go to 8
   55 continue
c
c     print*,jcount,' iterations required'
c
      do 92 ll=1, nj, 1
      do 92 lk=1,n
   92 xt(lk,ll,li)=xx(lk,ll)
      end if
c
      return
      end
c
c**********************************************************************
```

```
      subroutine temperature(kk,v,q,ut,Uoc,il4)
      implicit real*8(a-h,o-z)
      parameter(maxt=900)
      common /calc/ ai(maxt),u(222,900),ts(maxt),h,h1,h2,hcp,
     1hcn,rr
      common/const/ fc,r,t,frt,cur,ep,epf,eps,epp,epps,pi,nneg,
     1nprop,npos
      common/cprop/ sig,area,ct,dfs,Rad,cmax,rka,rkf,tmmax,g01
      common/temp/thk,htc,dudt,Cp,dens,tam,ncell,tin,lht
c
c     calculate open-circuit potential at present state of charge
      call ekin(1,1,ut,il4)
      Uoc=g01
c
c     if (kk.eq.2) print*,htc,dudt,ncell,cur,tam-273.15
c     per cell heat generation
      q=cur*(g01-v-t*dudt)
c  The heat transfer coefficient is for heat transferred out of
c  one side of the cell; it is defined based on cell area.
c  htcc is a per-cell heat transfer coefficient.
      if (lht.eq.0) then
       t11 = Ncell*dens*Cp*thk/rr
       t12 = t11*t + (Uoc-v)*cur*Ncell + htc*tam
       t13 = t11 + dudt*cur*Ncell + htc
         if (kk.ne.2) then
            t = t12/t13
         end if
         htcc=htc/Ncell
      else
**********Calculate htc instead of Temp **********************
c  For this case the temperature is assumed constant, and the
c  heat transfer coefficient required to keep it constant is
c  calculated as a function of time.  The heat transfer coef.
c  is calculated for heat transferred out of one side of the
c  cell stack.  Htcc is defined as a per-cell heat transfer
c  coefficient.
         if (t.ne.tam) then
           htc = cur*Ncell*(Uoc-v-t*dudt)/(t-tam)
         else
           htc = 0
         endif
         htcc=htc/Ncell
************************************************************
      endif
c
      return
```

```
      end

c**********************************************************************
      double precision function expf(x)
      implicit real*8 (a-h,o-z)
      expf=0.d0
      if(x.gt.-700.d0) expf=dexp(x)
      return
      end

C foil subroutines

c**********************************************************************
      subroutine ekin(j,lag,utz,il4)
      implicit real*8(a-h,o-z)
      parameter(maxt=900)
      common /n/ nx,nt,n1,n2,nj
      common/const/ fc,r,t,frt,cur,ep,epf,eps,epp,epps,pi,nneg,
     1nprop,npos
      common/power/ ed,Vold,ranode,rcathde
      common/var/ xp(10),xx(5,221),xi(5,221),xt(5,221,maxt)
      common/cprop/ sig,area,ct,dfs,Rad,cmax,rka,rkf,tmmax,g01
      common/temp/thk,htc,dudt,Cp,dens,tam,ncell,tin,lht
      common/mat/ b,d
      common/bnd/ a,c,g,x,y
      dimension b(10,10),d(10,21)
      dimension a(10,10),c(10,221),g(10),x(10,10),y(10,10)
c
c%%%%%%%%%%%%%%%%%%%%%%%%%%%%%%%%%%%%%%%%%%%%%%%%%%%%%%%%%%%%%%%%%%%%%%%
c
c     OPEN-CIRCUIT POTENTIAL FUNCTIONS:
c
c     g0 is the open-circuit potential in terms of the solid
c     concentration, xx(3,j),
c     g1 is the derivative of the open-circuit potential wrt
c     the solid concentration
c
c  &&&&&&&&&&&&&&&&&&&&&&&&&&&&&&&&&&
c
      if (lag.eq.1) xx(3,j)=utz*ct
      go to (1,2,3,4,5,6,7,8),npos
    1 go to 101  ! TiS2
    2 go to 102  ! Spinel Mn2O4 (lower plateau)
    3 go to 103  ! NaCoO2:  Sodium cobalt oxide
    4 go to 104  ! Spinel Mn2O4 (upper plateau)
    5 go to 105  ! Tungsten oxide (LixWO3 with 0<x<0.67)
```

```
     6 go to 106  ! CoO2 (Cobalt dioxide)
     7 go to 107  ! V2O5 (Vanadium oxide)
     8 go to 108  ! NiO2 (Nickel dioxide)
c
c  &&&&&&&&&&&&&&&&&&&&&&&&&&&&&&&&&
c     TiS2:
c
   101 delt=-5.58d-04
       zeta=8.1d0
       cT=2.9d04
       g0=2.17+(dlog((ct-xx(3,j))/xx(3,j))+delt*xx(3,j)+zeta)/frt
       g1=(delt-ct/xx(3,j)/(ct-xx(3,j)))/frt
       go to 98
c
c  &&&&&&&&&&&&&&&&&&&&&&&&&&&&&&&&&
c     Spinel Mn2O4 (lower plateau)
c
   102 c1=2.06307d0
       c2=-0.869705d0
       c3=8.65375d0
       c4=0.981258d0
       a1=c3*(xx(3,j)/ct-c4)
       a11=0.1d0
       a12=100.0d0
       a13=1.0d-02
       g0=c1+c2*(dtanh(a1))
       g0=g0+a11*expf(-a12*(xx(3,j)/ct-a13))
       g1=c2*c3/ct/(dcosh(a1))/(dcosh(a1))
       g1=g1-a11*a12/ct*(expf(-a12*(xx(3,j)/ct-a13)))
       go to 98
c
c  &&&&&&&&&&&&&&&&&&&&&&&&&&&&&&&&&
c     NaCoO2:  Sodium cobalt oxide (P2 phase, 0.3<y<0.92)
c
   103 c1=4.4108d0
       c2=-2.086d0
       c3=0.10465d0
       c4=133.42d0
       c5=89.825d0
       c6=0.16284d0
       c7=145.01d0
       c8=71.92d0
       c9=0.01d0
       c10=200.0d0
       c11=0.3d0
       c12=0.885d0
```

```
      a1=xx(3,j)/ct
      g0=c1+c2*a1+c3*dtanh(-c4*a1+c5)+c6*dtanh(-c7*a1+c8)+c9*
     1expf(-c10*(a1-c11))-c9*expf(c10*(a1-c12))
      g1=c2/ct-c3*c4/dcosh(-c4*a1+c5)/dcosh(-c4*a1+c5)/ct-c6*c7
     1/dcosh(-c7*a1+c8)/dcosh(-c7*a1+c8)/ct-c9*c10*expf(-c10*(a1-
     1c11))/ct-c9*c10*expf(c10*(a1-c12))/ct
      go to 98
c
c  &&&&&&&&&&&&&&&&&&&&&&&&&&&&&&&&&&
c     Spinel Mn2O4 (upper plateau)
c
  104 a1=4.06279d0
      a2=0.0677504d0
      a3=21.8502d0
      a4=12.8268d0
      a5=0.105734d0
      a6=1.00167d0
      a7=-0.379571d0
      a8=1.575994d0
      a9=0.045d0
      a10=71.69d0
      a11=0.01d0
      a12=200.0d0
      a13=0.19d0
      g0=a1+a2*dtanh(-a3*xx(3,j)/cT+a4)-a5*((a6-xx(3,j)/cT)**a7-
     1a8)-a9*expf(-a10*((xx(3,j)/cT)**8.0d0))+a11
     1*expf(-a12*(xx(3,j)/cT-a13))
      g1=(1.0d0/cT)*(-a2*a3/dcosh(-a3*xx(3,j)/cT+a4)/dcosh(-a3
     1*xx(3,j)/cT+a4)+a5*a7*(a6-xx(3,j)/cT)**(-1.0d0+a7)+
     1a9*a10*8.0d0*((xx(3,j)/cT)**7.0d0)*expf(-a10*
     1(xx(3,j)/cT)**8.0d0))-a11*a12/cT*expf(-a12*(xx(3,j)/cT-a13))
      if (g0.lt.1.0d0) g0=1.0d0
      if (g0.gt.5.0d0) then
      print*,'solid conc overload ',xx(3,j),j
      g0=5.0d0
      end if
      go to 98
c
c  &&&&&&&&&&&&&&&&&&&&&&&&&&&&&&&&&&
c     Tungsten oxide (LixWO3 with 0<x<0.67)
c     literature data from Whittingham et al
c
  105 c1=2.8767d0
      c2=-0.9046d0
      c3=0.76679d0
      c4=-0.15975d0
```

```
       c5=0.671d0
       g0=c1+c2*xx(3,j)/ct+c3*xx(3,j)*xx(3,j)/ct/ct+
      1c4*expf(100.0d0*(xx(3,j)/ct-0.671))
       g1=c2/ct+2.0d0*c3*xx(3,j)/ct/ct+
      1c4*100.0d0*expf(100.0d0*(xx(3,j)/ct-0.671))/ct
       go to 98
c
c  &&&&&&&&&&&&&&&&&&&&&&&&&&&&&&&&
c     CoO2 (Cobalt dioxide)
c     literature data from Goodenough et al.
c
  106 r1=4.825510
      r2=0.950237
      r3=0.913511
      r4=0.600492
      g0=r1-r2*expf(-((xx(3,j)/ct-r3)/r4)**2.0d0)
      g1=2.0d0*r2*(xx(3,j)/ct-r3)*expf(-((xx(3,j)/ct
     1-r3)/r4)**2.0d0)/r4/r4/ct
      go to 98
c
c  &&&&&&&&&&&&&&&&&&&&&&&&&&&&&&&&
c     V2O5 (Vanadium oxide)  0<y<0.95
c
  107 r1=3.3059d0
      r2=0.092769d0
      r3=14.362d0
      r4=6.6874d0
      r5=0.034252d0
      r6=100.0d0
      r7=0.96d0
      r8=0.00724d0
      r9=80.0d0
      r10=0.01d0
      a2=xx(3,j)/ct
      g0=r1+r2*dtanh(-r3*a2+r4)-r5*expf(r6*(a2-r7))+r8*expf(r9*
     1(r10-a2))
      g1=-r2*r3/dcosh(-r3*a2+r4)/dcosh(-r3*a2-r4)/ct-r5*r6*
     1expf(r6*(a2-r7))/ct-r8*r9*expf(r9*(r10-a2))/ct
      go to 98
c
c  &&&&&&&&&&&&&&&&&&&&&&&&&&&&&&&&
c     NiO2 (Nickel dioxide)  0.45<y<1.0
c
  108 r1=6.515d0
      r2=2.3192d0
      r3=5.3342d0
```

```
       r4=0.41082d0
       r5=200.0d0
       r6=0.44d0
       r7=0.24247d0
       r8=60.0d0
       r9=0.99d0
       a3=xx(3,j)/ct
       g0=r1+r2*a3-r3*a3**0.5d0+r4*expf(r5*(r6-a3))
      1-r7*expf(r8*(a3-r9))
       g1=r2/ct-0.5d0*r3*(xx(3,j)**-0.5d0)/ct**0.5d0
      1-r4*r5*expf(r5*(r6-a3))/ct-r7*r8*expf(r8*(a3-r9))/ct
       go to 98
c
c%%%%%%%%%%%%%%%%%%%%%%%%%%%%%%%%%%%%%%%%%%%%%%%%%%%%%%%%%%%%%%%%%%%%%%%%%%%
c
   98 if(j.eq.n1 .or. lag.eq.1) g01=g0
      if (lag.eq.1) go to 99
c
c%%%%%%%%%%%%%%%%%%%%%%%%%%%%%%%%%%%%%%%%%%%%%%%%%%%%%%%%%%%%%%%%%%%%%%%%%%%
c
c     KINETIC EXPRESSIONS
c
c     h0 is i0/nF, the exchange current density divided by nF.
c     h1 is the derivative of h0 wrt solid concentration, xx(3,j)
c     h2 is the derivative of h0 wrt electrolyte concen., xx(1,j)
c
c  &&&&&&&&&&&&&&&&&&&&&&&&&&&&&&&&&
c
c
c     NONAQUEOUS LIQUIDS
c
      if(il4.eq.0) then
      alpha=0.5d0
      alphc=0.5d0
      h0=rka*dsqrt(xx(1,j))*dsqrt(ct-xx(3,j))*dsqrt(xx(3,j))
      h1=-rka*dsqrt(xx(1,j))*dsqrt(ct-xx(3,j))*dsqrt(xx(3,j))
     1*(1.0d0/(ct-xx(3,j))-1.0d0/xx(3,j))/2.0d0
      h2=rka*dsqrt(ct-xx(3,j))*dsqrt(xx(3,j))/dsqrt(xx(1,j))/2.0d0
c
c  &&&&&&&&&&&&&&&&&&&&&&&&&&&&&&&&&
c
c     POLYMER
c
      else
      alpha=0.5d0
      alphc=0.5d0
```

```
      h0=rka*dsqrt(xx(1,j)*(cmax-xx(1,j))*(ct-xx(3,j))*xx(3,j))
      h1=h0*(0.5*ct-xx(3,j))/xx(3,j)/(ct-xx(3,j))
      h2=h0*(0.5*cmax-xx(1,j))/xx(1,j)/(cmax-xx(1,j))
      endif
c
c  &&&&&&&&&&&&&&&&&&&&&&&&&&&&&&&&&&
c
      r1=alpha*frt
      r2=r1*(xx(2,j)-fc*xx(5,j)*rcathde-g0)
c
      de=-2.d0*r2-r2**3/3.d0
      if(dabs(r2).gt.1.0d-7) de=expf(-r2)-expf(r2)
      pe=expf(-r2)+expf(r2)
      b(3,1)=h2*de
      b(3,2)=-h0*r1*pe
      b(3,3)=h1*de+h0*r1*g1*pe
      b(3,5)=1.0d0-b(3,2)*fc*rcathde
      g(3)=-h0*de-xx(5,j)
c
   99 return
      end
c**********************************************************************
      subroutine prop(nj,n1)
      implicit real*8(a-h,o-z)
      parameter(maxt=900)
      common/const/ fc,r,t,frt,cur,ep,epf,eps,epp,epps,pi,nneg,
     1nprop,npos
      common/var/ xp(10),xx(5,221),xi(5,221),xt(5,221,maxt)
      common/tprop/df(221),cd(221),tm(221),
     1ddf(221),dcd(221),dtm(221),dfu(221),d2fu(221)
c
      do 94 j=1,nj
      if(j .gt. n1) ee=ep
      if(j .le. n1) ee=eps
      go to (1,2,3,4,5,6),nprop
    1 go to 101  ! AsF6 in methyl acetate
    2 go to 102  ! Perchlorate in PEO
    3 go to 103  ! Sodium Triflate in PEO
    4 go to 104  ! LiPF6 in PC (Sony cell simulation)
    5 go to 105  ! Perchlorate in PC (West simulation)
    6 go to 106  ! Triflate in PEO
c
c  &&&&&&&&&&&&&&&&&&&&&&&&&&&&&&&&&&
c     AsF6 in methyl acetate
c
c     diffusion coefficient of the salt (m2/s)
```

```
  101 df(j)=(ee**1.5d0)*1.54d-09
      ddf(j)=0.0d0
c     conductivity of the salt (S/m)
      cd(j)=2.5d0*(ee**(1.5d0))
      dcd(j)=0.0d0
c     transference number of lithium
      tm(j)=0.20d0
      dtm(j)=0.0d0
c     activity factor for the salt
      dfu(j)=0.0d0
      d2fu(j)=0.0d0
      go to 99
c
c  &&&&&&&&&&&&&&&&&&&&&&&&&&&&&&&&&&
c     Perchlorate in PEO
c
c     diffusion coefficient of the salt (m2/s)
  102 df(j)=(ee**1.5d0)*1.78d-12
      ddf(j)=0.0d0
c     conductivity of the salt (S/m)
      cd(j)=1.6d-02*ee**(1.5d0)
      dcd(j)=0.0d0
c     transference number of lithium
      tm(j)=0.10d0
      dtm(j)=0.0d0
c     activity factor for the salt
      dfu(j)=0.0d0
      d2fu(j)=0.0d0
      go to 99
c
c  &&&&&&&&&&&&&&&&&&&&&&&&&&&&&&&&&&
c     Sodium Triflate in PEO
c
  103 r0=1.3041d-07
      r1=4.4978d-07
      r2=-3.1248d-07
      r3=-2.2383d-07
      r4=8.9264d-09
c
c     diffusion coefficient of the salt (m2/s)
      df(j)=0.0001d0*(ee**1.5d0)*(r0+r1*xx(1,j)/1000+
     1r2*((xx(1,j)/1000)**0.5d0) + r3*((xx(1,j)/1000)**1.5d0)
     1+ r4*((xx(1,j)/1000)**3.0d0))
      ddf(j)=0.0001d0*(ee**1.5d0)*(r1/1000d0 +
     10.5d0*r2*(xx(1,j)**(-0.5d0))/(1000.0d0**0.5d0)
     1+ 1.5d0*r3*(xx(1,j)**0.5d0)/1000d0**1.5d0 +
```

```
     13.0d0*r4*(xx(1,j)**2.0d0)/1000d0**3.0d0)
      if (xx(1,j).ge.3.0d03) then
      df(j)=(ee**1.5d0)*1.6477d-12
      ddf(j)=0.0d0
      end if
c     conductivity of the salt (S/m)
      r7=4.32d-05
      r8=0.00017d0
      r9=0.000153d0
      r10=3.73d-05
c
      cd(j)=100*(ee**(1.5d0))*(r7+r8*xx(1,j)/1000+r9*xx(1,j)
     1*xx(1,j)/1000000+r10*xx(1,j)*xx(1,j)*xx(1,j)/1000000000)
      dcd(j)=100*(ee**(1.5d0))*(r8/1000+2.0*r9*xx(1,j)/1000000
     1+3.0*r10*xx(1,j)*xx(1,j)/1000000000)
c
c     transference number of lithium
c
      if(xx(1,j).lt.0.3d03) then
      r5=0.32141d0
      r6=2.5768d0
      r11=71.369d0
      r12=643.63d0
      r13=1983.7d0
      r14=2008.d0
      r15=287.46d0
      tm(j)=r5-r6*xx(1,j)/1000.+r11*xx(1,j)*xx(1,j)/1000000.
     1-r12*((xx(1,j)/1000.)**(3.0d0))+r13*((xx(1,j)/1000.)**4.0d0)
     1-r14*((xx(1,j)/1000.)**(5.0d0))+r15*((xx(1,j)/1000.)**6.0d0)
      dtm(j)=-r6/1000.+2.0d0*r11*xx(1,j)/1000000.-
     13.0d0*r12*(xx(1,j)**2.0d0)/(1000.**3.0d0) +
     14.0d0*r13*(xx(1,j)**3.0d0)/(1000.**4.0d0) -
     15.0d0*r14*(xx(1,j)**4.0d0)/(1000.**5.0d0) +
     16.0d0*r15*(xx(1,j)**5.0d0)/(1000.**6.0d0)
      else
      tm(j)=0.0d0
      dtm(j)=0.0d0
      end if
c
      if(xx(1,j).ge.0.70d03) then
      r5=4.5679d0
      r6=4.506d0
      r11=0.60173d0
      r12=1.0698d0
      tm(j)=-r5+r6*dexp(-((xx(1,j)/1000.-r11)/r12)**2.)
      dtm(j)=-r6*(xx(1,j)/1000.-r11)*2.
```

```
     1*dexp(-((xx(1,j)/1000.-r11)/r12)**2.)/r12/r12/1000.
      end if
c
      if(xx(1,j).ge.2.58d03) then
      tm(j)=-4.4204d0
      dtm(j)=0.0d0
      end if
c
c     activity factor for the salt:  (dlnf/dc) and (d2lnf/dc2)
c
      if(xx(1,j).gt.0.45d03) then
      r17=0.98249d0
      r18=1.3527d0
      r19=0.71498d0
      r20=0.16715d0
      r21=0.014511d0
      thermf=r17-r18*xx(1,j)/1000.+r19*xx(1,j)*xx(1,j)/1000000.-
     1r20*xx(1,j)*xx(1,j)*xx(1,j)/1000000000.+r21*xx(1,j)*xx(1,j)
     1*xx(1,j)*xx(1,j)/1000000000000.
      dthermf=-r18/1000.+2.*r19*xx(1,j)/1000000.-
     13.*r20*xx(1,j)*xx(1,j)/1000000000.+4.*r21*xx(1,j)*xx(1,j)
     1*xx(1,j)/1000000000000.
      end if
c
      if(xx(1,j).le.0.45d03) then
      r23=0.99161d0
      r24=0.17804d0
      r25=55.653d0
      r26=303.57d0
      r27=590.97d0
      r28=400.21d0
      thermf=r23-r24*xx(1,j)/1000.-r25*xx(1,j)*xx(1,j)/1000000.+
     1r26*xx(1,j)*xx(1,j)*xx(1,j)/1000000000.-r27*xx(1,j)*xx(1,j)
     1*xx(1,j)*xx(1,j)/1000000000000.+r28*xx(1,j)*xx(1,j)*xx(1,j)
     1*xx(1,j)*xx(1,j)/1000000000000000.
      dthermf=-r24/1000.-2.*r25*xx(1,j)/1000000.+
     13.*r26*xx(1,j)*xx(1,j)/1000000000.-4.*r27*xx(1,j)
     1*xx(1,j)*xx(1,j)/1000000000000.+5.*r28*xx(1,j)*xx(1,j)
     1*xx(1,j)*xx(1,j)/1000000000000000.
      end if
c
      dfu(j)=(-1.+2.*thermf)/xx(1,j)
      d2fu(j)=1./xx(1,j)/xx(1,j)-2.*thermf/xx(1,j)/xx(1,j)+
     12.*dthermf/xx(1,j)
c
      if(xx(1,j).ge.3.00d03) then
```

```
      dfu(j)=-0.9520/xx(1,j)
      d2fu(j)=0.9520/xx(1,j)/xx(1,j)
      end if
      go to 99
c
c  &&&&&&&&&&&&&&&&&&&&&&&&&&&&&&&&&&
c     LiPF6 in PC (Sony cell simulation)
c
c     this is actually the diff coeff for perchlorate
c     diffusion coefficient of the salt (m2/s)
  104 df(j)=(ee**1.5d0)*2.50d-10
      ddf(j)=0.0d0
c     conductivity of the salt (S/m)
c     pmax=0.5409
      pmax=0.035d0
      pu=0.857d0
      aa=1.093
      bb=0.04d0
      rho=1.2041d03
      fun=pmax*((1.0d0/rho/pu)**aa)*expf(bb*((xx(1,j)/rho-pu)**2.0)
     1-(aa/pu)*(xx(1,j)/rho-pu))
      fun2=2.0d0*(bb/rho)*(xx(1,j)/rho-pu)-aa/pu/rho
      cd(j)=0.0001+(ee**1.5d0)*((xx(1,j))**aa)*fun
      dcd(j)=(ee**1.5d0)*fun*(aa*(xx(1,j)**(aa-1.0d0))+
     1(xx(1,j)**aa)*fun2)
c     transference number of lithium
      tm(j)=0.20d0
      dtm(j)=0.0d0
c     activity factor for the salt
      dfu(j)=0.0d0
      d2fu(j)=0.0d0
      go to 99
c  &&&&&&&&&&&&&&&&&&&&&&&&&&&&&&&&&&
c     Perchlorate in PC (West's simulation)
c
c     diffusion coefficient of the salt (m2/s)
  105 df(j)=(ee**1.5d0)*2.58d-10
      ddf(j)=0.0d0
c     conductivity of the salt (S/m)
      pmax=5.42d0
      pu=0.6616d0
      aa=0.855d0
      bb=-0.08d0
      rho=1.2041d03
      fun=pmax*((1.0d0/rho/pu)**aa)*expf(bb*((xx(1,j)/rho-
     1pu)**2.0)-(aa/pu)*(xx(1,j)/rho-pu))
```

```
      fun2=2.0d0*(bb/rho)*(xx(1,j)/rho-pu)-aa/pu/rho
      cd(j)=0.0001+(ee**1.5d0)*((xx(1,j))**aa)*fun
      dcd(j)=(ee**1.5d0)*fun*(aa*(xx(1,j)**(aa-1.0d0))
     1+(xx(1,j)**aa)*fun2)
c     transference number of lithium
      tm(j)=0.20d0
      dtm(j)=0.0d0
c     activity factor for the salt
      dfu(j)=0.0d0
      d2fu(j)=0.0d0
      go to 99
c
c  &&&&&&&&&&&&&&&&&&&&&&&&&&&&&&&&
c     Triflate in PEO
c
  106 r0=3.18466d-05
      r1=1.9915633d-06
      r2=-1.9504432d-09
      r3=6.307483d-13
      r4=-6.752235d-17
c     diffusion coefficient of the salt (m2/s)
      df(j)=(ee**1.5d0)*7.5d-12
      ddf(j)=0.0d0
c     conductivity of the salt (S/m)
      cd(j)=(ee**(1.5d0))*100.0d0*(r0 + r1*xx(1,j)+r2*xx(1,j)*
     1xx(1,j)+r3*xx(1,j)*xx(1,j)*xx(1,j)+r4*xx(1,j)**4.0d0)
      dcd(j)=(ee**1.5d0)*100.0d0*(r1 + 2.0d0*r2*xx(1,j) +
     13.0d0*r3*xx(1,j)**2.0d0+4.0d0*r4*xx(1,j)**3.0d0)
c     ****************************
c     ****************************
c*********new conductivity function  (S/m) ******************
c     rr0= 32.1374d0
c     rr1= -6.60932d0
c     rr2= -0.0251516d0
c     rr3=  0.0259545d0
c     rr4= -0.0019001d0
c     rr5=  3.41711d-5
c     rr6= 32.1262d0
c     rr7=-44.5889d0
c     rr8=  2.59756d0
c     rr9= -0.0631626d0
c     rr10= 0.000640897d0
c     rr11=-2.35565d-6
c
c     cx=xx(1,j)
c
```

```
c      ff1=((1.0d0+dtanh(rr0-cx**.5))/2.0d0)*
c     +(rr1 + rr2*cx**.5 + rr3*cx + rr4*cx**1.5 + rr5*cx**2)
c      ff2=((1.0d0+dtanh(-rr6+cx**.5))/2.0d0)*
c     +(rr7 + rr8*cx**.5 + rr9*cx + rr10*cx**1.5 + rr11*cx**2)
c      bb1=-1052.65d0
c      bb2=-182.053d0
c      bb3=3.74936d0
c      bb4=0.0242493d0
c      gg=(bb1+bb2*cx**.5+bb3*cx+bb4*cx**1.5)*(1.0/t-1.0/358.0d0)
c      cd(j)=(ee**(1.5d0))*100.0d0*cx*expf(dlog(10.)*(ff1+ff2+gg))
c
c      dff1=((1.0d0+dtanh(rr0-cx**.5))/2.0d0)*
c     +(.5*rr2/cx**.5 + rr3 + 1.5*rr4*cx**.5 + 2.0*rr5*cx)
c      dff2=(((1.0/(dcosh(rr0-cx**.5))**2))/(-4.0d0*cx**0.5))*
c     +(rr1 + rr2*cx**.5 + rr3*cx + rr4*cx**1.5 + rr5*cx**2)
c      dff3=((1.0d0+dtanh(-rr6+cx**.5))/2.0d0)*
c     +(.5*rr8/cx**.5 + rr9 + 1.5*rr10*cx**.5 + 2.0*rr11*cx)
c      dff4=(((1.0/(dcosh(-rr6+cx**.5))**2))/(4.0d0*cx**0.5))*
c     +(rr7 + rr8*cx**.5 + rr9*cx + rr10*cx**1.5 + rr11*cx**2)
c      dgg=(0.5*bb2/cx**0.5 + bb3 + 1.5*bb4*cx**0.5)*
c     +(1.0d0/t - 1.0d0/358.0d0)
c      b=dlog(10.)*(ff1+ff2+gg)
c      dbdc=dlog(10.)*(dff1+dff2+dff3+dff4+dgg)
c      dcd(j)=(ee**(1.5d0))*100.0d0*exp(b)*(1.0d0+cx*dbdc)
c      ****************************
c      ****************************
c      transference number of lithium
c      tm(j)=0.0107907d0 + 1.48837d-04*xx(1,j)
c      dtm(j)=1.48837d-04
       tm(j)=0.2d0
       dtm(j)=0.0d0
c      activity factor for the salt
       dfu(j)=0.0d0
       d2fu(j)=0.0d0
       go to 99
c
c  &&&&&&&&&&&&&&&&&&&&&&&&&&&&&&&&
c
   99 continue
   94 continue
c
       return
       end
c*********************************************************************
c      That's All Folks!
c*********************************************************************
```

## List of Symbols

| | |
|---|---|
| $a$ | specific interfacial area, $m^2/m^3$ |
| $a(\tau)$ | integrals defined by equation 2-41 |
| $a_A^{\theta}$ | property expressing secondary reference state, $dm^3$/mol |
| $A_i$ | integrals defined by equation 2-40 |
| $c$ | concentration of electrolyte, mol/$dm^3$ |
| $c_i$ | concentration of species $i$, mol/$dm^3$ |
| $c_s$ | concentration of lithium in solid phase, mol/$dm^3$ |
| $\hat{C}_p$ | heat capacity per unit mass of cell, J/kg·K |
| $D$,$D_s$ | diffusion coefficient of electrolyte and of lithium in the solid matrix, $cm^2/s$ |
| $\mathcal{D}_{ij}$ | pairwise interaction parameter between species $i$ and $j$, $cm^2/s$ |
| $E$ | specific energy of cell, W·hr/kg |
| $f_A$ | activity coefficient of salt |
| $f_{\pm}$ | mean molar activity coefficient of the salt |
| $F$ | Faraday's constant, 96,487 C/eq |
| $h$ | mesh spacing, m |
| $h_0$ | heat transfer coefficient of cell, $J/m^2 \cdot K \cdot s$ |
| $\mathbf{i}$ | current density, $mA/cm^2$ |

| | |
|---|---|
| $i_o$ | exchange current density, mA/cm$^2$ |
| $I$ | superficial current density, mA/cm$^2$ |
| $j_n$ | pore-wall flux across interface, mol/m$^2$·s |
| $k$ | reaction rate constant |
| $K_{ij}$ | frictional coefficient, J·s/m$^5$ |
| $L$ | thickness of cell, m |
| $M$ | mass per unit area of cell, kg/m$^2$ |
| $M_i$ | molecular weight of component $i$, g/mol |
| $n$ | number of electrons transferred in electrode reaction |
| $\mathbf{N}_i$ | molar flux of species $i$, mol/m$^2$·s |
| $P$ | average specific power of cell, W/kg |
| $r$ | radial distance in a particle of active material, m |
| $R$ | universal gas constant, 8.3143 J/mol·K |
| $R_s$ | radius of solid particles, m |
| $s_i$ | stoichiometric coefficient of species $i$ in electrode reaction |
| $t$ | time, s |
| $\Delta t$ | time step size, s |
| $t_i^0$ | transference number of species $i$ with respect to the solvent |
| $T$ | temperature, K |
| $U$ | open-circuit potential, V |

| | |
|---|---|
| $v_i$ | velocity of species *i*, m/s |
| $V$ | cell potential, V |
| $x$ | distance from the negative electrode current collector or from the Li foil electrode, m |
| $\overline{x}$ | value of variable $x$ at previous time step |
| $y$ | stoichiometric coefficient of lithium in insertion material, defined by $Li_yMO_z$ |
| $z_i$ | charge number of species *i* |
| $\alpha_a, \alpha_c$ | transfer coefficients |
| $\delta_s$ | thickness of separator, m |
| $\delta_+$ | thickness of composite positive electrode, m |
| $\delta_-$ | thickness of composite negative electrode, m |
| $\varepsilon$ | porosity |
| $\eta$ | overpotential, V |
| $\kappa$ | conductivity of electrolyte, S/cm |
| $\gamma_\pm$ | mean molal activity coefficient of the salt |
| $\nu_+, \nu_-$ | number of cations and anions into which a mole of electrolyte dissociates |
| $\rho_i$ | density of component *i*, $g/cm^3$ |
| $\sigma$ | conductivity of solid matrix, S/cm |
| $\tau$ | dimensionless time |
| $\mu_i$ | electrochemical potential of species *i*, J/mol |

| | |
|---|---|
| $\Phi$ | electrical potential, V |

Subscripts

| | |
|---|---|
| - | negative electrode |
| + | positive electrode |
| amb | ambient value |
| *e* | electrolyte |
| eff | effective value of transport property in porous medium |
| *f* | filler |
| ref | reference state |
| *s* | solid phase or separator |
| *t* | maximum concentration in insertion material |
| 1 | solid matrix |
| 2 | solution phase |

Superscripts

| | |
|---|---|
| 0 | with respect to the solvent or initial condition |
| $\theta$ | standard cell potential |

## References

[1] M. Lazzari and B. Scrosati, "A Cyclable Lithium Organic Electrolyte Cell Based on Two Intercalation Electrodes," *J. Electrochem. Soc.*, **127**, 773 (1980).

[2] K. M. Abraham, J. L. Goldman, and M. D. Dempsey, "Rechargeable Lithium/Vanadium Oxide Cells Utilizing 2Me-THF/$LiAsF_6$," *J. Electrochem. Soc.*, **128**, 2493-2501 (1981).

[3] J.-P. Gabano, Ed., *Lithium Batteries,* Academic Press, New York, N. Y. (1983).

[4] A. Hooper and J. M. North, "The Fabrication and Performance of All Solid State Polymer-Based Rechargeable Lithium Cells," *Solid State Ionics,* **9&10**, 1161-1166 (1983).

[5] M. Gauthier, D. Fauteux, G. Vassort, A. Belanger, M. Duval, P. Ricoux, J.-M. Chabagno, D. Muller, P. Rigaud, M. B. Armand, and D. Deroo, "Assessment of Polymer-Electrolyte Batteries for EV and Ambient Temperature Applications," *J. Electrochem. Soc.*, **132**, 1333-1340 (1985).

[6] Sony's Lithium Manganese Rechargeable Battery (AA Size), *JEC Press, Inc.,* p. 26 (February, 1988).

[7] Moli Energy's New Product Data Sheet, *JEC Battery Newsletter,* No. 6, p. 15 (Nov-Dec, 1988).

[8] Sanyo's Lithium Rechargeable Battery, *JEC Battery Newsletter,* No. 3, p. 15 (1989).

[9] D. Guyomard and J. M. Tarascon, "Li Metal-free Rechargeable $LiMn_2O_4$ Carbon Cells: Their Understanding and Optimization," *J. Electrochem. Soc.*, **139**, 937-948 (1992).

[10] S. Megahed and B. Scrosati, "Lithium-ion Rechargeable Batteries," *J. Power Sources,* **51**, 79-104 (1994).

[11] J. Newman, *Electrochemical Systems,* Prentice-Hall, Englewood Cliffs, New Jersey (1991).

[12] Y. Ma, M. Doyle, T. F. Fuller, M. M. Doeff, L. C. De Jonghe, and J. Newman, "The Measurement of a Complete Set of Transport Properties for a Concentrated Solid Polymer Electrolyte Solution," *J. Electrochem. Soc.*, **142**, 1859-1868 (1995).

[13] J. Newman and W. Tiedemann, "Porous Electrode Theory with Battery Applications," *AIChE J.*, **21**, 25-41 (1975).

[14] C. N. Satterfield and T. K. Sherwood, *The Role of Diffusion in Catalysis,* Addison-Wesley, Reading, MA (1963).

[15] R. E. Meredith and C. W. Tobias, "Conduction in Heterogeneous Systems," in *Advan. Electrochem. Electrochem. Eng.*, C. W. Tobias, Ed., **2**, 15-47 (1962).

[16] D. A. G. Bruggeman, *Annalen der Physik,* **24**, 636 (1935).

[17] K. West, T. Jacobsen, and S. Atlung, "Modeling of Porous Insertion Electrodes with Liquid Electrolyte," *J. Electrochem. Soc.*, **129**, 1480-1485 (1982).

[18] F. B. Hildebrand, *Advanced Calculus for Applications,* p. 463, Prentice-Hall Inc., Englewood Cliffs, New Jersey (1976).

[19] C. Wagner, "On the Numerical Solution of Volterra Integral Equations," *J. Mathematics and Physics,* **34**, 289-301 (1954).

[20] A. Acrivos and P. L. Chambré, "Laminar Boundary Layer Flows with Surface Reactions," *Ind. Eng. Chem.*, **49**, 1025-1029 (1957).

[21] M. J. Matlosz, *Experimental Methods and Software Tools for the Analysis of Electrochemical Systems,* Dissertation, University of California, Berkeley (1985).

[22] P. M. Shain, *Cyclic Voltammetry at a Rotating Disk, Electroreduction of Nitrate in Acidic Nickel Solutions, and Frequency-Response Analysis of Porous Electrodes,* Dissertation, University of California, Berkeley (1990).

[23] Z. Mao and R. E. White, "A Finite-Difference Method for Pseudo-Two-Dimensional Boundary Value Problems," *J. Electrochem. Soc.,* **141**, 151-156 (1994).

[24] C. A. C. Sequeira and A. Hooper, "The Study of Lithium Electrode Reversibility against PEO-$LiCF_3SO_3$ Polymeric Electrolytes," *Solid State Ionics,* **9&10**, 1131-1138 (1983).

[25] K. Kanehori, K. Matsumoto, K. Miyauchi, and T. Kudo, "Thin Film Solid Electrolyte and Its Application to Secondary Lithium Cell," *S. S. Ionics,* **9/10**, 1445-1448 (1983).

[26] C. Julien, "Thin Film Technology and Microbatteries," in *Lithium Batteries: New Materials and New Perspectives,* vol. 5, Ed., G. Pistoia, Elsevier Applied Science, North Holland, pp. 167-237 (1994).

[27] S. D. Jones, J. R. Akridge, and F. K. Shokoohi, "Thin Film Rechargeable Li Batteries," *S. S. Ionics,* **69**, 357-368 (1994).

[28] H. S. Carslaw and J. C. Jaeger, *Conduction of Heat in Solids,* Clarendon Press, Oxford, p. 112 (1959).

[29] C. R. Pals, M. Doyle, T. F. Fuller, and J. Newman, "Modeling of Adiabatic and Isothermal Galvanostatic Discharge Behavior of the Lithium/Polymer/Insertion Cell," *Douglas M. Bennion Memorial Symposium Proceedings Volume,* R. E. White and J. Newman, Eds., The Electrochemical Society Proceedings Series, Pennington, NJ (1994).

[30] C. R. Pals and J. Newman, "Thermal Modeling of the Lithium/Polymer Battery I. Discharge Behavior of a Single Cell," accepted by *J. Electrochem. Soc.*, May, 1995.

[31] C. R. Pals and J. Newman, "Thermal Modeling of the Lithium/Polymer Battery II. Temperature Profiles in a Cell Stack," accepted by *J. Electrochem. Soc.*, May, 1995.

[32] J. Van Zee, G. Kleine, R. E. White, and J. Newman, in *Electrochemical Cell Design,* R. E. White, Ed., pp. 377-389, Plenum Press, Inc., New York (1984).

[33] D. Fan and R. E. White, "Modification of Newman's BAND(J) Subroutine to Multi-Region Systems Containing Interior Boundaries: MBAND," *J. Electrochem. Soc.*, **138**, 1688-1691 (1991).

[34] R. Pollard, *Mathematical Modeling of the Lithium-Aluminum, Iron Sulfide Battery,* Dissertation, University of California, Berkeley (1979).

[35] S. V. Patankar, *Numerical Heat Transfer and Fluid Flow,* McGraw-Hill, New York (1980).

[36] A. C. West and T. F. Fuller, "Control-volume Techniques for Modeling of Fuel-cell and Battery Systems," submitted to *J. Electrochem. Soc.*, January 1995.

[37] T. F. Fuller, M. Doyle, and J. Newman, "Relaxation Phenomena in Lithium Ion Insertion Cells," *J. Electrochem. Soc.*, **141**, 982-990 (1994).

[38] M. Doyle, J. Newman, and J. Reimers, "A Quick Method of Measuring the Capacity *versus* Discharge Rate for a Dual Lithium Ion Insertion Cell Undergoing Cycling," *J. Power Sources,* **52**, 211-216 (1995).

[39] P. W. Atkins, *Physical Chemistry,* 4th. Ed., W. H. Freeman and Co., New York, p. 923 (1990).

[40] M. Doyle and J. Newman, "The Use of Mathematical Modeling in the Design of Lithium/Polymer Battery Systems," *Electrochim. Acta,* Proceedings of the 4th International Symposium on Polymer Electrolytes, June 1994.

[41] R. Fong, U. von Sacken, and J. R. Dahn, "Studies of Lithium Intercalation into Carbons Using Nonaqueous Electrochemical Cells," *J. Electrochem. Soc.,* **137**, 2009-2013 (1990).

[42] K. H. Cheng and M. S. Whittingham, "Lithium Incorporation in Tungsten Oxides," *S. S. Ionics,* **1**, 151-161 (1980).

[43] K. Mizushima, P. C. Jones, P. J. Wiseman, and J. B. Goodenough, "$Li_xCoO_2$ ($0<x<1$); A New Cathode Material for Batteries of High Energy," *S. S. Ionics,* **3&4**, 171-174 (1981).

[44] L. W. Shacklette, T. R. Jow, and L. Townsend, "Rechargeable Electrodes from Sodium Cobalt Bronzes," *J. Electrochem. Soc.,* **135**, 2669-2674 (1988).

[45] W. J. Macklin, R. J. Neat, and R. J. Powell, "Performance of Lithium-Manganese Oxide Spinel Electrodes in a Lithium Polymer Electrolyte Cell," *J. Power Sources,* **34**, 39-49 (1991).

[46] T. Ohzuku, M. Kitagawa, and T. Hirai, "Electrochemistry of Manganese Dioxide in Lithium Nonaquous Cell," *J. Electrochem. Soc.,* **137**, 769-775 (1990).

[47] J. R. Dahn, U. von Sacken, M. W. Juzkow, and H. Al-Janaby, "Rechargeable $LiNiO_2$/Carbon Cells," *J. Electrochem. Soc.,* **138**, 2207-2211 (1991).

[48] C. Delmas, H. Cognac-Auradou, J. M. Cocciantelli, M. Menetrier, and J. P. Doumerc, "The $Li_xV_2O_5$ System: An Overview of the Structure Modifications Induced by the Lithium Intercalation," *S. S. Ionics,* **69**, 257-264 (1994).

# Chapter 3

## Simulation of the Lithium Ion Consumer Battery

### 3.1 Introduction

In this work we will focus on the simulation of a lithium-ion battery developed at Bellcore in Red Bank, NJ.[1-6] The experimental prototype cell has the configuration:

$$Li_xC_6 \mid Li_yMn_2O_4,$$

which is becoming an increasingly popular alternative to $Li_xC_6 \mid Li_yCoO_2$ due to the low cost and stability of the materials. The system employs a plasticized polymer electrolyte, consisting of a nonaqueous carbonate solvent mixture and single lithium salt dispersed in an inert polymer matrix which provides mechanical support.[7] Cells are assembled in the discharged state, where they are air stable and free standing.

We will use this battery as our model system to explore many of the features of the computer program DUAL. This will allow us to evaluate the validity of the previously developed mathematical model by comparison with experimental data in the form of discharge curves. Also, we can explore the phenomena that occur during the charge and discharge of this system in order to understand what may limit these processes at higher rates.

The experimental prototype cell is first described, and relevant physical parameters are given. This requires us to obtain a significant amount of experimental data on the system, some of which are not presently available. Thus, in cases where data are not known, we will be forced to estimate values for particular parameters. Simulation results, including discharge curves and comparisons with experimental data, will be given next. Last, we will illustrate the use of the simulations in the design process. The experimental prototype cell was designed

more for fundamental studies without consideration to maximizing the volumetric and gravimetric energy density; this will be one of the goals of the present work.

### 3.2 Description of the system

A diagram of the cell under consideration is given in figure 3-1. The cell has the usual lithium-ion configuration, with each porous electrode consisting of a pseudo-homogeneous mixture of the active insertion material, polymer matrix, nonaqueous liquid electrolyte, and conductive filler additive. The conductive additive used is Super P Battery Black (MMM Carbon, Belgium). The current collectors are either aluminum (for the positive electrode) or copper (for the negative electrode). Details of the cell fabrication procedures have been published previously.[6,7] It is important to note that these procedures have been developed to the point that very reproducible cell behavior is obtained from the cells. The parameters required for the mathematical model can be classified as either transport, thermodynamic, or design-adjustable; we shall discuss them in that order.

The plasticized electrolyte is a multicomponent system; the five species being the polymer, two liquids, cation, and anion. The salt used is $LiPF_6$ in a nonaqueous liquid mixture of ethylene carbonate (EC) and dimethyl carbonate (DMC). The polymer matrix is a random copolymer of vinylidene fluoride and hexafluoropropylene, p(VdF-HFP). Two different liquid solvent ratios (EC:DMC) are used, depending on whether good low-temperature performance is required.[8] The ratio of polymer phase to liquid phase is generally held constant, with the liquid volume fraction equal to 0.724. Under concentrated solution theory, a five-species system requires ten independent transport properties to describe fully the transport processes in the electrolyte. These data include one conductivity, six diffusion coefficients, and three transport numbers. Unfortunately, very little of this information is available; in fact, the experimental

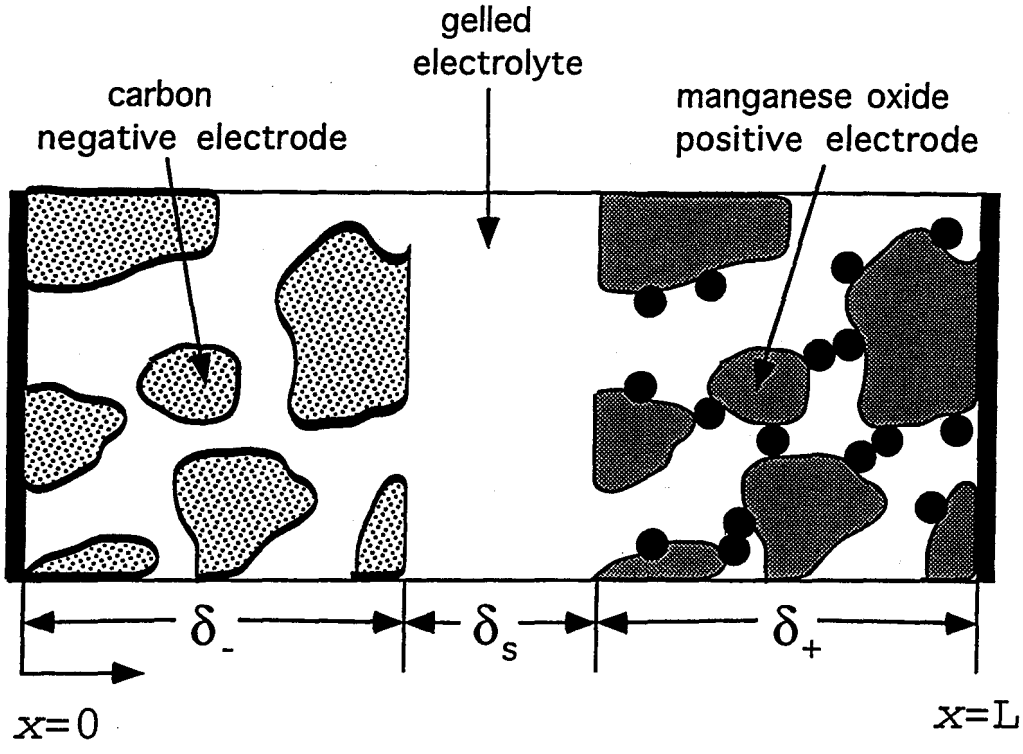


Figure 3-1. Diagram of Li-ion cell sandwich, consisting of composite negative and positive electrodes and separator. Smaller spheres in the positive electrode represent conducting filler.

methodology required to measure these properties has not yet even been developed. Thus, a full description of the electrolyte phase is not available. The data that are available include the conductivity of the plasticized electrolyte as a function of salt concentration, temperature, and solvent ratio EC/DMC.

The conductivity of the liquid/salt/polymer system consisting of a 2:1 v/v mixture of EC/DMC at 25°C was measured and fit to the following function of the salt concentration:

$$\kappa_\infty = 4.1253\times10^{-4} + 5.007\times10^{-3}c - 4.7212\times10^{-3}c^2 + 1.5094\times10^{-3}c^3 - 1.6018\times10^{-3}c^4 . \quad (3\text{-}1)$$

Alternatively, several of the experimental cells use $LiPF_6$ in a 1:2 v/v mixture of EC/DMC; this conductivity is given by

$$\kappa_\infty = 1.0793\times10^{-4} + 6.7461\times10^{-3}c - 5.2245\times10^{-3}c^2 + 1.3605\times10^{-3}c^3 - 1.1724\times10^{-3}c^4 . \quad (3\text{-}2)$$

The concentration, $c$, in these expressions is in $mol/dm^3$, the conductivity is in S/cm, and these functional fits are valid over the range of 0.10 to 4.0 M. The salt concentration is calculated based on the total volume of the plasticized electrolyte, *i.e.*, liquid and polymer phases. Both of these sets of data are given in figure 3-2, along with the fitting expressions.

We should remark that the conductivity of this system is not that expected under the assumption that the polymer matrix is an inert, insulating material. Data on the concentration dependence of the conductivity of the liquid electrolyte alone have also been measured. These data can be used in the Bruggeman relation,[9,10] along with the known volume fraction of the liquid in the plasticized electrolyte ($\varepsilon_{l,s}$=0.724), to estimate its conductivity:

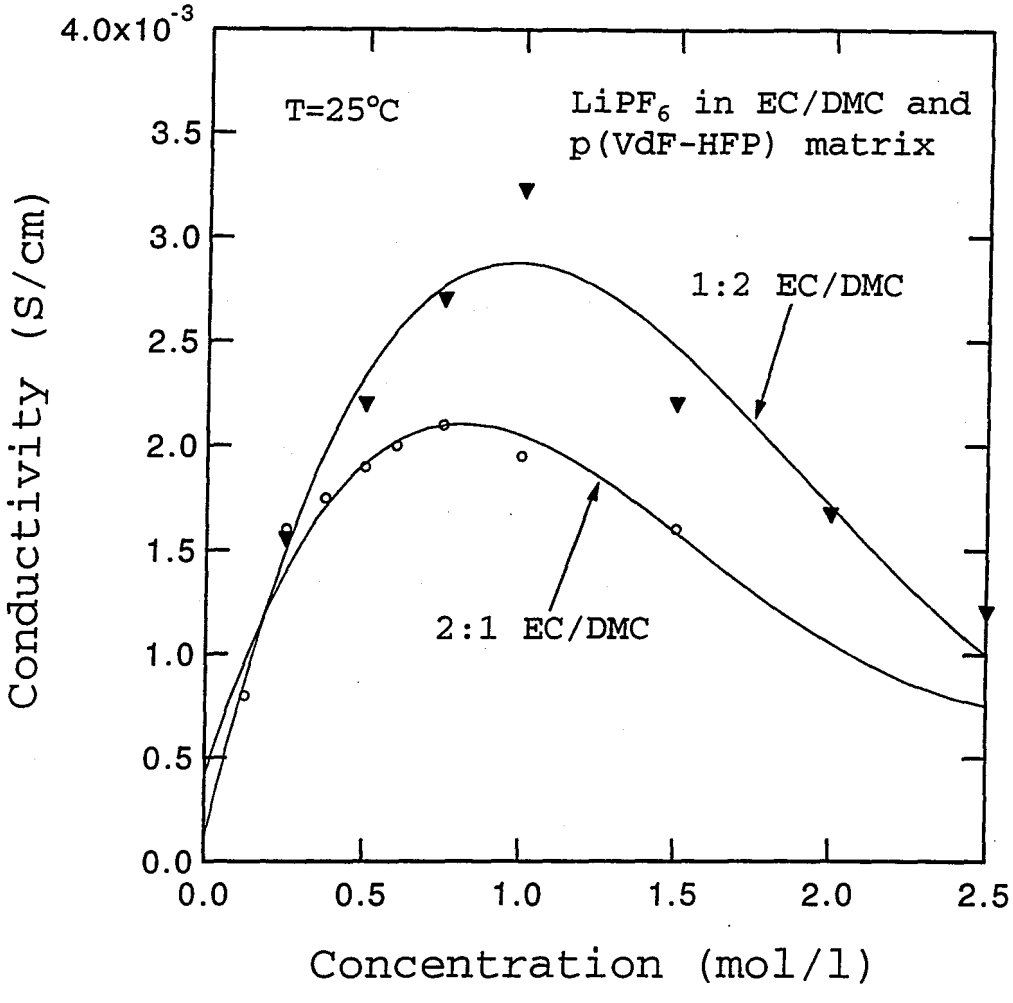


Figure 3-2. Conductivity data for the gelled electrolyte system $LiPF_6$ in EC/DMC and p(VdF-HFP) as a function of salt concentration. The solid lines are analytic fits given in the text.

$$\kappa_\infty = \varepsilon^{1.5}\kappa_l \,, \tag{3-3}$$

where $\kappa_l$ is the conductivity of the liquid phase alone. Upon comparison, one finds that the plasticized electrolyte has a lower conductivity than that predicted by the Bruggeman formula; a better fit is obtained by using an exponent of 4.5 in equation 3-3. These findings are demonstrated in figure 3-3, which compares both sets of conductivity data at 25°C with that predicted by the Bruggeman formula with exponents of 1.5 and 4.5. Considering the complexity of the polymer/liquid plasticized electrolyte mixture, especially solvation of the polymer by the solvent molecules, we should not necessarily expect the Bruggeman expression to hold. This type of effect is motivation for treating these systems as true quaternary mixtures under the framework of concentrated solution theory.

In the composite electrodes, effective values of the conductivity and salt diffusion coefficient apply. These are usually calculated from the true transport properties using expressions of the form:

$$\kappa = \frac{\varepsilon\kappa_\infty}{\tau} \quad \text{and} \quad D = \frac{\varepsilon D_\infty}{\tau} \,, \tag{3-4}$$

where $\tau$ is a tortuosity correction often related to $\varepsilon$ by $\tau = \varepsilon^{-0.5}$.[10] Accounting for the effective transport properties in the porous electrodes can be a difficult task, and past modeling work has often found it necessary to use $\tau$ as an adjustable parameter.[11] We will follow this procedure in the present simulations, assuming that both the conductivity and diffusion coefficient depend on porosity by the empirical relationship:

$$\kappa = \varepsilon^p \kappa_\infty \,, \tag{3-5}$$

where the exponent $p$ will be determined by fitting of the discharge-curve data.

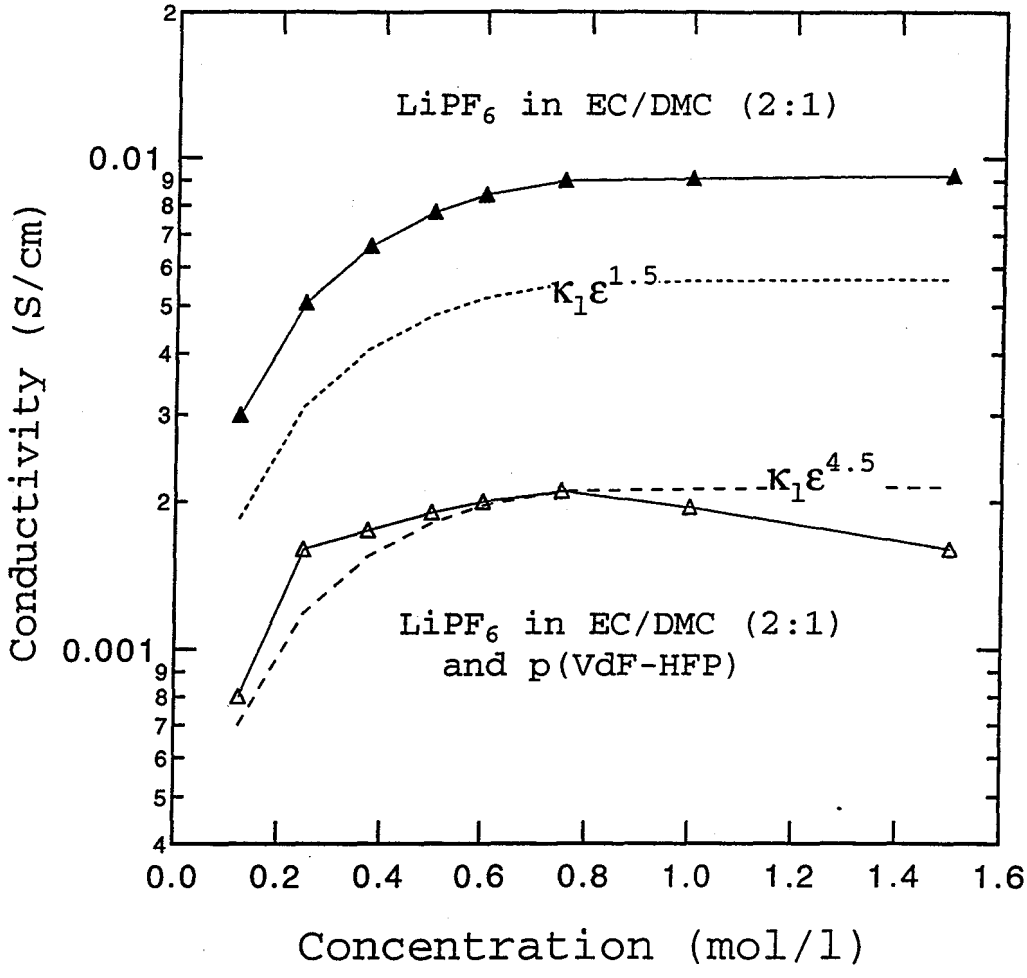


Figure 3-3. Comparison between conductivity data for the pure liquid electrolyte and the liquid plus polymer matrix (gelled) electrolyte. The dashed lines are the predictions of the Bruggeman correction for the volume fraction of the polymer phase.

Additional transport properties include the electronic conductivity and solid-phase lithium diffusion coefficient for each of the electrodes. The conductivity of the carbon electrode is assumed to be large. The manganese oxide electrode, on the other hand, has a poor electronic conductivity and good performance depends on the carbon additive. The electronic conductivity of the positive electrode is found by measuring the resistance to the passage of current through the porous-electrode matrix. This gives a value of $3.8\times10^{-2}$ S/cm for the conductivity of the positive-electrode matrix in the discharged state at T=25°C. The diffusion coefficient of lithium in the lithium manganese oxide spinel electrode has been reported[4] in the literature to be approximately $1\times10^{-9}$ $cm^2/s$. Diffusion coefficients in the carbon electrodes used in the experimental cells (Osaka Gas Mesophase Microbead MCMB 25-10 petroleum coke) are not presently known.

Thermodynamic and kinetic data for the overall cell reaction include an exchange current density and transfer coefficients for each half reaction, as well as open-circuit potential data. Kinetic data on the insertion reactions are not available and have been measured only rarely for any of these materials.[12-15] Insertion reactions are believed to be characterized by large exchange current densities. The fast charge-transfer process, along with the often slow

**Table 3.1.** Parameters for the electrodes.

| parameter | $Li_xC_6$ | $Li_yMn_2O_4$ |
|---|---|---|
| $D_s$ ($cm^2/s$) | $3.9\times10^{-10}$ | $1.0\times10^{-9}$ |
| $\sigma$ (S/cm) | 1.0 | 0.038 |
| $i_o$ ($mA/cm^2$) | 0.11 | 0.08 |
| $c_t$ ($mol/dm^3$) | 24.03 | 22.86 |
| $\rho_-,\rho_+$ ($g/cm^3$) | 1.90 | 4.14 |

**Table 3.2.** Design adjustable parameters.

| parameter | $Li_xC_6$ | $Li_yMn_2O_4$ |
|---|---|---|
| $\delta_-, \delta_+$ (μm) | 100 | 174 |
| $R_s$ (μm) | 12.5 | 8.5 |
| $c_s^o$ (mol/dm$^3$) | 14.66 | 4.10 |
| $\varepsilon_l$ | 0.357 | 0.444 |
| $\varepsilon_p$ | 0.146 | 0.186 |
| $\varepsilon_f$ | 0.026 | 0.073 |
| parameter | value | |
| $T$ (°C) | 25 | |
| $c^o$ (mol/dm$^3$) | 2.00 | |
| $\delta_s$ (μm) | 52 | |
| $\rho_l$ (g/cm$^3$) | 1.324 | |
| $\rho_p$ (g/cm$^3$) | 1.780 | |

diffusion process in the solid, makes the measurement of kinetic data difficult.[13] The open-circuit potential of each electrode is measured in separate cells by performing a very-low-rate discharge (60-hr discharge) *versus* a lithium electrode. The curve fit of each material's open-circuit potential as a function of its state of charge is given in Appendix 3-A. Since the mean molar activity coefficient of the salt is not known, we assume that the solution is ideal. The capacities of each of the electrode materials and densities of each component of the cell are given in Tables 3.1 and 3.2.

The design-adjustable parameters include electrode thicknesses and volume fractions, particle sizes, separator thickness, and initial cell temperature and salt concentration. Electrode thicknesses were measured before and after cell assembly to account for changes in thickness during the lamination steps. The volume fractions of each component were estimated using

mass fractions and component densities. We will compare modeling predictions with experimental data from three cells having various values of the electrode thicknesses and initial salt composition. The system parameters for cell #1 are illustrated in Table 3.2. The specific surface area per unit volume of each electrode is estimated by assuming that the electrode particles are spherical:

$$a = \frac{3(1-\varepsilon_l-\varepsilon_p-\varepsilon_f)}{R_s}. \tag{3-6}$$

We should also include here the initial states of charge of either electrode; however, due to side reactions on the first few cycles, these values are not precisely known and must instead be estimated from the lowest-rate discharge curve. Identical values for all simulation parameters, except for component thicknesses and initial states of charge, will be used for the different sets of simulations.

### 3.3 Simulation results

*Comparison of experimental and simulated discharge curves.* - First we examine the cell potential during galvanostatic discharge at 25°C at various current densities for cell #1. In figure 3-4 the cell potential is given as a function of attainable capacity for discharges at various multiples of the 1 C rate. The solid lines are simulation results, and the markers are experimental data. The 1 C rate is defined as the current density for which the discharge time is one hour; experimental data set this at 1.75 mA/cm$^2$. The capacity at the 0.1 C rate is then defined as full capacity, which is found to be 44.7 mAh for this cell (the cell area is 24 cm$^2$). The discharge curves given in figure 3-4 are at the 0.1 C, 0.5 C, 1 C, 2 C, 3 C, and 4 C rates. The experimental data were taken from a cell that was about 5 cycles into its life, where the

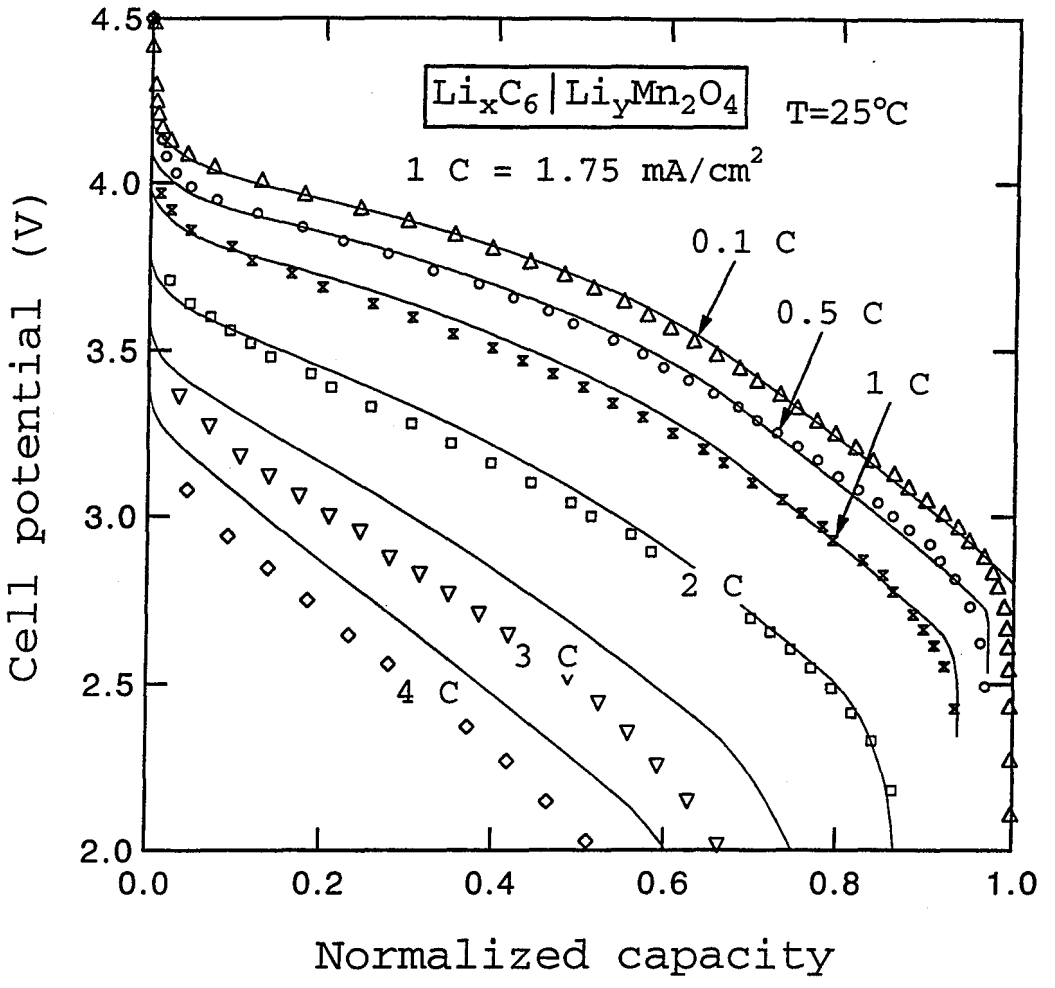


Figure 3-4. Cell potential *versus* fraction of attainable capacity for cell #1 at various discharge rates. The solid lines are simulation results, and the markers are experimental data.

behavior of the cell (*i.e.*, capacity) essentially had stabilized. The charging rate between experimental discharge curves was at the 0.2 C rate.

The initial states of charge of either electrode, $x^0$ and $y^0$, are difficult to determine in practice due to an irreversible side reaction occurring on the carbon electrode on the first cycle. These values can be determined by requiring the simulations to agree with the lowest-rate discharge curve, which nearly traces out the cell's open-circuit potential. This procedure leads to the values: $y^0$=0.18 and $x^0$=0.61. The initial positive electrode stoichiometry is approximately the lowest possible value attainable with the given open-circuit-potential (Appendix 3-A), as would be expected after a low-rate charge up to a cutoff of 4.5 V. As the cell is negative-electrode limited on discharge, the cell capacity is determined by the initial state of charge of the negative electrode.

The diffusion coefficient of lithium in the carbon electrode is used as an adjustable parameter to obtain the agreement seen in figure 3-4. We found that $D_{s,-}$=3.9×10$^{-10}$ cm$^2$/s gives the desired gradual loss of capacity at rates above 0.1 C, which can be explained by solid-state diffusion limitations. This value of $D_{s,-}$ can be determined with a high degree of accuracy from the discharge curves. The solid-state diffusion limitations are rather modest and are quickly dominated by the ohmic drop in the solution at higher discharge rates, above the 1 C rate. In fact, considering the practical desire to minimize the carbon electrode's surface area,[16] minor solid-phase diffusion limitations in this electrode signify an optimized particle size.

For completeness, we must consider that the experimental results could also be explained by using larger carbon particle sizes and literature data on the lithium diffusion coefficient in another petroleum coke material ($D_{s,-}$=5×10$^{-9}$cm$^2$/s, Conoco coke[4]). However, the average particle size used in the cells is readily available (12.5 μm), and the significantly larger particle

size needed to match figure 3-4 with this value of the diffusion coefficient is very unlikely (≈ 44 μm). The time constant for diffusion in the carbon particles, defined as $R_s^2/D$, is 1.1 hours. It is not possible to explain the loss of capacity at increasing rates with solution-phase diffusion limitations, as these would bring about a more severe decrease in capacity (see Appendix 3-B).[17]

A second adjustable parameter used in the simulations is a film resistance on either electrode surface. The resistance is treated by modifying the Butler-Volmer kinetic expression for the insertion reactions:

$$Fj_n = i_0 \left[ \exp\left[ \frac{\alpha_a F \eta_s}{RT} \right] - \exp\left[ -\frac{\alpha_c F \eta_s}{RT} \right] \right], \tag{3-7}$$

where the local surface overpotential is now defined as (compare equation 2-54)

$$\eta_s = \Phi_1 - \Phi_2 - U(c_s, T) - Fj_n R_f, \tag{3-8}$$

and $R_f$ is the value of the film resistance in $\Omega \cdot \text{cm}^2$. The simulations given in figure 3-4 employ a negative electrode film resistance of $R_{f,-} = 800\ \Omega \cdot \text{cm}^2$. This accounts for upwards of 25% of the overpotential in the cell at the 1 C rate. Some physical justification for this model is provided by the passivation of the carbon electrode known to occur on the first few cycles. However, as will be discussed later, it is not possible to determine the origin of this resistance with certainty using these simulations.

The agreement seen on figure 3-4 is excellent for the lower rates (below 3 C) but is not as good for the very high discharge rates (3 C and 4 C). The agreement at low rates is surprisingly good considering the lack of transport property data, particularly activity coefficient and transference number data, necessary for calculating the concentration overpotential. These factors apparently make only a minor contribution to the cell's overpotential. The main

contribution to the overpotential comes from ohmic drop in the electrolyte phase, where the Bruggeman exponent being used here is $p$=3.3. This equates to a positive electrode tortuosity of 2.9 (see equation 3-4), which is a reasonable value.[18] At higher rates, the experimental data exhibit a larger overpotential than the simulations. This increase in cell resistance at the higher discharge rates could not be explained by using unknown physical properties such as kinetic and solution-phase transport data as adjustable parameters in the simulations. The high-rate overpotential also cannot be modeled by decreasing the electronic conductivity of either electrode or by including contact resistances between particles in the porous electrodes.

We also attempted to model this increase in cell resistance using a mass-transfer resistance in the porous electrodes. Under certain operating conditions, it is possible for mass-transfer limitations to arise in the direction normal to the particles.[19] This can be described in an approximate manner by an expression of the form:

$$j_n = -k_m \left[ c - c_w \right] , \tag{3-9}$$

where $c_w$ is the value of the wall concentration. The value $c_w$, solved for using equation 3-9, is used in the Butler-Volmer equation to describe the concentration-dependence of the exchange-current density and local open-circuit potential. Using the values of $k_m$ as adjustable parameters, we were still not able to obtain better agreement with the data in figure 3-4, and this approach was abandoned.

As the film resistance is one of the main contributions to the overpotential in the cell, it warrants further discussion. The agreement between experimental and simulated discharge curves on figure 3-4 is much poorer if an extra source of internal resistance is not included in the simulations. It is possible to increase the value used for $R_{f,-}$ further and obtain better

agreement at the high discharge rates. This is demonstrated in figure 3-5, where discharge curves are given for values of $R_{f,-}$ equal to 900 and 1100 $\Omega \cdot cm^2$. The agreement at high dicharge rates becomes much better while that at the lower rates becomes progressively worse.

It is not possible to distinguish between the two electrodes when attempting to assign the film resistance. For example, figure 3-6 gives a comparison between simulations and the experimental cell data for cell #1 using no film on the negative electrode and a film resistance of 1500 $\Omega \cdot cm^2$ on the positive electrode. The agreement is very similar to that seen in figure 3-4. A larger value of the resistance must be used in the positive electrode because the average value of $j_n$ is smaller for a thicker electrode. In fact, the values of the resistances scale very well with the values of the average transfer-current density, which relate to the quantity:

$$<j_n> = \frac{IR_{s,i}}{3\varepsilon_i F \delta_i} \text{ goes as } \frac{R_{s,i}}{\varepsilon_i \delta_i} \text{ with } i = + \text{ or } -. \qquad (3\text{-}10)$$

We should note that another possible explanation for the internal resistance could be residual resistances located between the current collectors and the electrodes. Our conclusion from this is that additional resistance exists in the porous electrodes that is not properly explained by the present mathematical model, but the origin of this resistance is not known with certainty. Future work using discharge-curve data with individual half-cell potentials from a three-electrode cell, along with the computer simulations, may be used to determine the distribution of resistance between the two porous electrodes.

The values of the exchange current densities used for the insertion processes in this cell are: $i_{0,-}$=0.11 mA/cm$^2$ and $i_{0,+}$=0.08 mA/cm$^2$, evaluated at the initial conditions. We can compare these to values quoted in the literature for various insertion reactions: $i_0(TiS_2)$=0.06 mA/cm$^2$ and $i_0(V_2O_5)$=0.13 mA/cm$^2$.[13-15] Thus, the values used for the present system

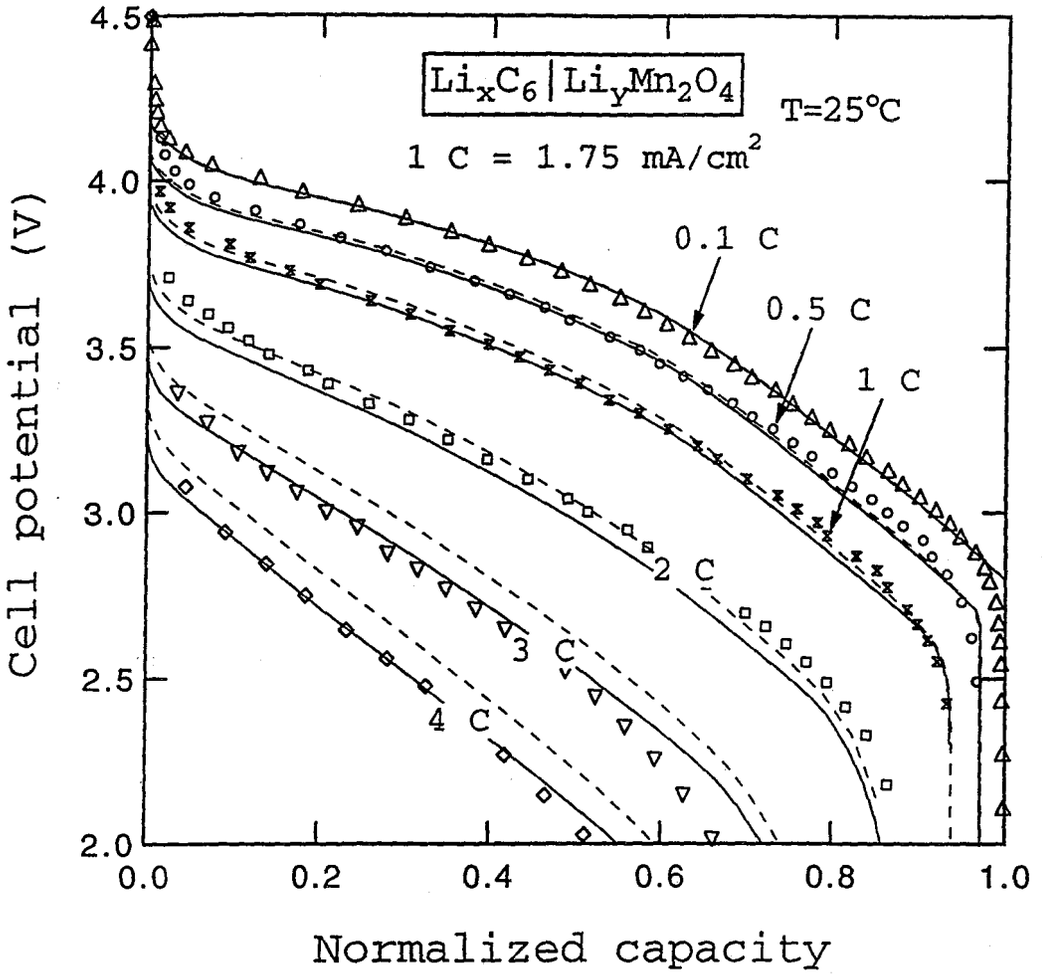


Figure 3-5. Effect of varying the negative electrode resistance on the discharge curves for cell #1. The solid lines are simulation results with a resistance of 1100 Ω cm$^2$, and the dashed lines use a value of 900 Ω cm$^2$.

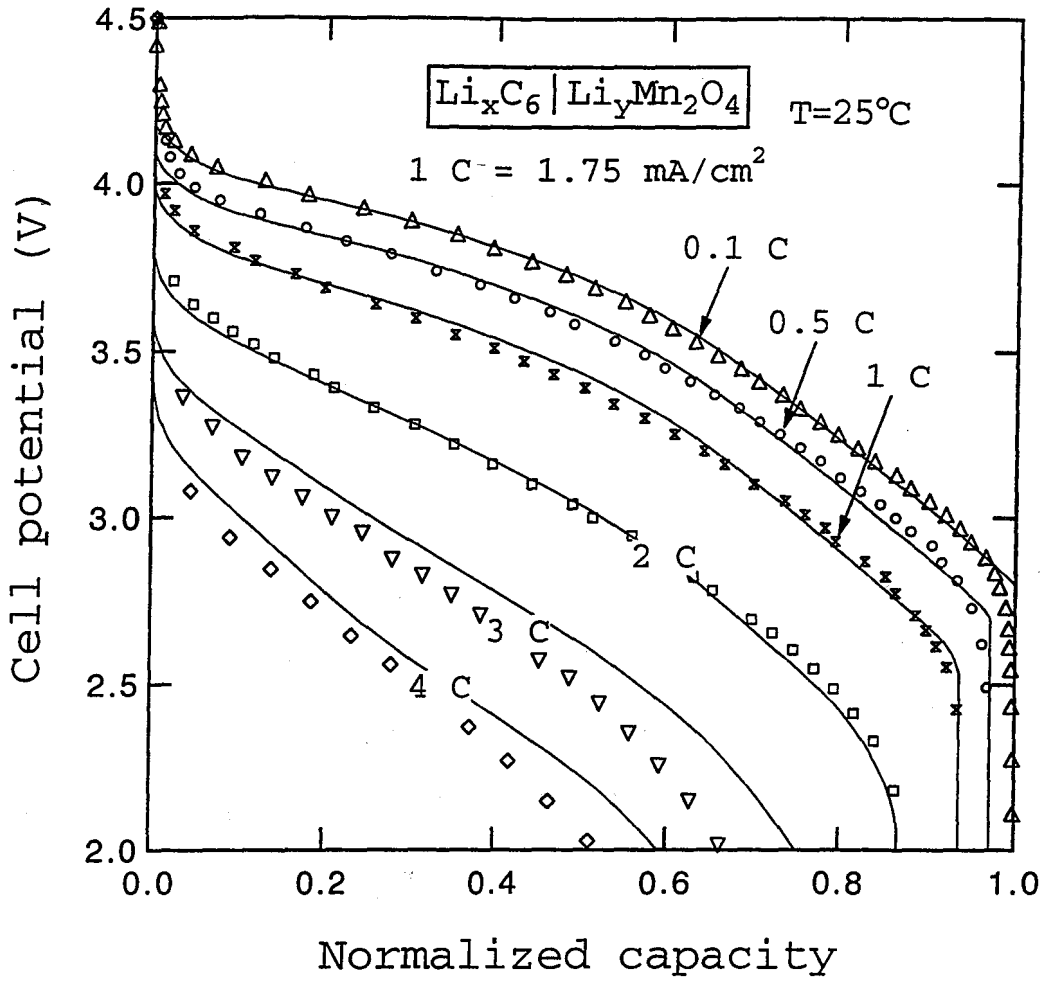


Figure 3-6. Cell potential *versus* fraction of attainable capacity for cell #1 at various discharge rates. The simulations assume a film resistance of 1500 $\Omega$ cm$^2$ exists on the positive electrode particles.

appear to be reasonable. Using larger values of $i_0$ in the electrodes makes little difference to the discharge curves, indicating that a reversible charge-transfer process exists. Even in the negative electrode, where the film resistance is assumed to exist, the value of $i_0$ is unimportant, and an equilibrium situation essentially is established with respect to the charge-transfer reaction.

The same simulated discharge curves from figure 3-4 are plotted in figure 3-7 as a function of the manganese electrode stoichiometric parameter, $y$ in $Li_yMn_2O_4$. Figure 3-7 demonstrates that this cell achieves a maximum stoichiometry in the positive electrode of $y$=0.77; this indicates that the cell is negative-electrode limited, as the carbon runs out of lithium before the manganese oxide is fully utilized. The cell cycles over a range of $y$ of 0.59, which is 71% of the maximum value of $\Delta y$=0.83. A common way to express the utilization is in terms of the attainable capacity of the manganese oxide electrode; for cell #1 one finds that 87.3 mAh/g of manganese oxide ($LiMn_2O_4$) is being utilized (out of a theoretical value of 148 mAh/g if $\Delta y$=1).

Next we consider discharge curves for cell #2, which is identical in design to cell #1 except for the component thicknesses and initial salt composition. Components of cell #2 have the following thicknesses: $\delta_-$=128 μm, $\delta_s$=76 μm, and $\delta_+$=190 μm. The electrolytic solution used in cell #2 is 1 M $LiPF_6$ in a 2:1 ratio of EC/DMC. Unless otherwise noted, all of the simulation parameters identified earlier for cell #1 will be used in the following simulations. Theoretical and experimental discharge curves for cell #2 are given in figure 3-8 for various discharge rates. The 1 C rate is equal to 2.08 mA/cm$^2$; simulated discharge curves are given for the 0.2 C, 1 C, 2 C, 3 C, 4 C, 5 C, and 7 C rates. Experimental data are available at the 0.2 C, 1 C, 3 C, 4 C, and 5 C rates. As before, the $n$ C rate is defined as a multiple of the 1 C rate.

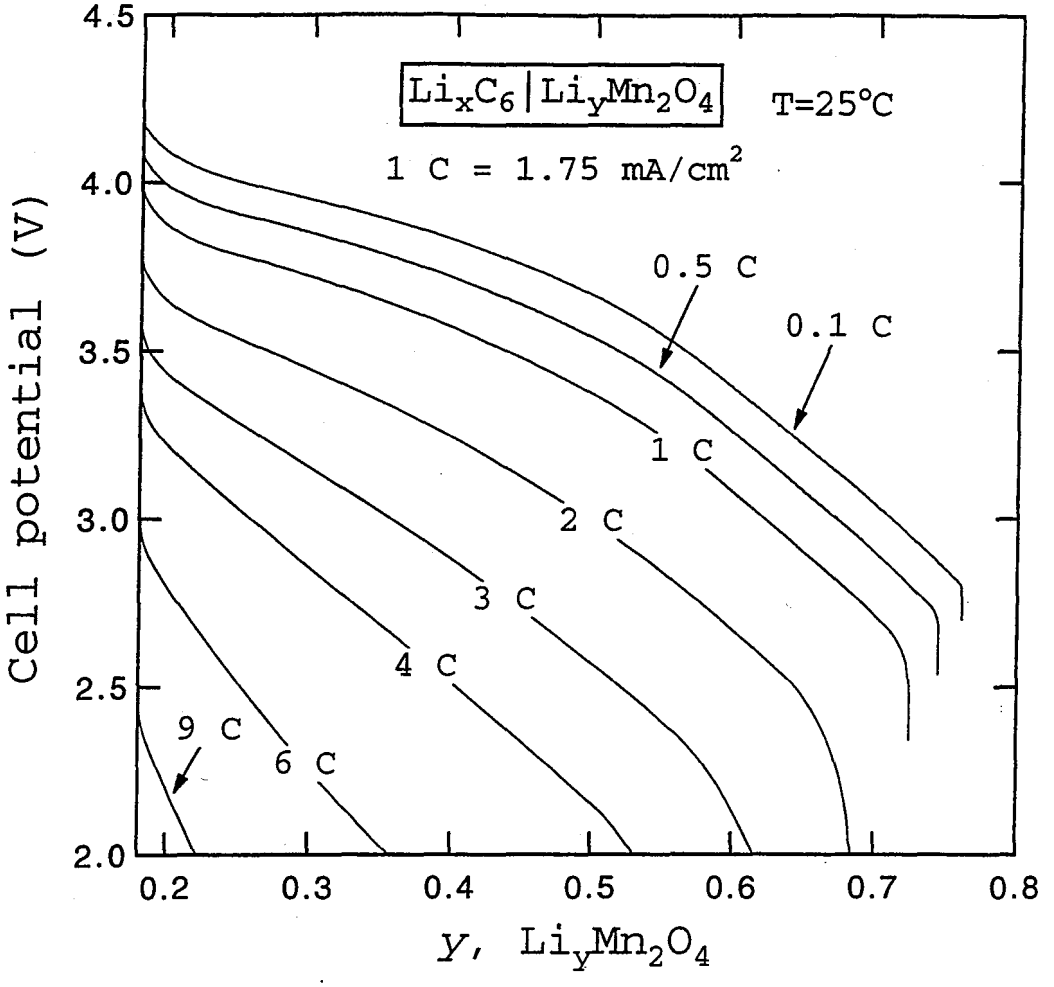


Figure 3-7. Cell potential *versus* utilization of positive electrode for cell #1 at various discharge rates. Discharge rates are given as a multiple of the 1 C rate.

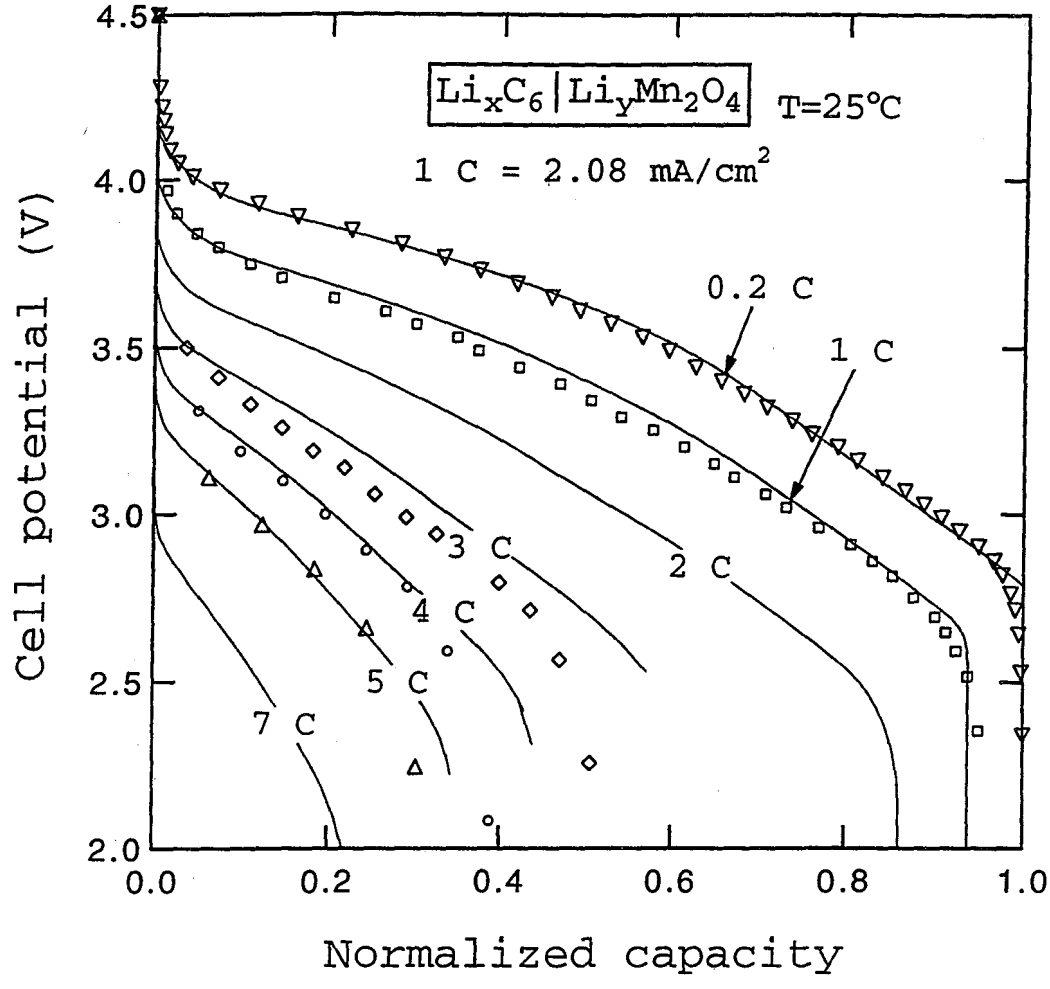


Figure 3-8. Experimental discharge curves, *i.e* cell potential *versus* fraction of attainable capacity, for cell #2 at various discharge rates. The solid lines are simulations, and the markers are experimental data.

The simulated discharge curves for cell #2 show good agreement with the experimental data over the whole range of discharge rates. The initial states of charge for cell #2 were found to be $x^0$=0.52 and $y^0$=0.17. The lower value of $x^0$ for this cell compared to cell #1 is a result of the fact that these experimental discharge curves were taken for a cell that had already been cycled over 50 times, causing some capacity fading. This capacity loss is reflected in the amount of cyclable lithium in the carbon electrode in the charged state, as well as in the final stoichiometry of the manganese oxide electrode. Similarly to the behavior of cell #1, we find that cell #2 is dominated by solution-phase ohmic drop and film resistances, and also has modest solid-phase diffusion limitations at the moderate discharge rates (1 C and 2 C).

Unlike cell #1, this cell begins to exhibit solution-phase diffusion limitations at rates above the 2 C rate. This is the cause of the rapid loss of capacity at these higher discharge rates. The simulations do only a moderate job of capturing this region of the discharge curves; the transport properties used for the electrolyte are $D$=9×10$^{-7}$ cm$^2$/s and $t_+^0$=0.36. In the simulations of cell #1, the values of these transport properties had little effect on the discharge curves. Here, on the other hand, they dominate the behavior of the curves in this one region. Cell #2 has diffusion limitations in the solution phase where cell #1 did not because of the difference in initial salt concentrations.

The transference number and diffusion coefficient used in the simulations are chosen to give the best agreement with the discharge curves for cell #2 and cell #3 (data for cell #3 to follow). We can compare these values with those for 1 M lithium perchlorate in propylene carbonate: $D$=2.58×10$^{-6}$ cm$^2$/s and $t_+^0$=0.20.[20,21] The plasticized electrolyte used in these cells appears to have a lower diffusion coefficient than a pure liquid electrolyte, but a somewhat larger transference number. A more relevant comparison would be between the values of the

ratio:

$$D_+ = \frac{D}{1 - t_+^0}, \tag{3-11}$$

which is equal to the lithium ion diffusion coefficient for a dilute solution. This ratio still retains significance in a concentrated solution as it directly relates to the size of the concentration gradient formed in the cell at steady state:

$$\nabla c = \frac{I(1 - t_+^0)}{FD}. \tag{3-12}$$

The value of $D_+$ for 1 M $LiPF_6$ in EC/DMC with p(VdF-HFP) is calculated to be $1.4\times10^{-6}$ $cm^2/s$; for comparison $D_+$ for 1 M $LiClO_4$ in PC is $3.2\times10^{-6}$ $cm^2/s$. As has been found before, although the plasticized electrolyte is essentially a solid material, its transport properties are comparable to those of a liquid solution.

It was not possible to obtain perfect agreement between the simulations and the experimental data using any combination of $t_+^0$ and $D$. This is to be expected when one considers that the transport properties will likely vary with salt concentration whereas we have assumed constant values. Also, our treatment of the complex plasticized-electrolyte blend as a binary electrolyte is probably not valid. We consider the present treatment of the transport processes in the plasticized electrolyte to be an initial approximation which should be followed by a more rigorous experimental characterization of the system under the framework of concentrated solution theory.

In addition to the discharge performance of the system, it is also necessary to examine the behavior of the cell on charge. This is not studied as thoroughly as the discharge process

because charging tends to be carried out at lower rates. However, in some applications, *e.g.*, electric vehicles, the ability of a system to charge at high rates can be just as important as high-rate discharges. In general, for a lithium-ion cell, one would expect the charge behavior to be similar to the discharge behavior. This symmetry is destroyed by the solid-phase diffusion limitations in the carbon electrode as well as different values for design parameters, such as the active material loading, used in either electrode.

In figure 3-9, we compare simulated charging curves to experimental data. The cell used here is nearly identical to cell #2, with only slightly different electrode thicknesses ($\delta_+$=213 μm and $\delta_-$=134 μm). The 1 C rate for this cell is defined as 2.29 mA/cm$^2$; charging curves are given for the 0.18 C, 0.33 C, 0.5 C, and 1 C rates. Each charging curve was preceded by a discharge at the 1 C rate, except for the 0.18 C curve which was preceded by a 0.18 C-rate discharge. There is some uncertainty in these comparisons because of the effect of the previous moderate-rate discharge on the charging curves. The system is able to recharge to completion for rates up to nearly the 1 C rate (which is still defined with respect to the one-hour discharge). At higher rates, there is a rapid loss of capacity due to the imposition of the cutoff potential. This is more pronounced than in the discharge curves because the upper cutoff potential (4.5 V) is closer to the open-circuit potential than the lower cutoff potential (2.0 V).

The simulations appear to agree reasonably well with the data, particularly with the expected times to reach the 4.5 V cutoff potential. However, the simulations do seem to underestimate systematically the overpotential in the cell on charge. Diffusion limitations are absent from the cell during charging, both in the solution and the solid phases. For the solid state, we conclude that the manganese oxide diffusion coefficient measured previously is accurate,[4] and the particle size used in these cells is satisfactory. Solid-phase diffusion limitations

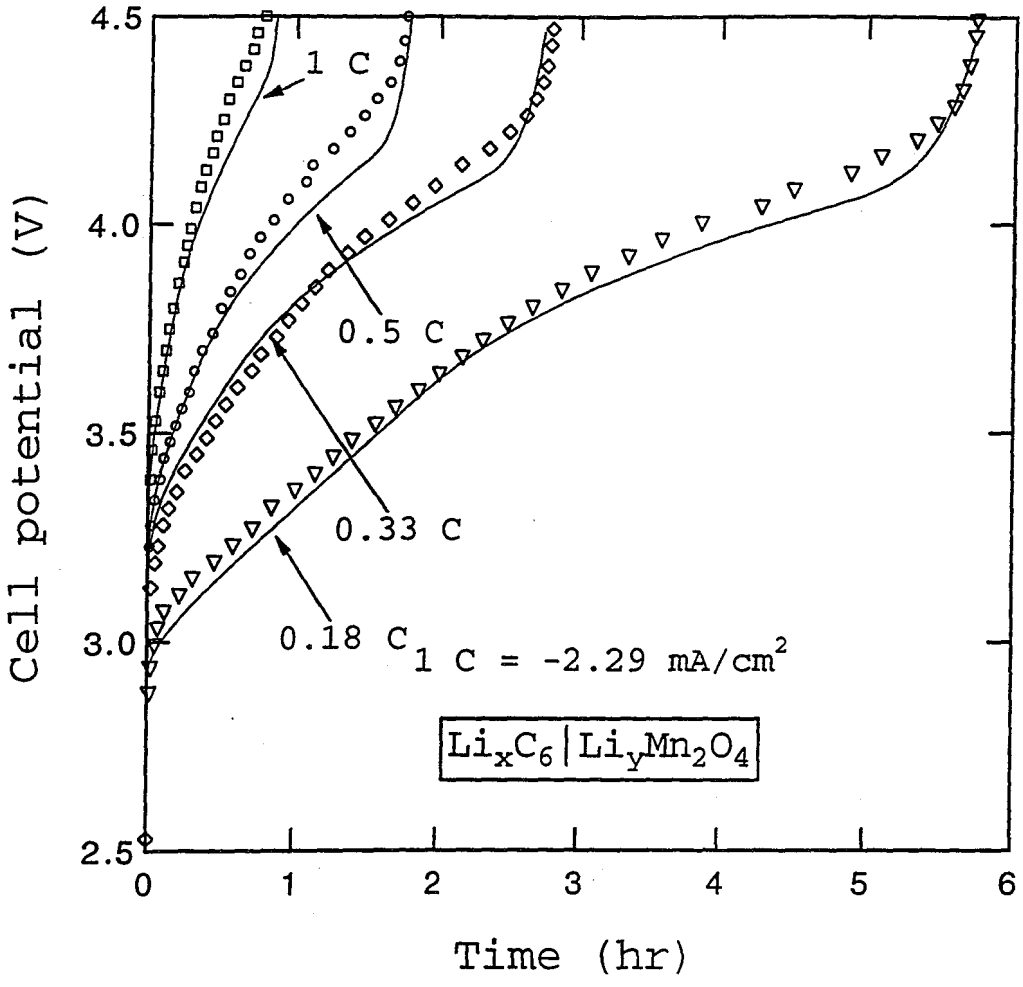


Figure 3-9. Comparison of simulation results to experimental charge curves, *i.e.* cell potential *versus* time, for an experimental cell at various charge rates at 25°C.

in the negative electrode have little impact on the charging process because the carbon electrode's final stoichiometry is only $x$=0.6 on average. We should note that significant solid-phase diffusion limitations at high rates will increase the possibility of having lithium metal plate on the negative electrode. It is possible to simulate charging conditions for which the negative electrode overpotential goes below 0 V *versus* Li at the end of a charge, a point that will be explored later. Diffusion limitations in the solution phase seen in the discharge curves are not seen here because the charging process is confined to low to moderate rates.

The last comparison between the simulations and experimental data that we make is with a very thick cell referred to as cell #3. This cell was fabricated by laminating together two electrodes of the type used in cell #2 to form each electrode for cell #3. The thicknesses of the electrodes in cell #3 are $\delta_+$=366 μm and $\delta_-$=244 μm. The experimental discharge curves are given in figure 3-10, along with the simulated curves at the 0.1 C, 0.2 C, 0.5 C, 1 C, 2 C, and 2.5 C rates. The 1 C rate is defined as 4.17 mA/cm$^2$, the cell area is 24 cm$^2$, and the capacity of cell #3 is 96 mAh. The simulations agree well with the experimental data over the full range of discharge rates. The lowest-rate discharge curve in figure 3-10 attains less capacity than the 0.2 C-rate discharge simply due to capacity fading of this fresh cell (the 0.1 C-rate discharge was taken last).

For cell #3 we found it necessary to use a substantially larger value of the film resistance, $R_{f,-}$=2400 Ω·cm$^2$, to fit the experimental discharge curves. This is three times the value used for the earlier cells. Among the possibilities to account for this observation, the lamination process used to fabricate electrodes could be the source of the extra resistance in the cell. The process consists of thermally laminating individual electrode layers, consisting of active electrode particles and the electrolyte, together with current collecting grids, followed by passing the

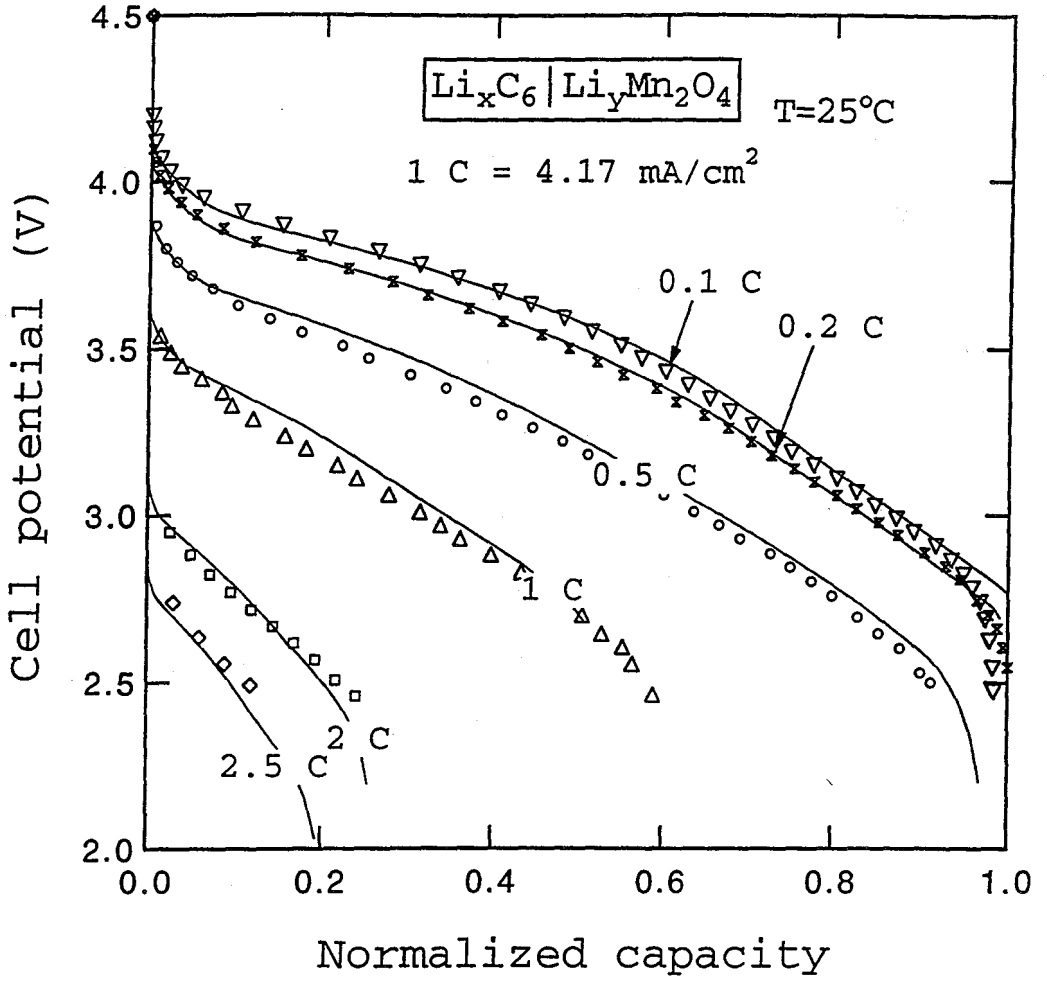


Figure 3-10. Cell potential *versus* the fraction of attainable capacity for cell #3 at various discharge rates. The solid lines are simulations, and the markers are experimental data.

electrodes and separator through the laminator together to form the full-cell sandwich.[6] The interface temperature during the lamination will depend on the thickness of the electrode layers, as the same lamination temperature was used for both thick and thin electrodes. Thus, higher resistances in the thicker electrodes might be explained by incomplete melting of the separator/composite electrode interfaces. Again, comparisons between experimental and theoretical half-cell potentials could be used to support this theory, as we would expect to see the resistance distributed rather equally between the two porous electrodes if this were the case.

Solution-phase diffusion limitations have become more prominent for cell #3 due to the increase in electrode thicknesses. A closer examination of the comparisons between experiment and theory shows that the simulated discharge curves fall off earlier than the experimental data at the highest rates. Even with this minor deficiency in the simulations, we are fairly confident in the accuracy of the values used for $D$ and $t_+^0$ for this system. One finds that changing either of these numbers by about 20% in either direction rapidly leads to very poor agreement with the experimental high-rate dischage curves.

*Discussion of impact of irreversible side reaction on Li-ion simulations*. - It was mentioned previously that there is some difficulty in the determination of the initial states-of-charge of either electrode in a lithium-ion battery. This is a direct consequence of an irreversible side reaction that proceeds between lithium ions and/or the solvent and the fresh carbon electrode surface. This side reaction appears to form a stable, protective film on the carbon which allows the electrode to continue to operate without further reaction; an identical process is thought to occur on the bare lithium surface in nonaqueous liquid electrolytes.[22] Unfortunately, the initial loss of lithium ions in forming this film causes electrodes that are initially balanced in capacity to be thrown out of balance. This necessarily results in a diminished utilization and hence a

decreased specific energy for the battery.

It is helpful to examine the initial few cycles of a fresh lithium-ion cell in order to understand this loss of capacity. Figure 3-11 is a schematic of the capacity of each electrode during the first full cycle of the cell. The capacity is measured by the stoichiometric parameters for either electrode, $x$ and $y$. We assume that the capacities of the electrodes are initially perfectly balanced; this requirement can be quantified by the following relationship between the electrode characteristics:

$$\Delta x C_- \delta_- \varepsilon_- \rho_- = \Delta y C_+ \delta_+ \varepsilon_+ \rho_+ , \tag{3-13}$$

where we define $C$ as the theoretical capacity of the insertion material in mAh/g:

$$C_i = \frac{F}{3.6\, M_i} , \tag{3-14}$$

$M_i$ being the molecular weight of the starting material $LiMn_2O_4$ or $C_6$. Often the criterion for balanced capacities is expressed as a requirement for a specific mass ratio between the two components:

$$\gamma = \frac{\delta_+ \varepsilon_+ \rho_+}{\delta_- \varepsilon_- \rho_-} = \frac{\Delta x C_-}{\Delta y C_+} . \tag{3-15}$$

The values of $\Delta x$ and $\Delta y$ are the inherent cycling ranges for the two materials, assumed to be $\Delta x$=0.61 and $\Delta y$=0.83. For the present system, one finds that $\gamma$=1.8.

The fresh lithium-ion cell is prepared in the discharged state; thus the initial states of charge of the electrodes are assumed to be $x^0$=0.0 and $y^0$=1.0. These values could be obtained, for example, by x-ray diffraction of the powder samples prior to cell assembly. The carbon sur-

face is assumed to be in its unreacted state initially, although it is likely that side reactions with the surface would proceed as soon as the materials were in contact. We will visualize the film formed on the carbon surface as a sink for lithium having a known capacity that is a function of the surface area of the electrode only; this is represented by the lower box below the carbon electrode on figure 3-11a. It is known that this film forms over the first few cycles of the cell; however, for the schematic purposes of figure 3-11, we shall assume that it is completely formed after the first cycle.

Examining the first charge of the fresh cell of figure 3-11b, one sees that the lithium ions taken from the manganese oxide electrode can either insert into the carbon electrode or react on the surface to form the film. Thus, at the end of this charging period, the final stoichiometry of the carbon electrode depends on the amount of lithium that reacted in forming the film as well as the capacity of the positive electrode. If the capacities are initially balanced, because of the lithium lost to the film, the carbon electrode will not reach its maximum utilization. On the first discharge of the cell, the lithium that had managed to intercalate into the carbon is now available to insert into the positive electrode. Because of the initial loss of lithium, there is no longer sufficient lithium to bring the positive electrode up to its full capacity, as pictured in figure 3-11c. Depending on the lithium capacity of the film, this may limit practical positive electrode utilizations to 50 to 75% of the theoretical capacity (for $\Delta y$=0.83).

How can this situation be improved? First, one could consider using a thicker positive electrode so that the capacities of the two electrodes are not balanced in the fresh cell. The added positive electrode material should provide extra lithium ions to form the film on the carbon surface, while still bringing the carbon electrode up to its maximum capacity on charge. It is important to note that one will still not be able to attain full utilization of the manganese

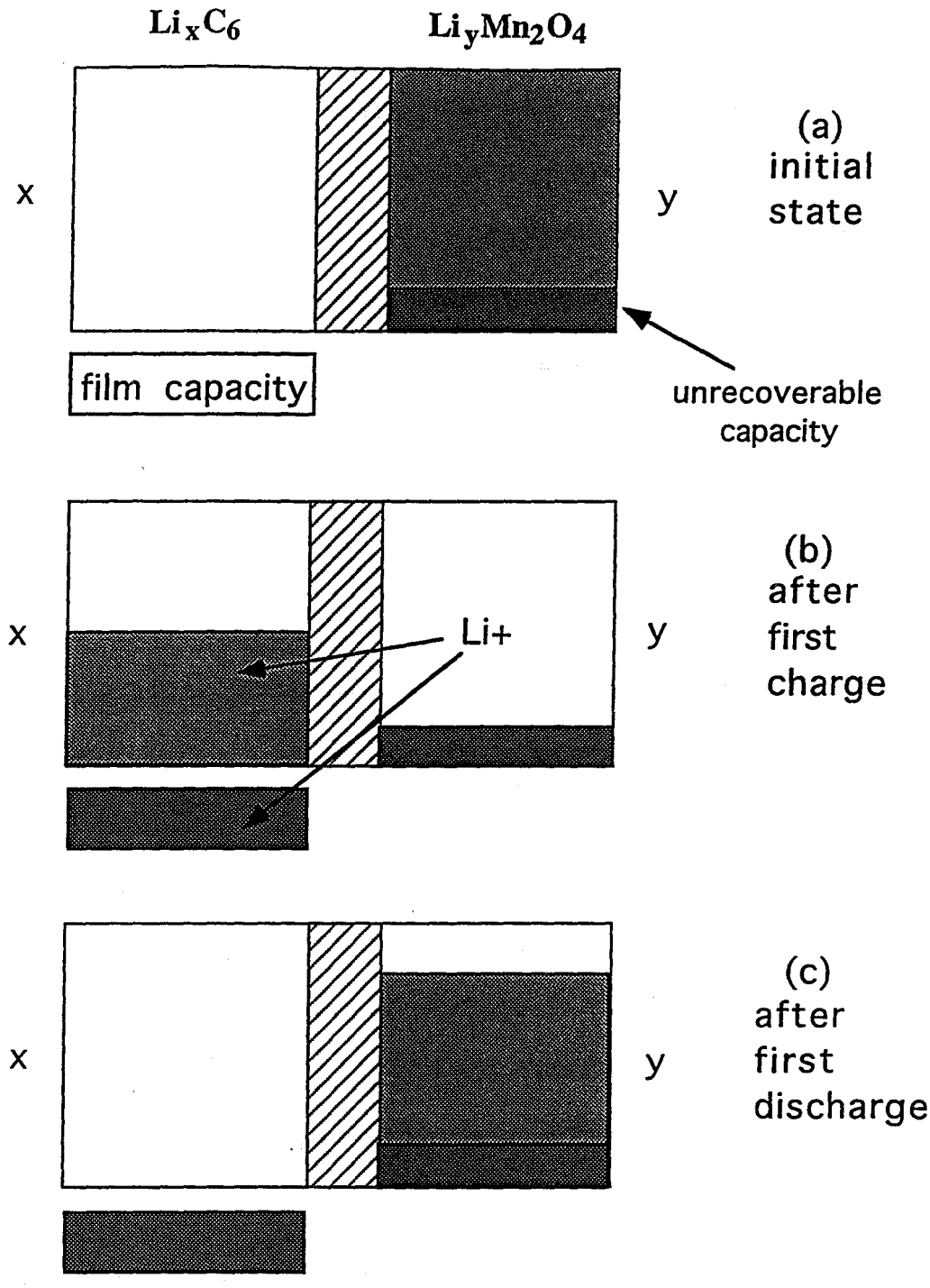


Figure 3-11. Schematic representation of loss of lithium-ion cell capacity to irreversible film formation on carbon electrode during the first cycle.

oxide electrode; the lithium lost to form the film cannot be regained by increasing the positive electrode thickness. The optimum positive electrode thickness will correspond to the amount required by stoichiometry plus an amount that is equal in capacity to the film capacity. As the capacity of the film is unlikely to be known, this can be determined in practice by using a published method.[4,5] This involves monitoring the potential of either electrode *versus* a reference electrode in solution during the first few cycles of a fresh cell. When the thickness of the positive electrode (or the mass of positive electrode material) has been optimized, the potential of the carbon electrode should just reach zero at the end of the first charge, indicating that there is enough extra capacity to form the film and still attain 100% utilization of the carbon electrode.

This procedure was followed successfully for the experimental cells discussed above. For example, with cell #1 we found that the initial state of charge of the negative electrode was $x^0$=0.61. Examination of the open-circuit potential of carbon (Appendix B) indicates that the lithium potential at this state of charge is about 50 mV *vs.* lithium. This is the lowest value at which one could safely operate, indicating that the initial mass ratio was indeed optimized. The optimum mass ratio found using the reference-electrode measurements was approximately 2.1;[4] this can be compared to the mass ratio required for a balanced cell of about 1.8 (with $\Delta x$=0.61 and $\Delta y$=0.83). Thus, we have 16.7% excess capacity in the positive electrode, which is a measure of the amount of lithium needed to form a stable film on the carbon surface; better carbon electrodes are being sought in order to reduce these losses.[22]

An attractive solution to this capacity loss problem would involve having the initial state of charge of the manganese oxide electrode be $Li_yMn_2O_4$ with $1<y<2$.[4] The extra lithium in the manganese oxide electrode initially could be balanced with the film capacity. This should be possible in theory, as the reaction:

$$LiMn_2O_4 + xLi^+ + e^- \rightleftarrows Li_{1+x}Mn_2O_4$$

is known to proceed at a lower plateau at ≈ 3V *vs.* lithium. However, the spinel structure of manganese oxide commonly used in the lithium-ion cells does not cycle reversibly between these two plateau regions. That is, once the additional lithium atoms are inserted into the crystal structure, the spinel structure is no longer the most stable, and an irreversible transformation occurs spontaneously.[23] Also, costs associated with chemical agents such as LiI presently used to carry out this reaction would prohibit large-scale production of $Li_yMn_2O_4$ with $y>1$. Other possible solutions to this capacity-loss problem involve preforming the film; this could involve either an extra lithium source in the cell or cycling of the carbon electrode prior to battery assembly. It is probable that all of these options will be explored in the future.

The problem that this situation creates for numerical simulations is that the initial state of charge of the electrode is not known after the first cycle. Without reference electrodes, it is not possible to tell whether coulombs being passed are inserting into the electrode rather than forming the carbon film. One cannot simply equate the charge passed through an external circuit to the stoichiometry of the insertion electrode, *e.g.*, $\Delta x$. To determine the initial state of charge, we can examine the capacity obtained at some low-rate discharge such as 0.1 C; assuming the cell is negative-electrode limited, we find

$$x^0 = \frac{It_d}{C\_\delta\_\varepsilon\_\rho\_}, \tag{3-16}$$

where $I$ is the current density and $t_d$ the discharge time for some low-rate discharge. This expression assumes that we have discharged to a low potential so that the final value of $x$ is zero. It is also difficult to maximize $x^0$ in practice because the carbon film capacity seems to depend on the type of carbon used, the components of the electrolytic solution, and additives to

the electrode or solution. One is thus required to go through the experimental effort to measure the film capacity with each new material development in the system.

*Effect of positive electrode electronic conductivity on discharge curves.* - There is interest in examining the effect of decreasing values of the manganese oxide electrode's electronic conductivity. This material has a poor intrinsic conductivity, and it is necessary to add a certain amount of conductive additive (usually carbon black) in order to operate the battery successfully. Generally, the optimum carbon content is found experimentally by discharging cells with increasing amounts of carbon additive until increasing the carbon content further has no noticeable effect on discharge curves. Alternatively, one may test the dc-resistance of porous manganese oxide electrodes with various carbon contents. It is often found that the resistivity of the electrode as a function of carbon content follows a percolation model; thus, above a certain threshold carbon content the resistance drops dramatically (the so-called percolation limit). The carbon content should be minimized as a practical matter not only because of penalties to the specific energy but also to limit unwanted side reactions on the positive electrode that have been associated with carbon black additive levels.[24] Using the simulations, one can increase the electrode resistance in order to investigate the consequences of a less-than-desired carbon content on cell performance.

From our experimental measurements, the electronic conductivity of the manganese oxide electrode with carbon black additive in the discharged state is found to be $6\times10^{-3}$ S/cm. This value includes the full porous electrode, with solution phase also; if we correct this for the finite volume of the electrode material by using the Bruggeman factor, an inherent conductivity for the manganese oxide plus carbon is $3.8\times10^{-2}$ S/cm. Figure 3-12 gives discharge curves for decreasing values of the electronic conductivity of the positive electrode. These galvanostatic

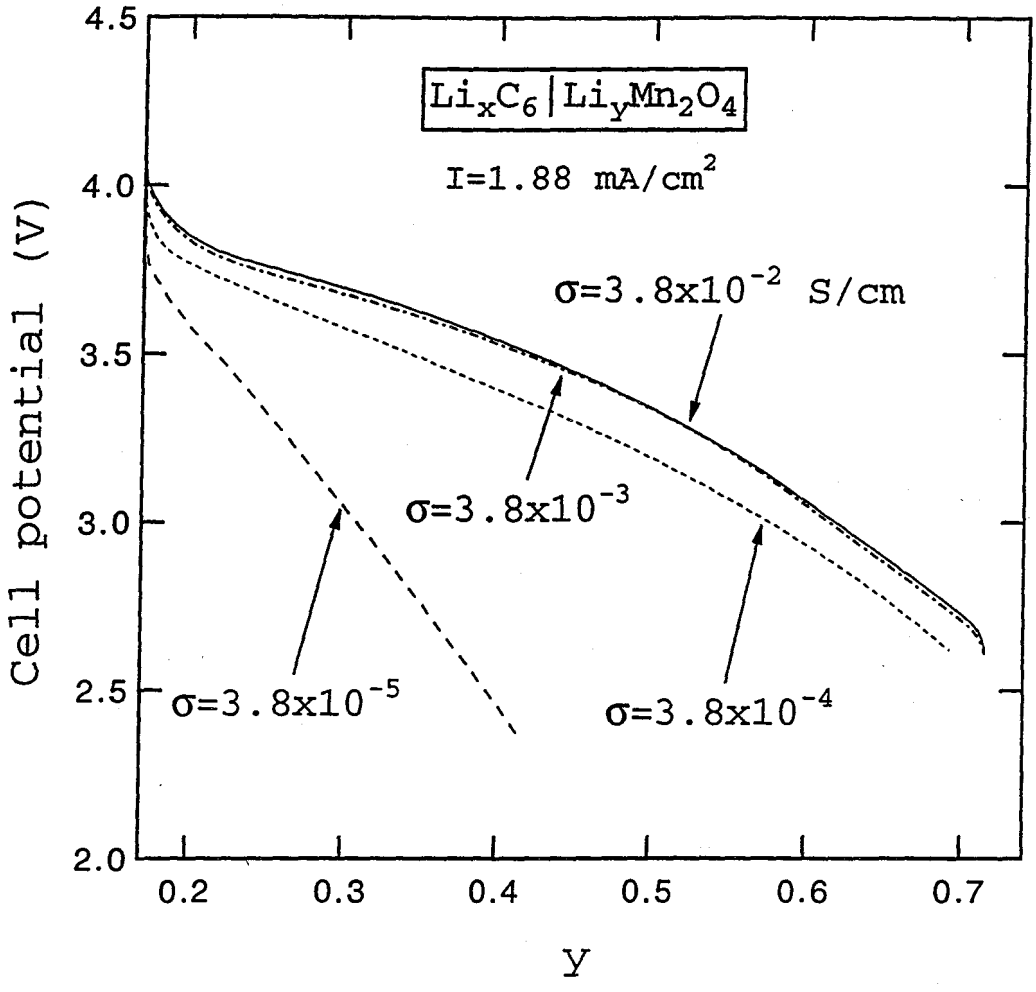


Figure 3-12. Simulated cell potential *versus* state of charge for cell #2 at the 1 C rate for various values of the positive electrode matrix electronic conductivity. The conductivity is reduced from its measured value of 0.038 S/cm.

discharges are for cell #2 at I=1.88 mA/cm$^2$ and 25°C. The electronic conductivity can be reduced by one order of magnitude with little impact on the discharge curve. Then, however, as the conductivity is decreased further, a large drop in utilization occurs. This effect is seen when the electronic conductivity decreases below the ionic conductivity of the solution, causing the system to be ohmically-limited due to the positive electrode.

*Assessment of capacity-rate data using the signature-curve method.* - It is useful to test periodically the rate behavior of a cell undergoing steady cycling. This information is useful to assess the high-rate performance of a cell, which gives information of the power capabilities of the system. Also, the very-low-rate discharge capacity is needed to determine whether capacity fading seen on extended cycling is due to reversible or irreversible capacity loss. Unfortunately, the process of cycling and testing cells is very time consuming, and it is thus beneficial to be able to determine this information in as rapid a manner as possible. For this reason, several battery manufacturers, including some in the lithium-ion battery area, have developed a rapid method of obtaining capacity-rate data for cells.

The process consists of carrying out successive discharges starting with the highest rate and each followed by a lower rate discharge and relaxation period but no charging step. The capacity attained at a given rate is assumed to be the cumulative capacity up to that point. The resulting discharge curve has been dubbed the "signature-curve" for a cell by Moli Energy.[25] This method is much faster than carrying out each discharge and charge separately because most of the cell's capacity is consumed at the higher discharge rates. We demonstrate this process in figure 3-13, where a simulated signature-curve discharge for cell #2 is given (dashed line). Also given on figure 3-13 are individual discharge curves at the 4 C, 3 C, 2 C, and 1 C rates (solid lines). The signature curve pictured here consists of a series of discharges at the 4

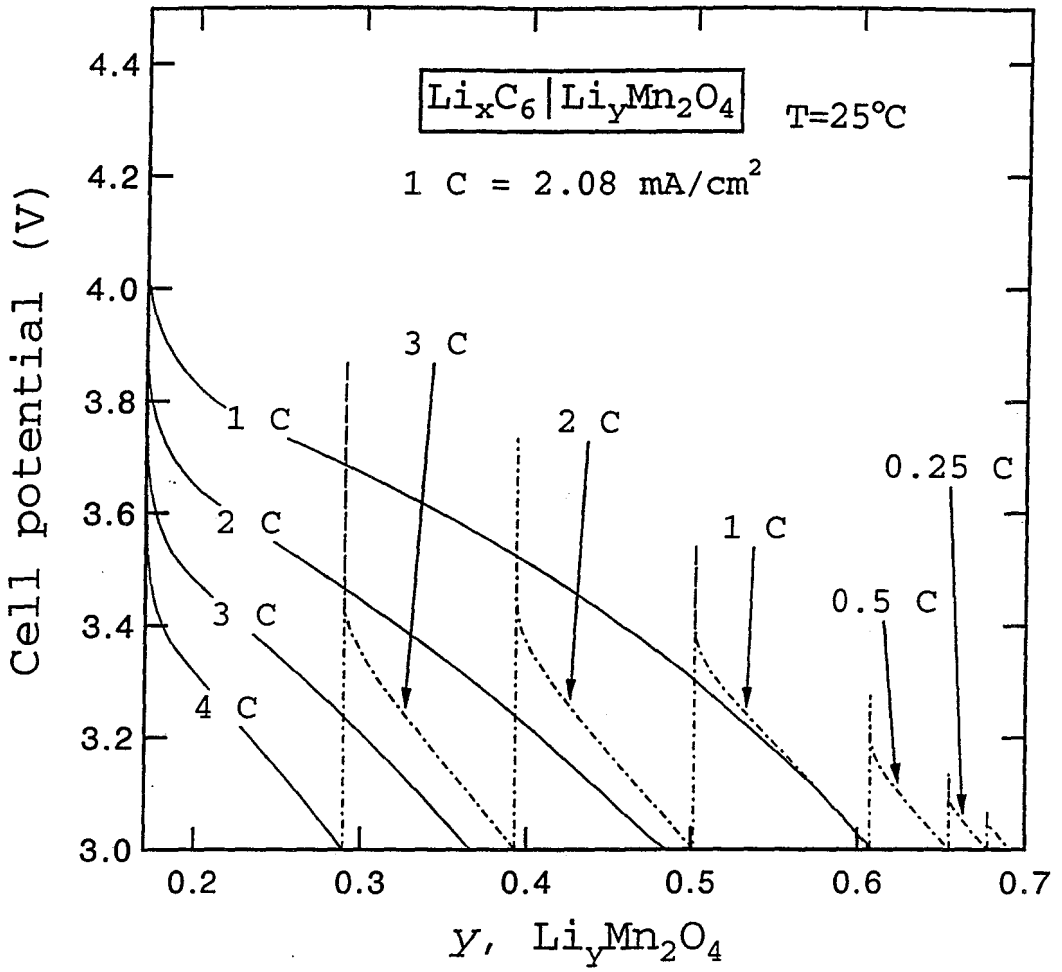


Figure 3-13. Signature-curve predictions for the capacity/rate behavior of cell #2 compared with several individual discharge curves.

C, 3 C, 2 C, 1 C, 0.5 C, 0.2 C, and 0.1 C rates, each followed by a five-minute relaxation period.

The capacity of the cell (to the 3 V cutoff potential) is defined as the intercept of the discharge curve on the abscissa. One can use the individual discharge curves to compare with the predictions for the signature-curve method. It is apparent that the signature curve overestimates the capacity of the cell at the higher rates (3 C and 2 C). Individual discharge curves at rates below the 1 C rate (not pictured here) obtain the same capacity as the signature curve. The reason for the discrepency between capacity predictions at high rates is due to relaxation processes occurring during the five-minute rest period. This time allows lithium to redistribute in the insertion electrodes, giving more favorable conditions for the next discharge. This effect is compounded by using closely spaced high-rate discharges in the signature curve, such as the 4 C, 3 C, and 2 C rates used here. Lower rate discharges are not affected by these processes. The optimal procedure for using the signature-curve method to obtain accurate capacity-rate data has been discussed in the literature.[25]

*Profiles of variables across the full cell.* - One of the unique strengths of battery modeling is its ability to predict the distributions of current, potential, and concentrations across the full cell during its operation. This often will provide information that is either difficult or impossible to determine experimentally, as well as improve our understanding of the phenomena occurring inside of the cells. We will focus on the transient profiles of all of the variables across cell #1 during a 1 C-rate discharge at 25°C, providing profiles of variables in the other cells and at higher rates for comparison only. All of the profiles will be plotted against normalized distances, either using the total cell thickness or the particle radius, as appropriate.

First, figure 3-14 gives salt concentration profiles across the full cell during the galvanostatic discharge. The solution used in cell #1 is 2 M $LiPF_6$ in a 1:2 ratio mixture of EC/DMC.

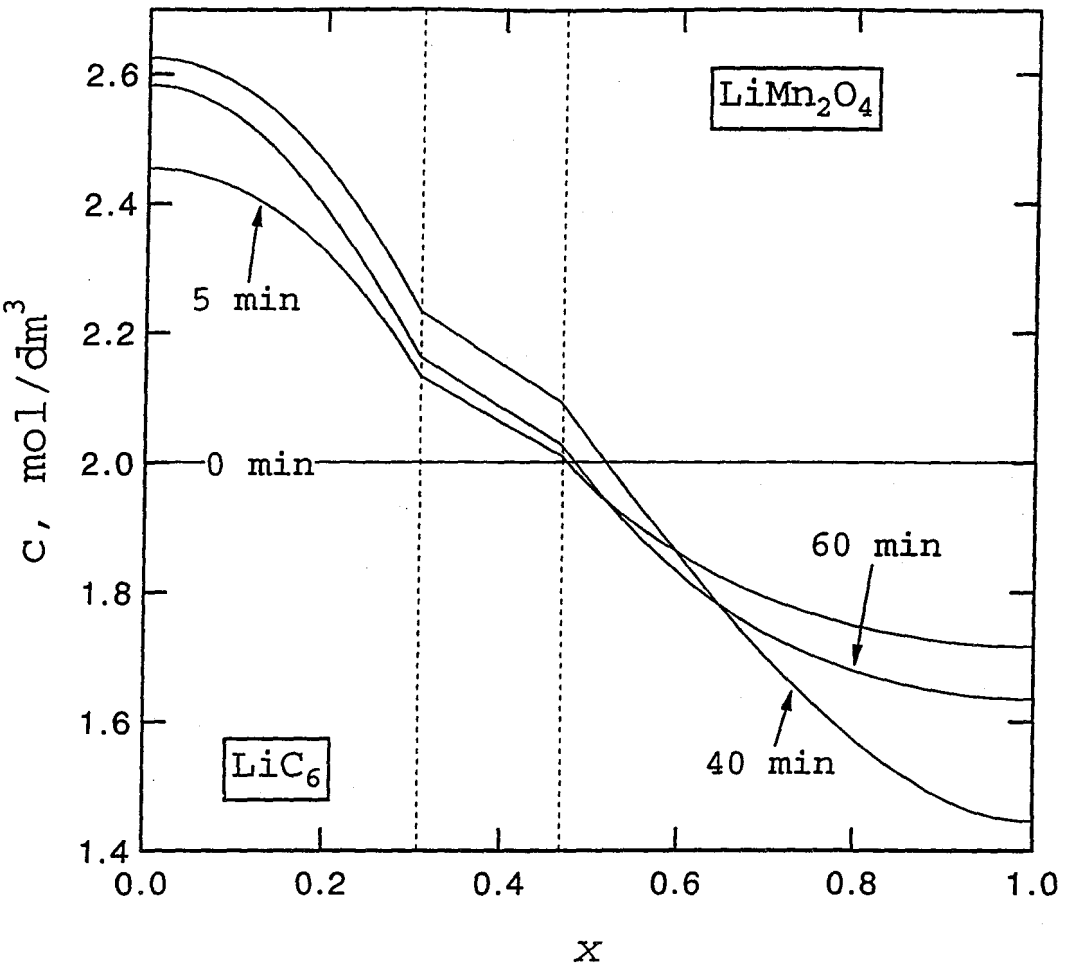


Figure 3-14. Salt concentration profiles across cell #1 during galvanostatic discharge at the 1 C rate. The separator region is set off by dashed lines. Time since the beginning of discharge is given in minutes.

The salt diffusion coefficient is assumed to be constant and equal to $9\times10^{-7}$ $cm^2/s$, whereas the lithium ion transference number used is 0.36. Solution-phase diffusion is sufficiently fast that a limiting current is not reached at the 1 C rate. Since the time constant for diffusion, $L^2/D$, is equal to 0.3 hr, the profiles have time to reach their pseudo-steady-state form (given by equation 3-12) and as manifested by a nearly constant concentration gradient in the separator. The maximum concentration reached in cell #1 at the 1 C rate is about 2.6 M, increasing to 3.4 M at the 4 C rate; at these high concentrations, salt-solubility limitations could be a concern. However, the onset of salt precipitation is difficult to predict in practice due to the possibility of supersaturation.

For comparison, figure 3-15 shows the concentration profiles in cell #2 during the 3 C-rate discharge. The lower initial salt concentration, as well as the high-rate discharge, causes the salt concentration to be driven to zero in the positive electrode after approximately eight minutes. This is the cause of the abrupt loss of capacity in figure 3-8 at rates above the 3 C rate. At even higher discharge rates, the salt concentration can be driven to zero near the front of the positive electrode first. This is demonstrated in figure 3-16, which gives profiles for cell #2 at the 5 C discharge rate. Only four minutes into this discharge, the salt concentration near the front of the electrode reaches zero, and the cell cuts off shortly thereafter.

The solution-phase potential, $\Phi_2$, is plotted in figure 3-17 across the full cell at various times during a 1 C-rate galvanostatic discharge for cell #1. For convenience, the arbitrary zero for the potential has been shifted in this figure to the center of the separator. The difference in the potential across the cell gives an indication of the solution-phase potential drop, which includes contributions from ohmic drop and concentration overpotential. This total potential drop is initially about 60 mV, increasing to 140 mV by the end of discharge. This can be com-

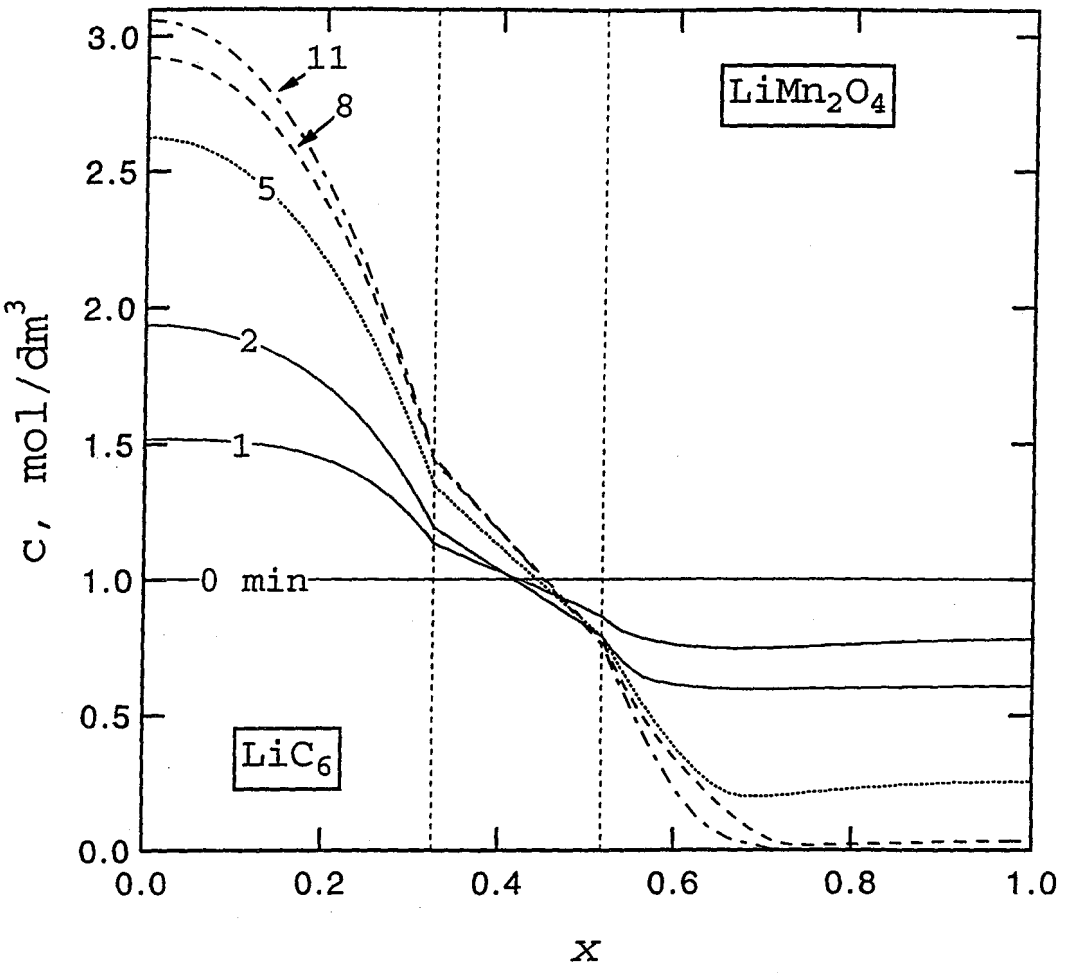


Figure 3-15. Salt concentration profiles across cell #2 during galvanostatic discharge at the 3 C rate ($I=6.25$ mA/cm$^2$). The separator region is set off by dashed lines. Time since the beginning of discharge is given in minutes.

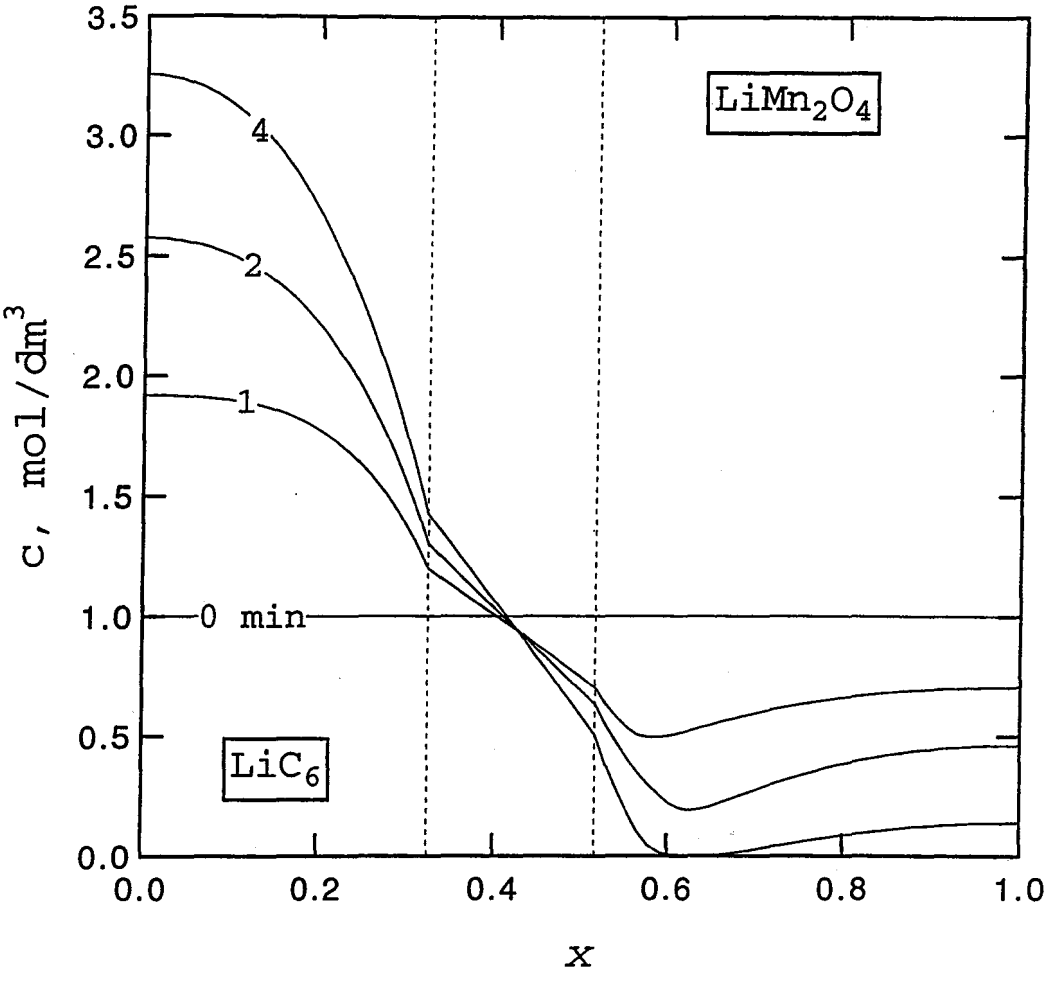


Figure 3-16. Salt concentration profiles across cell #2 during galvanostatic discharge at the 5 C rate ($I=10.5$ mA/cm$^2$). The separator region is set off by dashed lines. Time since the beginning of discharge is given in minutes.

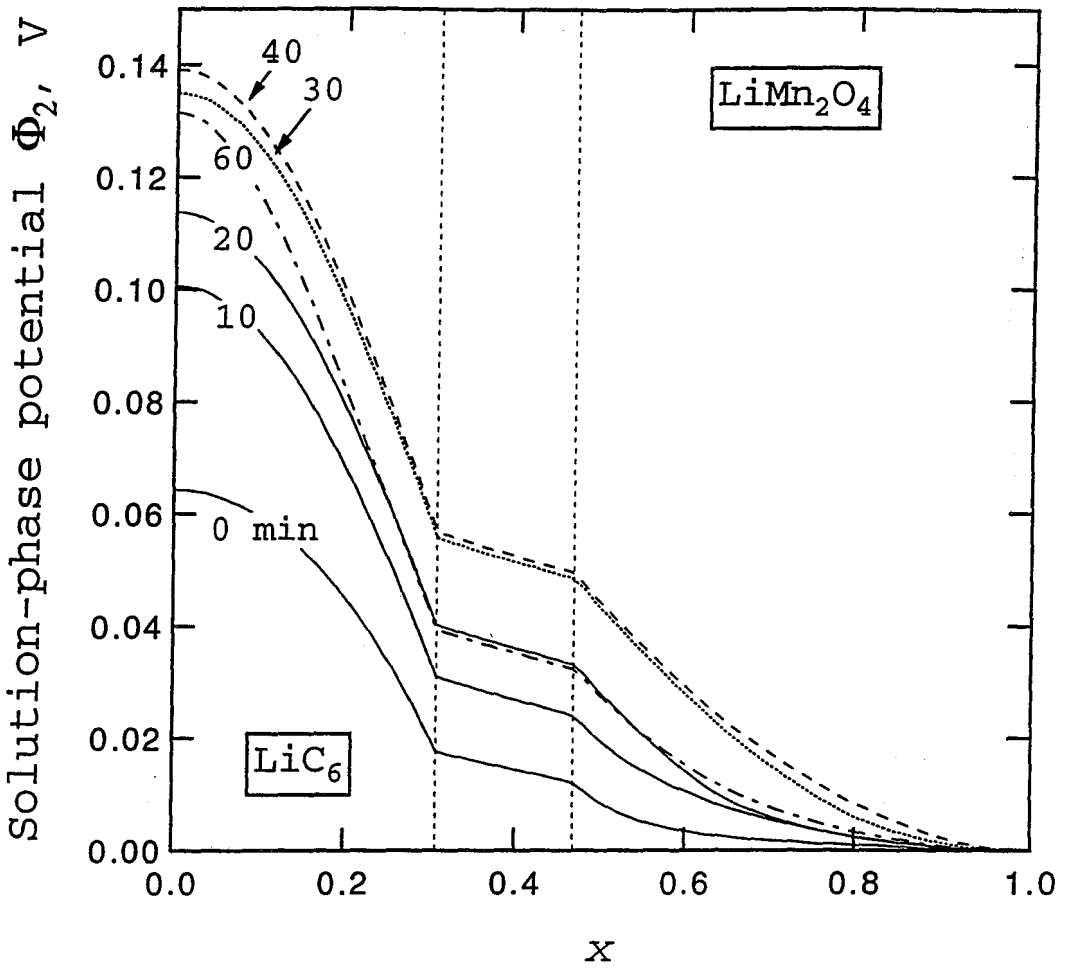


Figure 3-17. Solution-phase potential profiles across cell #1 during galvanostatic discharge at the 1 C rate. The separator region is set off by dashed lines. Time since the beginning of discharge is given in minutes.

pared to the total overpotential in the cell, defined as the difference between the cell potential and the open-circuit potential, which increases from 200 mV to 400 mV over the course of the discharge. As expected, the solution-phase potential drop is the dominant contribution to the total overpotential. Most of the potential drop occurs in the two electrodes, not in the separator. Thus, increasing the volume fraction of the liquid phase of the plasticized-electrolyte mixture in the porous electrodes should bring about a substantial decrease in the ohmic drop, whereas decreasing the separator thickness should cause only a minor improvement. This latter point has been confirmed experimentally.

Next, in figure 3-18, we examine profiles of the current density in solution across the cell under identical conditions to figure 3-17. The current density across the separator region is equal to the applied current density, 1.75 $mA/cm^2$. Inside of either porous electrode, the solution-phase current density decreases as one approaches the current collectors because lithium ions are transferring betweeen the solution and solid phases, leading to an increase in the electronic component of the current density. At the current collectors, the current density in solution reaches zero, and all of the current is carried by electrons. Although the shape of these curves gives one an indication of where the insertion reactions are occurring, figure 3-18 is not particularly interesting as this information is more easily obtained directly from the plots of reaction-rate distribution.

The pore-wall flux, or reaction-rate distribution, for lithium through the interface of either porous electrode is plotted in figure 3-19 during a 1 C-rate galvanostatic discharge. The transfer current density is directly related to the pore-wall flux through the expression,

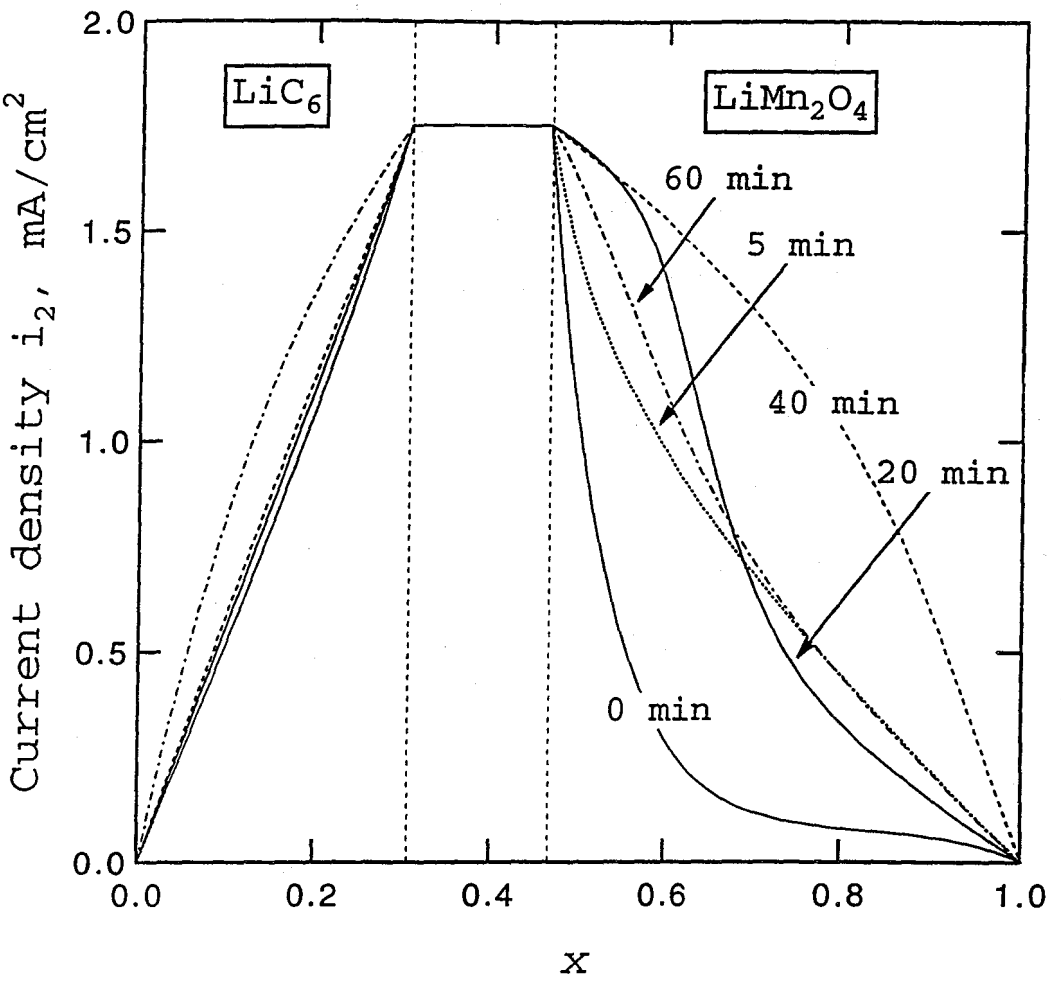


Figure 3-18. Solution-phase current density across cell #1 during galvanostatic discharge at the 1 C rate. The separator region is set off by dashed lines. Time since the beginning of discharge is given in minutes.

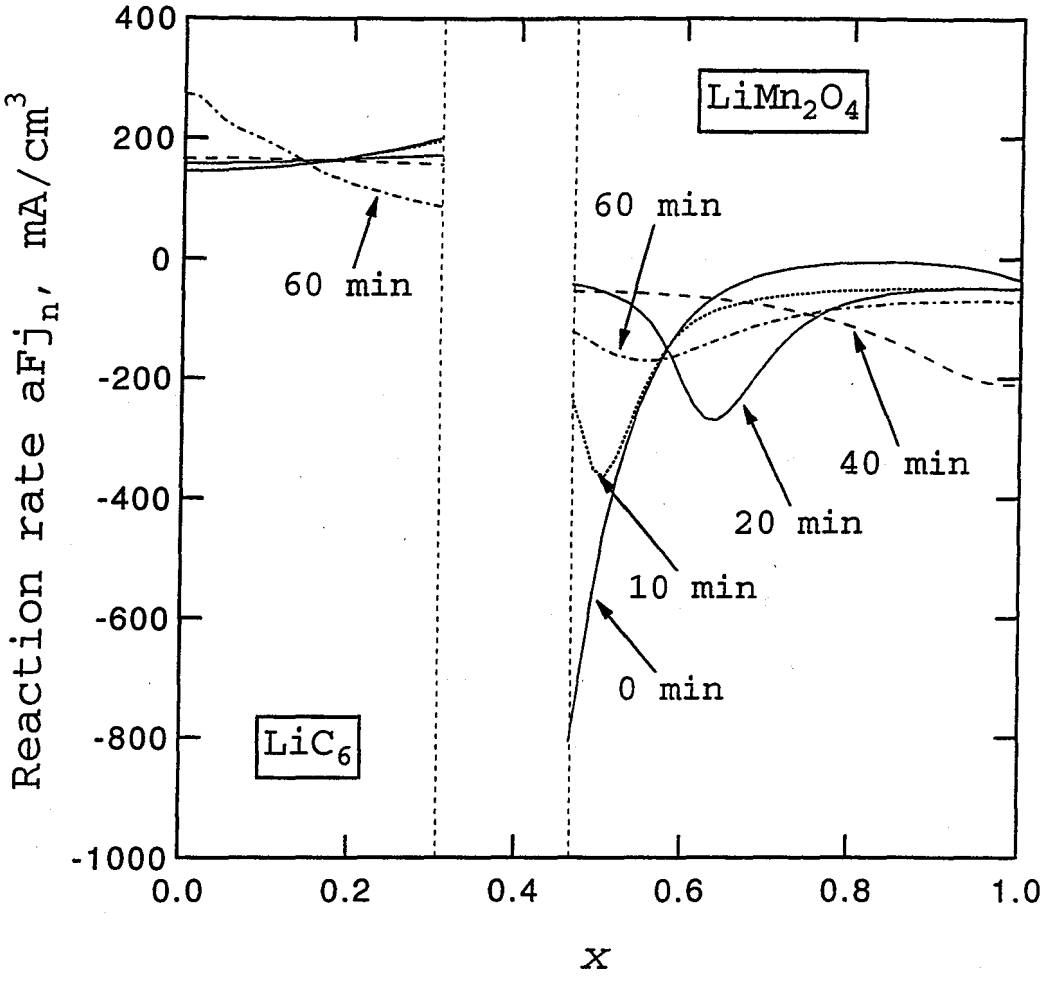


Figure 3-19. Reaction-rate distribution across cell #1 during galvanostatic discharge at the 1 C rate. The separator region is set off by dashed lines. Time since the beginning of discharge is given in minutes.

$$\frac{\partial i_2}{\partial x} = aFj_n \,. \tag{3-17}$$

The pore-wall flux is negative for the positive electrode because lithium ions are being transferred out of solution and into the solid phase. The reaction rate is distributed nonuniformly through the positive electrode but is fairly uniform in the negative electrode. For the negative electrode, the current distribution is more uniform because the open-circuit potential function is sloped, causing lithium to favor deinserting from regions with a higher lithium concentration, as well as because of the film resistance assumed to exist on the electrode surface. Both of these phenomena shift the current distribution from the ohmically-dominated case to resemble a kinetically-dominated, uniform distribution. Near to the end of the discharge (60 min), the reaction begins to favor the back of the negative electrode; this occurs when the front becomes exhausted because of the initially higher current densities in this region.

The situation in the positive electrode is more complicated. As the open-circuit potential of the manganese electrode is flat in the region from $y$=0.2 to 0.6, the reaction distribution resembles an ohmically-limited reaction-zone model (see Appendix 3-A). The insertion reaction proceeds to its completion ($y$=0.6) at a given point before penetrating further into the depths of the positive electrode. Then, the $U$ curve has a slight dip at around $y$=0.6 followed by a second plateau region, causing another reaction front to develop and move though the electrode consuming the rest of the attainable capacity. We barely see this second reaction front in figure 3-19 (60 min) because the average utilization of the manganese electrode is only about $y$=0.73 at the end of a 1 C rate discharge.

Another way to examine the insertion-reaction distributions is to plot the lithium concentration in the solid phase across the two electrodes. The surface value of the lithium concentra-

tion, $c_s$, is plotted in terms of the stoichiometric parameters $x$ and $y$ (*i.e.*, $c_s/c_t$) in figure 3-20 for a 1 C-rate galvanostatic discharge of cell #1. The surface concentration is equal to the average lithium concentration or active material utilization in the absence of solid-state diffusion limitations. This figure allows one to determine which parts of the porous electrodes are being utilized effectively, information that is very difficult to obtain experimentally. Examining figure 3-20, one finds that the state of charge in the negative electrode varies from approximately 0.61 to 0 while that in the positive electrode goes from 0.17 to about 0.73. This corresponds to a positive electrode utilization of 67.5% or 83 mAh/g of $LiMn_2O_4$ at the 1 C rate.

Figure 3-20 can be viewed as a quantitative version of figure 3-11, and can be compared directly to figures 3-11b and 3-11c. The distribution of utilized capacity in either electrode during the discharge follows from the discussion of the reaction-rate distributions shown in figure 3-19. Early in the discharge (5 min curves), the electrodes are utilized primarily in the regions nearest the separator because of the dominance of solution-phase ohmic drop. Later (20 min), the utilization of the negative electrode is more uniform while that of the positive electrode develops a front-like behavior. The details of the distributions of utilized material and their relationship to material properties such as the open-circuit potential for the insertion process have been discussed elsewhere.[26-28]

The mathematical model can also be used to explore the concentration gradients that develop inside the solid insertion electrode particles. Diffusion limitations existing in the carbon electrode lead us to examine the size of the gradient in these particles during the discharge. It is possible to examine profiles at any position into the electrode, but we shall focus on a point near the separator because the final profiles are nearly independent of position. Although the particles near the separator boundary become polarized first, this "limiting current" quickly pro-

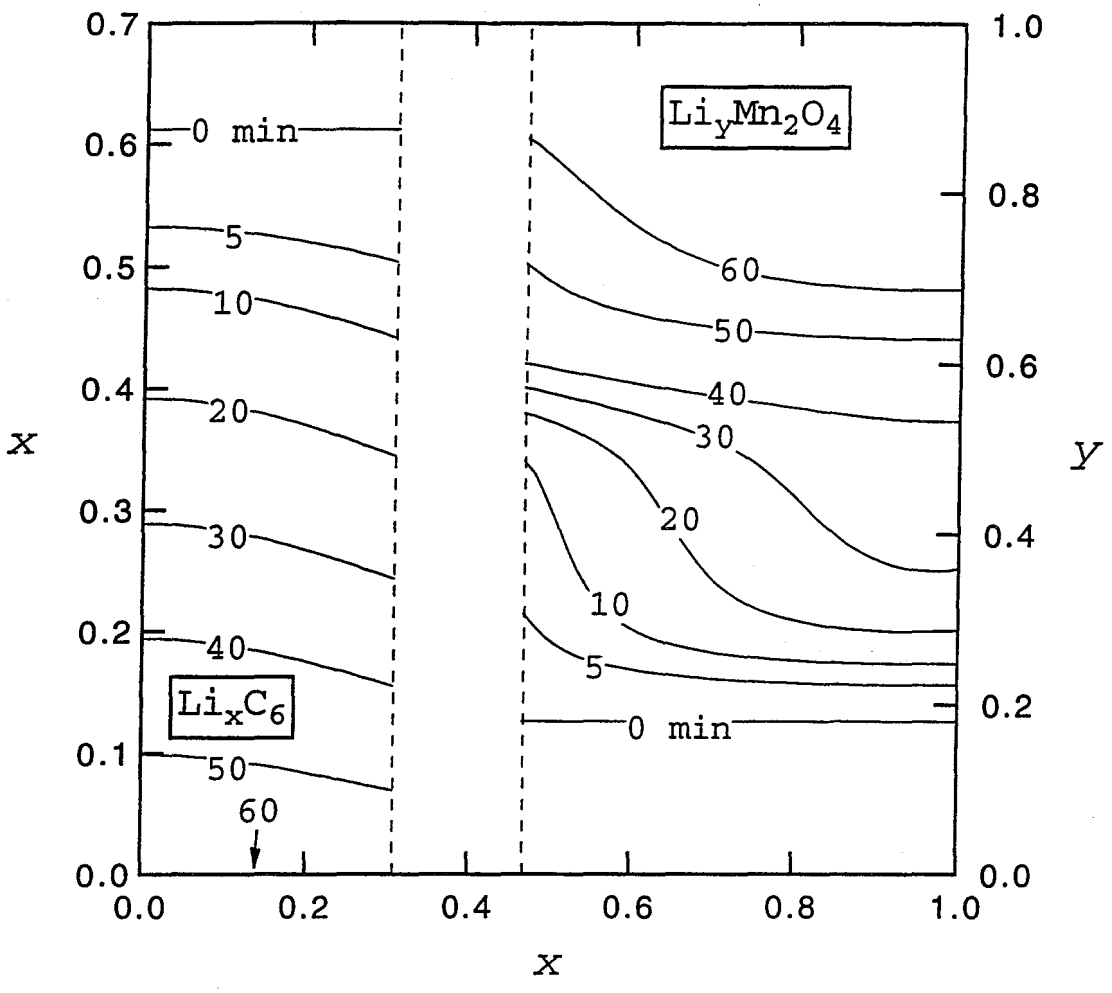


Figure 3-20. Local utilization of active material across the full cell during galvanostatic discharge of cell #1 at the 1 C rate. The separator region is set off by dashed lines.

pagates into the depths of the electrode as the particles in the front no longer can provide the necessary current. In figure 3-21 are various concentration profiles inside of a carbon particle at the end of discharges at different rates (0.5 C, 1 C, and 2 C) for cell #1. Since the concentration gradient scales with the current, at higher rates a larger fraction of the active material is not accessible at the end of the discharge. This scaling is almost, but not quite exactly, linear because the larger current will also influence the reaction-rate distribution.

To demonstrate the dependence of the solid-phase concentration profiles on distance across the electrode, figure 3-22 gives profiles as a function of time at two positions into the negative electrode during a 1 C-rate discharge of cell #2. The solid lines are taken from a particle near the electrode/separator boundary, whereas the dashed lines are for a particle at the back of the electrode. The concentration profiles develop rather quickly into their pseudo-steady-state form:[17]

$$c_s(r=0) - c_s(r) = \frac{-Ir^2}{2aFD_{s,-}\delta_- R_{s,-}} . \tag{3-18}$$

The solid-phase concentration at the back of the porous electrode is slightly greater than that at the front over the full discharge, as would be expected.

During the charging process, it is important to avoid the formation of solid lithium metal on the surface of the carbon electrode. As the cell is negative-electrode limited, it is not obvious that this can be avoided during high-rate charges. In figure 3-23 we examine profiles of the local overpotential, $\Phi_1 - \Phi_2$, across the negative electrode as a function of time during the 1 C-rate charging of cell #2. The potential $\Phi_2$ is defined with respect to a lithium reference electrode, and when $\Phi_1 - \Phi_2$ reaches zero, the lithium plating reaction becomes thermodynamically favorable. Figure 3-23 demonstrates that this may occur near the end of the 1 C-rate

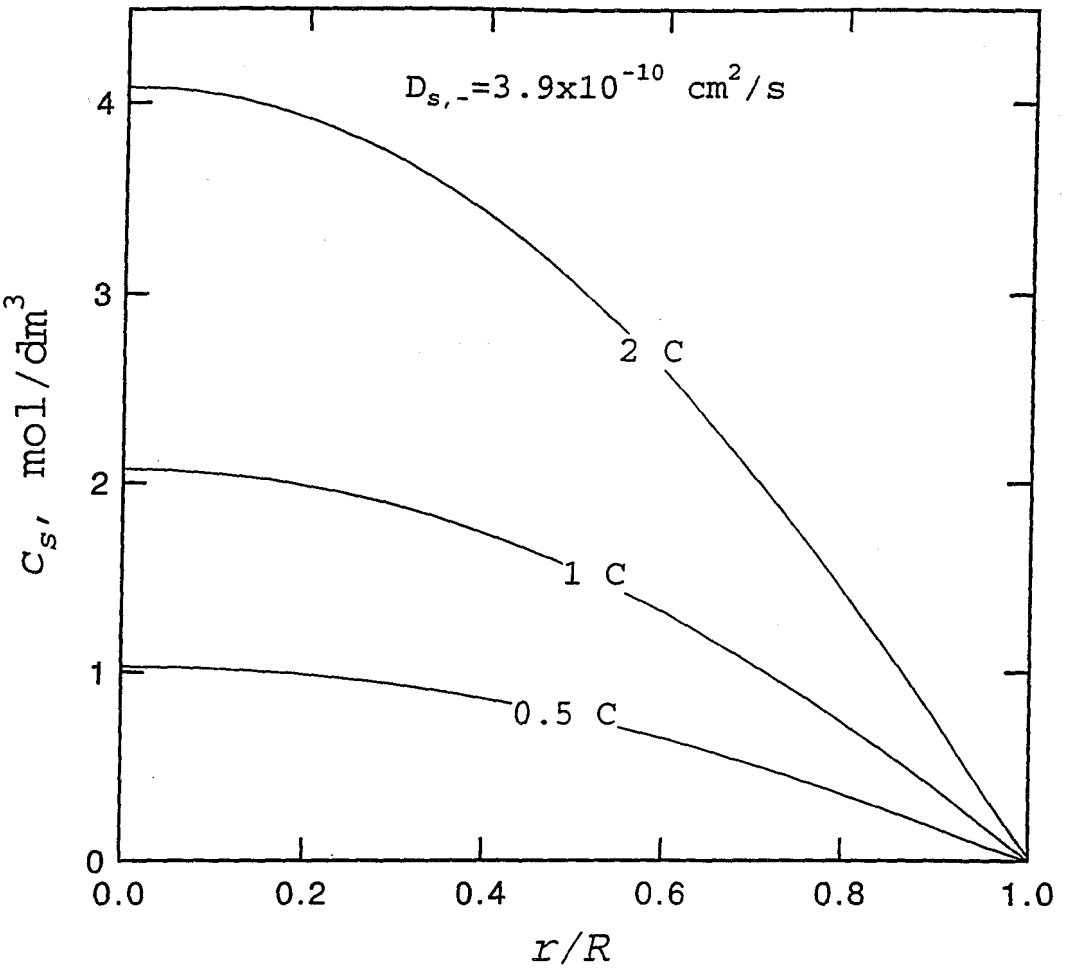


Figure 3-21. Concentration profiles of lithium inside a solid carbon particle near the front of the negative electrode for cell #1. The discharge rates are given on the figure as a fraction of the 1 C rate, and the time is near the end of discharge.

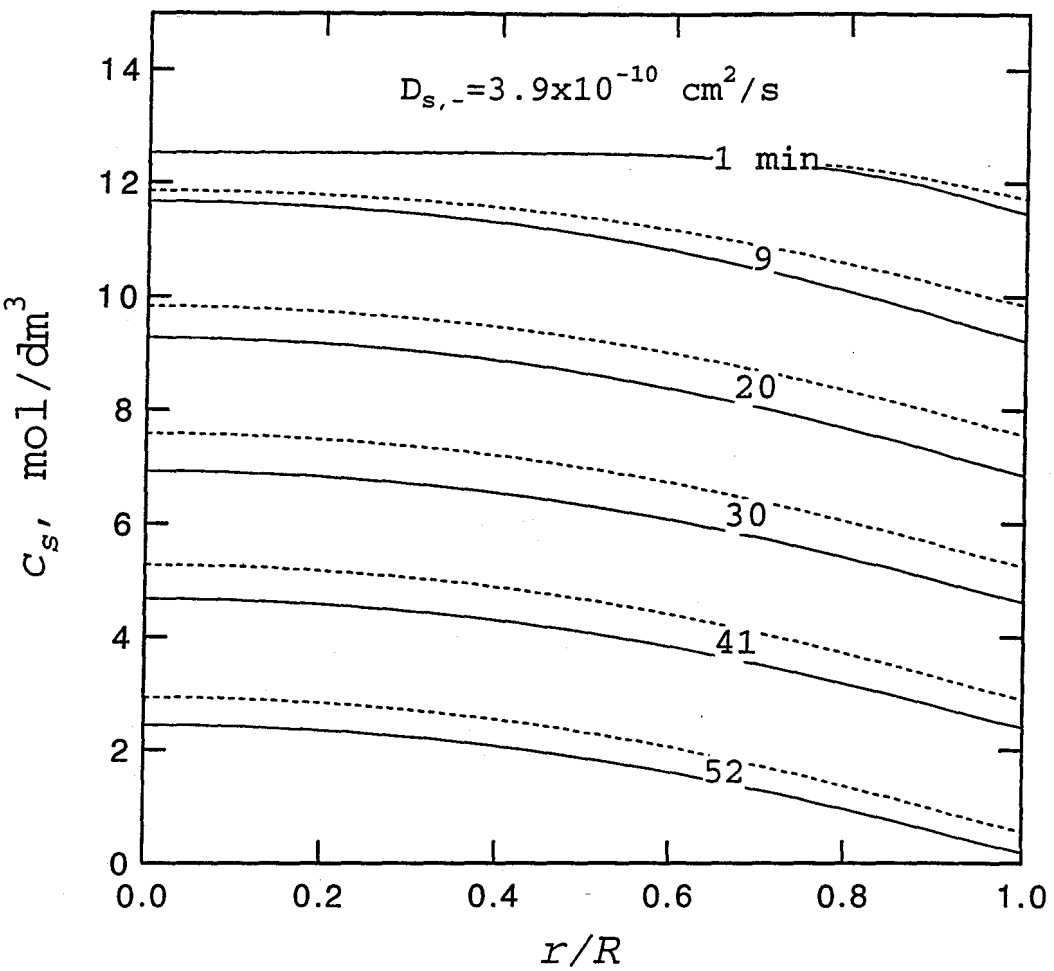


Figure 3-22. Concentration profiles of lithium inside a solid carbon particle at two different positions in the negative porous electrode. The solid lines are near the front and the dashed lines the back of the electrode. The current density is I=2.08 mA/cm$^2$, and cell #2 is used.

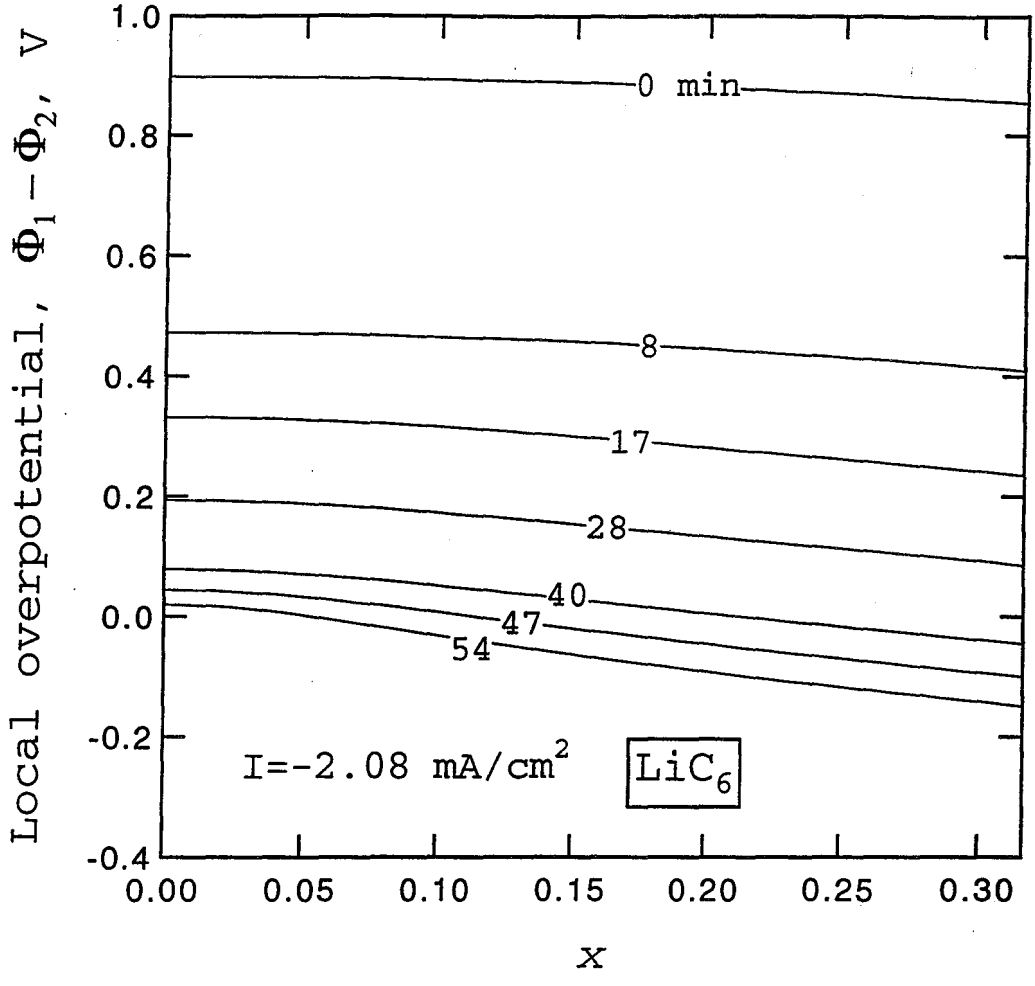


Figure 3-23. The distribution of the potential difference between the solid and solution phases in the negative electrode during the 1 C-rate charge of cell #2. Time since the beginning of the charge is given on the figure.

charge at the negative electrode/separator boundary. A nonuniform current distribution in the negative electrode causes the front of the electrode to be filled with lithium earlier than the back, leading to the drop in the overpotential at the front. This problem becomes worse as the charging rate is increased. Lithium plating may occur, but this will depend on the kinetics of the reaction, as it must compete with the lithium insertion reaction. Also, the initial lithium deposition may be hindered somewhat by the need to develop an overpotential for nucleation of lithium metal.

In certain applications it can be important for a battery to attain large peak specific powers. An electric-vehicle battery, for example, needs to provide a peak specific power (W/kg) for a thirty-second current pulse that is two to four times the specific energy of the battery (Wh/kg).[29] We can use the simulations to predict the peak specific power available from the three experimental cells examined above. The peak power is that available over a thirty-second period when the cell is discharged at increasing rates to a 2.0 V cutoff potential from a given initial discharge condition. The mass used in these calculations includes all cell components and current collectors (see equation 3-21) but not the container and peripherals. The values used here have not been optimized.

Figure 3-24 gives the results for the peak specific power for each of the three cells as a function of the depth of discharge. The peak power decreases steadily during the discharge, due primarily to the increasing distance that ions must flow in solution to reach the reaction zone and the decreasing open-circuit potential of the cell. Cells #1 and #2 have similar power capabilities, decreasing from about 300 W/kg near the beginning of discharge to 200 W/kg at the end. Cell #2 performs slightly better than cell #1, even with somewhat thicker electrodes, because the average ionic conductivity of cell #1 is lower ($c^0$=2 M). Cell #3 achieves a sub-

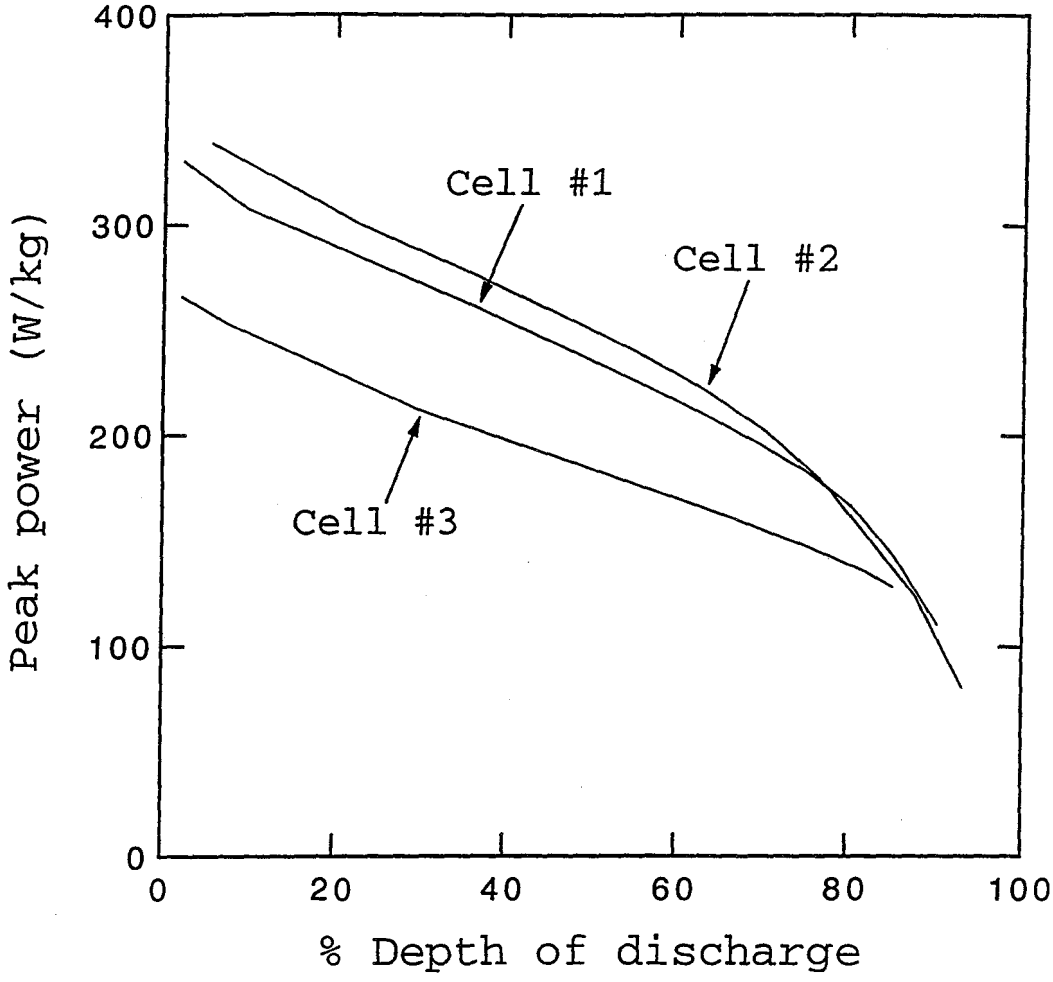


Figure 3-24. The peak specific power for a 30-s pulse of current after a galvanostatic discharge to different %DOD. The initial discharge is at the 1 C rate at 25°C for each cell.

stantially lower peak power because of its thicker electrodes. These simulations demonstrate that the specific power available from the lithium-ion cell should be over twice the specific energy.

*Effect of temperature on the discharge curves*. - An advantage of lithium rechargeable battery systems is often said to be their good performance over a wide range of temperatures. For this reason, it is important to examine discharge curves at temperatures other than 25°C. In figure 3-25 we present several experimental discharge curves for cell #1 at 0°C at various discharge rates. The 1 C rate is still defined as 1.75 $mA/cm^2$, the one-hour discharge rate at 25°C; other rates are given as multiples of the 1 C rate. The low-temperature performance of the cell is poorer than that at 25°C; even at the 0.1 C rate the cell is obtaining only about 87% of the full capacity. Experimental discharge curves for cell #1 at 55°C are given in figure 3-26. The high-temperature performance of the cell is quite good. The loss of capacity at the 0.5 C and 1 C rates seen in figure 3-4 and attributed to solid-phase diffusion limitations is somewhat reduced at 55°C.

Simulated discharge curves at 0 and 55°C are not given in figures 3-25 and 3-26. We find that the simulations do not agree well with the experimental data for temperatures other than 25°C. Data on the ionic conductivity at various temperatures is known. However, other properties that depend on temperature have not been measured. In particular, the temperature dependence of the solid-phase diffusion coefficient in the carbon electrode and the open-circuit potentials can not be ignored. Poor agreement between simulations and experimental data is attributed to these effects. Future work may involve the measurement of these data, followed by more detailed modeling work at other temperatures.

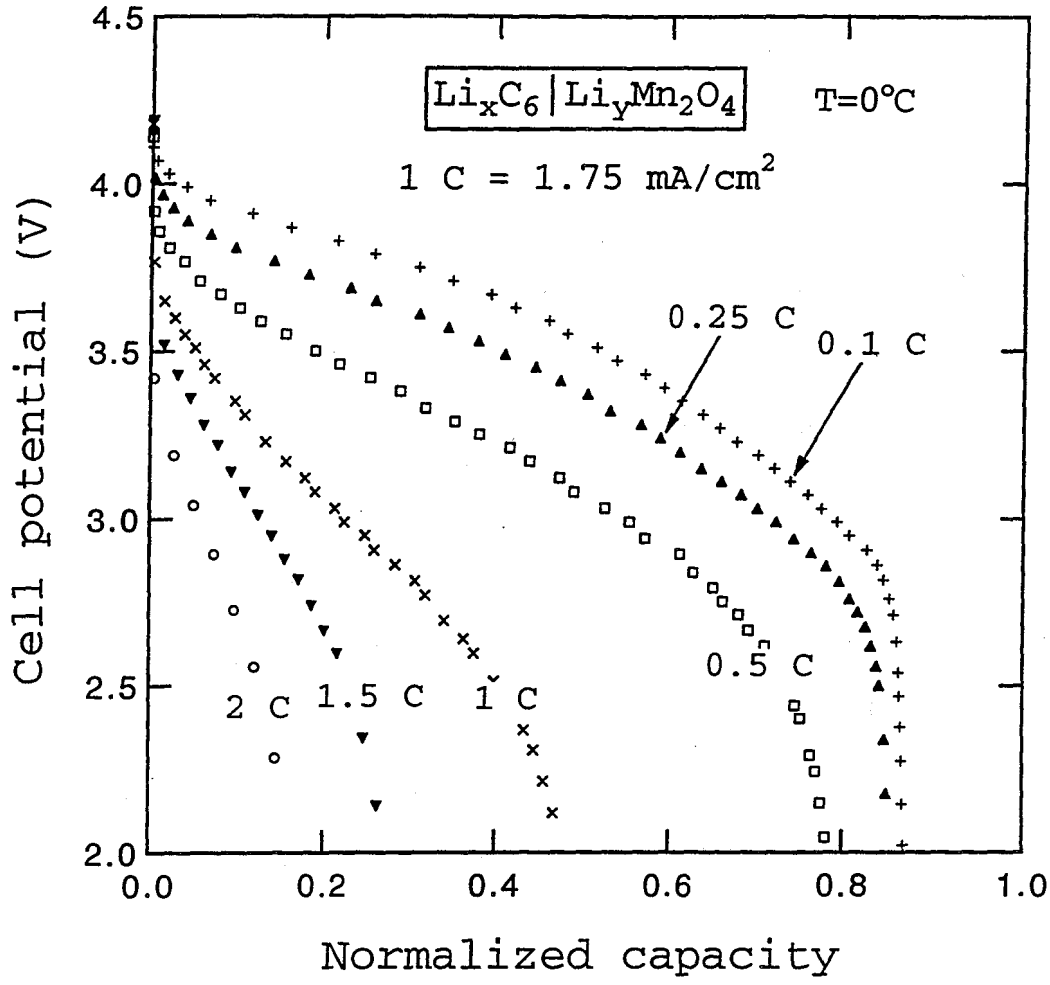


Figure 3-25. Experimental data on cell potential *versus* the fraction of attainable capacity for cell #1 at various discharge rates at 0°C.

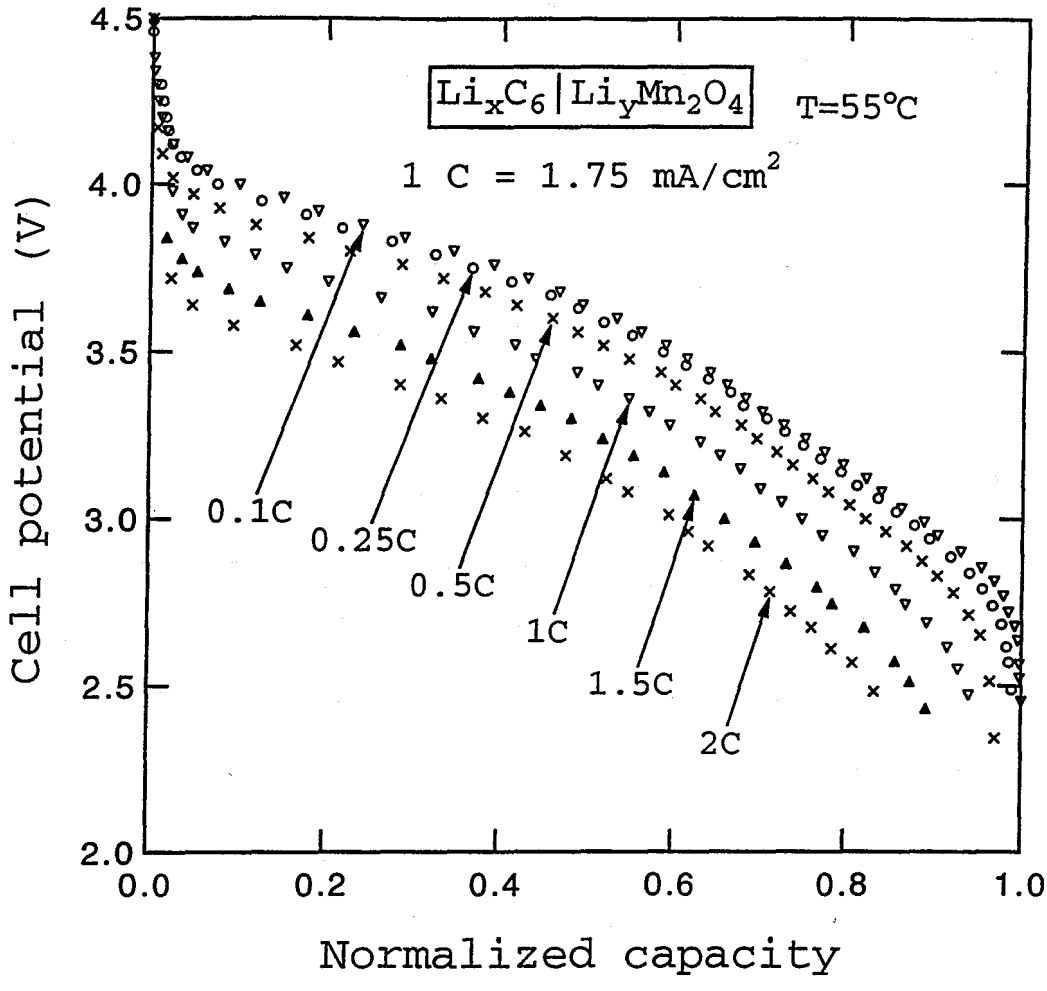


Figure 3-26. Experimental data on cell potential *versus* fraction of the attainable capacity for cell #1 at various discharge rates at 55°C.

*Discharge curves for a graphite negative electrode.* - For comparison purposes, an experimental cell was fabricated that used graphite (Lonza KS-6) as the negative electrode material instead of petroleum coke. This cell had the following design specifications:

$$\delta_-=83\ \mu m,\ \delta_s=76\ \mu m,\ \delta_+=187\ \mu m$$

$$\varepsilon_-=0.42,\ \varepsilon_{l,-}=0.46,\ \varepsilon_{p,-}=0.12,\ \varepsilon_{f,-}=0.00$$

In addition, the negative electrode particle size was reduced to $R_{s,-}=4\ \mu m$. The volume fractions for the composite positive electrode were identical to those given in Table 3.2. The density of the graphite was measured and found to be 2.25 g/cm$^3$; this gives a mass ratio for the cell of $\gamma=2.93$. The larger value for $\gamma$ compared to previous cells is just due to the larger capacity of the graphitic carbon for lithium insertion. Using equation 3-15, we find that the theoretical mass ratio for this cell is $\gamma=2.62$. The open-circuit potential for the graphite being used was measured and is given in Appendix 3-A.

In figure 3-27 we give the comparison between experimental and theoretical discharge curves for this cell. The 1 C rate is defined at I=1.67 mA/cm$^2$, and the total (normalizing) cell capacity is 40.0 mAh. The initial states of charge for this cell are found to be $x^0=0.72$ and $y^0=0.18$. The value of $x^0$ is too low considering the range of capacity accessible with the graphite (the open-circuit-potential curve suggests $x^0$ should be closer to 0.95). This indicates that the mass ratio used was too low; not enough extra capacity existed in the positive electrode to make full use of the negative capacity. A better value for the mass ratio would have been $\gamma=3.5$. The graphite cell can attain the full capacity at rates up to the 2 C rate. As the carbon particle size is significantly smaller than that used earlier, we no longer see solid-phase diffusion limitations. Similarly to earlier cells, solution-phase diffusion limitations dominate

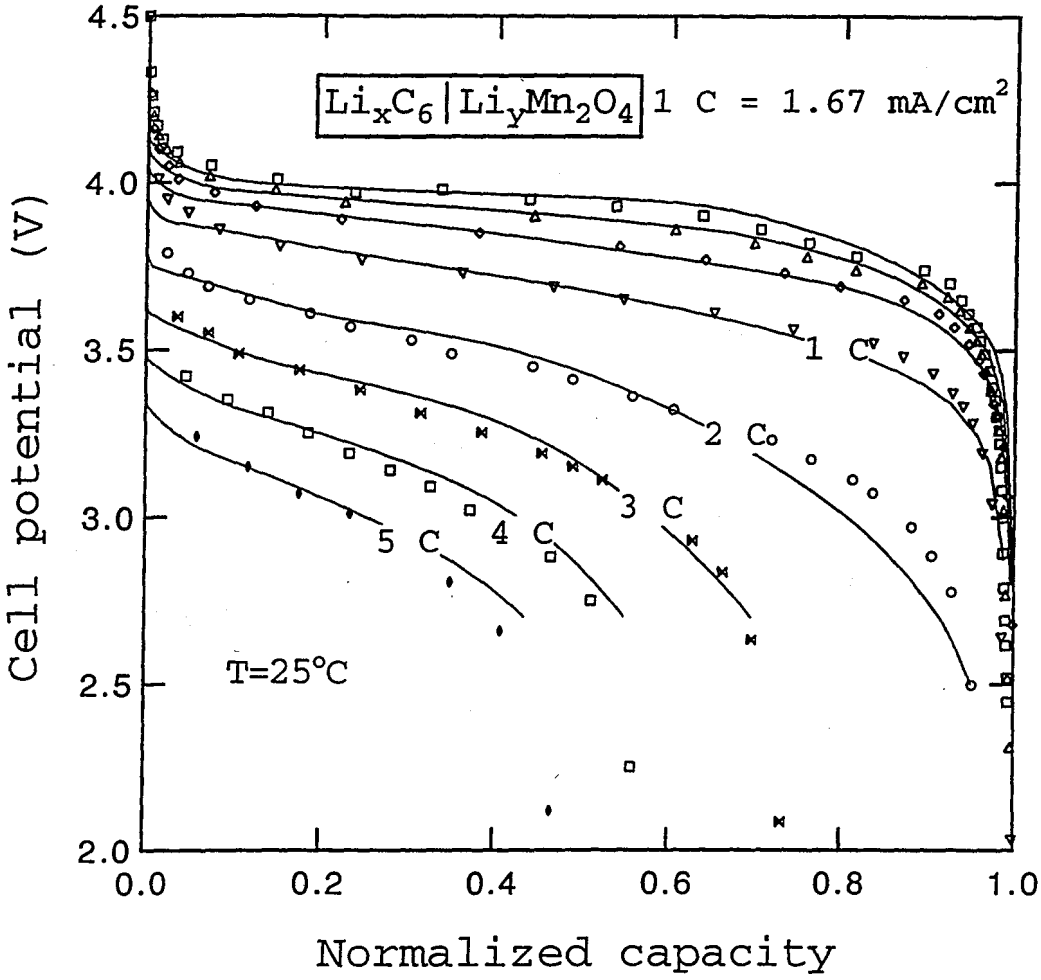


Figure 3-27. Comparison of simulated to experimental discharge curves, *i.e.*, cell potential *versus* the fraction of attainable capacity, for a Li-ion cell having a graphite negative electrode. The solid lines are the simulations, and the markers are the experimental data.

the discharge curves at rates above the 2 C rate. The same negative electrode resistance used earlier, $R_{f,-}$=800 $\Omega \cdot cm^2$, is used here, but a larger value of the tortuosity factor was required, $p$=7.2. The larger value of $p$ for this cell is disturbing; we are at a loss to explain this at present. One would not expect the use of a different electrode material to have such a drastic effect on the solution-phase transport properties. As far as we know, the positive electrode in this cell was nearly identical to positive electrodes used in earlier cells in its composition and structure.

### 3.4 Design and optimization considerations

The full potential of mathematical modeling is realized when one attempts to optimize a new battery system. If done through experimental work only, this process may be very time consuming as the number of parameters that can be varied is large. With a mathematical model, on the other hand, the process of varying system parameters and determining the overall performance is greatly expedited. But, to have confidence in the results, the model must have been proved to represent accurately the system behavior. The optimization process will usually involve extrapolation of the battery's behavior into regions of parameter space where experimental data do not exist. Models that are too simplified, or ones that involve excessive parameter fitting using a specific configuration, will be unlikely to provide good results under these conditions. In any case, an optimum battery configuration determined from mathematical modeling should be viewed as an initial guess at the true optimum system, which can act as a starting point for the experimental design effort.

In the present case, the modeling results shown above have demonstrated a good deal of flexibility in describing the lithium-ion cell. Several different cell configurations were studied, including different electrode thicknesses and initial salt concentrations, under conditions of charge and discharge. Some parameter fitting was required, but these same values applied to all

of the experimental cell designs. The only exception was the film resistance on cell #3, and this effect was ascribed to the manufacturing technique. Thus, we do have some hope of providing accurate results while carrying out the optimization of this battery. Next, we must ask what it is that we wish to optimize and how this is to be accomplished.

We assume that one wants to attain the highest possible specific energy for a known application. The Ragone plot, defined as the specific energy as a function of the average specific power, is a useful tool for this purpose. Integration of the instantaneous power delivered over the time of discharge gives the specific energy

$$E = \frac{1}{M}\int_0^{t_d} IV\mathrm{d}t\,, \tag{3-19}$$

and the average specific power is then:

$$P = \frac{E}{t_d}\,. \tag{3-20}$$

Each of these quantities depends on the current density; theoretical Ragone plots are generated by running simulations for many values of $I$ and calculating $E$ and $P$ from each simulation.

Figure 3-28 shows simulated Ragone plots for the experimental cells #1, #2, and #3. The major difference among these configurations is in the electrode thicknesses, with cell #3 being significantly thicker than cells #1 and #2. The mass used in these calculations includes all of the cell components and separator and current collectors, but not cell casing and other external battery masses. The current collectors are each assumed to be 25 μm in thickness, and the densities of aluminum and copper are taken to be 2.70 and 8.93 g/cm$^3$, respectively. The mass per unit area of the cell, $M$, in units of kg/m$^2$ is

$$M = \delta_{-}\left[\rho_{-}(1-\varepsilon_l-\varepsilon_p-\varepsilon_f)_{-}+\rho_l\varepsilon_l+\rho_p\varepsilon_p+\rho_f\varepsilon_f\right]+\delta_s\left[\rho_l\varepsilon_l+\rho_p\varepsilon_p\right] + \delta_{+}\left[\rho_{+}(1-\varepsilon_l-\varepsilon_p-\varepsilon_f)_{+}+\rho_l\varepsilon_l+\rho_p\varepsilon_p+\rho_f\varepsilon_f\right]+0.29\,. \quad (3\text{-}21)$$

The constant addend to equation 3-21 accounts for the current-collector masses. Because this value of $M$ does not include other components of the final battery, the energies and powers given in figure 3-28 will be higher than actual values. Examining figure 3-28, we find that these cell configurations are predicted to achieve from 68 to 84 Wh/kg. Generally, one expects the specific energy to increase and the specific power to decrease as the electrode thicknesses are increased. In agreement with this, the specific power is found to decrease substantially for cell #3, whereas the specific energy is larger than that of cells #1 and #2. Differences between cell #1 and #2 are due to the slightly different thicknesses as well as the fact that cell #1 uses an initial salt concentration of 2 M. The higher salt concentration in cell #1 leads to a lower conductivity and thus to lower specific powers on the far right of figure 3-28. Including other battery component masses in these calculations would only accentuate the differences between the Ragone plots of these cells.

The specific energy found for cell #3, 84 Wh/kg, is lower than that obtained by some $LiCoO_2$ systems such as the Sony phone cell (80 to 110 Wh/kg),[30] especially when one considers that the additional battery component masses will reduce this value further. This motivates us to use the computer simulations to consider different configurations in an attempt to increase $E$. We are confident that a larger specific energy can be achieved with this system because of the location of the "knee" of the Ragone plots in figure 3-28. The "knee" is the region of the plot at higher power values where the specific energy begins to fall off. The discharge time corresponding to this region is generally where one wants to operate for a given design.[31] This allows nearly the maximum specific energy to be obtained at the highest

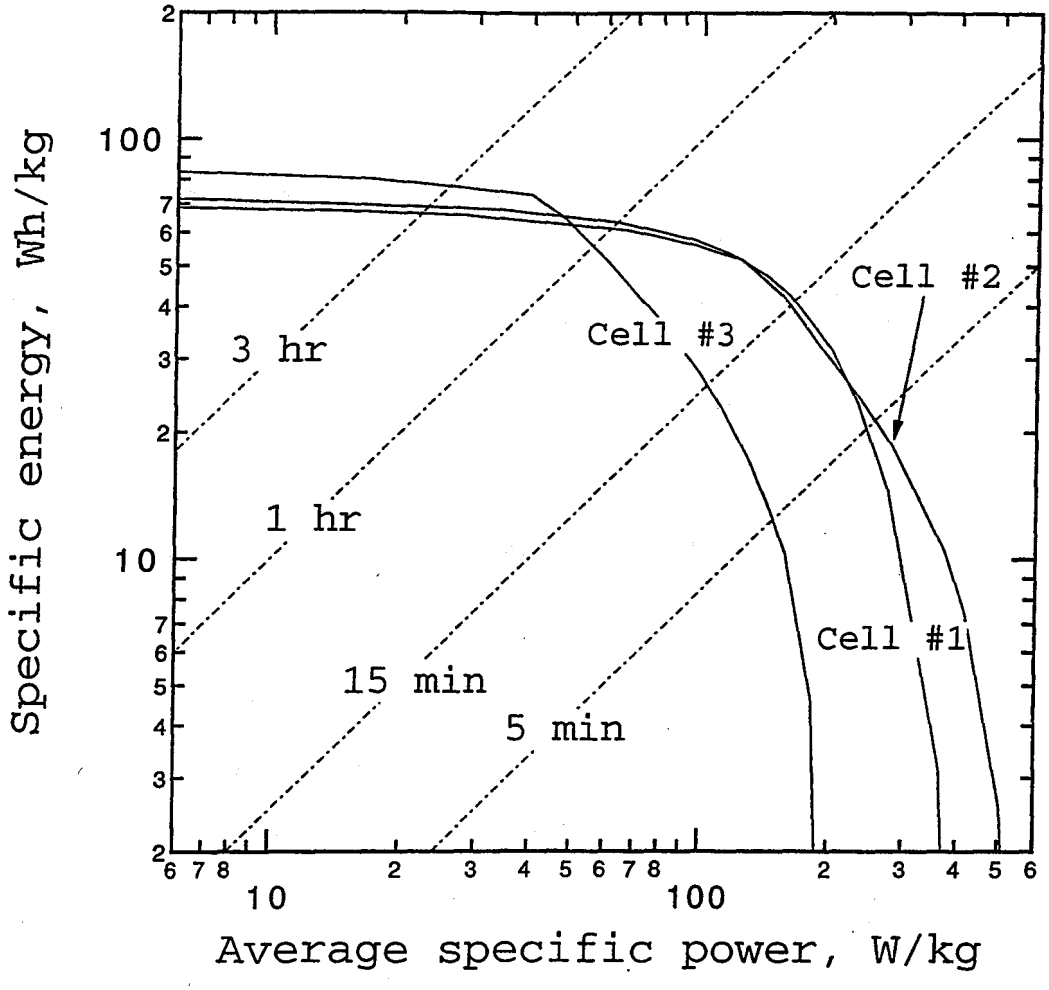


Figure 3-28. Comparison of Ragone plots for the three cell designs. The mass used here is based on porous electrodes, electrolyte, separator, and current collectors only. The dashed lines are curves of constant discharge time.

possible specific power. From the curves on figure 3-28, for example, we find cell #3 is well-suited for a two-hour discharge whereas cells #1 and #2 are appropriate for a thirty-minute discharge. As we are usually interested in longer discharge times (3 hours for electric vehicles, 5 to 6 hours for laptop computers, *etc.*), it should be possible to sacrifice some of the power presently being obtained to achieve higher values of the specific energy. We are naturally led to explore using thicker and/or more dense electrodes to increase the specific energy.

As explained by Newman,[32] it is necessary to be clear about what is to be optimized and what is to be held fixed when carrying out the optimization process. We assume that a given discharge time is required for some particular application. Then we wish to optimize $E$ by varying the electrode thicknesses, volume fractions, and current density. The other parameters given in Tables 3.1 and 3.2 are assumed to be fixed, including the temperature, initial salt concentration, and separator thickness. We will also fix the positive to negative electrode mass ratio at 2.1. As the active material volume fractions are varied, it is assumed that the same ratio of conductive filler to active material found in Table 3.2 must be used (giving 24% by volume of the active material in the positive electrode and 5% in the negative). The separator thickness will be fixed at $\delta_s$=52 μm, and the initial salt concentration is taken to be $c^0$=1 M. We can return to the issue of optimizing the initial salt concentration later. Also, the ratio of polymer to liquid in the plasticized electrolyte will be fixed, both in the separator region and in the composite electrodes. We should note here that we assume a symmetric system is desired, where the rate behavior of the cell on charge and discharge will be similar. If high discharge rates only are needed, then the design of either electrode may be different.

The optimization procedure then is to vary the design-adjustable parameters, generate Ragone plots for each design, and use these plots to identify an optimum configuration. This is

a time-consuming process, even with the computer program, which we can expedite for the present system by using analytic models of the discharge of an ohmically-dominated lithium-ion cell.[32] These results provide correlations for the optimum values of the electrode thickness and porosity as a function of a dimensionless discharge time, ratio of separator to electrode density, and residual mass content. We can then use these values as a first guess when carrying out more refined optimizations using the computer program. For illustrative purposes, we will consider here the case of a battery designed for laptop-computer applications with a desired discharge time of 6 hours. The resulting design parameters using the ohmically-dominated model are:

$$\delta_-=452\ \mu m,\ \delta_+=512\ \mu m$$

$$\varepsilon_-=0.779,\ \varepsilon_{l,-}=0.130,\ \varepsilon_{p,-}=0.050,\ \varepsilon_{f,-}=0.041$$

$$\varepsilon_+=0.662,\ \varepsilon_{l,+}=0.125,\ \varepsilon_{p,+}=0.047,\ \varepsilon_{f,+}=0.166$$

This shows that significantly thicker and more dense electrodes are required compared to those used in the present designs. The larger volume fractions for the active materials predicted here may not be attainable with the present manufacturing processes, a constraint that could be brought into the above optimization process.[32]

These parameters can next be tested in the full mathematical model, and the performance of this system evaluated. We immediately find that the ohmically-dominated "optimized" system has severe solution-phase diffusion limitations. This is to be expected considering that the above model is an idealized one in which concentration variations are not considered, and thus the resulting design has very thick and dense porous electrodes where diffusion problems will be magnified. The specific energy for this system, predicted with the full-cell-sandwich model, is 195 Wh/kg. However, the cell will obtain only a small fraction of this at the C/6 rate.

We can still use this first set of system parameters as a starting point in the optimization process, and proceed by reducing electrode thicknesses and volume fractions until an optimum is reached. Reducing either the thicknesses or volume fractions alone does not produce an optimum configuration. Instead, the best system is one in which both thicknesses and volume fractions are reduced simultaneously. This procedure generates the following system parameters:

$$\delta_-=309\ \mu m,\ \delta_+=321\ \mu m$$

$$\varepsilon_-=0.520,\ \varepsilon_{l,-}=0.329,\ \varepsilon_{p,-}=0.125,\ \varepsilon_{f,-}=0.026$$

$$\varepsilon_+=0.480,\ \varepsilon_{l,+}=0.293,\ \varepsilon_{p,+}=0.112,\ \varepsilon_{f,+}=0.115$$

The specific energy predicted for this design is 115 Wh/kg, which is a 35% improvement over cell #3. This value of the specific energy could be competitive with $LiCoO_2$ systems even when additional battery masses are considered.

To compare these designs, the simulated Ragone plot (using the full-cell-sandwich model) is given for the above system in figure 3-29, along with that of the experimental cell #3. The optimum configuration given above appears similar to cell #3 on figure 3-29, but gives a higher specific energy by sacrificing some of the power available in the two-hour to five-minute discharge range. This system attains higher powers at very high discharge rates (times less than five minutes) due to the thinner separator. In general, the optimum configuration appears to be one in which all of the major limitations in the cell are balanced at the discharge rate of interest. Thus, the configuration given above should begin to show solution-phase diffusion limitations at rates just above the six-hour rate.

The fact that the optimum design is determined by the balance of solution-phase diffusion limitations and ohmic drop indicates that optimizing the initial salt concentration is an

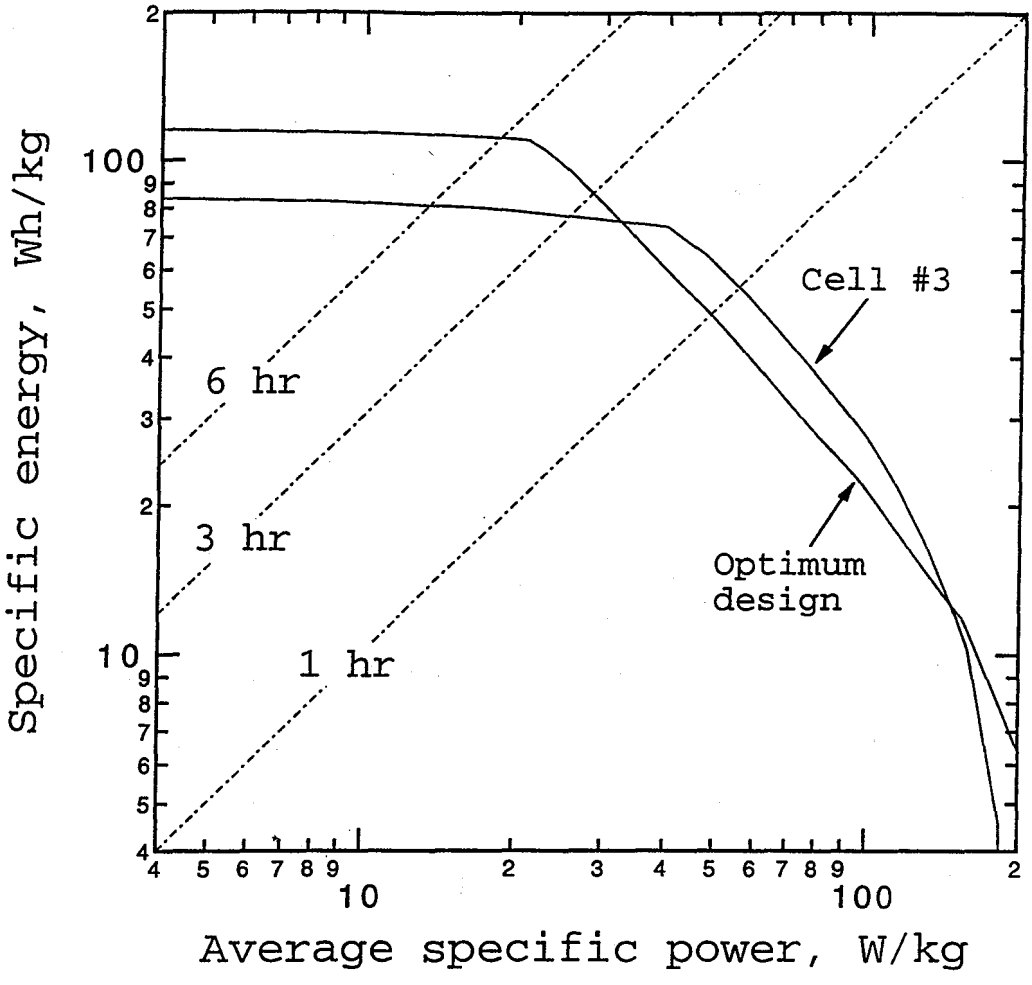


Figure 3-29. Ragone plots for simulated cell design compared to results for cell #3. The mass used is based on porous electrodes, electrolyte, separator, and current collectors only. The dashed lines are curves of constant discharge time.

important issue. Increasing the initial salt concentration above 1 M will shift the optimum design to thicker and more dense electrodes as diffusion limitations are delayed, leading to increased specific energies. This will continue up to salt concentrations of around 2 M, after which the decreasing ionic conductivity and the possibility of salt precipitation become issues. However, the optimum salt concentration must factor in the cost of the salt, which for $LiPF_6$ is substantial. For this reason, one may wish to consider the use of a combination of two salts having different anions (*e.g.*, $LiPF_6$ and $LiBF_4$), which may provide a cheaper alternative that still fulfills the desired purpose.

### 3.5 Conclusions

We have used computer simulations to model and predict the performance of a lithium-ion cell consisting of a carbon negative electrode, a plasticized electrolyte containing $LiPF_6$/EC/DMC in p(VdF-HFP), and a lithium manganese oxide positive electrode. The simulations are compared to experimental data for cells having various electrode thicknesses and different electrolyte compositions. Excellent agreement between theory and experiment is obtained when the lithium diffusion coefficient in the carbon electrode, an electrode film resistance, and an effective ionic conductivity in the porous electrodes are used as adjustable parameters. This system is determined to be dominated by ohmic drop in the plasticized-electrolyte phase. Minor solid-phase diffusion limitations exist in the carbon electrode. The simulations suggest that the lithium diffusion coefficient in the carbon material is $D_{s,-}=3.9\times10^{-10}$ cm$^2$/s. Solution-phase diffusion limitations become a concern when the electrode thicknesses are increased and the initial salt concentration decreased to 1 M. Using the diffusion-limited region of the discharge curves to fit the transport properties in the plasticized electrolyte gives $D=9\times10^{-7}$ cm$^2$/s and $t_+^0=0.36$. The kinetics for the lithium ion insertion reaction are confirmed

to be practically reversible.

The calculated specific energy of the battery in its present designs is from 68 to 84 Wh/kg, with the mass based on the composite electrodes, separator, and current collectors. These cells have good moderate-rate performance and are well-suited for applications with 30-minute to one-hour discharge times. Larger specific energies are obtained with less porous, thicker electrodes; simulations suggest that it is possible to obtain 115 Wh/kg with a system optimized for a six-hour discharge time. The optimum system will exhibit a compromise of solution-phase diffusion limitations and ohmic drop at the six-hour rate. The peak specific power for the experimental cells is predicted to fall from about 300 W/kg near the beginning of discharge to 200 W/kg at the end of discharge.

**Acknowledgements**

We gratefully acknowledge the assistance of Antoni S. Gozdz, Caroline Schmutz, and Jean-Marie Tarascon from Bellcore in Red Bank, NJ, for allowing us to use experimental data from their lithium-ion cells in this work. In addition, the conductivity data given in figures 3-2 and 3-3 were measured by Antoni S. Gozdz.

## Appendix 3-A Open-circuit potential data for the insertion materials

The open-circuit potential *versus* state of charge for manganese dioxide was measured at Bellcore and fit to the function

$$U = 4.19829 + 0.0565661\ \tanh\left[-14.5546y + 8.60942\right] - 0.0275479\left[\frac{1}{(0.998432-y)^{0.492465}} - 1.90111\right] - 0.157123\exp\left(-0.04738y^{8}\right) + 0.810239\exp\left[-40(y-0.133875)\right], \quad \text{(A-1)}$$

where $y$ is the amount of lithium inserted in $Li_yMn_2O_4$. This curve fit is given as figure 3-30. Similarly, for the carbon electrode

$$U = -0.16 + 1.32\exp\left(-3.0x\right), \quad \text{(A-2)}$$

where $x$ is the value defined by the formula $Li_xC_6$. This fit is presented as figure 3-31. The open-circuit potential data above correspond to the potential of the insertion material *versus* lithium during a very-low-rate discharge (C/60).

The open-circuit potential for graphitic carbon was fit to the following function:

$$U = 0.7222 + 0.13868x + 0.028952x^{0.5} - 0.017189x^{-1} + 0.0019144x^{-1.5} + 0.28082\exp\left[15(0.06-x)\right] - 0.79844\exp\left[0.44649(x-0.92)\right], \quad \text{(A-3)}$$

where $x$ is again the value defined by the formula $Li_xC_6$. This curve fit is given in figure 3-32. The data for this fit were measured at Bellcore at the C/11 rate, and the open-circuit potential is considered to be less accurate as a result.

## Appendix 3-B Simplified model of cell dominated by solid-state diffusion limitations

It may be possible to distinguish between solid and solution-phase diffusion limitations by developing log-log plots of the capacity *versus* discharge rate for the battery. The slope of these plots should reflect the main limitation in the system under high-rate discharge. The

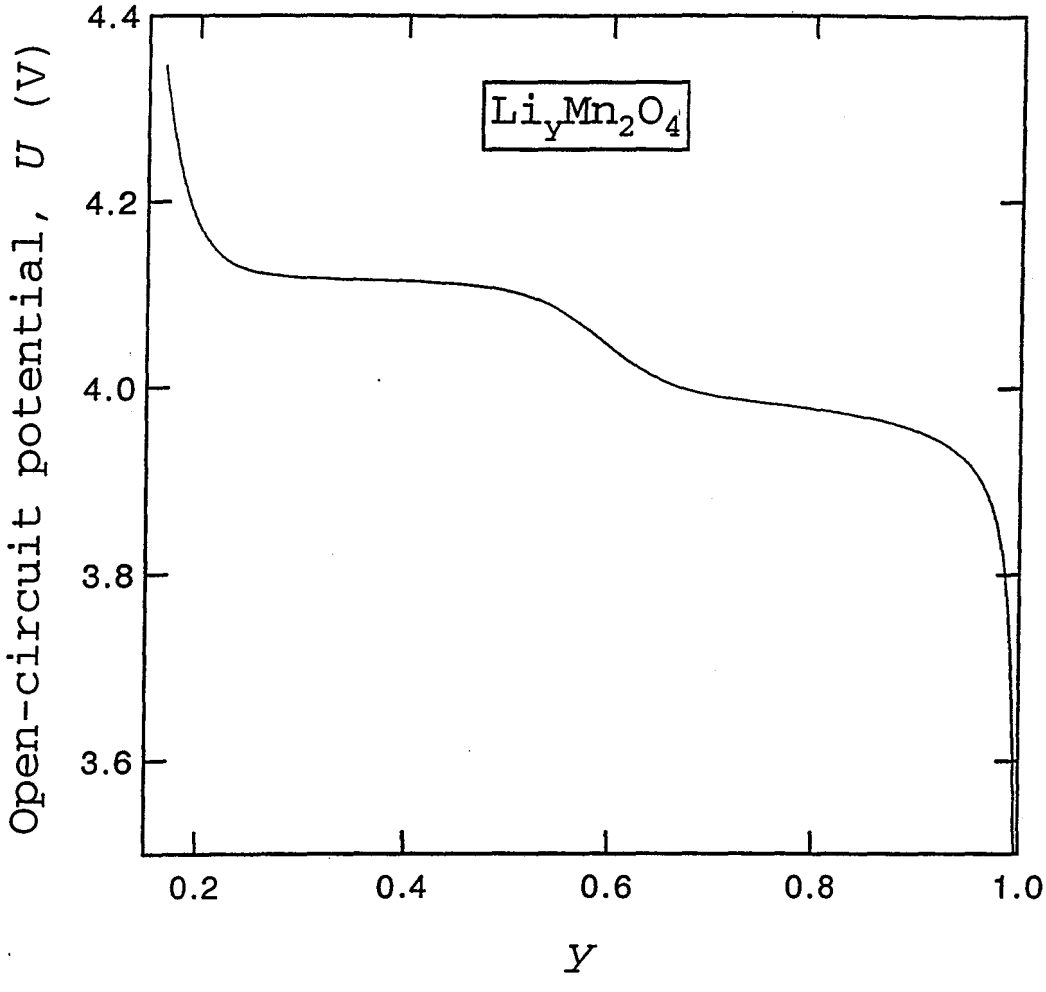


Figure 3-30. The open-circuit potential of lithium-manganese-oxide spinel as a function of the state of charge relative to solid lithium. (Fitted from discharge data at the C/60 rate.)

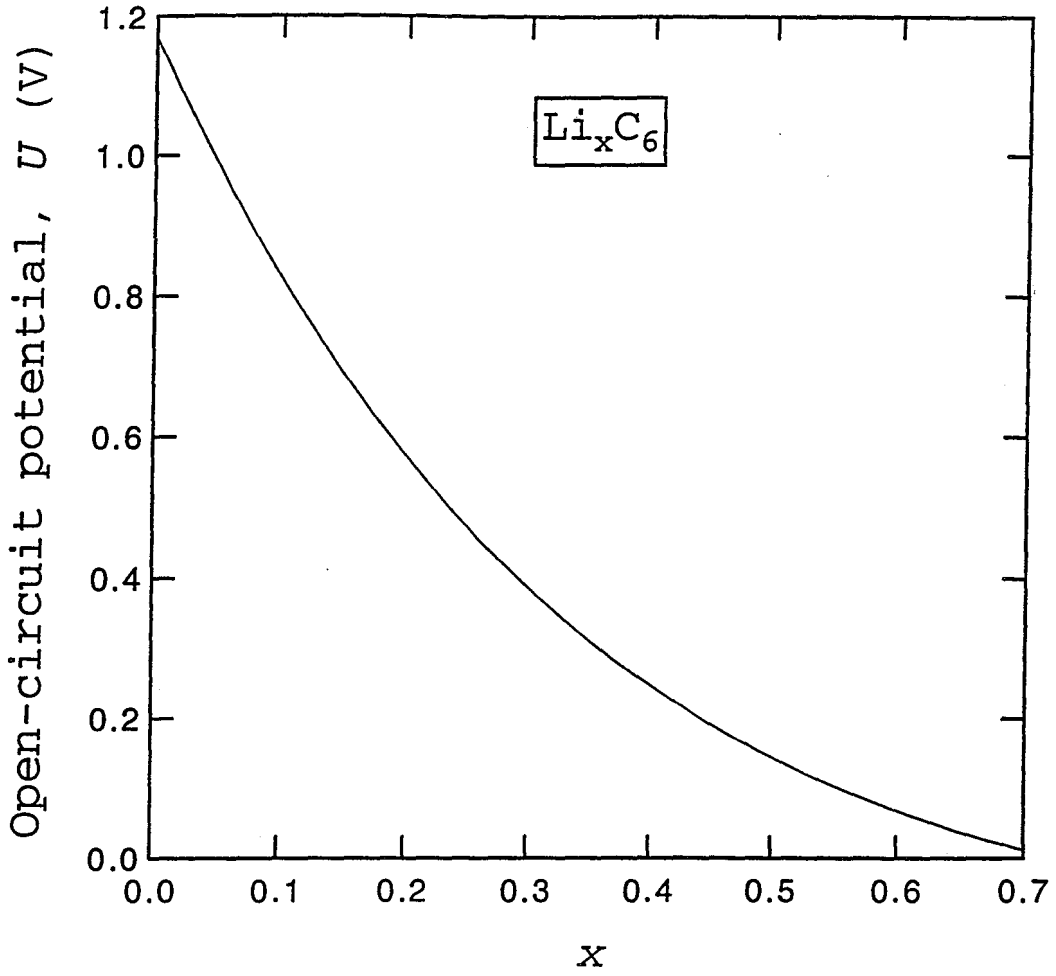


Figure 3-31. The open-circuit potential of petroleum coke ($Li_xC_6$, Osaka Gas MCMB 25-10) as a function of state of charge relative to the potential of solid lithium. (Fitted from discharge data at the C/60 rate.)

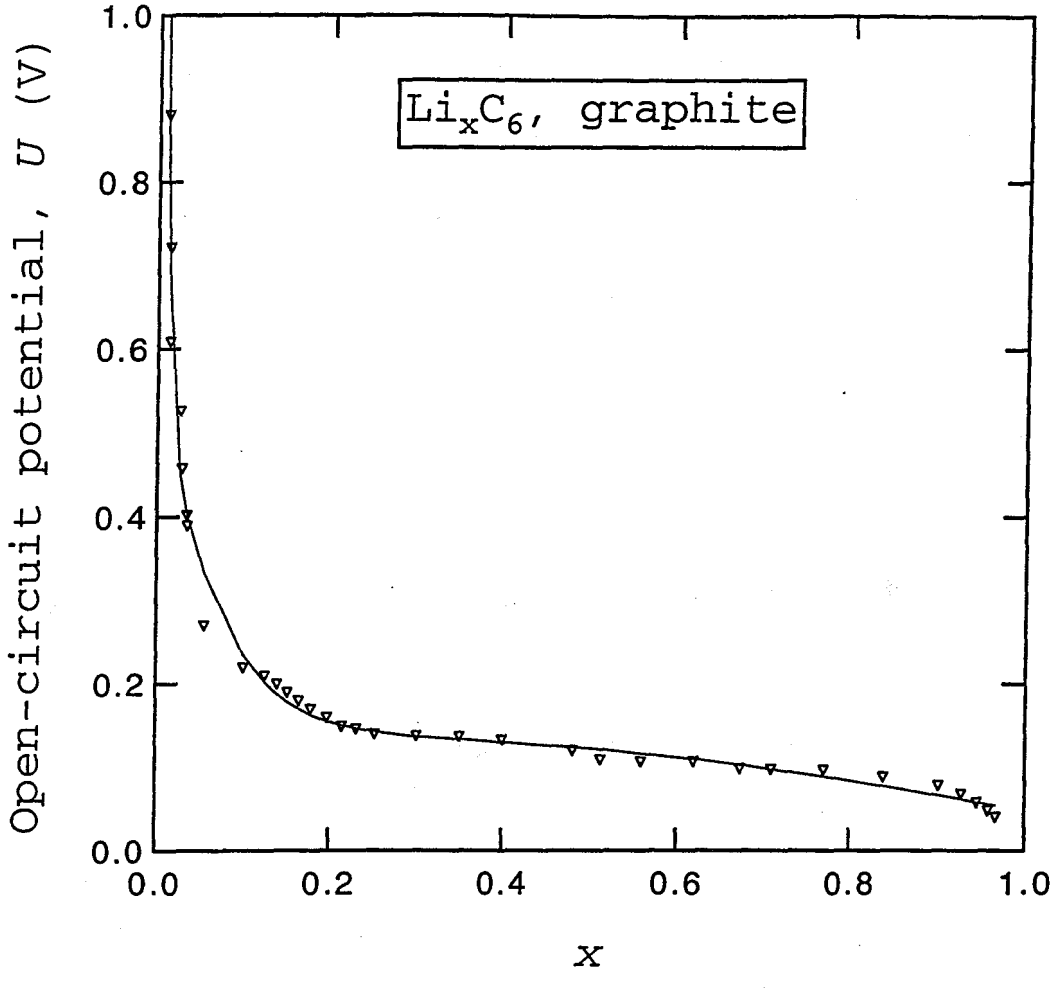


Figure 3-32. The open-circuit potential of graphite ($Li_xC_6$, Lonza KS-6) as a function of the state of charge relative to the potential of solid lithium at the same electrolyte concentration. (Fitted from discharge data at the C/11 rate.)

development of simplified models of the discharge process can be used to extract this slope from theoretical predictions. This approach to modeling the discharge behavior has been taken in previous work; a primary example is the work of Tiedemann and Newman[32,33] on ohmically-limited reaction-zone models of the discharge process.

We have developed useful analytic solutions in previous work,[17] covering the following cases:

1. Ohmically limited cell having an open-circuit potential that varies linearly with state of charge.

2. Cell dominated by solution-phase diffusion limitations with a constant reaction rate through the porous electrode.

3. Cell dominated by solution-phase diffusion limitations with a reaction occurring only at the front face of the porous electrode.

These analytic solutions for the discharge process allow us to extract the characteristic slopes on a log-log capacity-rate plot for each of the above phenomena. One typically finds that solution-phase diffusion limitations lead to slopes of -2 and smaller at low rates, which then approaches -1 at very high rates. An ohmically-limited model, on the other hand, gives a slope on a log-log energy/power (Ragone) plot of -1 in a certain region.

For the present situation, we are motivated to consider a battery discharge limited by solid-state diffusion of lithium into the host oxide structure. It is assumed that solution-phase concentration variations can be neglected and that the reaction-rate distribution in the porous electrode is uniform. This last assumption is necessary in order to decouple the governing equations; consideration of a nonuniform current distribution quickly leads to models that

require numerical solution, which we attempt to avoid here. The reaction-rate distribution is assumed to be equal to its average value. We also assume that the diffusion coefficient of lithium inside the insertion material is a constant. If severe diffusion limitations exist, it is possible to estimate the battery capacity by relating the discharge time to the time to reach a limiting current in the solid phase. The mathematical formulation of the problem is then

$$\frac{\partial c_s}{\partial t} = \frac{D_s}{r^2}\frac{\partial}{\partial r}\left[r^2\frac{\partial c_s}{\partial r}\right]. \tag{B-1}$$

Boundary conditions include

$$\frac{\partial c_s}{\partial r}(t,\ r=0) = 0\,, \tag{B-2}$$

$$-D_s\frac{\partial c_s}{\partial r}(t,\ r=R_s) = \frac{I}{aF\delta_-}\,,$$

$$c_s(t=0,\ r) = c_t\,.$$

A solution to this problem can be found,[34] but it is expressed as an infinite series that is cumbersome to evaluate.

At this point it is convenient to develop solutions to equation B-1 that are valid for short and long times; these illustrate the behavior of the system without being too complicated to be useful. For short discharge times, or high rates, a planar diffusion model is valid, giving the following relationship between discharge time and rate

$$t_d = \frac{\pi c_t^2 F^2 D_s a\delta_-}{4I^2}. \tag{B-3}$$

From this one would predict:

$$C = \frac{It_d}{M} = \frac{\pi c_t^2 F^2 D_s a \delta\_}{4MI}, \tag{B-4}$$

where the mass $M$ is given by equation 3-21, for example. Thus, the capacity is inversely proportional to the rate at high rates.

For longer times, or lower rates, a pseudo-steady-state is established in the particles. That this is relevant can be seen by examining solid-phase concentration profiles in the carbon particles given in figure 3-22. In our experience, this condition is usually satisfied by lithium-ion cells in practice.[27,28] Then the equation to be solved becomes:

$$0 = \frac{D_s}{r^2}\frac{\partial}{\partial r}\left[r^2 \frac{\partial c_s}{\partial r}\right], \tag{B-5}$$

with the required boundary conditions given in B-2. This leads to a steady concentration profile of the form

$$c_s(r=0) - c_s(r) = \frac{-Ir^2}{2aFD_s\delta\_R_s}. \tag{B-6}$$

The discharge time is approximated by the time for the concentration of lithium at the surface to reach zero. The capacity can then be calculated as

$$C = \frac{F\varepsilon\_\delta\_}{M}\left[c_t - \bar{c}_s\right], \tag{B-7}$$

with $\bar{c}_s$ representing the average concentration of lithium in the solid at the end of discharge. This leads to:

$$C = \frac{F\varepsilon\_\delta\_}{M}\left[c_t - \frac{R_s I}{3aFD_s\delta\_}\right]. \tag{B-8}$$

For low rates, a log-log plot of capacity *versus* rate will then have the form

$$\log C = \log\left[\frac{F\varepsilon\_\delta\_c_t}{M}\right] - \frac{0.767R_s I}{aF\delta\_D_s c_t}. \tag{B-9}$$

The slope is extracted from two regimes of behavior; at low to moderate rates the steady-state solution to the diffusion equation shows that log $C$ should be linearly proportional to the current, while at high rates, one finds that a slope of -1 on the log-log plot is approached. Thus, solid-phase diffusion limitations appear to provide fundamentally different capacity-rate behavior than solution-phase diffusion limitations at low to moderate rates. At very high rates, on the other hand, each provides a slope of -1, and these cases should be difficult to separate.

## List of Symbols

| | |
|---|---|
| $a$ | specific interfacial area, $m^2/m^3$ |
| $c_s$ | concentration of lithium in solid, $mol/dm^3$ |
| $c$ | concentration of salt, $mol/dm^3$ |
| $C$ | theoretical capacity of material, mAh/g |
| $D$ | salt diffusion coefficient, $cm^2/s$ |
| $D_s$ | diffusion coefficient of lithium in the solid electrode particles, $cm^2/s$ |
| $E$ | specific energy, Wh/kg |

| | |
|---|---|
| $F$ | Faraday's constant, 96,487 C/eq |
| $i_1$ | electronic current density in the solid phase, mA/cm$^2$ |
| $i_2$ | ionic current density in the solution phase, mA/cm$^2$ |
| $I$ | superficial current density, mA/cm$^2$ |
| $j_n$ | pore wall flux of lithium ions, mol/cm$^2$s |
| $k_m$ | mass transfer coefficient, m/s |
| $L$ | total cell thickness, m |
| $M$ | mass per unit area of cell, g/cm$^2$ |
| $M_i$ | molecular weight of species $i$, g/mol |
| $p$ | exponent related to effective transport properties defined in equation 3-5 |
| $P$ | average specific power, W/kg |
| $R_f$ | film resistance, $\Omega \cdot$cm$^2$ |
| $R_s$ | radius of positive electrode material, m |
| $t$ | time, s |
| $t_d$ | discharge time, s |
| $t_+^0$ | transference number of lithium ion defined with respect to the solvent |
| $T$ | temperature, K |
| $U$ | open-circuit potential, V |
| $V$ | cell potential, V |
| $x$ | dimensionless distance from the negative electrode/current collector boundary, cm |

| | |
|---|---|
| $x$ | stoichiometric coefficient in negative electrode defined by $Li_xC_6$ |
| $y$ | stoichiometric coefficient in positive electrode defined by $Li_yMn_2O_4$ |
| $\alpha$ | transfer coefficient for electrochemical reaction |
| $\gamma$ | mass ratio of positive to negative active material |
| $\delta_i$ | thickness of cell component $i$, m |
| $\varepsilon_i$ | volume fraction of component $i$ |
| $\eta_s$ | surface overpotential, V |
| $\kappa$ | ionic conductivity of electrolyte, S/cm |
| $\rho$ | density of material, $g/cm^3$ |
| $\sigma$ | electronic conductivity of solid matrix, S/cm |
| $\tau$ | tortuosity factor |
| $\Phi$ | electrical potential, V |

Subscripts

| | |
|---|---|
| - | negative electrode |
| + | positive electrode |
| $e$ | electrolyte |
| $f$ | conducting filler additive |
| $l$ | liquid component of plasticized electrolyte |
| $p$ | polymer component of plasticized electrolyte |

| | |
|---|---|
| *s* | separator or solid phase |
| *t* | maximum concentration in intercalation material |
| 1 | solid matrix phase |
| 2 | solution phase |
| ∞ | transport property measured without the composite electrodes |

Superscripts

| | |
|---|---|
| 0 | with respect to the solvent or initial condition |

## References

[1] J. M. Tarascon, E. Wang, F. K. Shokoohi, W. R. McKinnon, and S. Colson, "The Spinel Phase of $LiMn_2O_4$ as a Cathode in Secondary Lithium Cells," *J. Electrochem. Soc.*, **138**, 2859-2864 (1991).

[2] P. Barboux, J. M. Tarascon, and F. K. Shokoohi, "The Use of Acetates as Precursors for the Low-Temperature Synthesis of $LiMn_2O_4$ and $LiCoO_2$ Intercalation Compounds," *J. Solid State Chem.*, **94**, 185-196 (1991).

[3] J. M. Tarascon and D. Guyomard, "Li Metal-Free Rechargeable Batteries Based on $Li_{1+x}Mn_2O_4$ Cathodes ($0<x<1$) and Carbon Anodes," *J. Electrochem. Soc.*, **138**, 2864-2868 (1991).

[4] D. Guyomard and J. M. Tarascon, "Li Metal-Free Rechargeable $LiMn_2O_4$/Carbon Cells: Their Understanding and Optimization," *J. Electrochem. Soc.*, **138**, 937-948 (1992).

[5] J. M. Tarascon and D. Guyomard, "The $Li_{1+x}Mn_2O_4$/C Rocking-Chair System: A Review," *Electrochim. Acta,* **38**, 1221-1231 (1993).

[6] C. Schmutz, J. M. Tarascon, A. S. Gozdz, P. C. Warren, and F. K. Shokoohi, "A New Rechargeable Plastic Li-Ion Battery," Lithium Battery Symposium, Electrochemical Society Meeting, Miami Beach, FL, October 9-14, 1994.

[7] A. S. Gozdz, J. M. Tarascon, O. S. Gebizlioglu, C. N. Schmutz, P. C. Warren, and F. K. Shokoohi, "A New Hybrid Polymer Electrolyte For Lithium-Ion Rechargeable Batteries," Lithium Battery Symposium, Electrochemical Society Meeting, Miami Beach, FL, October 9-14, 1994.

[8] J. M. Tarascon and D. Guyomard, "New Electrolyte Compositions Stable over the 0 to 5 V Voltage Range and Compatible with the $Li_{1+x}Mn_2O_4$/carbon Li-ion Cells," *S. S. Ionics,* **69**, 293-305 (1994).

[9] D. A. G. Bruggeman, *Annalen der Physik,* **24**, 636 (1935).

[10] R. E. Meredith and C. W. Tobias, "Conduction in Heterogeneous Systems," in *Advan. Electrochem. Electrochem. Eng.,* C. W. Tobias, Ed., **2**, 15-47 (1962).

[11] D. Fan and R. E. White, "A Mathematical Model of a Sealed Nickel-Cadmium Battery," *J. Electrochem. Soc.,* **138**, 17-25 (1991).

[12] C. Ho, I. D. Raistrick, and R. A. Huggins, "Application of A-C Techniques to the Study of Lithium Diffusion in Tungsten Trioxide Thin Films," *J. Electrochem. Soc.,* **127**, 343-350 (1980).

[13] A. J. Vaccaro, T. Palanisamy, R. L. Kerr, and J. T. Maloy, "Electrochemical Investigations of Alkali-Metal Intercalation Reactions in $TiS_2$: Chronoamperometric Determination of Mass and Charge Transport Properties of Liquid Electrolyte Systems," *J. Electrochem. Soc.*, **129**, 682-688 (1982).

[14] M. G. S. R. Thomas, P. G. Bruce, and J. B. Goodenough, "AC Impedance Analysis of Polycrystalline Insertion Electrodes: Application to $Li_{1-x}CoO_2$," *J. Electrochem. Soc.*, **132**, 1521-1528 (1985).

[15] J. Farcy, R. Messina, and J. Perichon, "Kinetic Study of the Lithium Electroinsertion in $V_2O_5$ by Impedance Spectroscopy," *J. Electrochem. Soc.*, **137**, 1337-1341 (1990).

[16] W. Ebner, D. Fouchard, and L. Xie, "The $LiNiO_2$/Carbon Lithium-Ion Battery," *S. S. Ionics,* **69**, 238-256 (1994).

[17] M. Doyle and J. Newman, "Analysis of Capacity-Rate Behavior using Simplified Models for the Discharge Process of Lithium Batteries," submitted to *J. Appl. Electrochem.*, June 1995.

[18] C. N. Satterfield and T. K. Sherwood, *The Role of Diffusion in Catalysis,* Addison-Wesley, Reading, MA, p. 21 (1963).

[19] J. Newman and W. Tiedemann, "Porous Electrode Theory with Battery Applications," *AIChE J.*, **21**, 25-41 (1975).

[20] J. M. Sullivan, D. C. Hanson, and R. Keller, "Diffusion Coefficients in Propylene Carbonate, Dimethyl Formamide, Acetonitrile, and Methyl Formate," *J. Electrochem. Soc.*, **117**, 779-780 (1970).

[21] R. Jasinski, "Electrochemistry and Application of Propylene Carbonate," *Advan. Electrochem. Electrochem. Eng.*, C. W. Tobias, Ed., **8**, 253-335 (1972).

[22] J. Dahn, "Carbons and Graphites as Substitutes for the Lithium Anode," in *Lithium Batteries: New Materials and New Perspectives,* vol. 5, Ed., G. Pistoia, Elsevier Applied Science, North Holland, pp. 1-47 (1994).

[23] R. J. Gummow, A. de Kock, and M. M. Thackeray, "Improved Capacity Retention in Rechargeable 4 V Lithium/Lithium-Manganese Oxide (Spinel) Cells," *S. S. Ionics,* **69**, 59-67 (1994).

[24] D. Guyomard and J. M. Tarascon, "The Carbon/$Li_{1+x}Mn_2O_4$ System," *S. S. Ionics,* **69**, 222-237 (1994).

[25] M. Doyle, J. Newman, and J. Reimers, "A Quick Method of Measuring the Capacity versus Discharge Rate for a Dual Lithium Ion Insertion Cell Undergoing Cycling," *J. Power Sources,* **52**, 211-216 (1995).

[26] M. Doyle, T. F. Fuller, and J. Newman, "Modeling of Galvanostatic Charge and Discharge of the Lithium/Polymer/Insertion Cell," *J. Electrochem. Soc.,* **140**, 1526-1533 (1993).

[27] T. F. Fuller, M. Doyle, and J. Newman, "Simulation and Optimization of the Dual Lithium Ion Insertion Cell," *J. Electrochem. Soc.,* **141**, 1-10 (1994).

[28] T. F. Fuller, M. Doyle, and J. Newman, "Relaxation Phenomena in Lithium Ion Insertion Cells," *J. Electrochem. Soc.,* **141**, 982-990 (1994).

[29] E. J. Cairns, "A New Opportunity for Electrochemical Energy Conversion," *Interface,* **1**, 38-39 (1992).

[30] K. Ozawa, "Lithium-ion Rechargeable Batteries with $LiCoO_2$ and Carbon Electrodes: The $LiCoO_2$/C System," *S. S. Ionics,* **69**, 212-221 (1994).

[31] G. G. Trost, V. Edwards, and J. S. Newman, "Electrochemical Reaction Engineering," in *Chemical Reaction and Reactor Engineering,* J. J. Carberry and A. Varma, Eds., Marcel Dekker, Inc., New York, pp. 923-972 (1987).

[32] J. Newman, "Optimization of Porosity and Thickness of a Battery Electrode by Means of a Reaction-Zone Model," *J. Electrochem. Soc.,* **142**, 97-101 (1995).

[33] W. Tiedemann and J. Newman, "Maximum Effective Capacity in an Ohmically Limited Porous Electrode," *J. Electrochem. Soc.,* **122**, 1482-1485 (1975).

[34] H. S. Carslaw and J. C. Jaeger, *Conduction of Heat in Solids,* Clarendon Press, Oxford, p. 242 (1959).

# Chapter 4

## Measurement of Transport Properties in Solid Polymer Electrolytes

### 4.1 Introduction

The field of polymer electrolytes has seen enormous growth in the last twenty years because of the wide range of properties that can be synthesized into the polymer structure. This includes ionically conducting polymers such as poly(ethylene oxide), cation exchange polymers having a liquid-phase cosolvent such as Nafion,® and electronically conducting polymer electrodes such as polypyrrole. For ionically-conducting polymers, research has focused on the attainment of ever-increasing values of the conductivity. Many theoretical studies on the conduction mechanism in polymer electrolytes have been performed.[1] A microscopic understanding of the conduction mechanism is very important in the design and synthesis of novel, more conductive polymers. However, as far as battery performance is concerned, the ionic conductivity is only one of several transport properties that determine what makes a good polymer electrolyte.

Polymer electrolyte solutions are generally nonideal and concentrated, as demonstrated from activity coefficient measurements,[2] the concentration dependence of the conductivity,[3] and studies of ion-pairing and aggregation processes.[1,4] Therefore, in order to describe completely and properly the transport processes in these materials, it is necessary to have $n(n-1)/2$ transport properties, where $n$ is the number of independent species in solution. Thus, for example, for a binary salt in a polymer solvent, three independent species exist (polymer, anion, and cation), giving three independent transport properties. These properties can be chosen to be the conductivity, salt diffusion coefficient, and the transference number of one species. The binary electrolyte has been very popular in lithium-based battery systems; however, there have not

been comprehensive measurements of all of the transport properties for any single polymer-salt solution. This is due foremost to difficulties in the measurement of the transference number in solid polymer systems.

The most popular polymer electrolyte for lithium batteries has been poly(ethylene oxide) (PEO), first suggested for this application in 1979 by Armand.[5] PEO has a reasonable ionic conductivity with a wide range of lithium salts above its melting point (≈ 65°C), where it has an amorphous phase present. In general, complexes between PEO and salts may have complicated equilibria involving several different crystalline and amorphous phases; however, the existence of an amorphous phase is critical to attain a substantial ionic conductivity.

It is generally accepted that PEO solvates by direct interaction of the cation with ether oxygens on the polymer chain, with chain flexibility being an important aspect of the interactions in order for several oxygens to surround a given cation. This microscopic model is the origin of the convention of referring to salt concentrations in PEO by the ratio of monomer units to cation, $n$ in $PEO_nLiX$, as this gives one a picture of the microscopic solvation situation. The importance of the cation-ether group interactions is also demonstrated by examining the conductivities of solutions of polyoxymethylene $(CH_2\text{-}O)_n$ and polyoxetane $(CH_2\text{-}CH_2\text{-}CH_2\text{-}O)_n$; neither of these materials shows appreciable conductivity due to nonoptimal spacing of the ether sites.[5] On the other hand, the more recently developed and better-conducting polymer electrolyte poly(bis-methoxyethoxyethoxy phosphazene) is purely amorphous and has a monomer possessing side chains similar to PEO in molecular structure.[6]

In addition to lithium salts, there have also been studies and applications using several other cations in PEO, including $Na^+$, $K^+$, $Mg^{2+}$, $Ca^{2+}$, $Cu^{2+}$, and $Zn^{2+}$.[6-10] The anions used in these systems are usually large, soft anions with delocalized electronic charge; this allows

the polymer to solubilize the salt without the need for specific interactions with the anionic species. Some popular anions in the literature for battery applications have included trifluoromethanesulfonate ($CF_3SO_3^-$), tetrafluoroborate ($BF_4^-$), perchlorate ($ClO_4^-$), hexafluoroarsenate ($AsF_6^-$), and hexafluorophosphate ($PF_6^-$).[11] Since these anions tend to be rather expensive, reduction of the salt concentration used in the battery is advantageous.

The experimental work in this chapter will focus on the measurement of a complete set of transport properties for a single salt in PEO at a single temperature. The salt chosen is $NaCF_3SO_3$ ($0.1<c(M)<2.6$ at 85°C). The experiments will be analyzed using concentrated solution theory. Thus, the three transport properties are independent functions of salt concentration and temperature, and the solution may be nonideal.

## 4.2 Theoretical development

The solution is described using a macroscopic model with the three independent species chosen to be $Na^+$, $CF_3SO_3^-$, and PEO. One does not need to take into account the microscopic speciation, *i.e.*, the actual species that exist in the solution, as long as ion-exchange reactions are fast enough to be considered in equilibrium. The concentration dependence of the transport properties will naturally reflect the equilibria of the microscopic processes. The three transport properties necessary to describe this system are the conductivity, salt diffusion coefficient, and sodium ion transference number. These properties can be related to three pairwise interaction parameters $\mathcal{D}_{ij}$ through the expressions:[12]

$$\frac{1}{\kappa} = \frac{-RT}{c_T z_+ z_- F^2}\left[\frac{1}{\mathcal{D}_\pm} - \frac{c_0 z_-}{c_+(z_+\mathcal{D}_{0+} - z_-\mathcal{D}_{0-})}\right], \tag{4-1}$$

$$D = \frac{c_T}{c_0}\left[1 + \frac{d\ln \gamma_\pm}{d\ln m}\right]\left[\frac{\mathcal{D}_{0+}\mathcal{D}_{0-}(z_+ - z_-)}{z_+\mathcal{D}_{0+} - z_-\mathcal{D}_{0-}}\right], \tag{4-2}$$

and

$$t_+^0 = 1 - t_-^0 = \frac{z_+\mathcal{D}_{0+}}{z_+\mathcal{D}_{0+} - z_-\mathcal{D}_{0-}}. \tag{4-3}$$

It is possible that the $\mathcal{D}_{ij}$ may be less concentration dependent than the measured set of transport properties.

For many salts in PEO, complicated phase equilibria exist between an amorphous phase and one or several salt/PEO crystalline phases of various stoichiometries.[3] It is now agreed upon that the amorphous salt/PEO phase is responsible for ionic conduction.[5] This phase equilibrium information is not yet available for PEO and $NaCF_3SO_3$. If a true phase equilibrium existed between an amorphous phase of given composition and a single crystalline phase of given composition, then addition of increasing amounts of salt would simply enrich the crystalline phase (*i.e.*, lead to an increasing crysalline phase volume fraction). This would lead to a steady decrease in conductivity with salt concentration, as the crystalline phase would be a barrier to conduction. Examination of both phase diagram and conductivity data for PEO and $LiCF_3SO_3$ shows that the expected behavior is not obeyed.[3,13] The attainment of a true equilibrium in these systems may be a slow process. For the present work, we ignore the possibility of phase equilibrium processes and treat the solution as a single-phase mixture.

The conductivity is determined by employing the standard ac-impedance method. The salt diffusion coefficient is found by using the method of restricted diffusion,[14] with the concentration difference related to the potential of the cell.[15] The theoretical analysis of this method for concentrated electrolyte solutions has been performed by Chapman *et al.*[14] We

apply a constant current to the cell:

$$\text{Na} \mid \text{PEO}_n\,\text{NaCF}_3\text{SO}_3 \mid \text{Na}$$

for sufficient time to set up a concentration gradient. The current is then interrupted, and the potential of the cell is monitored as the concentration profile relaxes. The salt diffusion coefficient is calculated from the slope of a plot of $\ln(\Delta\Phi)$ *versus* time,

$$\text{slope} = -\frac{\pi^2 D}{L^2}, \tag{4-4}$$

where $L$ is the cell thickness. This diffusion coefficient approaches the value $D(c_\infty)$ rapidly as the concentration profile relaxes.

To measure the transference number it is useful to use concentration-cell data. The potential of a cell of the form:

$$\text{Na} \mid \text{PEO}_n\text{NaCF}_3\text{SO}_3 \mid \text{PEO}_m\text{NaCF}_3\text{SO}_3 \mid \text{Na}$$

can be expressed by using a sodium reference electrode in solution to assess the local potential gradient:

$$\nabla\Phi = \frac{2RT}{F}\left[1 + \frac{d\ln f_\pm}{d\ln c}\right]\left[1 - t_+^0\right]\nabla\ln c\,. \tag{4-5}$$

The potential across the full cell is then:

$$U = \frac{2RT}{F}\int_{x=0}^{L}\left[1 + \frac{d\ln f_\pm}{d\ln c}\right]\left[1 - t_+^0\right]\frac{\partial\ln c}{\partial x}\mathrm{d}x\,. \tag{4-6}$$

The potential of this cell depends only on the concentrations at the two electrode surfaces.

However, it is evident that the measurement combines both the transference number and the thermodynamic factor. This latter quantity is just a specific function of the salt activity coefficient's concentration dependence:

$$1 + \frac{d\ln f_{\pm}}{d\ln c} . \tag{4-7}$$

The thermodynamic factor is unity for an ideal solution. Unfortunately, we cannot expect that the concentrated polymer electrolyte solution will be ideal.

The measurement of the salt activity coefficient in these solutions without the knowledge of the transference number has not been achieved yet. Many methods that are used in low-molecular-weight solvents cannot be used in solid polymer systems, such as boiling-point elevation, vapor pressure, *etc.* A possible electrochemical method would involve measuring the concentration dependence of the potential of the following cell:

$$\mathrm{X} \mid \mathrm{PEO}_n\mathrm{NaX} \mid \mathrm{Na}.$$

The X above denotes an electrode reversible to the anion. Unfortunately, it is difficult to develop such an electrode with the unusual anionic species used in these solutions. Some attempt has been made to use poly(ethylene imide) in a cell of the following form for this purpose:[16,17]

$$\mathrm{Li} \mid \mathrm{PEO}_n\mathrm{LiCF_3SO_3} \mid \mathrm{PEI}_m\mathrm{CuCF_3SO_3} \mid \mathrm{Cu}.$$

To date, none of these results have been published. For now, we must assume that the value of the transference number is necessary to calculate the activity coefficient.

### 4.3 Analysis of the galvanostatic polarization experiment

Although we cannot determine $t_+^0$ directly from concentration-cell data, we can make use of these data as a relationship between cell potential and concentration difference. Consider the galvanostatic polarization of a cell of the form: Na|PEO$_n$NaCF$_3$SO$_3$|Na for short enough times so that semi-infinite diffusion conditions apply at either electrode. The current is passed for a sufficient amount of time to establish a concentration gradient at the surfaces, but less than the diffusion time of the cell ($t_i$<0.05$\frac{L^2}{D}$ ). An identical situation exists in the Hittorf cell; the excess salt on one side of the cell (or the depleted salt on the other side) is directly proportional to the transference number at the bulk concentration. Instead of attempting to measure the total excess salt on either side, we instead monitor the potential of the cell after current interruption. The potential can then be used to find the concentration difference across the cell as a function of the current density $I$ and the time passed $t_i$, as we can show that $\Delta c$ is a single-valued function of $It_i^{1/2}$.

The experiment can be modeled with the two equations:

$$\frac{\partial c}{\partial t} + \mathbf{v}^{\square}\cdot\nabla c = \nabla\cdot\left[D\nabla c\right] - \frac{c_0\bar{V}_0}{F}\left[\mathbf{i}\cdot\nabla t_+^0\right], \tag{4-8}$$

$$\nabla\cdot\mathbf{v}^{\square} = -\frac{\bar{V}_e}{F}\left[\mathbf{i}\cdot\nabla t_+^0\right], \tag{4-9}$$

where $\mathbf{v}^{\square}$ denotes the volume-average velocity.[14] The quantity referred to as $Q$ and defined in Chapman *et al.*[14] is arbitrarily taken to equal zero. We have assumed that the partial molar volume of the salt is constant. For the semi-infinite diffusion problem posed above, the boundary conditions are

$$c = c_\infty \text{ both at } t=0 \text{ and at } x=\infty, \tag{4-10}$$

$$\frac{\partial c}{\partial x} = -\frac{I(1-t_+^0)}{FD} \text{ at } x=0, \tag{4-11}$$

and

$$v_x^{\square} = \frac{\bar{V}_e I t_-^0}{F} \text{ at } x=0. \tag{4-12}$$

Notice that a fluid motion exists due to the flow of current in the solution; this is usually negligible.[18,19]

For a very-thin cell, it is valid to consider the one-dimensional forms of equations 4-8 and 4-9. As with any semi-infinite diffusion problem, it is useful to use the similarity-transformed variable

$$\eta = \frac{x}{2(D(c_\infty)t)^{1/2}}. \tag{4-13}$$

We also define a dimensionless time according to

$$\tau = \frac{2t_-^0(c_\infty)}{D^{1/2}(c_\infty)Fc_\infty} I t^{1/2}, \tag{4-14}$$

where $D(c_\infty)$ and $t_-^0(c_\infty)$ refer to the properties evaluated at the bulk concentration. This definition emphasizes the importance of the parameter $It_i^{1/2}$. Substitution of these definitions above gives the following differential equations in $\tau$ and $\eta$,

$$2\tau\frac{\partial c}{\partial \tau}-2\eta\frac{\partial c}{\partial \eta}-\frac{D}{D(c_\infty)}\frac{\partial^2 c}{\partial \eta^2}=\frac{1}{D(c_\infty)}\frac{dD}{dc}\left[\frac{\partial c}{\partial \eta}\right]^2$$
$$-c_0\bar{V}_0\frac{c_\infty}{t_-^0(c_\infty)}\frac{dt_+^0}{dc}\tau\frac{\partial c}{\partial \eta}-\frac{Fc_\infty}{It_-^0(c_\infty)}v_x^{\square}\tau\frac{\partial c}{\partial \eta}, \tag{4-15}$$

and

$$\frac{\partial v_x^{\square}}{\partial \eta}=-\frac{\bar{V}_e I}{F}\frac{dt_+^0}{dc}\frac{\partial c}{\partial \eta}. \tag{4-16}$$

To complete the nondimensionalization of the problem, we define a dimensionless concentration and a volume-average velocity as

$$\Theta=\frac{c-c_\infty}{\tau c_\infty} \quad \text{and} \quad Y=\frac{Fv_x^{\square}}{\bar{V}_e It_-^0(c_\infty)}. \tag{4-17}$$

This leads to

$$2\tau\frac{\partial \Theta}{\partial \tau}+2\Theta-2\eta\frac{\partial \Theta}{\partial \eta}-\frac{D}{D(c_\infty)}\frac{\partial^2 \Theta}{\partial \eta^2}=\tau\frac{c_\infty}{D(c_\infty)}\frac{dD}{dc}\left[\frac{\partial \Theta}{\partial \eta}\right]^2$$
$$-\tau c_0\bar{V}_0\frac{c_\infty}{t_-^0(c_\infty)}\frac{dt_+^0}{dc}\frac{\partial \Theta}{\partial \eta}-\tau c_\infty\bar{V}_e Y\frac{\partial \Theta}{\partial \eta}, \tag{4-18}$$

and

$$\frac{\partial Y}{\partial \eta}=-\tau\frac{c_\infty}{t_-^0(c_\infty)}\frac{dt_+^0}{dc}\frac{\partial \Theta}{\partial \eta}. \tag{4-19}$$

For constant physical properties, $\partial\Theta/\partial\tau = 0$, and the left side of equation 4-18 has the familiar solution involving the integrated error function:[20]

$$\Theta(\eta) = \text{ierfc}\,\eta\,. \tag{4-20}$$

The perturbation in the parameter $\tau$ is evident in the terms on the right sides of equations 4-18 and 4-19, all of which involve the variable physical properties.

The boundary conditions on these equations become

$$\frac{\partial\Theta}{\partial\eta} = -\frac{t_-^0}{t_-^0(c_\infty)}\frac{D(c_\infty)}{D} \quad \text{at} \quad \eta = 0\,, \tag{4-21}$$

$$Y = 1 \quad \text{at} \quad \eta = 0\,, \tag{4-22}$$

$$\text{and} \quad \Theta = 0 \quad \text{at} \quad \eta = \infty\,. \tag{4-23}$$

Thus, the concentration scales with $It_i^{1/2}$, although not necessarily linearly, even in the concentrated binary electrolyte with an arbitrary variation of physical properties. If we calculate the values of $\tau$ used in the present experiments, we find that $\tau<0.1$ at all times. From equation 4-18, it is apparent that as $\tau$ approaches zero, the solution for constant transport properties, equation 4-20, is valid.

In the present experiment we are most interested in the concentration difference between the two electrodes immediately after current interruption. We can find this from equation 4-20 in its dimensional form; by evaluating $\Theta$ at $x=0$ and multiplying by 2 to account for the full cell with two electrodes we find,

$$\Delta c = \frac{4t_-^0}{F(\pi D)^{1/2}}(It_i^{1/2})\,. \tag{4-24}$$

This relationship apparently will hold as $It_i^{1/2}$ approaches zero. We can achieve this experimentally by using short times and small current densities in our experimental method. The

deviation of $\Delta c$ from this dilute-solution theory form can be predicted by solution of the full equation numerically. This will be explored in section 4.6 and is used to verify the validity of the linear expression 4-24 under typical experimental conditions.

Having a relationship between the concentration difference in the cell and the value of the transference number, the potential measured can be compared with concentration-cell data to determine $t_-^0$. This is achieved by preparing a plot of the potential difference across the cell $U$ *versus* the value of the experimental parameter $It_i^{1/2}$. The slope of these plots at the origin will be referred to as $m$. By the combination of equations 4-5 and 4-24, we find that the transference number is given by

$$t_-^0 = \frac{mc_\infty F(\pi D)^{1/2}}{4} \Big/ \left[\frac{dU}{d\ln c}\right] . \tag{4-25}$$

The values of $t_-^0$ and $D$ apply at the bulk concentration $c_\infty$. The quantity $\frac{dU}{d\ln c}$ is the slope of the concentration-cell data, plotted in logarithmic form, and also applies at the bulk concentration $c_\infty$. Note that this calculation requires three experimentally-derived quantities: $D$, $m$, and $\frac{dU}{d\ln c}$, all evaluated effectively at $c_\infty$.

With the transference number known, it is a simple matter to back out the thermodynamic factor from the concentration-cell data. This is calculated from:

$$\left[1 + \frac{d\ln f_\pm}{d\ln c}\right] = \frac{-F}{2RTt_-^0}\left[\frac{dU}{d\ln c}\right] , \tag{4-26}$$

and must be evaluated as a function of the salt concentration. If desired, the thermodynamic factor can be used to calculate the activity coefficient directly by integration with the applica-

tion of the infinite dilution condition of ideality (*i.e.*, $f_{\pm} \rightarrow 1$ as $c \rightarrow 0$). However, as the activity coefficient only appears in the governing equations in the form above, there is little motivation to perform this calculation.

### 4.4 Experimental details

The polymer films were prepared using the solvent-casting method. Mixtures of different salt weight fractions were made by dissolving poly(ethylene oxide) (avg. M.W.=$5\times10^6$ g/mol, Aldrich) and sodium trifluoromethanesulfonate in the desired ratio in acetonitrile (Aldrich, HPLC grade), and then casting onto a Teflon-coated glass plate. After air-drying for a period of hours, the films were dried in a vacuum oven for at least three days. The films were generally about 100 μm thick with very uniform thicknesses. Thicker films were formed by stacking and heating together a sufficient number of films to the desired thickness.

The salt concentration was calculated using the weight fraction and solution density,

$$c = \frac{\rho\omega_e}{M_e}. \tag{4-27}$$

By assuming a constant partial molar volume for the salt, we were able to correlate our density data with the expression:

$$\frac{1}{\rho} = \frac{1}{\rho^0_{PEO}} + \omega_e\left[\frac{\bar{V}_e}{M_e} - \frac{1}{\rho^0_{PEO}}\right]. \tag{4-28}$$

This gives $\bar{V}_e$ = 36 cm$^3$/mol. The density calculated from this equation is used above to calculate the salt concentration. All experiments were carried out over the range of salt concentrations: $0.14<c(\text{mol/dm}^3)<2.58$, corresponding to $160<n<8$ in the formula $PEO_nNaCF_3SO_3$. The concentration-cell data were taken over a wider range of concentrations:

$0.05<c(\text{mol/dm}^3)<4.71$, to improve the accuracy in the differentiation of the data.

Sodium (Alfa) was melted, filtered through coarse stainless steel wool, then heated at 400°C with small amounts of titanium sponge. The purified sodium was rolled between sheets of polyethylene to form thin foil electrodes. Experimental cells of the form: $\text{Na|PEO}_n\text{NaCF}_3\text{SO}_3\text{|Na}$ were assembled in a helium-filled glove box with the oxygen level less than 1 ppm. The cells were heated to 85°C at least five hours prior to testing. A convection oven with a Eurotherm temperature controller was used as the heating source. Temperature variation was less than 1.0°C during cell operation.

Conductivities were measured using the Solatron Schlumberger SI 1286 Electrochemical Interface and 1254 Four-channel Frequency Response Analyzer. The cells were assembled as above and then transferred into an external convection oven. Strict temperature control was maintained, including having the same thermal history for each sample to ensure that the pseudo-equilibrium state of each polymer film was identical. The working area of the cells was 0.9 $\text{cm}^2$ for all experiments. Impedance data were taken over a wide range of frequencies and plotted in the Nyquist (complex plane) form. The ionic conductivity was obtained from the high-frequency intercept of the impedance data with the real axis.

Restricted-diffusion experiments were carried out entirely in the helium-filled glove box. Cells were polarized in the galvanostatic mode using a computer-driven PAR 371 potentiostat/galvanostat and software developed in the De Jonghe laboratory. Generally about ten to fifteen minutes of polarization time at current densities of 0.1 to 0.3 $\text{mA/cm}^2$ were used to establish the concentration gradient, although for the very dilute solutions smaller currents and/or times are needed. One must avoid exceeding the limiting current, which can be estimated prior to the experiments and used as a guide to the choice of a proper current density.

The cells had a working area of 0.9 $cm^2$ and thicknesses on the order of 300 to 400 μm. An identical procedure was used for assembling the cells for the transference number measurements. Polarization times should be much shorter, on the order of one to two minutes, to assure that semi-infinite diffusion conditions apply during the experiments. Similar current densities and film thicknesses were used as in the restricted-diffusion experiments.

For the concentration-cell experiments, it is necessary to assemble the cell, heat it to the temperature of interest, and then measure the potential, without allowing the concentration gradient to relax to the electrode surfaces. This requires a very long diffusion time, on the order of several hours, and thus a slightly different cell configuration was used. Instead of placing the two films face to face, we overlap the films edgewise, and place electrodes on the two ends. This gives a diffusion length of several centimeters, and a diffusion time on the order of days. It is possible to have this large distance between the two electrodes because no current flows during the experiment; otherwise the ohmic drop would be prohibitively large. The potential difference is measured across the concentration cell with the Keithley 642 Electrometer.

### 4.5 Results and discussion

The ionic conductivity of $PEO_nNaCF_3SO_3$ solutions at 85°C is similar in form but slightly higher in magnitude than that of $PEO_nLiCF_3SO_3$ solutions. In figure 4-1, the conductivity is given as a function of the salt concentration. The conductivity increases with concentration steeply until going through a maximum of $3.3\times10^{-4}$ S/cm at $c$=1.09 mol/$dm^3$ ($n$=20). At higher salt concentrations than this, the conductivity falls off, supporting the theory that chain entanglement due to transient ionic cross-linking leads to lower mobilities for the ionic species.[1] The conductivity of the lithium analog also exhibits a maximum at a similar concentration ($\kappa=2.1\times10^{-4}$ S/cm at $n$=18), although it also shows a local maximum at very low

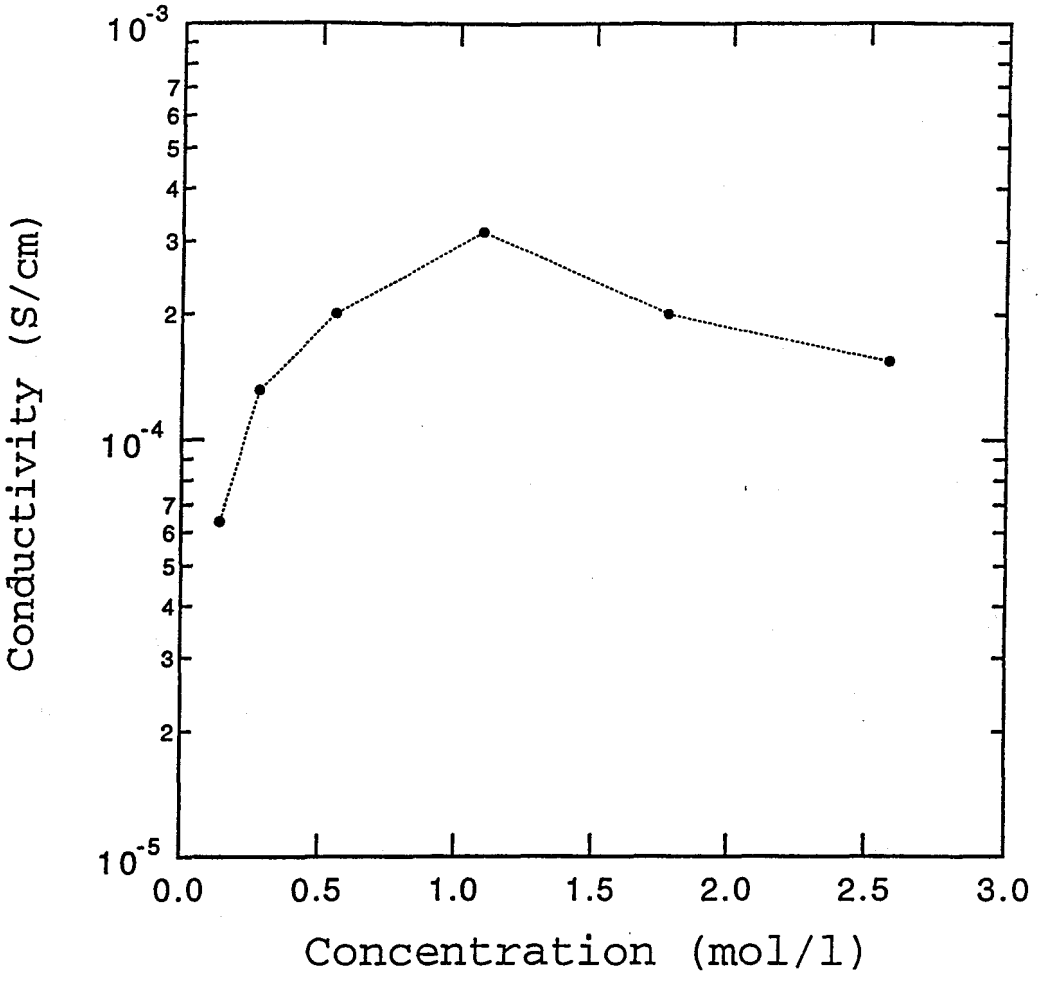


Figure 4-1. Logarithmic plot of the ionic conductivity of $NaCF_3SO_3$ in PEO at 85°C. Data obtained using ac-impedance methods.

concentrations ($\kappa$=2.0×10$^{-4}$ S/cm at $n$=100) not seen for sodium.[3,21] It is possible that a second maximum would be seen in this system also if more data points had been taken in the dilute range. On the other hand, research has shown that this second maximum is sensitive to the content of residual catalyst impurities used in the synthesis of poly(ethylene oxide).[3]

The method of restricted diffusion involves the measurement of the potential of a cell undergoing relaxation of a concentration gradient. Any arbitrary initial profile will eventually decay with a time constant related to $D(c_\infty)$; other processes such as thermal and momentum transport occur on much shorter time scales than the diffusion process. An example of this plot is given as figure 4-2 for the electrolyte $PEO_{55}NaCF_3SO_3$. The slope is taken after sufficient time has elapsed for linear behavior to be observed. This happens very quickly for the present polymer electrolyte solution, within about five minutes on figure 4-2. However, the most accurate value of $D(c_\infty)$ is found from 20 to 60 minutes into the relaxation, which corresponds to potential differences of from 8 to 2 mV. At very low potentials, the potentiostat reading can become erratic and settle to a nonzero value, as it reflects the slow side reaction between the sodium electrode and the electrolyte. We were able to improve the data by subtracting this steady-state value of the potential from the data before taking the natural logarithm; this leads to straight-line behavior over the largest possible range of times. The time for the overall relaxation of the concentration profile can be estimated from the diffusion time, $L^2/D$, to be approximately one hour. For liquid solvent systems, where $D$ is expected to be much larger, the time constant for diffusion is smaller, and a longer diffusion length $L$ should be used in the experiment.

Plots of the form of figure 4-2 are used to calculate $D$, given in figure 4-3 as a function of bulk salt concentration. The diffusion coefficient varies with salt concentration, decreasing

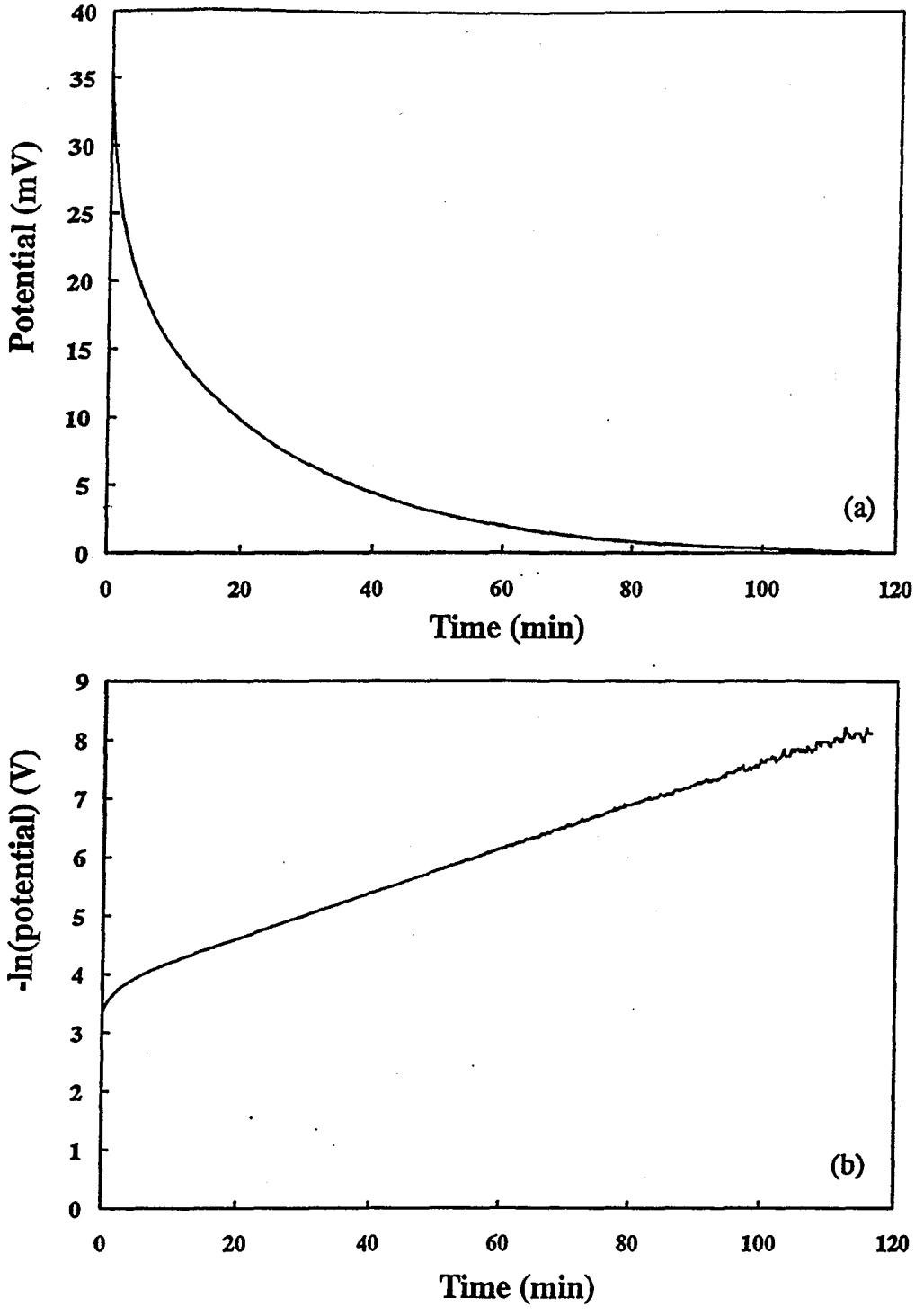


Figure 4-2. Diffusion-coefficient measurement of $NaCF_3SO_3$ in PEO at 85°C using the restricted-diffusion method. A polarized cell, $Na/PEO_{55}NaCF_3SO_3/Na$, relaxes back to its initial condition shown by (a) potential *vs.* time, and (b) natural logarithm of potential *vs.* time.

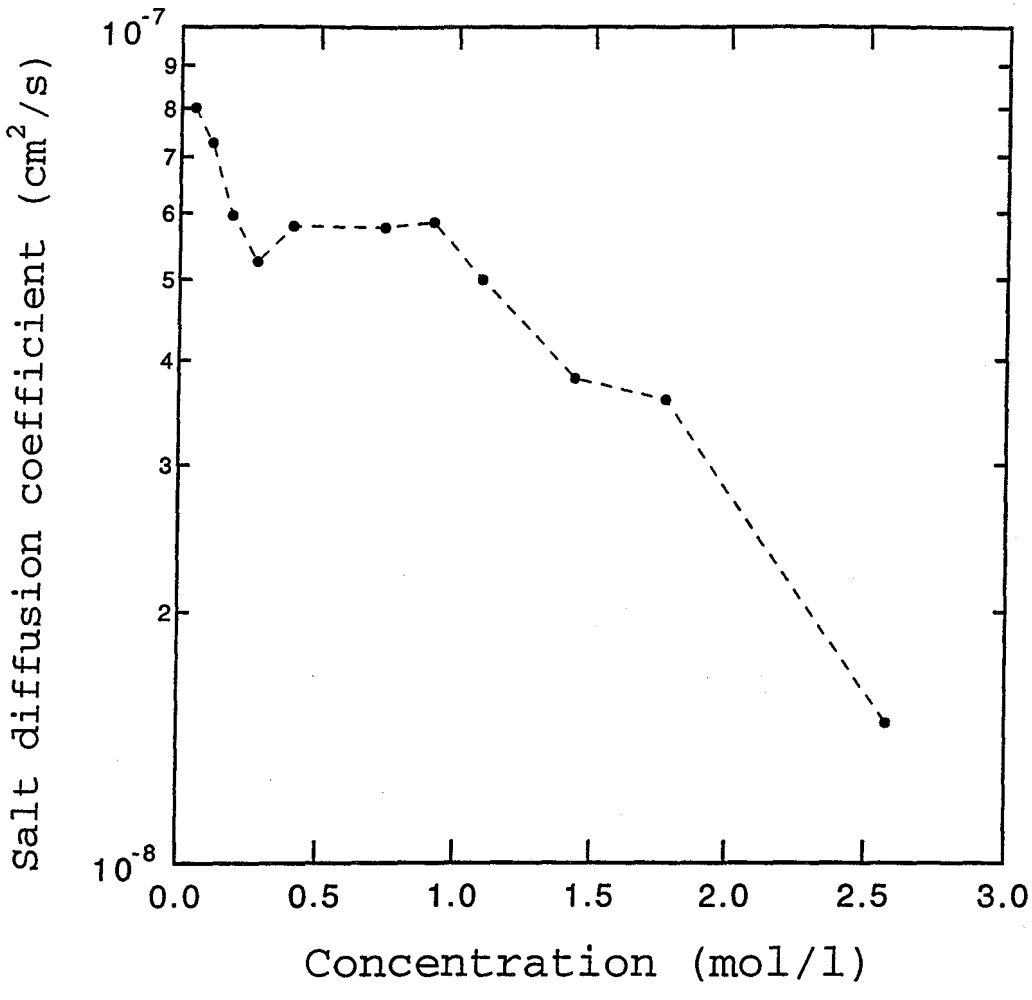


Figure 4-3. Calculated diffusion coefficient of $NaCF_3SO_3$ in PEO at 85°C. Data were obtained by using the method of restricted diffusion.

with concentration at all data points except for a local minimum at the concentration of 0.28 mol/dm$^3$ (n=80). The values found for the diffusion coefficient of sodium triflate are similar to the values reported for the diffusion coefficient of lithium triflate ($D$=7.5×10$^{-8}$ cm$^2$/s at n=45).[2] The steady decrease in the salt diffusion coefficient at high salt concentrations suggests a mechanism similar to that seen in the conductivity data, *i.e.*, increasing salt concentration is leading to increased chain entanglement and decreased ion mobility.

The error in these diffusion coefficient values can be estimated from the variance in the measurements of film thickness and the relaxation time constant. The following formula is used to calculate the error:

$$\left[\frac{\sigma_D}{D}\right]^2 = \left[\frac{2\sigma_L}{L}\right]^2 + \left[\frac{\sigma_s}{s}\right]^2,$$

where σ is the standard deviation for a given measurement. Following this procedure leads to predicted errors of from 1.5 to 6.0% for the measured diffusion coefficients. As an example, we will perform this calculation for the $n$=55 case whose data are illustrated in figure 4-2. The film thickness was measured five times over the area of a given sample to assess the scatter in this measurement. This gave a standard deviation of 2.44 μm for a 400 μm film. The error in the measurement of the time constant for the relaxation process is related to the range over which one chooses to fit the slope of figure 4-2. Taking various ranges of relaxation time and determining the slope, we can calculate a standard deviation for this set of data to be 8.64×10$^{-4}$ min$^{-1}$. Based on both the scatter in the thickness measurements and the slope of figure 4-2, we estimate the precision of this diffusion coefficient value to be 2.6 % using the above equation.

Concentration cells of the form Na|PEO$_n$NaCF$_3$SO$_3$|PEO$_m$NaCF$_3$SO$_3$|Na, where $m$=8 and $n$ varies from 4 to 500, were prepared as described in the Experimental section. In figure

4-4 we present the potential difference of these cells as a function of the natural logarithm of the concentration; the markers represent data points, and the solid line is a curve fit discussed in the next paragraph. Data points on figure 4-4 represent the average value of 2 to 5 experiments for each concentration difference. Note that these data are approximately linear over small ranges of the salt concentration, a result that will be used later in determining the transference number.

Although there is about 1 to 4 mV of scatter in the concentration-cell data, we chose to use a highly accurate six-parameter fit to the data instead of a more smooth curve. We made this choice because of the extreme sensitivity of the calculated transference numbers to the differentiation of this data fit. The data were fit by the equation

$$U = v(0) + v(1)c + v(2)\exp\left[-v(3)c\right] + v(4)\exp\left[-v(5)c\right], \qquad (4\text{-}29)$$

with the fitting parameters

$$v(0)=3.2807\,,\ v(1)=-0.0020545\,,\ v(2)=62.521$$

$$v(3)=0.0018733\,,\ v(4)=130.33\,,\ \text{and}\ v(5)=0.028355\,,$$

where $U$ is in mV and $c$ is in mol/dm$^3$. The slope of equation 4-29 is the important quantity for evaluation of the transference number and thermodynamic factor.

It is interesting to compare the concentration-cell data for $NaCF_3SO_3$ in PEO with those for $LiCF_3SO_3$. These data are taken from the literature;[2] unfortunately, we have only four data points available and these cover a limited range of salt concentrations. The two sets of data are compared in figure 4-5; we have shifted the literature data's zero point (n=20) up to the value of our data (remember that only the slopes of these data have physical meaning). Note that the

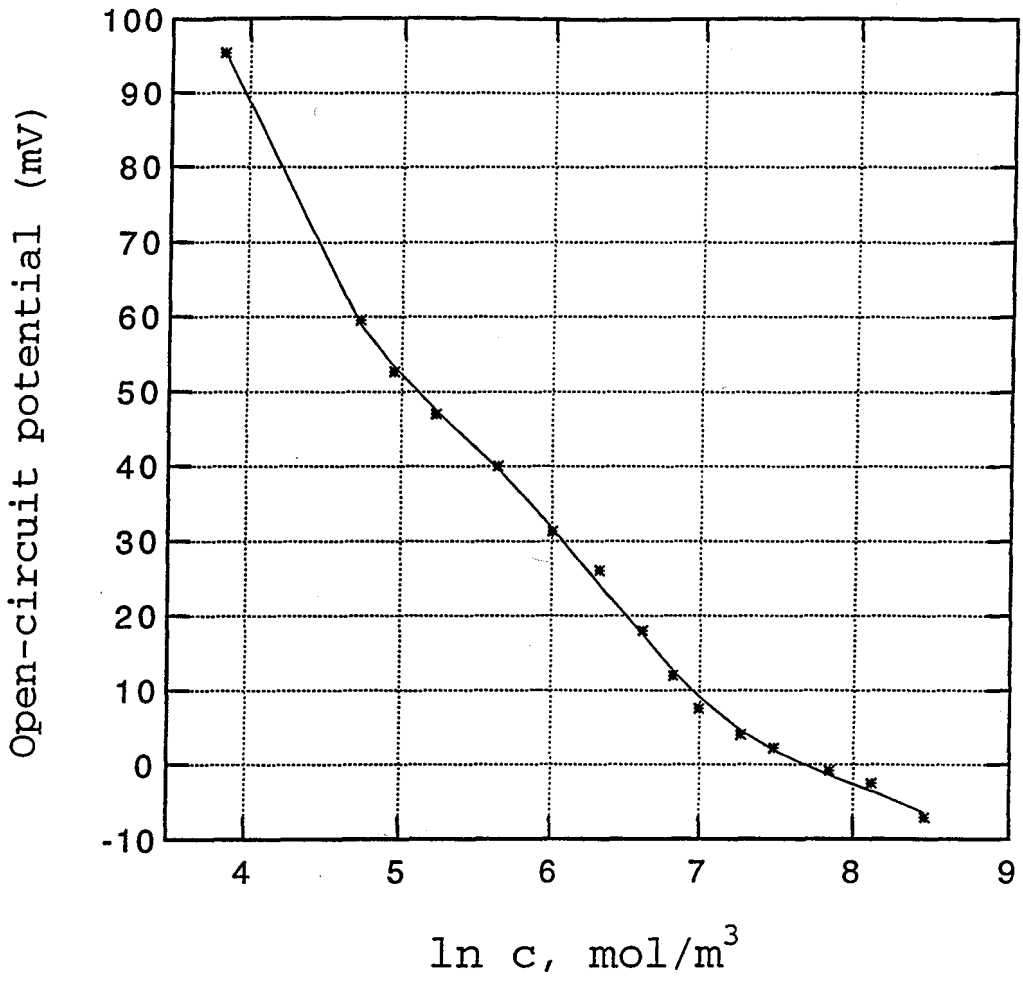


Figure 4-4. Data taken from concentration cells of the form $Na/PEO_nNaCF_3SO_3/PEO_mNaCF_3SO_3/Na$ at 85°C with m fixed and n varied from 4 to 500. The solid line is a fit to the data.

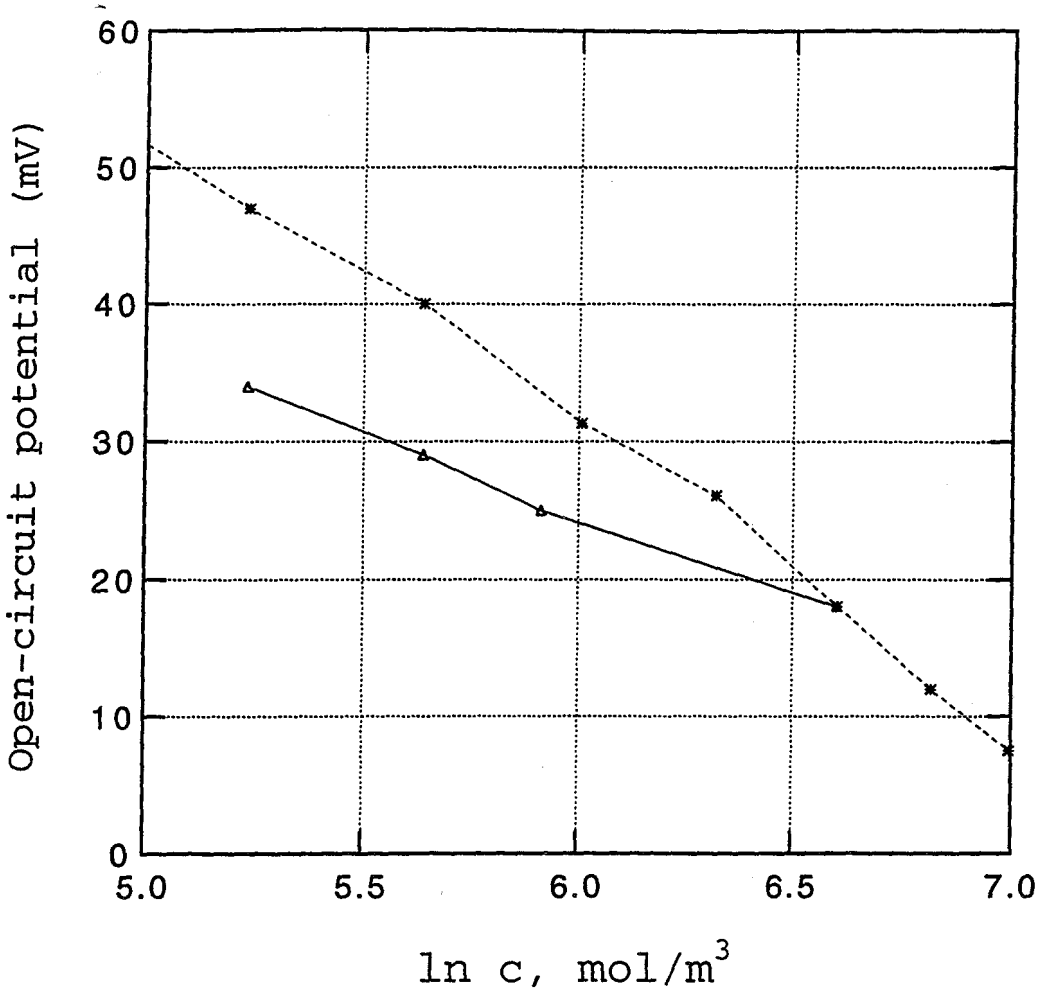


Figure 4-5. Comparison of data taken from lithium and sodium concentration cells of the form $M/PEO_nMCF_3SO_3/PEO_mMCF_3SO_3/M$ at 85°C. The lithium data, indicated by the solid line, are taken from the literature.

data for $LiCF_3SO_3$ have a smaller slope than that for the sodium data. This indicates that over this concentration range lithium triflate either has a larger value of $t_+^0$ or a smaller thermodynamic factor or both. The slopes appear to be getting more nearly equal as the salt concentration decreases, which we might expect as both solutions will become ideal.

Galvanostatic polarization of cells of the form $Na|PEO_nNaCF_3SO_3|Na$ provides a second experiment needed to extract the transference number and thermodynamic factor separately from the concentration-cell data. After passing current through this cell for a given time, the current is interrupted, and the cell potential is recorded. The potential difference across the cell as a function of the quantity $(It_i^{1/2})$ is plotted. In figure 4-6 we present the experimental results in the form of $\Delta\Phi$ *versus* $(It_i^{1/2})$ for several values of $n$ in $PEO_nNaCF_3SO_3$. These plots are linear for small values of $(It_i^{1/2})$, as predicted in the theoretical development (equation 4-12) and then deviate upwards at larger values. The slope of this plot near the origin, *i.e.*, as $(It_i^{1/2})$ approaches zero, which we refer to as $m$, is the important experimental quantity. We do find the predicted linear dependence over the whole range of concentrations used here, *i.e.*, from $n=8$ to $n=500$, when small enough values of $(It_i^{1/2})$ are used. Figure 4-7 gives the experimental data for the slopes $m$ as a function of the bulk salt concentration. Bear in mind that figure 4-6 can be extrapolated rigorously into the third quadrant because the two electrodes are symmetric and the curves are odd in $(It_i^{1/2})$. The value of $m$ is approximately constant at 3.45 $\Omega cm^2/s^{1/2}$ for salt concentrations above 0.5 $mol/dm^3$.

The transference number of the sodium ion *versus* concentration, calculated using equation 4-25, is presented in figure 4-8. At the higher concentrations these transference numbers are lower than any of the values reported for $LiCF_3SO_3$ in PEO, which tend to range from 0 to 0.5. The transference number decreases from its maximum value of 0.31 in the most dilute

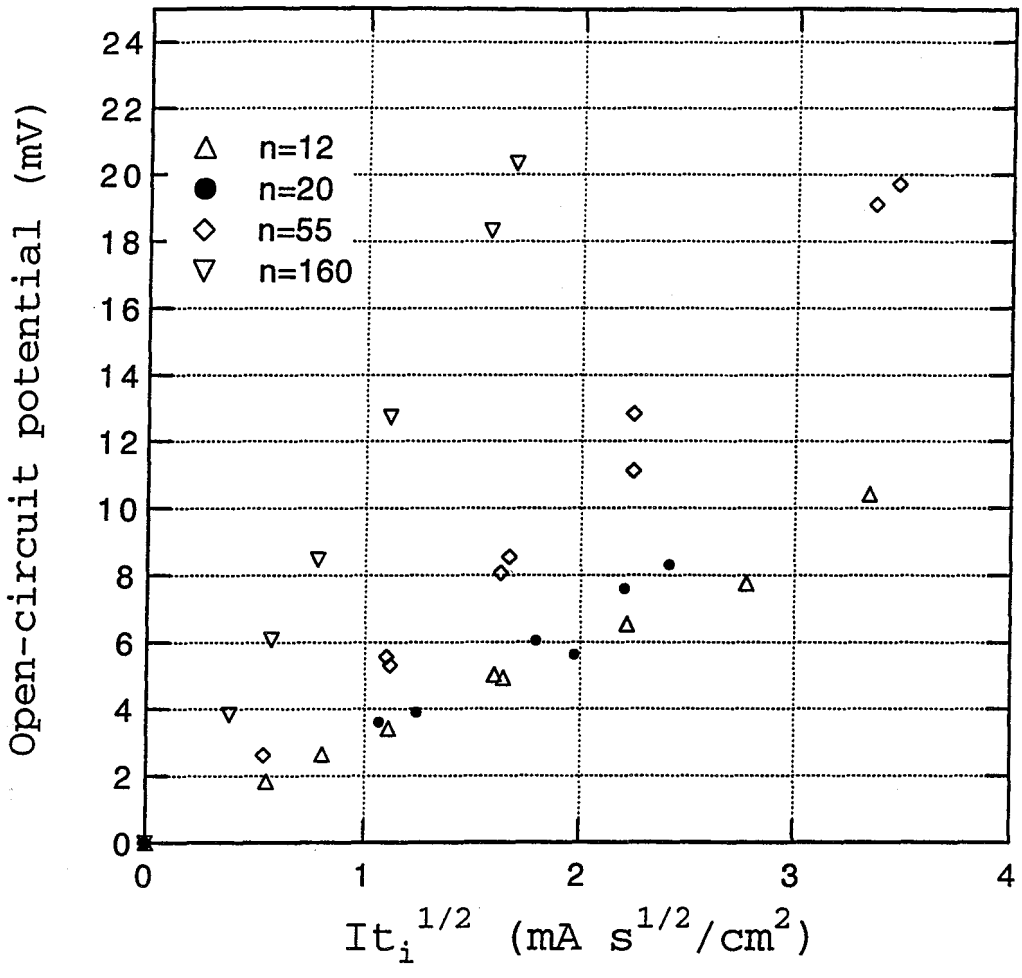


Figure 4-6. Experimental data from galvanostatic polarization for various bulk concentrations. The slope of the data at the origin is the important experimental quantity.

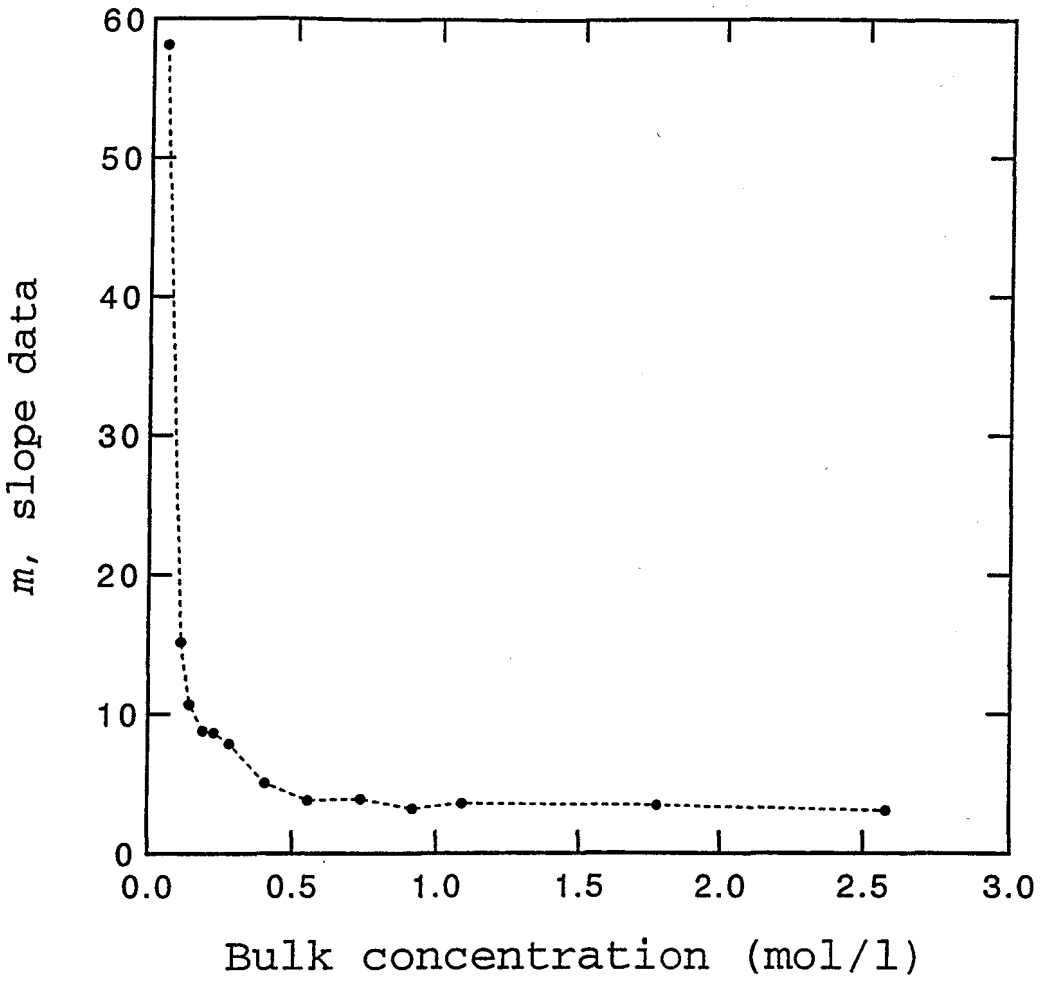


Figure 4-7. Slopes of galvanostatic polarization plots as a function of bulk salt concentration for $NaCF_3SO_3$ in PEO at 85°C. The slope is taken at the origin and is used to calculate the transference number.

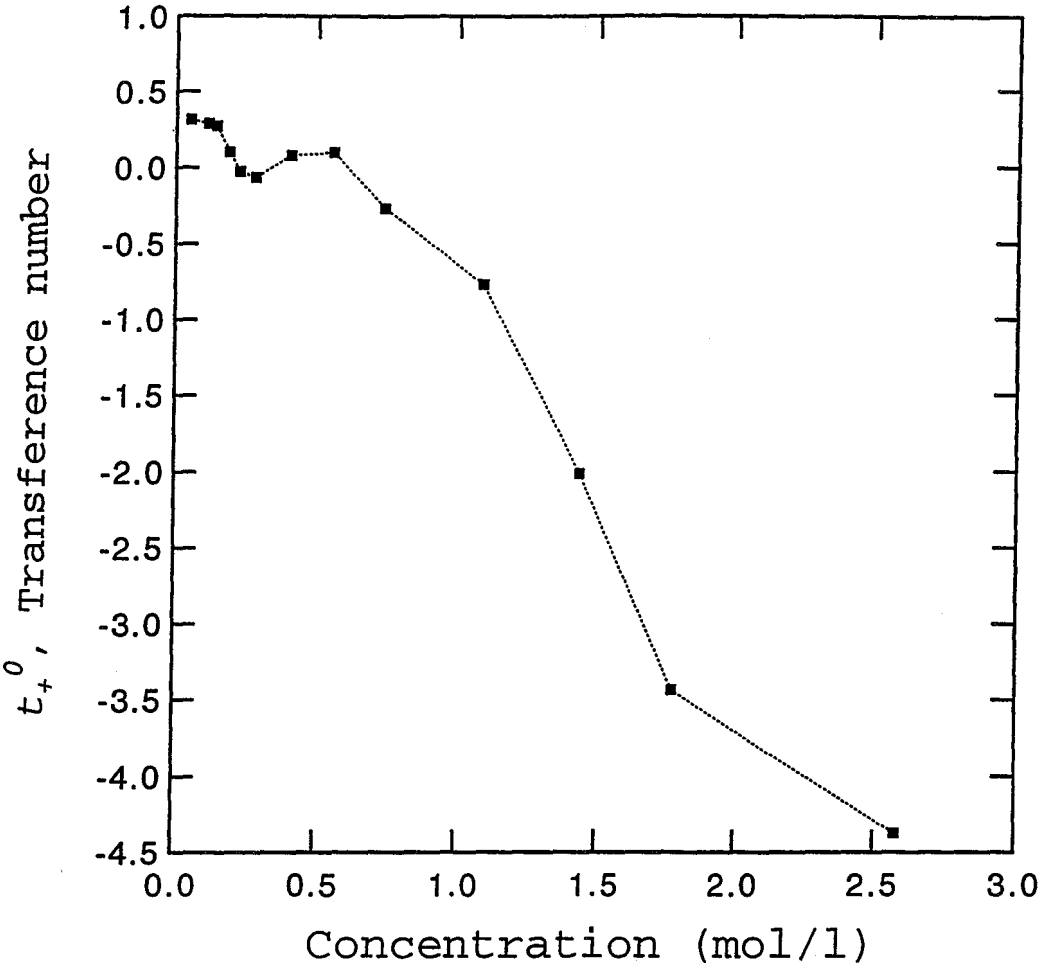


Figure 4-8. Transference number of the sodium ion in $PEO_nNaCF_3SO_3$ solutions at 85°C. The method of measurement is given in the text.

solution (0.05 mol/dm$^3$) to a minimum of -4.4 in the most concentrated (2.58 mol/dm$^3$). The transference number steadily decreases above the concentration of 0.56 mol/dm$^3$ (n=40), where it goes through a local maximum of 0.09, and is negative over a large range of salt concentrations. A negative transference number has been seen for other systems, and has been explained in terms of complexation reactions.[22] These results suggest the formation of mobile triplets consisting of two anions and one cation; however, considering the complexity of the results in figure 4-8, it is unlikely that any simple speciation model would accurately describe this system. We will explore this point in section 4.8.

The practical significance of these results is that large concentration gradients must develop in the polymer electrolyte in order to sustain current flow, a detrimental situation for battery performance. As has been discussed previously,[23] it is still possible for a polymer electrolyte battery with a cationic transference number of zero or even less than zero to operate successfully. However, on discharge this cell will develop large salt concentration gradients; the magnitude of the concentration difference can be estimated from the steady-state value:

$$\Delta c = \frac{I(1 - t_+^0)L}{FD}. \tag{4-30}$$

This may lead to severe diffusion limitations or to salt solubility problems, depending on several factors such as the cell design and other physical properties.[24] Interestingly, if we had a symmetrical cell having electrodes reversible to the anion, the steady-state concentration difference would be

$$\Delta c = -\frac{It_+^0 L}{FD}, \tag{4-31}$$

which actually changes sign when $t_+^0$ goes through zero. A battery that operated using anion-reversible electrodes would be best served by having $t_+^0$ identically zero, rather than less than zero, for then no concentration gradients at all would exist.

With the transference number known, we can use equation 4-14 to calculate the thermodynamic factor, $\left[1 + \frac{d\ln f_{\pm}}{d\ln c}\right]$. This quantity is given in figure 4-9 as a function of the salt concentration. The thermodynamic factor generally decreases with concentration from its dilute value, 0.64 at 0.11 mol/dm$^3$, until starting to level off at very high concentrations at the value of 0.02. The data have a local maximum at n=40, similar to both the transference number and diffusion coefficient data. For the most dilute concentrations, the thermodynamic factor seems to be approaching unity, which is the ideal-solution result. These activity-coefficient results are a verification of the strong nonideality of solid-polymer-electrolyte solutions. Apparently one has to go to much lower concentrations than was done here ($n$>200) to reach an ideal solution. It is easy to show that, with such small values for the thermodynamic factor, making the erroneous assumption that this polymer electrolyte is an ideal solution would lead to large errors in the calculated transference numbers.

We should stress here the sensitivity of these results to the differentiation of the concentration-cell data. This is especially true for the most dilute data points because the slope $\frac{\mathrm{d}U}{\mathrm{d}\ln c}$ is largest in this region. We recommend taking as many data points as possible from the concentration-cell experiments, including points well outside of the range of concentrations being studied, to assure the highest possible accuracy in the calculated transference numbers

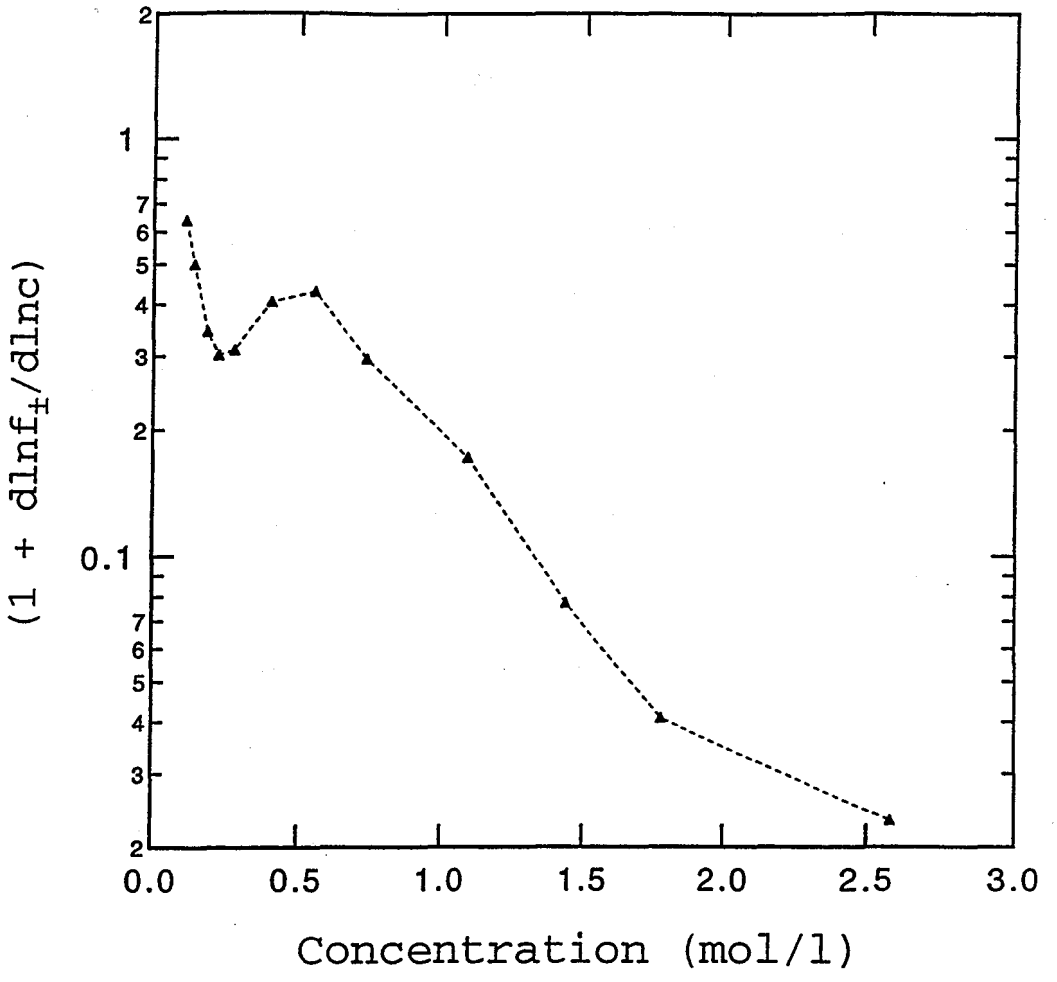


Figure 4-9. Semi-log plot of the thermodynamic factor for $NaCF_3SO_3$ in PEO at 85°C as a function of the salt concentration.

and thermodynamic factor.

### 4.6 Simulation of the galvanostatic polarization experiments

With all necessary properties known, it is possible to use numerical solutions of the governing equations to simulate the experimental method. This can be used to support the validity of the aforementioned assumptions as well as providing more detailed information about the concentration profiles during the experiments. It is especially interesting to examine the time required to reach a limiting current, as well as the effect of using too thin a membrane such that semi-infinite diffusion conditions no longer apply. We would like to avoid either of these situations in practice.

The simulations use the same parameters and cell specifications as in the experimental work, as well as all of the variable physical properties. The following two equations are solved simultaneously:

$$\frac{\partial c}{\partial t} = \nabla\cdot\left[D\nabla c\right] - \frac{c_0\bar{V}_0}{F}\left[\mathbf{i}\cdot\nabla t_+^0\right], \tag{4-32}$$

$$\mathbf{i} = -\kappa\nabla\Phi + \frac{2\kappa RT}{F}\left[1+\frac{d\ln f_\pm}{d\ln c}\right]\left[1-t_+^0\right]\nabla\ln c. \tag{4-33}$$

Equations 4-32 and 4-33 are solved by converting them into finite-difference equations which are subsequently linearized and solved using BAND.[12] We neglect the effect of the fluid motion, generated by the flow of current, on the concentration profiles, as this can be shown to have only a very minor effect.[18,19] Because all of the action is confined to the region near the surface of the electrodes, a savings in computational effort is obtained by using either a variable mesh spacing or scaling the equations (with $x/t^{1/2}$) to recognize this fact. The computer

program for simulation of the galvanostatic polarization experiment, called CHECK, is given in Appendix 4-A.

Starting with one of the more concentrated data points, figure 4-10 gives concentration profiles for the galvanostatic polarization of a $PEO_{12}NaCF_3SO_3$ solution. These profiles are generated by passing a current density of 0.4 $mA/cm^2$ across the 350 μm film for four minutes. Note first that the concentration profiles have not propagated across the full cell; semi-infinite diffusion conditions still apply. The impact of the variable physical properties is quite prominent, leading to steeper profiles at the anode and a quicker propagation rate at the cathode. Both the diffusion coefficient and transference number decrease with concentration steadily over these concentrations. The profiles given in figure 4-10 are equally spaced in time at thirty-second intervals.

We are most interested in comparisons of numerical simulations with the experimental data in the form of $\Delta\Phi$ *versus* $(It_i^{1/2})$ for various bulk salt concentrations. These simulations were carried out for all of the concentrations used in the transference-number experiments; however, we shall discuss only a few of them here. The simulations generally agreed well with the experimental data out to large values of $(It_i^{1/2})$. The worst agreement was seen at the two extreme data points, $n$=500 and $n$=8, which suggests errors in the extrapolation of concentration-cell data.

Figure 4-11 demonstrates the comparison between theoretical simulations and experimental data for the $n$=500 case. Various lines are generated by using the variable physical properties measured previously and different, constant values of the thermodynamic factor. It was difficult to measure the thermodynamic factor for the $n$=500 data point earlier because of its extreme sensitivity to the extrapolation and differentiation of the concentration-cell data. With

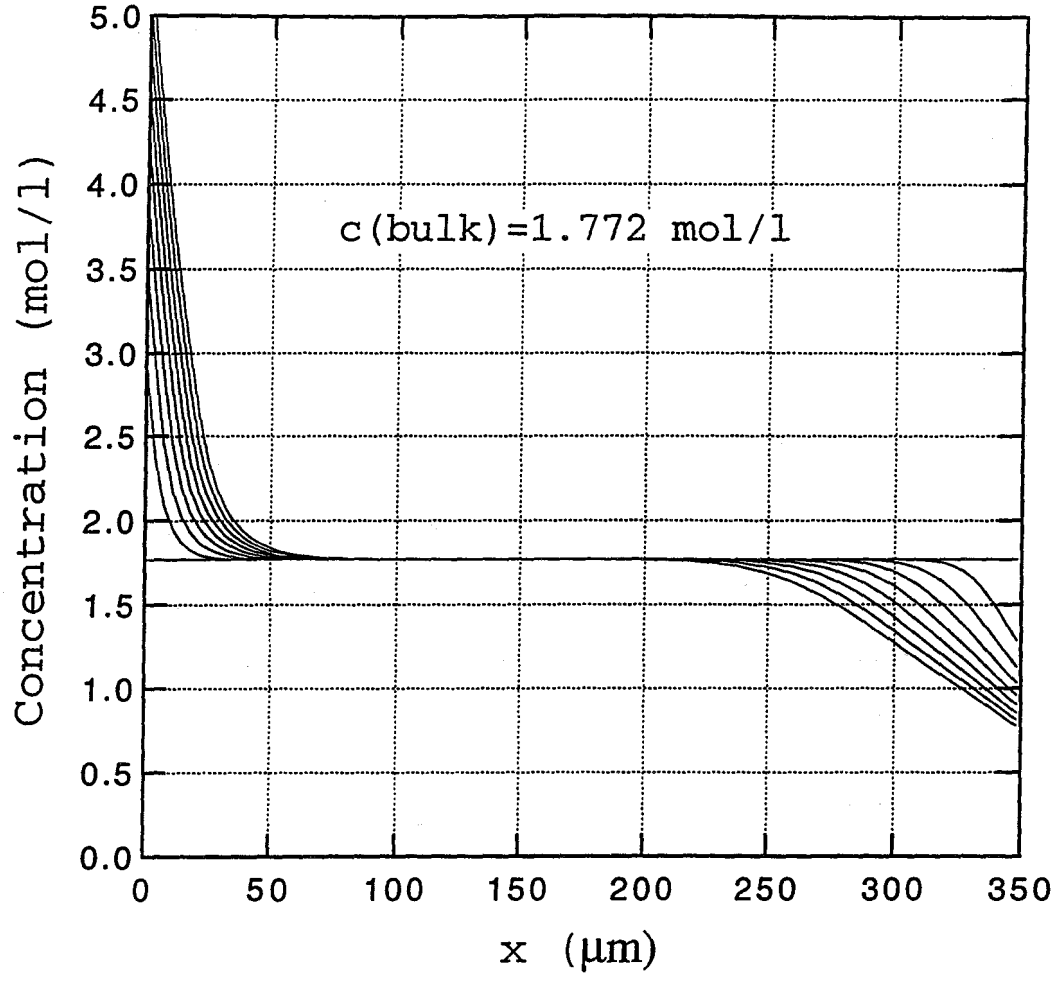


Figure 4-10. Concentration profiles across the cell $Na/PEO_{12}NaCF_3SO_3/Na$ taken at thirty-second intervals during a galvanostatic polarization for four minutes at 85°C. These simulations use the measured variable physical properties.

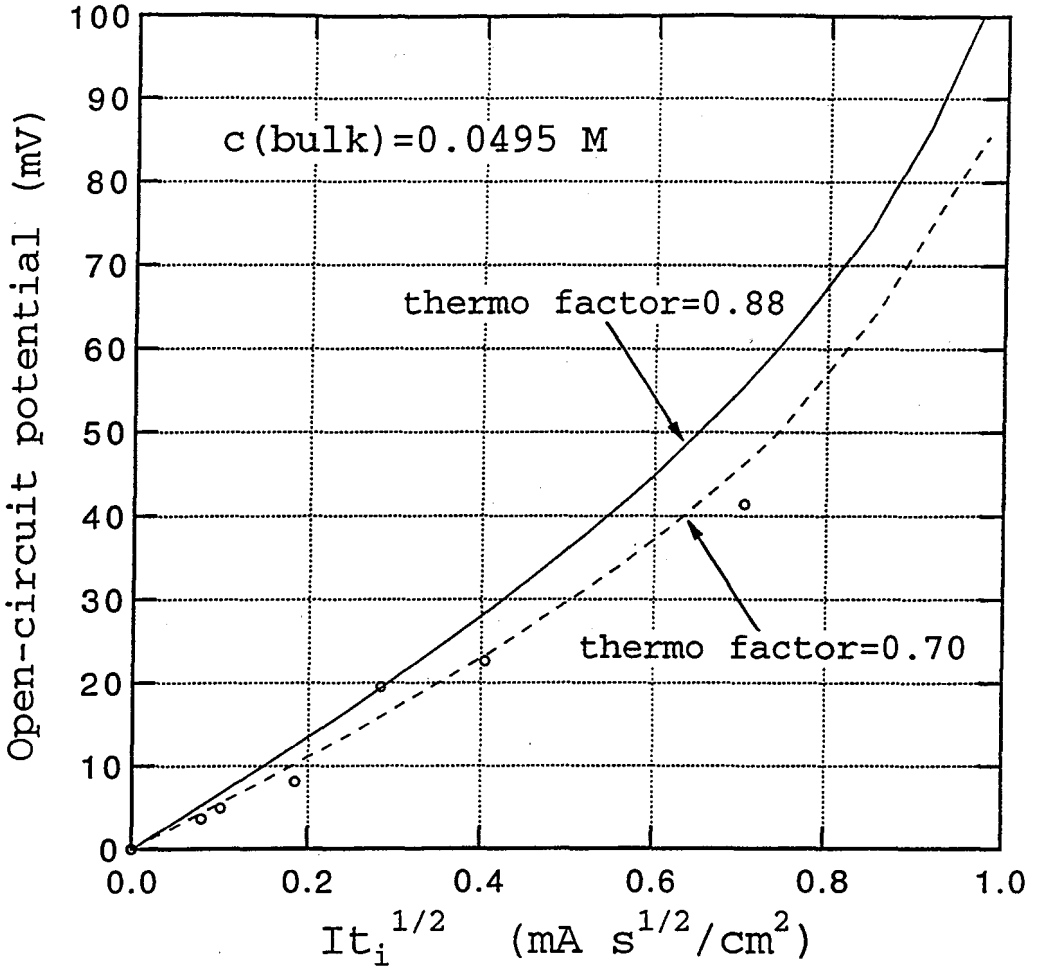


Figure 4-11. Data taken from polarized cells of the form $Na/PEO_{500}NaCF_3SO_3/Na$ at 85°C. The lines are the result of numerical simulations using the measured, variable transport properties but constant values for the thermodynamic factor.

figure 4-11, it is clear that the value of the thermodynamic factor is close to 0.7. Thus, we find that even in the most dilute solution used ($c$=0.049 M), the solid polymer electrolyte is still nonideal.

Agreement between simulation and experiment is excellent for the rest of the dilute data points. For example, figure 4-12 presents the experimental data and simulation results for the $n$=200, $n$=160, and $n$=100 cases. The simulation results generally exhibit the same deviation upwards from linearity on these plots at larger values of $It_i^{1/2}$ as seen in the experimental data. As stated earlier, this effect is caused by the variable physical properties; we will explore this in more detail in section 4.7. This agreement between the experimental data and the numerical simulations, especially at larger values of $It_i^{1/2}$, gives us confidence in our interpretation of the experimental method.

By using the simulations to explore the use of different values of the experimental parameters, it is found that a deviation upwards from linearity on figure 4-12 is not the only possible result. Instead, this will depend on the details of the experimental conditions, in particular the membrane thicknesses being used. For example, once semi-infinite diffusion conditions no longer apply, the potential difference across the cell begins to level off with $It_i^{1/2}$. On the other hand, if a limiting current is reached, then the curve does have a positive deviation from linearity. In our experimental work, we were careful to obey the semi-infinite diffusion conditions, which explains why we generally observed a positive deviation.

The most concentrated solutions are interesting to examine in more detail because large concentration gradients develop in these cells, making the experiments most sensitive to the variable physical properties. Also, as high salt concentrations will usually be used in polymer electrolyte batteries, these cases are most relevant to practical devices. Figures 4-13 and 4-14

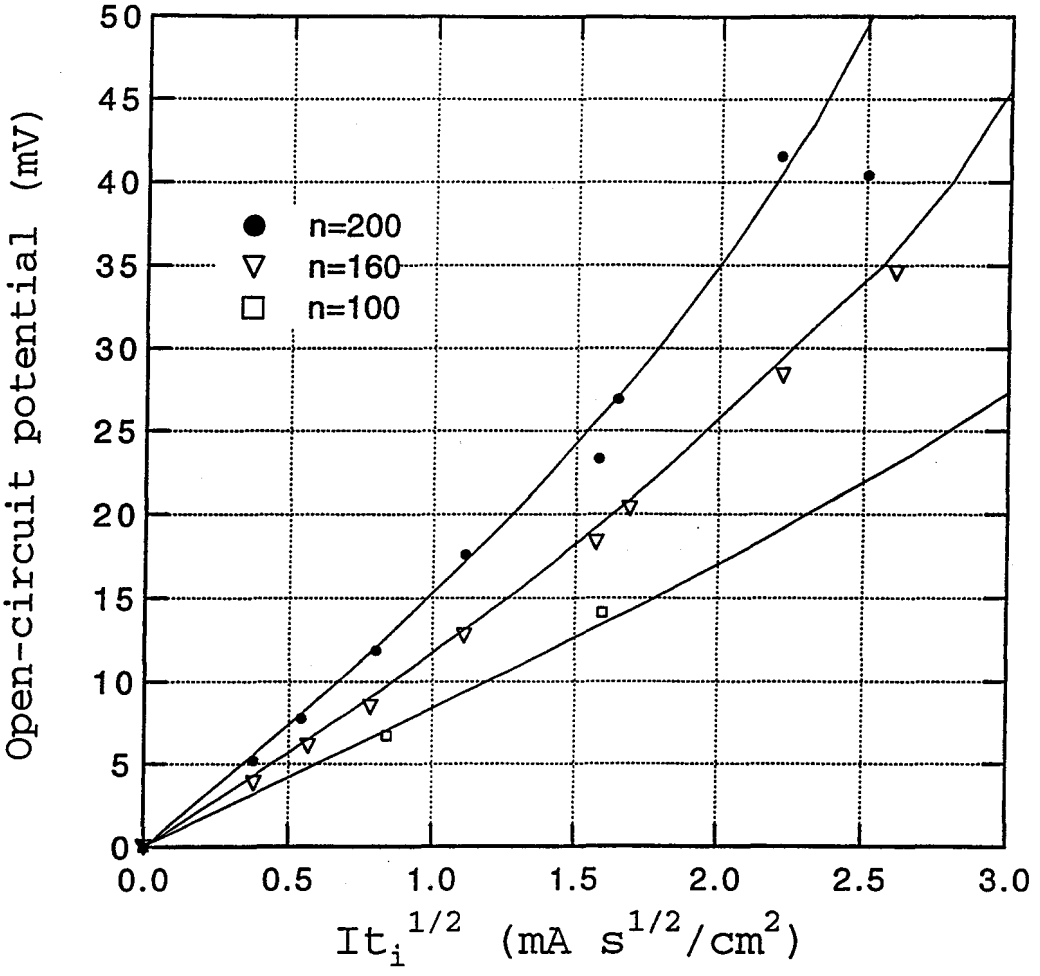


Figure 4-12. Data taken from polarized cells of the form $Na/PEO_nNaCF_3SO_3/Na$ for n=200, n=160, and n=100 at 85°C. The solid lines are the results of numerical simulations using variable physical properties.

give the comparison between experimental data and simulations for the $n$=20 and $n$=12 data points. The solid lines are the simulation results using variable physical properties and the markers are experimental data. The agreement in both figures is quite good, although the simulations in figure 4-14 appear to have a different curvature from the experimental data. Considering the scatter in the data, we cannot say for sure whether this is the result of poor physical property fits. We should point out that the solid line in figure 4-14 is very sensitive to the curve fits used to describe the concentration dependences of the physical properties. It is difficult to develop a single function that describes accurately the concentration-dependence of $t_+^0$ or $\left[1 + \frac{\partial \ln f_\pm}{\partial \ln c}\right]$ over the whole range of salt concentrations.

The $n$=8 data, given as figure 4-15, is even more difficult to explain with the numerical simulations. Here again we have problems with the curve fits for the transport properties; however, this problem becomes more serious now because the cell is accessing concentrations well outside the range of the experimental data. Even for relatively small values of ($It_i^{1/2}$) of around 4 to 5, concentrations of over five molar are reached on the anodic side. Because we do not know how the physical properties vary above 2.58 M, we assume that they are constant and equal to their initial values at $c$=2.58 M. The solid line on figure 4-15 is the simulation result using variable physical properties over the range that they have been measured and constant properties above $c$=2.58 M. This curve appears to be too low, which could indicate that a minor increase in the thermodynamic factor at the higher salt concentrations is needed.

The simulations can also provide the values of the wall concentrations as a function of $It_i^{1/2}$ during the experiments. For example, figure 4-16 gives the concentration adjacent to either electrode for the $n$=160 solution as a function of the experimental parameter. The solid line is

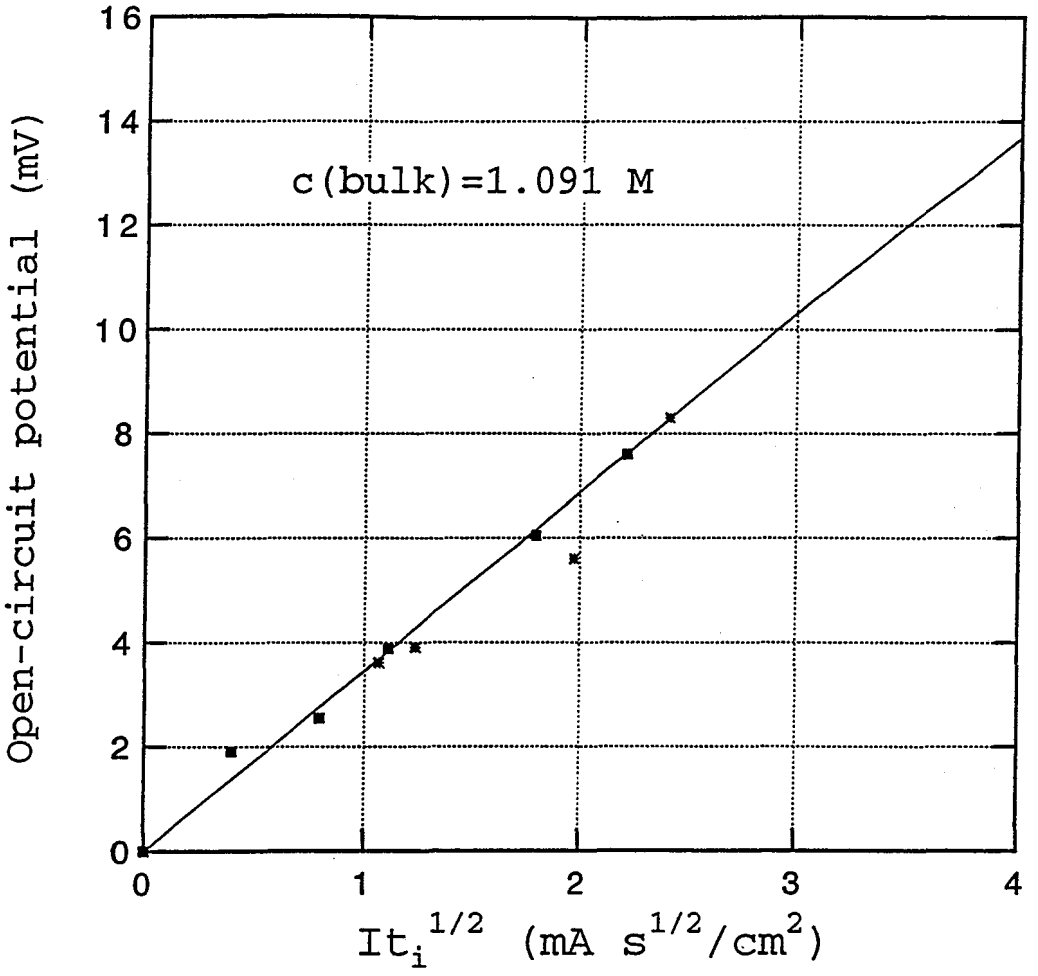


Figure 4-13. Data taken from polarized cells of the form $Na/PEO_{20}NaCF_3SO_3/Na$ at 85°C. The solid line is the result of numerical simulations using variable physical properties.

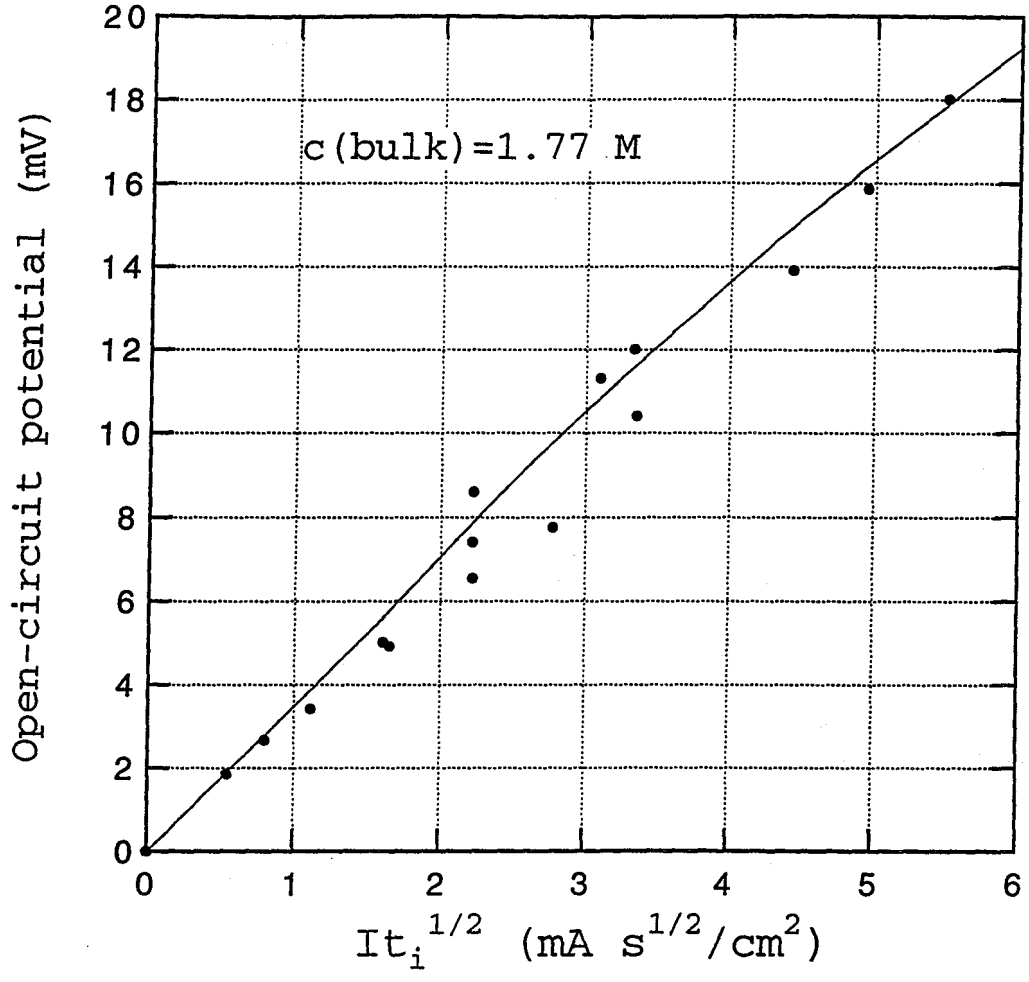


Figure 4-14. Data taken from polarized cells of the form $Na/PEO_{12}NaCF_3SO_3/Na$ at 85°C. The solid line is the result of numerical simulations using variable physical properties.

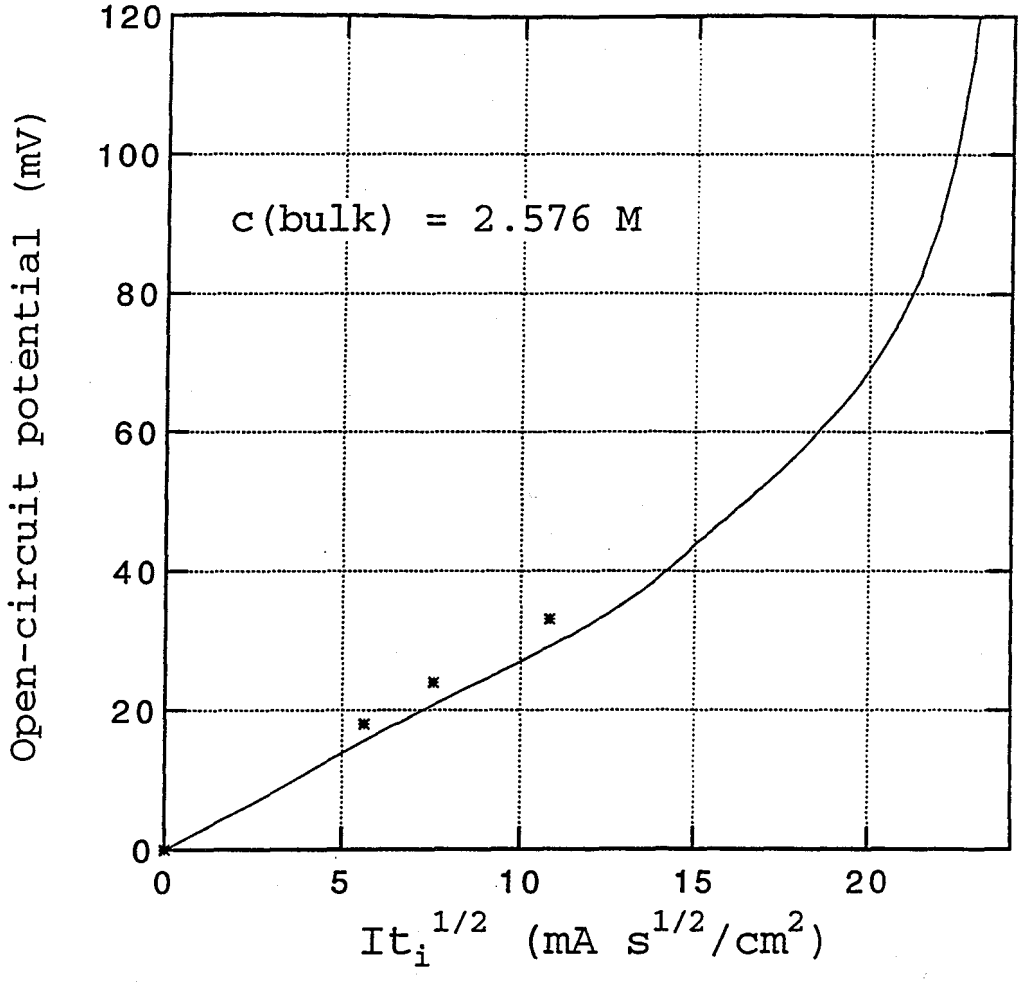


Figure 4-15. Data taken from polarized cells of the form $Na/PEO_8NaCF_3SO_3/Na$ at 85°C. The solid line is the result of numerical simulations using variable physical properties when below 2.58 M and constant physical properties above this concentration.

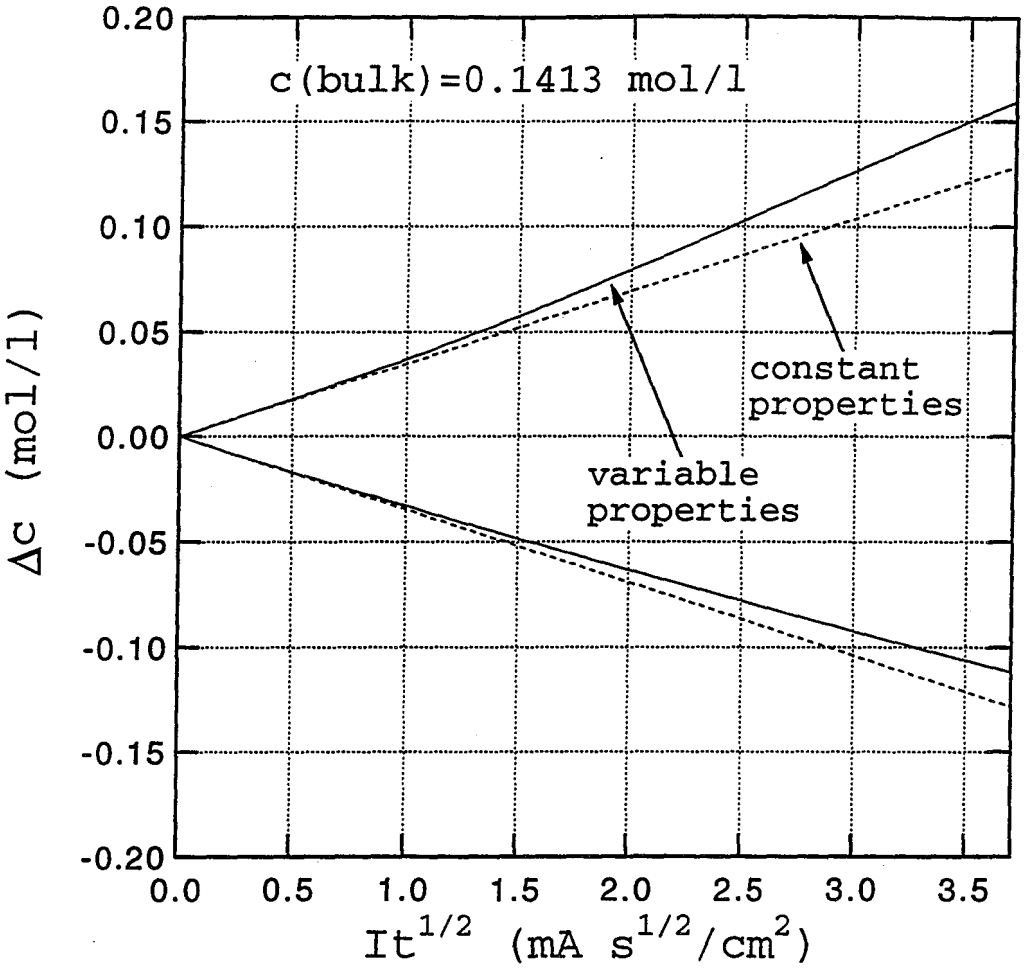


Figure 4-16. Concentration difference between either electrode and the bulk for a cell of the form $Na/PEO_{160}NaCF_3SO_3/Na$ at 85°C. The solid line is the theoretical prediction for the experiments using the measured, variable physical properties.

the variable physical property result, and the dashed line assumes constant physical properties. The concentration change which the current induces on either side of the cell is not symmetric, in constrast to the prediction from dilute-solution theory. Instead, on figure 4-16 we find that a larger concentration change occurs at the anode than at the cathode. This effect will be explained in the analysis of section 4.7. The use of too large a value of $It_i^{1/2}$ can lead to a limiting current at the cathode. This is the main consideration for the more dilute data points.

In figure 4-17 we give the concentrations at each electrode for the $n$=12 case. Figure 4-17, for $n$=12, is similar to figure 4-10, which gave full-cell concentration profiles during a galvanostatic polarization. Here we see much larger concentration changes occurring at either electrode during the passage of current than with the $n$=160 case. For figure 4-17, even at the relatively small values of $It_i^{1/2}$ of one to two, we find that concentration differences approaching one molar exist across the cell. At larger values of $It_i^{1/2}$, the concentration changes vary in a complicated manner due to the variable physical properties. We should note that the anodic curve for $n$=12 becomes linear above a concentration of about 2.8 M because the physical properties have been taken to be constant above this value. For the more concentrated solutions such as these, it is more likely that one would exceed the salt solubility limit at the anode than reach a limiting current at the cathode. Predicting this fact without a numerical solution of the governing equations that includes the effect of variable transport properties would be very difficult. The choice of proper polarization times in the more concentrated solutions is thus not a trivial matter as one must avoid both exceeding the salt solubility limit and reaching the limiting current.

This last point may be particularly important for batteries using $PEO_nNaCF_3SO_3$, as the value of $n$ is likely to be at least 8. For example, when the following cell:

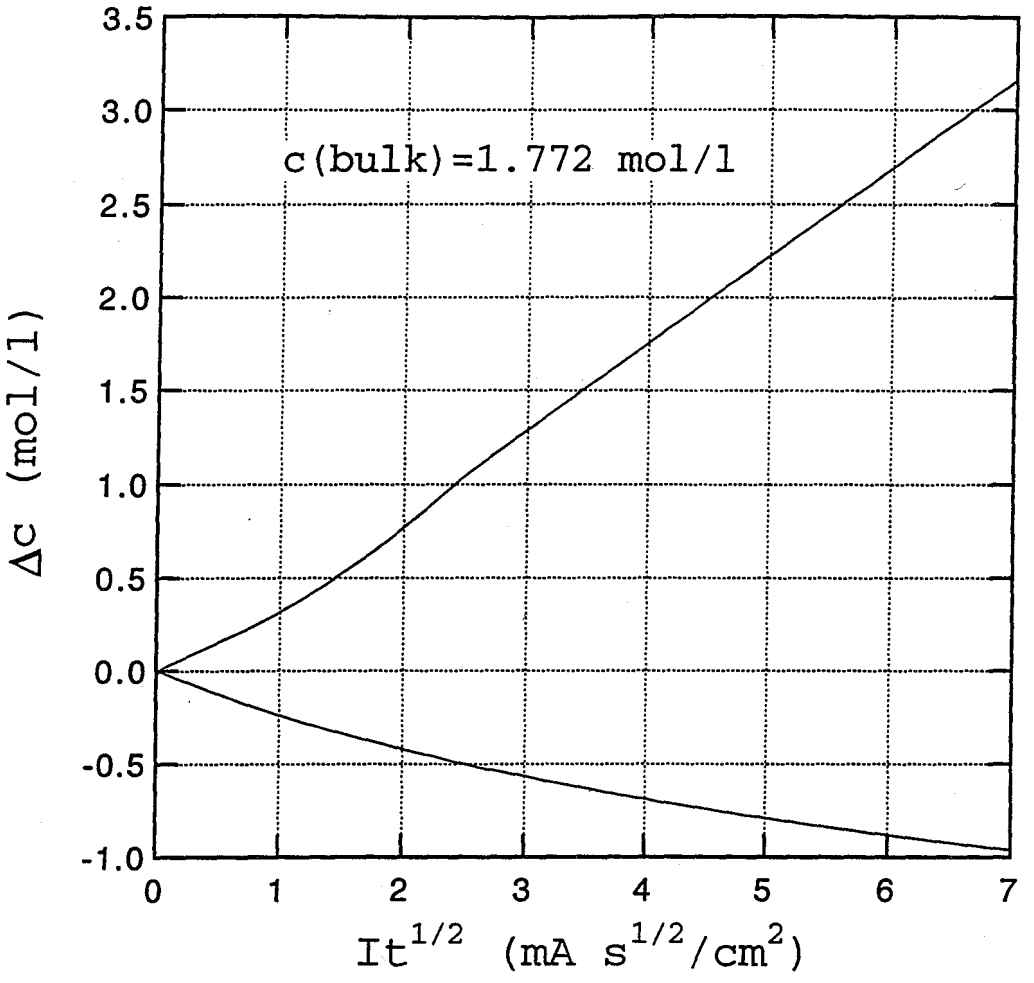


Figure 4-17. Concentration difference between either electrode and the bulk for a cell of the form $Na/PEO_{12}NaCF_3SO_3/Na$ at 85°C. This is the theoretical prediction for the polarization experiments using the measured physical properties.

$$Na|PEO_8NaCF_3SO_3|Na_{0.7}CoO_2$$

is discharged at increasing rates, one finds the discharge curves given in figure 4-18a.[25] Based on the above findings, as well as simulation results for the full battery that will not be discussed here, it is believed that the rate capability of this cell is limited by salt precipitation processes on the sodium foil electrode during discharge. Some evidence for this is found by comparison with discharge curves for the cell:

$$Na|PEO_{20}NaCF_3SO_3|Na_{0.7}CoO_2$$

which are given in figure 4-18b. This cell has a lower initial salt concentration, yet still attains a higher fraction of the available capacity at the higher discharge rates. This is simply due to the delay of the onset of salt precipitation brought about by using a lower initial salt concentration with better initial transport properties. With known values of the transport properties, one could use these data along will a battery modeling program to determine the optimum initial salt concentration to use in the cell.

To study the salt precipitation process in more detail, we constructed cells of the form: $Na|PEO_8NaCF_3SO_3|Na$. These were discharged at constant rate while monitoring the potential difference across the cell. When the potential difference changes abruptly, we assume that either salt precipitation or a limiting current has been reached; the time for this to happen is referred to as the transition time. Given the experimental conditions, primarily thickness of PEO film and current density, we can use the computer program CHECK to simulate these transition-time experiments just as was done with the galvanostatic polarization experiment.

Data for several experiments are compared in figure 4-19. Each experiment is followed by an extended rest period (≈2 hr) during which the cell potential and concentration profiles are

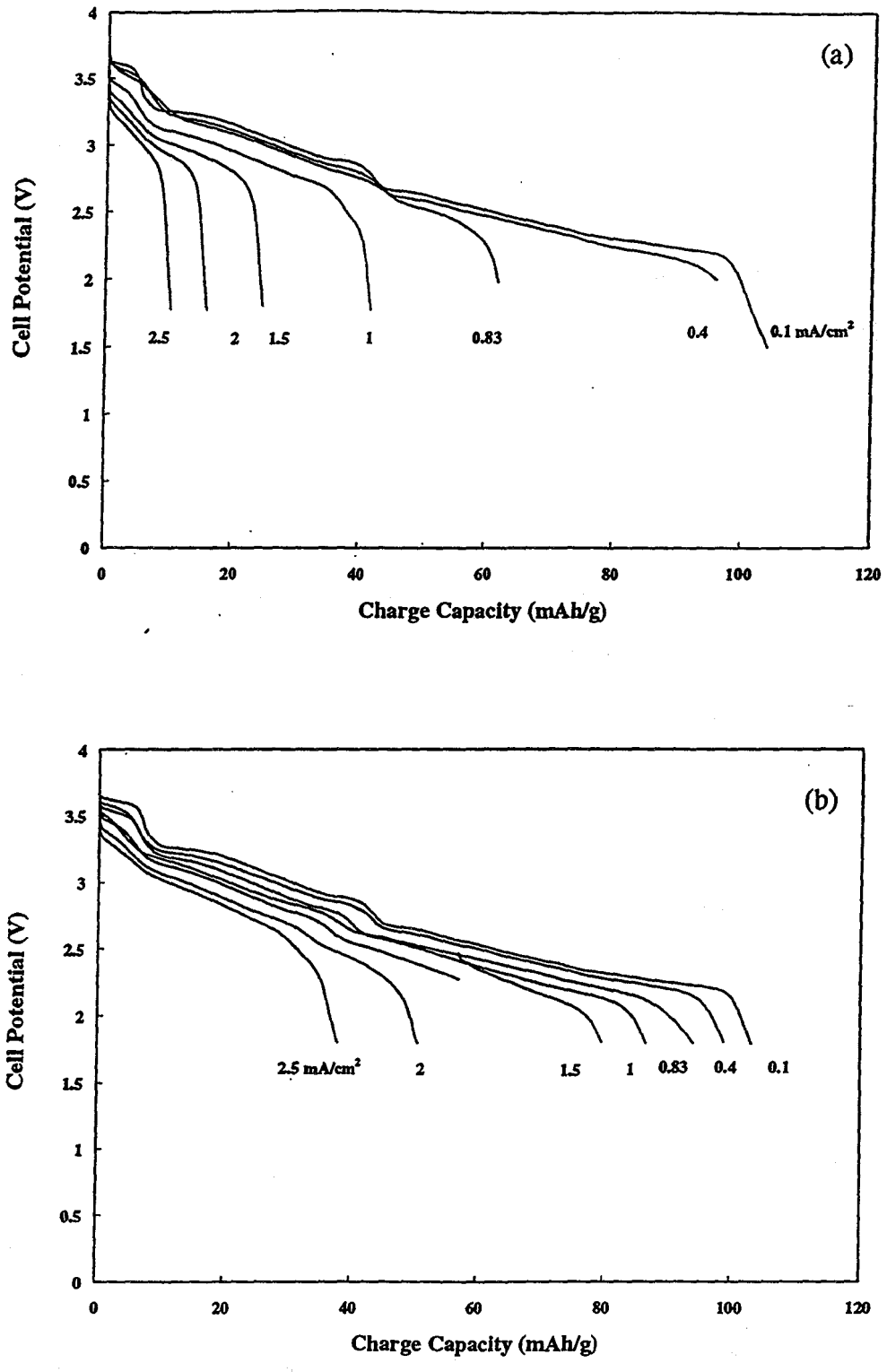


Figure 4-18. Discharge curves for $Na/PEO_nNaCF_3SO_3/Na_xCoO_2$, where (a) n = 8, and (b) n = 20.

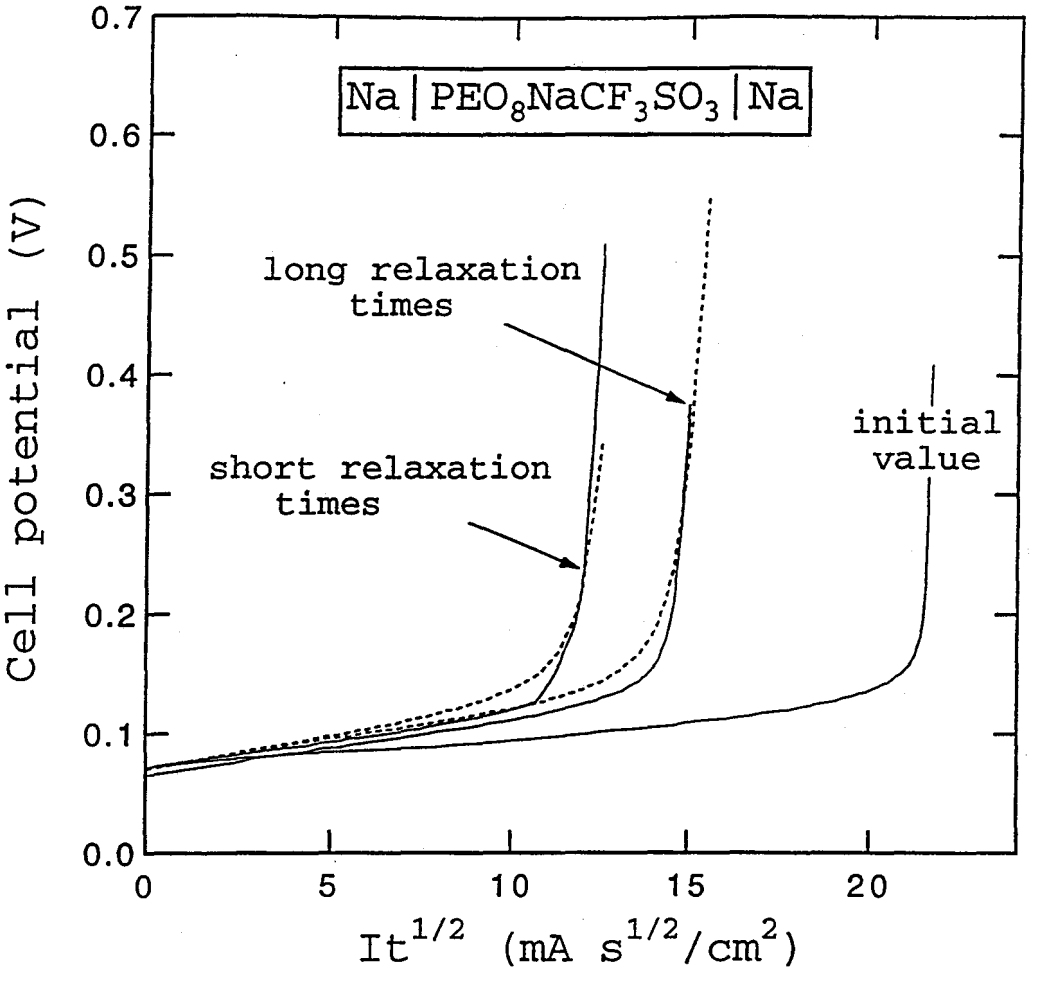


Figure 4-19. Transition-time experiments for the system: $Na/PEO_8NaCF_3SO_3/Na$ at 85°C. The same current density was used in each of the experiments. The resulting transition time depends on the amount of time between successive experiments.

allowed to relax back to their initial values. For repeated experiments using the same current density ($I$=0.55 mA/cm$^2$), the transition time varies as a function of relaxation time. This indicates an effect of the previous history, probably the initial salt precipitation process. To describe properly cell behavior, in particular the failure at high rates for the cells described earlier, one would need to study the kinetics of the salt precipitation/dissolution process in more detail. For now, we can use the results given in figure 4-15 to interpret the salt preciption phenomenon. By comparing the transition times (in units of $It_i^{1/2}$) with the wall concentrations, we can identify roughly the values of the supersaturation concentration of the salt. As earlier, we must assume that the transport properties are constant and at their bulk values for salt concentrations above 2.58 M. Also, we need to check that the violation of the thick-cell assumption does not invalidate the use of figure 4-15.

The first transition time in figure 4-19, using a fresh cell, occurs at $It_i^{1/2}$=21.4 mA·s$^{1/2}$/cm$^2$. According to the simulations, this equates to wall concentrations of about 0.10 M and 12.80 M at the cathode and anode, respectively. This large anode concentration is staggering, as one would initially expect the largest salt concentration the poly(ethylene oxide) could support would be that of the polymer/salt crystalline complex $PEO_3NaCF_3SO_3$, corresponding to $c$=5.94 M (we should note that the exact stoichiometry of this complex for $NaCF_3SO_3$ has not been identified, but a three to one ratio is seen with many other lithium and sodium salts in PEO). However, we need to stress that the values of physical properties at the higher salt concentrations are not known, and much error may have resulted from our extrapolation of the values at $c$=2.58 M. The cathode concentration is nearly zero at this large value of ($It_i^{1/2}$); considering experimental error, we cannot completely discount the possibility that the initial limiting current results from driving the salt concentration to zero at the cathode. Later experiments

of this type should incorporate a reference electrode which could be used to separate changes in the potential at either electrode. Detailed computer simulations of this transition-time experiment show that the concentration profiles have sufficient time to develop across the full separator.

Later transitions in figure 4-19 occur at shorter times, the smallest being around $It_i^{1/2}$=11.0. That the transition time eventually converges on a steady value is easiest to see in figure 4-20. Here we have carried out successive transition-time experiments allowing only sufficient time for concentration profiles to relax before repeating the experiment ($L^2/D$≈1 hr). We assume that this should most closely resemble a true transition time as the effect of salt dissolution kinetics should be minimized. From the results given in figure 4-20, we find that the transition time is approaching the value $It_i^{1/2}$=10.5. Simulations show that this corresponds to wall concentrations of 0.70 and 7.83 M. This anode concentration is still larger than the value of 5.94 M that we earlier rationalized as a possible maximum, but is now significantly less than the initial "fresh" cell value. As the cathode concentration in this experiment is no longer nearly zero, we are more confident that it is indeed a salt precipitation process and not a true limiting current that we are experiencing. Again, in order to model properly any battery that made use of a concentrated $PEO_nNaCF_3SO_3$ electrolyte, one would need to explore the kinetics of the salt precipitation/dissolution process in more detail than was done here.

### 4.7 Effect of variable physical properties on the galvanostatic polarization experiments

An interesting limiting case of equation 4-8 that has the advantage of allowing an analytic solution is that of a constant diffusion coefficient and a linear variation of transference number with concentration. Considering the experimental data, for which the transference number was found to decrease strongly with concentration, this is a reasonable approximation. We will

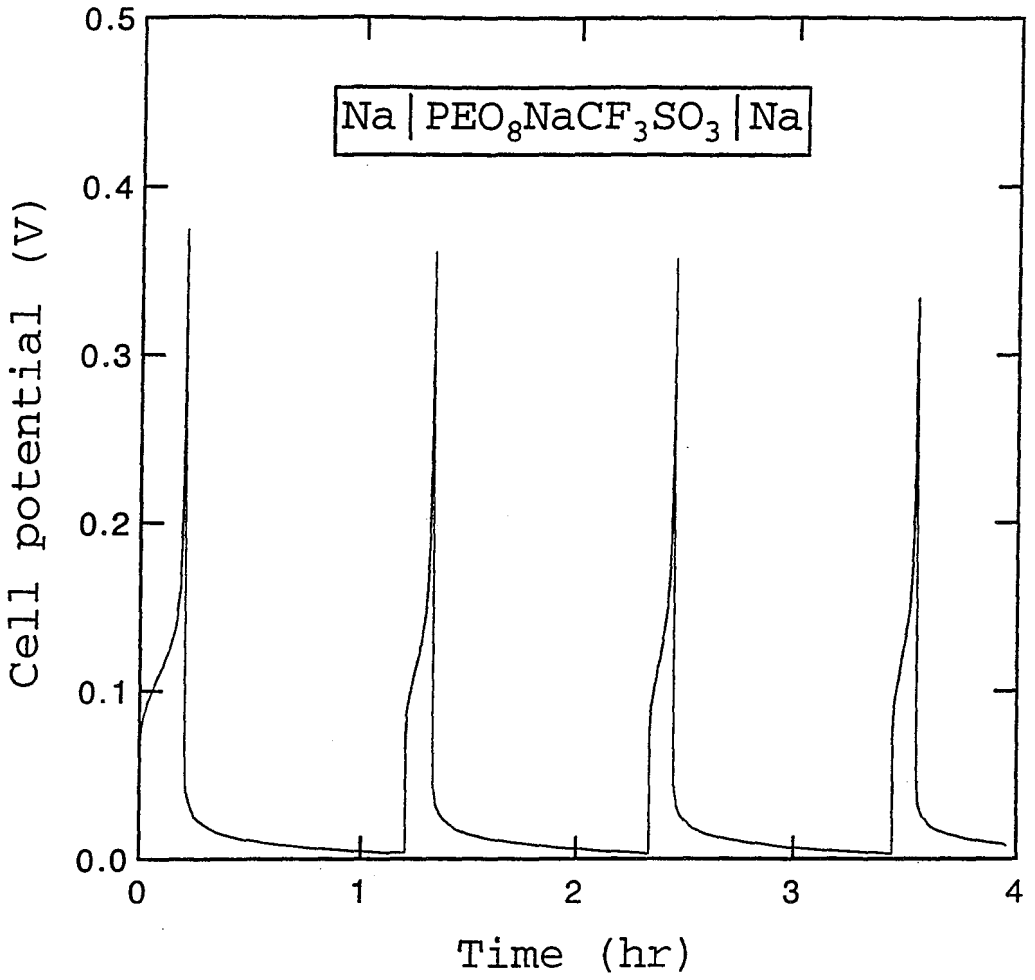


Figure 4-20. Transition-time experiments for the system $Na/PEO_8NaCF_3SO_3/Na$ at 85°C. Constant-current discharges are performed on the same cell until a transition time is reached, each followed by a one-hour relaxation period.

consider equation 4-8 in one-dimension, for this simplified case we have

$$\frac{\partial c}{\partial t} = D\frac{\partial^2 c}{\partial x^2} - \frac{I}{nF}\frac{dt_+^0}{dc}\frac{\partial c}{\partial x}. \tag{4-34}$$

We have also assumed here that convective flows due to the passage of current can be neglected. For a transference number that varies linearly with concentration, it is valid to expand the transference number at the wall in terms of its bulk value, so that the boundary condition at the wall is

$$\frac{\partial c}{\partial x}(x=0) = -\frac{I}{FD}\left[t_-^0(c_\infty) - \frac{dt_+^0}{dc}(c-c_\infty)\right]. \tag{4-35}$$

For this example, it is best not to use the similarity variable transformation because we would like to solve an equation with constant coefficients. We also use different definitions for the dimensionless time and concentration. These variables become, respectively,

$$t_* = \frac{(t_-^0(c_\infty))^2 I^2 t}{DF^2 c_\infty^2}, \tag{4-36}$$

and

$$\theta = \frac{c-c_\infty}{c_\infty}. \tag{4-37}$$

Substitution into the governing equation gives

$$\frac{\partial \theta}{\partial t_*} = \frac{D^2F^2c_\infty^2}{(t_-^0(c_\infty))^2 I^2}\frac{\partial^2\theta}{\partial x^2} - \frac{DFc_\infty^2}{(t_-^0(c_\infty))^2 I}\frac{dt_+^0}{dc}\frac{\partial\theta}{\partial x}. \tag{4-38}$$

The boundary condition is then

$$\frac{\partial\theta}{\partial x}(t_*, x=0) = -\frac{It_-^0(c_\infty)}{FDc_\infty} + \frac{I}{FD}\frac{dt_+^0}{dc}\theta . \tag{4-39}$$

With a dimensionless distance defined as

$$Z = \frac{It_-^0}{FDc_\infty}x , \tag{4-40}$$

the differential equation 4-38 becomes

$$\frac{\partial\theta}{\partial t_*} = \frac{\partial^2\theta}{\partial Z^2} - A\frac{\partial\theta}{\partial Z} , \tag{4-41}$$

with the boundary conditions

$$\theta(t_*, Z=\infty) = 0 \quad \text{and} \quad \theta(t_*=0, Z) = 0 , \tag{4-42}$$

$$\text{and} \quad \frac{\partial\theta}{\partial Z}(t_*, Z=0) = -1 + A\theta . \tag{4-43}$$

Above, we have defined for convenience the quantity

$$A = \frac{c_\infty}{t_-^0(c_\infty)}\frac{dt_+^0}{dc} . \tag{4-44}$$

The Laplace transform of this equation has the following solution,

$$\bar{\theta} = \frac{1}{s(A + r)}\exp(-rZ) , \tag{4-45}$$

with

$$r = \frac{2s}{A + (A^2 + 4s)^{1/2}}. \tag{4-46}$$

Since we are interested in the behavior of θ at the surface ($Z$=0), we evaluate equation 4-45 at $Z$=0 and expand for short times (or large values of $s$)

$$\bar{\theta}(Z=0) = \frac{1}{s^{3/2}} - \frac{A}{2s^2} + \frac{A^2}{2^3 s^{5/2}} + \frac{A^4}{2^7 s^{7/2}} + O(s^{-9/2}). \tag{4-47}$$

Inversion of this equation gives

$$\theta(Z=0) = 2\left[\frac{t_*}{\pi}\right]^{1/2} - \frac{At_*}{2} + \frac{A^2 t_*^{3/2}}{6\pi^{1/2}} + O(t_*^2). \tag{4-48}$$

One can obtain the concentration difference across the cell once equation 4-48 is expressed in terms of the original parameters. The concentration difference after a constant-current polarization is

$$\Delta c = \frac{2t_-^0}{FD^{1/2}} (It_t^{1/2}) \left[\frac{1}{\pi^{1/2}} - \frac{\zeta}{8} + \frac{\zeta^2}{12\pi^{1/2}} + O(\zeta^4)\right], \tag{4-49}$$

where the perturbation parameter ζ is

$$\zeta = \frac{2At_-^0}{FD^{1/2}c_\infty} (It_t^{1/2}). \tag{4-50}$$

The parameter ζ is proportional to the slope of figure 4-8, as can be seen by examining the definition of $A$ given in equation 4-44. One can show that $\zeta < 0.1$ over the range of concentrations covered in this work. The asymmetry seen in $\Delta c$ between either electrode and the bulk solution is evident in equation 4-49. This same result was seen previously from the full numeri-

cal solution discussed in connection with figure 4-16. Equation 4-49 shows that a larger salt concentration difference will develop at the anode than at the cathode if the transference number decreases with concentration; this is just the result seen in figure 4-16.

Equation 4-49 leads to the following potential difference across the cell,

$$\Delta\Phi = \frac{4t_-^0}{c_\infty F D^{1/2}} \left[\frac{dU}{d\ln c}\right] (It_i^{1/2}) \left[\frac{1}{\pi^{1/2}} + \frac{\zeta^2}{12\pi^{1/2}} + O(\zeta^4)\right] . \qquad (4\text{-}51)$$

Notice that the first correction term in equation 4-51 is of $O(\zeta^2)$ because the terms of $O(\zeta)$ from either side of the cell in equation 4-51 cancel one another, a fortuitous situation. (We earlier observed that figure 4-6 must be odd in $It_i^{1/2}$.) This also implies that a variable transference number will lead to a positive deviation from linearity on plots of the form of figure 4-6 no matter which way the transference number varies with salt concentration. Equation 4-51 allows one to simulate the polarization experiment up to larger values of $(It_i^{1/2})$ where the linear dependence of $\Delta\Phi$ on $(It_i^{1/2})$ no longer holds. However, with the small values of $\zeta$ generally used in the present experiments, we confirm that linear behavior should always be observed near the origin. Of course, at larger values of $(It_i^{1/2})$ it is possible to see the curvature effects evident in equation 4-51.

### 4.8 Microscopic speciation models

It is useful to discuss the issue of speciation in more detail in order to elucidate some of the effects of ion-ion interactions on the macroscopic transport parameters. Consider, for example, a case where the three independent species in solution are assumed to be $Na^+$, $Na(CF_3SO_3)_2^-$, and the polymer. We wish to determine how the macroscopic transference number which is measured in practice reflects this microscopic distribution of species. If we

refer to the sodium cation as species 1 and the sodium ditriflate anion as species 2, the fluxes of each species in the absence of concentration gradients are

$$N_1^* = -u_1 F c_1^* \nabla \Phi , \tag{4-52}$$

$$N_2^* = u_2 F c_2^* \nabla \Phi , \tag{4-53}$$

where the superscript * denotes the actual species in solution. We take $\nabla c = 0$ because $t_+^0$ is defined in the absence of concentration gradients. It is assumed that the mobilities of the true species in solution, given by $u_1$ and $u_2$, would be less concentration dependent than the macroscopic transport parameters.

As any practical experiment or device will be able to determine only the net amount of sodium transported across the cell, we can write the apparent fluxes as

$$N_{Na^+} = N_1^* + N_2^* , \tag{4-54}$$

$$N_{CF_3SO_3^-} = 2N_2^* . \tag{4-55}$$

The current flow in solution is

$$i = F(N_1^* - N_2^*) . \tag{4-56}$$

This allows us to calculate the experimentally accessible transference number as

$$t_{Na^+}^0 = \frac{F N_{Na^+}}{i} = \frac{u_1 - u_2}{u_1 + u_2} , \tag{4-57}$$

where we also made use here of the electroneutrality condition. From this we find that even this simple model is able to justify a negative value for the measurable transference number

when $u_2 > u_1$, *i.e.*, when mobile negative triplet ions exist. Also, one should note that the existence of ion pairs does not affect the value of the macroscopic transference number because the transference number is defined in the absence of concentration gradients. Even if we had allowed an equilibrium to exist among the above species and a neutral ion pair, we would have found the same result for equation 4-57.

If we wish to explore more complicated models of the microscopic speciation, we must include equilibrium constants for the various ion-exchange processes. For example, consider the case when there are the following species in solution: $Na^+$, $CF_3SO_3^-$, $Na(CF_3SO_3)_i^{(i-1)-}$, and the polymer, where $i$ runs from 1 to $n$. We will hereafter refer to these species with the subscripts 1 through $N$ ($N$=$n$+3), where 1 is the sodium ion, 2 the triflate ion, *etc.*, and species $N$ is the polymer. As we have ($n$+3) species but only 3 of these are independent, we can write $n$ expressions of reaction equilibrium of the form

$$K_i = \frac{c_i}{c_1 c_2^{(i-2)}}, \text{ where } i=3, ..., (N-1). \tag{4-58}$$

From electroneutrality,

$$c_1 = c_2 + c_4 + 2c_5 + \cdots + (N-4)\, c_{(N-1)}. \tag{4-59}$$

Combination of this with the $n$ equilibrium expressions gives

$$c_1 = \frac{c_2}{1 - K_4 c_2^2 - K_5 c_2^3 - \cdots - K_{(N-1)} c_2^{(N-3)}}. \tag{4-60}$$

Following the same procedure outlined above, we write an expression for the apparent flux of sodium in terms of the actual flux of each species

$$N_{Na^+} = N_1^* + N_4^* + N_5^* + \cdots + N_{(N-1)}^* \,. \tag{4-61}$$

The total current flow is

$$i = F\ (N_1^* - N_2^* - N_4^* - 2N_5^* - \cdots - (N-4)N_{(N-1)}^*)\,. \tag{4-62}$$

For simplicity, we define the following quantities,

$$A = u_1 - u_4K_4c_2^2 - 2u_5K_5c_2^3 - \cdots - (N-4)u_{(N-1)}K_{(N-1)}c_2^{(N-3)}\,, \tag{4-63}$$

$$B = u_1 + u_4K_4c_2^2 + 4u_5K_5c_2^3 + \cdots + (N-4)^2u_{(N-1)}K_{(N-1)}c_2^{(N-3)}\,, \tag{4-64}$$

$$C = 1 - K_4c_2^2 - K_5c_2^3 - \cdots - K_{(N-1)}c_2^{(N-3)}\,. \tag{4-65}$$

Thus, the transference number can be expressed as

$$t_+^0 = \frac{A}{B + u_1C}\,. \tag{4-66}$$

An expression of this sort could theoretically be used to describe the concentration dependence of the macroscopic transference number in terms of the presumed constant mobilities of the individual species and their equilibrium relationships. However, as these mobilities and equilibrium constants are unlikely to be available, we simply use this expression to explore the possible values of $t_+^0$. One can show that equation 4-66 will provide negative values of $t_+^0$ under certain conditions, although it will never give a value smaller than negative one.

A model of speciation that could provide transference numbers with arbitrarily large negative values would include species of the form: $Na^+$, $CF_3SO_3^-$, $Na_i(CF_3SO_3)_{(i+1)}^-$, and the polymer, where $i$ runs from 1 to $n$. The advantage of this model, as far as explaining values of $t_+^0 < -1$, is that the negative species carry many more sodium ions than current because they

are all univalent. However, considering the infinite number of combinations of species that may exist in solution and the lack of quantitative data on these species, we should not suggest that the above considerations are evidence of the existence of specific species. Again, we must emphasize that the transport processes in solution are described completely by the three macroscopic, concentration-dependent transport properties, and any further studies surrounding speciation are extraneous. If one's only purpose is to model the performance of an electrochemical device that utilizes a solid polymer electrolyte, the information contained in the three transport properties is sufficient.

We shall conclude this section by saying a few more words about the issue of microscopic speciation and its effect on the macroscopic transport properties. It is certainly true that the presence of species other than the stoichiometric ones will have an effect on the measured transport properties. This was demonstrated above using simple theoretical transport models. However, it is not necessary to be aware of the exact microscopic species that exist in solution in order to measure the macroscopic transport properties. This is a fundamental tenet of macroscopic physical theories that arises frequently in thermodynamics, and is also relevant in transport phenomena. Mobilities of the microscopic species, while interesting from a theoretical perspective and possibly accessible by spectroscopic means, are not measurable using macroscopic experiments involving current, voltage, and salt concentration. It is just those combinations of microscopic information defined as the transference number, ionic conductivity, and salt diffusion coefficient that are experimentally accessible by macroscopic methods.

## 4.9 Simulation of the potentiostatic polarization experiment

A significant amount of effort has been put into the development of a method to measure $t_+^0$ in solid polymer electrolytes using the potentiostatic polarization of a symmetric cell.[26-33] This method has now been used by several researchers to evaluate and compare transport processes in various polymer electrolytes.[34-39] Although it was understood from the beginning that this method is valid only for an ideal, dilute solution,[28] the implications of this fact on the measurements have been rarely mentioned.[33] Instead, much discussion of the impact of microscopic speciation on the measurements, especially the existence of ion pairs, has been published.[36,37] In fact, as mentioned earlier, issues surrounding speciation should not affect the measurement of the macroscopic transference number, while assumptions of solution ideality when analyzing experimental results may have drastic consequences. In this section, we will analyze the potentiostatic polarization experiment under the framework of concentrated solution theory in order to identify the transport property information that is accessible. In particular, we should like to elucidate the impact of solution nonideality on the experimental method.

The potentiostaic polarization, or "steady-state current," method of measuring $t_+^0$ uses the standard cell of the form: Li|$PEO_n$LiX|Li. A small, constant potential difference is applied between the two lithium electrodes, and the current that flows initially and at the steady state is recorded. This experiment is demonstrated for the Na|$PEO_8NaCF_3SO_3$|Na cell in figure 4-21. Initially, the transference number was simply equated to the ratio of the steady state to the initial current flow:[26]

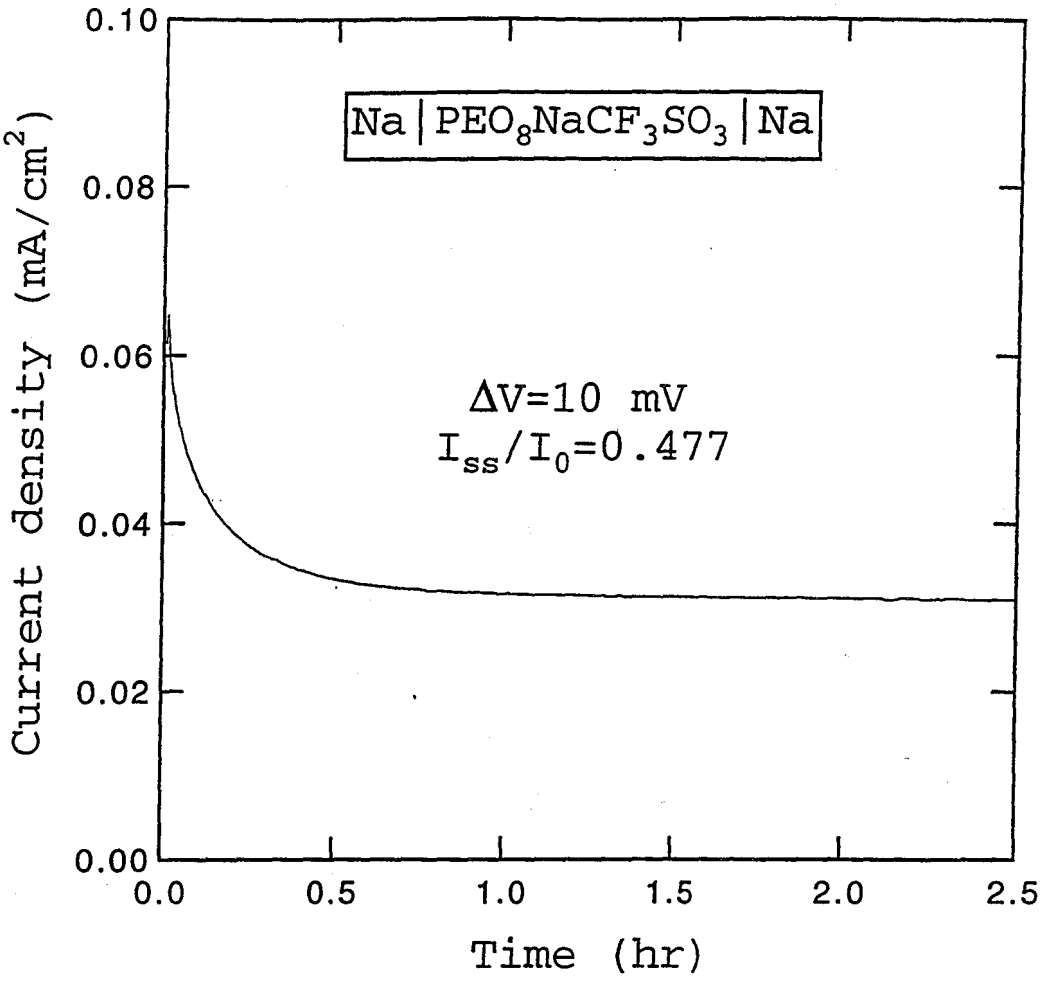


Figure 4-21. Application of the steady-state current method to $PEO_8NaCF_3SO_3$ at 85°C. The current density is monitored during a constant-potential discharge of a symmetric cell.

$$t_+^0 = \frac{I_{ss}}{I_0}. \tag{4-67}$$

Later, it was realized that a significant error may result from neglected kinetic resistances when using this formula. Thus, in later publications it has become more popular to use the following expression:

$$t_+^0 = \frac{I_{ss}\left[\Delta V - I_0 R_0\right]}{I_0\left[\Delta V - I_{ss} R_{ss}\right]}, \tag{4-68}$$

where $R$ is the interfacial (electrode kinetic) resistance and $\Delta V$ is the potential difference applied across the cell.

To analyze this experiment, we imagine using a lithium reference electrode in solution to define the potential. We assume that a reaction of the form

$$\sum_i s_i M_i^{z_i} \rightleftarrows n e^-$$

is equilibrated on the reference electrode. Then, the general expression for the reference electrode potential, $V$, is given by Newman:[12]

$$\nabla V = -\frac{I}{\kappa} - \frac{RT}{nF}\sum_i s_i \nabla \ln c_i f_{i,n} - \frac{RT}{F}\sum_j \frac{t_j^0}{z_j}\nabla \ln c_j f_{j,n}. \tag{4-69}$$

The molar activity coefficients used here, $f_{i,n}$, are defined with respect to the reference species $n$.[12] In the present case, we have a binary electrolyte with the species taken to be $Li^+$, $X^-$, and PEO. The reference electrode reaction is then:

$$\mathrm{Li} \rightleftarrows \mathrm{Li}^+ + \mathrm{e}^- .$$

The potential gradient then simplifies to:

$$\nabla V = -\frac{I}{\kappa} + \frac{2RT}{F}\left[1 + \frac{d\ln f_\pm}{d\ln c}\right]\left[1 - t_+^0\right]\nabla \ln c \,. \tag{4-70}$$

To find the total potential drop across the electrolyte we integrate 4-70 in one dimension across the cell of length $L$,

$$V(L) - V(0) = -I\int_0^L \frac{1}{\kappa}\mathrm{d}y + \frac{2RT}{F}\int_0^L \left[1 + \frac{d\ln f_\pm}{d\ln c}\right]\left[1 - t_+^0\right]\frac{\partial \ln c}{\partial y}\mathrm{d}y \,. \tag{4-71}$$

To evaluate this expression we must know how each of the physical properties appearing here varies with salt concentration. We can take $V(L)$=0 as an arbitrary condition on the potential.

At this point it becomes reasonable (for purposes of illustration) to make the approximation that the ionic conductivity, transference number, and thermodynamic factor can be treated as constants. This becomes more accurate for small potential differences, of course, and could be rigorously checked using the computer program CHECK. With this assumption, we have

$$V = \frac{IL}{\kappa} - \frac{2RT}{F}\left[1 + \frac{d\ln f_\pm}{d\ln c}\right]\left[1 - t_+^0\right]\ln\left[\frac{c(y=L)}{c(y=0)}\right] . \tag{4-72}$$

This expression can be evaluated at both initial and steady-state conditions in order to determine the current flow as a function of the potential difference. First, at the initial conditions, we have $\nabla c$=0 and

$$V_0 = \frac{I_0 L}{\kappa}. \tag{4-73}$$

At steady state, the concentration gradients in the cell are established in such a way as to have zero anion flux. The anion flux with respect to the polymer solvent can be written:

$$\mathbf{N}_- = -D\nabla c - \frac{I(1-t_+^0)}{F} + c\,\mathbf{v}_0, \tag{4-74}$$

where $\mathbf{v}_0$ is the solvent velocity which will hereafter be assumed to equal zero. When $\mathbf{N}_-$ is set equal to zero, one finds

$$\nabla c = -\frac{I_{ss}(1-t_+^0)}{FD}. \tag{4-75}$$

Integrating equation 4-75 and substituting into 4-72 gives

$$V_{ss} = \frac{I_{ss}L}{\kappa} - \frac{2RT}{F}\left[1 + \frac{d\ln f_\pm}{d\ln c}\right]\left[1 - t_+^0\right]\ln\left[\frac{c_0 - \delta}{c_0 + \delta}\right], \tag{4-76}$$

where

$$\delta = \frac{I_{ss}(1-t_+^0)L}{2FD}. \tag{4-77}$$

Now we again make use of the assumption of small concentration gradients such that $\delta << c_0$, giving

$$V_{ss} = \frac{I_{ss}L}{\kappa} + \frac{2RTI_{ss}L}{F^2 D c_0}\left[1 + \frac{d\ln f_\pm}{d\ln c}\right]\left[1 - t_+^0\right]^2. \tag{4-78}$$

Note that $V$ is linearly related to $I$ as long as $\delta << c_0$.

Having expressions for $I_0$ and $I_{ss}$ in terms of $V$, we must relate $V$ to the potential impressed across the full cell, $\Delta V$:

$$\Delta V = V + \eta_{s,a} - \eta_{s,c} \,. \tag{4-79}$$

The surface overpotentials can be estimated by assuming linear kinetics and a constant exchange current density, then

$$\eta_{s,a} - \eta_{s,c} = IR_{\text{eff}} \,, \tag{4-80}$$

where

$$R_{\text{eff}} = 2\left[R_f + \frac{RT}{i_0 F(\alpha_a + \alpha_c)}\right] . \tag{4-81}$$

Here $R_f$ is an inherent film resistance and $R_{\text{eff}}$ is the effective interfacial resistance, presumably measurable using ac-impedance techniques. The film resistance, $R_f$, can be a function of time (on the time scale of the experiment) but is assumed independent of the salt concentration. Combination of equations 4-73 and 4-78 with 4-79 and 4-80 gives the final expression:

$$\frac{I_{ss}\left[\Delta V - I_0 R_0\right]}{I_0\left[\Delta V - I_{ss} R_{ss}\right]} = \frac{1}{1 + \dfrac{2RT\kappa}{F^2 D c_0}\left[1 + \dfrac{d\ln f_{\pm}}{d\ln c}\right]\left[1 - t_+^0\right]^2} \,. \tag{4-82}$$

We have referred to the initial effective resistance as $R_0$ and the steady-state value as $R_{ss}$. This can also be written to eliminate $\Delta V$ as:

$$\frac{I_{ss}}{I_0} = \frac{1 + \frac{\kappa R_0}{L}}{1 + \frac{\kappa R_{ss}}{L} + \frac{2RT\kappa}{F^2 D c_0}\left[1 + \frac{d\ln f_{\pm}}{d\ln c}\right]\left[1 - t_+^0\right]^2}. \tag{4-83}$$

Comparing the final expressions 4-68 and 4-82, we find widely different results. For example, equation 4-68 predicts that the transference number must have a value between zero and unity. Equation 4-82, on the other hand, places no such limit. It is perhaps one of the wonders of dilute solution theory that the expression 4-82 does indeed reduce to 4-68 in the limit of an ideal, infinitely dilute solution. To see this, we must first assume that the mean molar activity coefficient is constant, giving a thermodynamic factor of unity. Next, we apply the dilute solution theoretical expressions for the various transport properties in terms of individual ionic mobilities,

$$\kappa = F^2\left[u_+ + u_-\right]c\,, \tag{4-84}$$

$$D = 2RT\left[\frac{u_+ u_-}{u_+ + u_-}\right], \tag{4-85}$$

$$t_+^0 = \frac{u_+}{u_+ + u_-}. \tag{4-86}$$

This leads to the result given in equation 4-68 directly. Thus, as was initially stated, the formula 4-68 applies only to the ideal, dilute solution. That these assumptions do not hold for typical solid polymer electrolytes is simple to prove. For example, if we examine the dilute solution theory expression 4-84 for the ionic conductivity, we find that it predicts a linear dependence on salt concentration. Experimental data show that this does not hold even at very dilute concentrations ($c$<0.1 M).[3]

The next question is what consequence does the expression 4-82 have for the steady-state current method. First, we realize that the steady-state current, even with the assumptions previously made, depends not only on the value of the transference number, but also on the salt diffusion coefficient, thermodynamic factor, and ionic conductivity. Thus, without prior knowledge of all of these data, it is not possible to obtain the transference number from the steady-state current. Also, very large errors in the measured transference number will result from ignoring these differences in the two formulas. As an example, we can consider the case of 2.58 M $NaCF_3SO_3$ in poly(ethylene oxide) at 85°C. The transport properties for this system are known as functions of the salt concentration from our previous work (section 4.5).[40] Assuming the properties to be constant and equal to their bulk values stated earlier, we can plug the following numbers into equation 4-82:

$$D=1.47\times10^{-8}\ \mathrm{cm^2/s},$$

$$\kappa=1.54\times10^{-4}\ \mathrm{S/cm},$$

$$t_+^0=-4.38,$$

$$\text{and}\quad \left[1+\frac{\partial \ln f_\pm}{\partial \ln c}\right]=0.023,$$

giving a value of:

$$\frac{I_{ss}\left[\Delta V - I_0 R_0\right]}{I_0\left[\Delta V - I_{ss} R_{ss}\right]} = 0.37. \qquad (4\text{-}87)$$

Notice the error that would result from incorrectly interpreting this number as the value of the sodium ion transference number.

It has been suggested that the ratio of steady state to initial current might be a useful piece of information to evaluate a given polymer electrolyte's transport behavior, even if it does not give one a direct measure of the lithium-ion transference number. This quantity has been called the "limiting current fraction" by some. We see now that this ratio will approach unity as either the salt diffusion coefficient or lithium-ion transference number is increased, or as the thermodynamic factor or ionic conductivity is decreased. Since all but the last of these criteria would be desirable properties for a polymer electrolyte, the above statement is to some extent true. However, it is certainly preferable to use the values of the measurable, macroscopic transport properties to evaluate various candidate polymer electrolytes instead of relying on quantities like the limiting current fraction, which contain a convolution of information.

Also, it is not true that the limiting current fraction is directly relevant to the performance of practical electrochemical devices. First, most devices will be run at a constant current, and the main transport issue is then how large a current can be sustained before a "limiting" current is reached in the polymer electrolyte, *i.e.*, before one drives the salt concentration to zero or above its supersaturation value. Thus, the main issue has to do with the size of the concentration gradients that develop in the cell during the passage of current. With a highly nonideal electrolyte, a large value of the limiting current fraction can still lead to the development of large concentration gradients upon passage of current. With the above example, the actual concentration gradient would be 8.5 times greater according to equation 4-75 with the correct value of the transference number rather than a value inferred incorrectly from a limiting current fraction.

When comparing the various methods that have been devised to measure the transference number that depend on the current/voltage behavior of a symmetric cell, it has not escaped our

attention that the quantity

$$\frac{2RT}{F^2Dc_\infty}\left[1+\frac{\partial \ln f_\pm}{\partial \ln c}\right]\left[1-t_+^0\right]^2 \tag{4-88}$$

appears in each case. For example, we can compare the potentiostatic (or steady-state current) method of equation 4-82, the galvanostatic method developed in section 4.3, and the ac-impedance method;[41] in each case we find that the quantity measured is related to 4-88 through various conversion factors. For example, from the above expression 4-82 one can show:

$$\frac{2RT}{F^2Dc_\infty}\left[1+\frac{\partial \ln f_\pm}{\partial \ln c}\right]\left[1-t_+^0\right]^2 = \frac{1}{2\kappa}\left[\frac{I_0\left[\Delta V - I_{ss}R_{ss}\right]}{I_{ss}\left[\Delta V - I_0R_0\right]}-1\right]. \tag{4-89}$$

For the ac-impedance experiment one finds:[41]

$$\frac{2RT}{F^2Dc_\infty}\left[1+\frac{\partial \ln f_\pm}{\partial \ln c}\right]\left[1-t_+^0\right]^2 = \frac{Z_\omega(0)A}{c_0\bar{V}_0L}, \tag{4-90}$$

where $Z_\omega(0)$ is the width of the low-frequency impedance loop. For the galvanostatic polarization method,

$$\frac{2RT}{F^2Dc_\infty}\left[1+\frac{\partial \ln f_\pm}{\partial \ln c}\right]\left[1-t_+^0\right]^2 = \frac{m\pi^{1/2}}{4D^{1/2}}, \tag{4-91}$$

with $m$ defined as the slope of a plot of $\Delta\Phi$ *versus* $(It_i^{1/2})$. This similarity among the experimental techniques is a natural result of the experimental approach and the governing transport relations. It should not be possible to avoid the thermodynamic factor when using the potential difference of the cell to ascertain the transference number.

Another consequence of the above analogy between methods is that any one of the above experiments could be combined with concentration-cell data to obtain the transference number. Assuming that the concentration-cell data in the form of *U versus* ln *c* are linear over the range of concentrations in the cell, one finds:

$$\left[\frac{\mathrm{d}U}{\mathrm{d}\ln c}\right] = \frac{2RT}{F}\left[1 + \frac{\partial \ln f_{\pm}}{\partial \ln c}\right]\left[1 - t_{+}^{0}\right] . \qquad (4\text{-}92)$$

Thus, the slope of concentration-cell data can be combined with any of the above equations 4-89, 90, or 91 to isolate the transference number. Note that in each case we still require the value of the salt diffusion coefficient. Along these same lines, we should point out that these two sets of data can also be used to calculate the thermodynamic factor without knowledge of $t_{+}^{0}$. Combination of the concentration-cell data with the quantity given by equation 4-88 provides the following:

$$\frac{1}{2RTDc_{\infty}}\left[\frac{\mathrm{d}U}{\mathrm{d}\ln c}\right]^{2}\left[1 + \frac{\partial \ln f_{\pm}}{\partial \ln c}\right]^{-1} . \qquad (4\text{-}93)$$

This idea was also mentioned by Pollard.[41] As this method requires the square of the slope from the concentration-cell data, one would expect errors introduced from the differentiation to be magnified.

### 4.10 Comparison of methods to measure $t_{+}^{0}$ in SPE's

It should now be possible to reflect on the utility of the present method of measuring the transference number in comparison to methods that have been used by others. Some of the problems involved in measuring $t_{+}^{0}$ in a solid polymer electrolyte have been discussed already in section 4.2. The results given above also support the fact that these solutions are both

concentrated and nonideal, so that assumptions of constant transport properties or of solution ideality fail even at the most dilute concentrations used in the present work. The criteria that we will use to compare the experimental methods are then their validity for a nonideal, concentrated electrolyte, experimental difficulty, and ability to ascertain a differential transport property.

The two most popular methods to date to measure $t_+^0$ have been the potentiostatic polarization method and the ac-impedance-based methods. The former of these was discussed in detail in section 4.9, where it was concluded that the method in its present form cannot be used to measure the transference number. Instead, the ratio of steady state to initial currents is determined by a function of all three of the macroscopic transport parameters as well as the mean molar activity coefficient of the salt. The ac-impedance methods presently in use can be derived from equations given by Macdonald.[42-44] For example, the following expression has been used to calculate the transference number from particular characteristics of the low-frequency impedance response of a symmetric cell:[45,46]

$$t_-^0 = \left[1 + \frac{R_b}{Z_\omega(0)}\right]^{-1}. \qquad (4\text{-}94)$$

The theoretical origins of this expression are in dilute solution theory, so we have the same problems with this expression as with those discussed earlier for the steady-state current method (*e.g.*, equation 4-68). This is the most probable explanation for discrepencies found between the results of these and other methods.[38,47] A detailed critique of the ac-impedance methods from the standpoint of concentrated-solution theory has already appeared in the literature and supports these conclusions.[41]

Another possible method is the measurement of limiting currents at a microelectrode surface; this experiment allows one to obtain the transference number as long as the salt diffusion coefficient is known. The limiting current to a disk electrode in a semiinfinite medium is given by:

$$i_{\text{lim}} = \frac{4nFDc_{\infty}}{\pi a(1 - t_{+}^{0})}. \tag{4-95}$$

As the cell is completely polarized during this measurement, the value that one obtains is an average value over the range of concentrations in the cell, which must then be deconvoluted to find a differential transport property.[48] There are also practical difficulties with these experiments that must be overcome involving the contact between the polymer electrolyte and the microelectrode surface. This has been achieved with low-molecular-weight polyethers, such as poly(ethylene glycol dimethyl ether) (PEGDM, MW=400), but the limiting current data were not used to obtain transport properties.[49]

The most direct measurement of the transference number from a theoretical perspective comes from the Hittorf method.[50-52] Although not known for its accuracy, the Hittorf method was the first and has historically been the most popular method to measure transference numbers in both liquid and solid systems. Current is passed across the standard Li|PEO|Li cell using thick PEO films so that concentration changes are confined to the region near the electrode surfaces. The transference number is found by comparing the net concentration change adjacent to either electrode with the total coulombs passed through the cell:

$$t_{-}^{0} = \frac{FL\Delta c}{It}, \tag{4-96}$$

where $L$ is the thickness of one section and $\Delta c$ is the change in concentration due to the electrolysis. To assure that concentration gradients do not propagate into the center of the cell, it is best to use a four-compartment cell; the concentration of salt in each of the two inner compartments should not change from the initial value.

This measurement has been made successfully by one group in a high-molecular-weight PEO-based system, but only one salt at a single concentration was studied.[51] It is interesting that this measurement gave one of the lowest values for $t_+^0$ yet reported (0.06). The difficulty with this method lies in the fact that the polymer must be sectioned and analyzed after the passage of current. This leads to problems of separating the polymer electrolyte from the electrode surfaces, which has motivated researchers to use either lithium-alloy or lead electrodes where separation is easier.[53] Also, longer diffusion lengths (perhaps 1 to 2 cm) become necessary in order to section the polymer easily; however, these longer diffusion lengths make passing current difficult for poorly conducting polymer electrolytes.

Considering the above techniques, we see that there exist either problems with the validity or experimental difficulties in each case. For this reason, one is motivated to consider more subtle approaches that make use of more than one experimental quantity. The class of experiments described earlier, that rely on the current/voltage behavior of a symmetric cell, represents just such an approach. We found earlier that these experiments are able to access the quantity:

$$\frac{2RT}{F^2 D c_\infty}\left[1+\frac{\partial \ln f_\pm}{\partial \ln c}\right]\left[1-t_+^0\right]^2 \tag{4-97}$$

which, when combined with concentration-cell data in the form given in equation 4-92, lead to:

$$\frac{1}{FDc_\infty}\left[\frac{\mathrm{d}U}{\mathrm{d}\ln c}\right]\left[1-t_+^0\right]. \tag{4-98}$$

In section 4.9 three approaches were described: one being the galvanostatic polarization used in the present work in section 4.5, another being the popular potentiostatic polarization (or steady-state current) method, and a third being an ac-impedance based technique. Comparing these three methods, we would prefer to use the galvanostatic polarization technique. The potentiostatic polarization method has the disadvantage of setting up steady concentration gradients that make measurement of differential transport properties impossible. Unlike with the galvanostatic polarization technique, it is not clear that as the size of the potential step is made small, the effect of the variable physical properties will disappear.

Ac-impedance-based techniques are appealing because the alternating-current signal minimizes the formation of concentration gradients during measurements. This should allow one to measure differential values of transport properties. However, it is often difficult to resolve accurately the low-frequency loop on the Nyquist plot.[41] On the other hand, an ac-impedance measurement does have the advantage of potentially giving the value of the salt diffusion coefficient in the same experiment. Alternating-current impedance data as a function of frequency can provide the salt diffusion coefficient at the bulk concentration from either the frequency maximum on the low-frequency loop:[41]

$$D = \frac{\pi L^2 f_{\max}}{5.080}, \tag{4-99}$$

or from the slope, $l$, of a plot of Re(Z) *versus* $(\omega/2\pi)^{-1/2}$:[41]

$$D = \frac{\pi L^2 l^2}{Z_\omega^2(0)} . \qquad (4\text{-}100)$$

With very slow diffusion processes, such as those in solid polymer electrolytes at lower temperatures, data in the low-frequency domain can be difficult to obtain.

Based on the above analyses, we conclude that no single method of measuring the transference number in solid polymer electrolyte solutions is clearly the best method. At the present time, there appears to be a tradeoff between the experimental difficulty and the theoretical simplicity of the various methods that are available. The Hittorf method, which still has not overcome fully some experimental difficulties, is the most direct method from a theoretical perspective. Whereas the method presented in the present work has the advantage of experimental simplicity, the result is sensitive to the values of several other experimental quantities such as the salt diffusion coefficient and the concentration-cell data. Considering this state of affairs, it seems likely that future research will lead to the development of even more novel methods of measuring either the transference number or, more likely, the salt activity coefficient in solid-polymer-electrolyte solutions.

### 4.11 Conclusions

We have measured a full set of transport properties for one solid-polymer-electrolyte system: sodium trifluoromethanesulfonate ($NaCF_3SO_3$) in poly(ethylene oxide) (PEO) over the concentration range of 0.1 to 2.6 mol/dm$^3$ at a temperature of 85°C. The conductivity was measured with ac-impedance from the high-frequency intercept on the real axis of a complex-plane plot. The conductivity was found to vary with concentration in a manner similar to that of $LiCF_3SO_3$ in PEO. The salt diffusion coefficient was measured using restricted diffusion with the concentration difference extracted from the potential of the cell. Diffusion coefficients

were also found to vary with concentration in a manner similar to the conductivity.

The sodium ion transference number was measured by combining concentration-cell data with the results of dc-polarization experiments. This method is easy to perform experimentally and does not require the assumption of an ideal polymer electrolyte solution. The resulting transference numbers decreased strongly with concentration, going from around 0.31 in the most dilute solution (0.05 mol/dm$^3$) to -4.37 in the most concentrated solution (2.58 mol/dm$^3$). Some discussion of the impact of microscopic speciation on the macroscopic transport properties is given to rationalize the large negative transference numbers obtained. The thermodynamic factor is also calculated and found to decrease with increasing salt concentration. The values found for this parameter indicate that this solid-polymer-electrolyte solution is highly nonideal.

## Acknowledgements

We gratefully acknowledge the assistance of Yanping Ma of the De Jonghe laboratory in the Department of Materials Science and Mineral Engineering at U. C. Berkeley and the Materials Sciences Division of the Lawrence Berkeley Laboratory for the experimental results given in this chapter. This work was supported by the Assistant Secretary for Energy Efficiency and Renewable Energy, Office of Transportation Technologies, Electric and Hybrid Propulsion Division of the U. S. Department of Energy under Contract No. DE-AC03-76SF00098.

## Appendix 4-A Computer program and data file CHECK

CHECK data file

```
20          3.5d-04     200         358.15      -0.030d0
1.0d00      1.0d0       1.50d0      8           0.50d0
8.00d03     3.750d-02   3.750d-02   5.0d0       0.000d0
0           2           1           0
6
0.1881d03
0.28096d03
0.22515d03
1.091d03
1.7724d03
2.576d03
```

CHECK data file comments

line 1: lim,hs,nj,t,xi(2,1)
- lim, limit on number of iterations
- hs, thickness of separator (m)
- nj, number of nodes in separator
- t, temperature (K)
- xi(2,1), initial potential (V)

line 2: rr,eps,cur,numb,fact
- rr, size of time step (s)
- eps, volume fraction of electrolyte in separator
- cur, current density for discharge (A/m2)
- numb, number of successive discharges to carry out
- fact, factor by which to increment time of successive discharges (min)

line 3: cmax,rka,rkc,resttime,restcur
- cmax, maximum concentration in polymer electrolyte (mol/m3)
- rka, exchange current density for anode
- rkc, exchange current density for cathode
- resttime, time of rest period between discharges (min)
- restcur, current density during rest period (A/m2)

line 4: il1,il2,il3,il4
- il1, 1 for long print-out 0 for short print-out
- il2, 1/il2 = fraction of nodes in long print-out
- il3, 1/il3 = fraction of time steps in long print-out
- il4, 1 for polymer, 0 for liquid electrolyte

line 5: nmax
- nmax, number of bulk concentrations to test

line 6 onward: xc(i)
- xc, bulk concentration (mol/m3)

CHECK program code

```
************************************************************************
c
c       AUTOCHECK.FOR
c       Retooled on 1/16/95
c
c       Binary, concentrated electrolyte solution between cation
c       reversible electrodes.
c
c       Performs either galvanostatic or potentiostatic
c       polarization experiments automatically according
c       to specifications in input file.
c
c       Includes variable transport properties
c
c       Has current PEO+NaCF3SO3 properties as of 8/1/94
c
c***********************************************************************
      implicit real*8(a-h,o-z)
      common /n/ nx,nt,nj
      common /calc/ u(822,1600),ts(1600),h
      common/const/ fc,r,t,frt,cur,eps,pi
      common/ssblock/ xp0(2),xx0(2,821),term(821)
      common/var/ xp(10),xx(2,821),xi(2,821),xt(2,821,1600)
      common/cprop/ cmax,rka,rkc,hs,rr
      common/results/ fact,nmax,mmax,xc(20),wconc2(20,100),
     1wconc(20,100),pot(20,100)
      common/tprop/df(821),cd(821),tm(821),
     1ddf(821),dcd(821),dtm(821),dfu(821),d2fu(821)
      dimension cu(2),rc(2)
c
      n=2
c     n is number of equations
      data fc/96487.0d0/, r/8.314d0/, pi/3.141592653589d0/
c***********************************************************************
c     read in parameters and boundary conditions
c
      read *,lim,hs,nj,t,xi(2,1)
c     lim is number of iterations, hs is thickness of separator,
c     nj is number of nodes in separator, t is temperature
      read *,rr,eps,cur,numb,factor
      read *,cmax,rka,rkc,resttime,restcur
      read *,il1,il2,il3,il4
      read *,nmax
      read *,(xc(i),i=1,nmax)
```

```
c
c     xc is the bulk concentration
c     cu is the current, rc is the time to discharge
c
      h=hs/(nj-1)
      frt=fc/(r*t)
c     Fix discharge current
      cu(1)=cur
c     Fixed relaxation time of one minute
      cu(2)=restcur
      rc(2)=resttime
c     Specify number of time changes:
      fact=factor
      mmax=numb
c*************************************************************
c     Loop for bulk concentrations:
      do 233 lk=1, nmax
      xi(1,1)=xc(lk)
c     print*,'bulk conc is ',xc(lk)
      xi(1,nj)=xi(1,1)
      do 232 lm=1, mmax
      rc(1)=fact*lm
c     print*,'time is ',rc(1)
      rr=1.0d0
c     Real time counter in seconds:
      ts(1)=0.00d0
      cur=cu(1)
      k=1
c
c     procedure guess sets the initial values/guesses:
      call guess(n)
c
      print*,'    CHECK VERSION 1.0'
      print*,' '
      print*,'cell pot  ','material','       time'
      print*,'  (V)     ','balance','        (min)'
c
c*************************************************************
c
      ncue2=0
      time=60.0d0*rc(1)
  123 k=k+1
      nt=k-1
c
  122 if(time.gt.ts(k-1)) then
c     print*,'time is ',ts(k-1),k
```

```
      ts(k)=ts(k-1)+rr
      call comp(n,lim,k,il2,il3,ncue2,lk)
      do 11 i=1,n
      do 11 j=1,nj
   11 xt(i,j,k)=xx(i,j)
      call cellpot(k,il4,vv)
c     print*,'stuff is ',k,cur,vv,ts(k)
      go to 123
c
      else
c     stop discharge
      if (abs(time-ts(k-1)).le.0.1d0) then
      cur=0.0d0
      rr=1.0d-03
      ts(k)=ts(k-1)+rr
      call comp(n,lim,k,il2,il3,1,lk)
      do 15 i=1,n
      do 15 j=1,nj
   15 xt(i,j,k)=xx(i,j)
c     print*,'potential at interrupt ',xt(2,1,k)
c     print*,'wall conc. at interrupt ',xt(1,1,k)
c     print*,'time of interrupt ',ts(k)
      pot(lk,lm)=xt(2,1,k)
      wconc(lk,lm)=xt(1,1,k)
      wconc2(lk,lm)=xt(1,nj,k)
      go to 198
      else
c     overshot the time required:
      k=k-1
      ncue2=1
      rr=rr/2.0d0
      go to 122
      endif
c
c     start post-pulse relaxation period:
  198 cur=cu(2)
      time=60.0d0*(rc(2)+rc(1))
      rr=1.0d0
  124 k=k+1
      nt=k-1
      if(time.gt.ts(k-1)) then
      ts(k)=ts(k-1)+rr
      ncue2=0
c     print*,'stuff',k,cur,ncue2,ts(k)
      call comp(n,lim,k,il2,il3,ncue2,lk)
      do 12 i=1,n
```

```
      do 12 j=1,nj
   12 xt(i,j,k)=xx(i,j)
      call cellpot(k,il4,vv)
      go to 124
      end if
      end if
      call nucamb(lk,n,il2,1,il1)
  232 end do
      cur=cu(1)
      il3=0
      call nucamb(lk,n,il2,il3,il1)
  233 end do
c
      end
c
c*********************************************************************
      subroutine comp(n,lim,kk,il2,il3,ncue2,lk)
      implicit real*8(a-h,o-z)
      common /n/ nx,nt,nj
      common /calc/ u(822,1600),ts(1600),h
      common/const/ fc,r,t,frt,cur,eps,pi
      common/ssblock/ xp0(2),xx0(2,821),term(821)
      common/var/ xp(10),xx(2,821),xi(2,821),xt(2,821,1600)
      common/cprop/ cmax,rka,rkc,hs,rr
      common/results/ fact,nmax,mmax,xc(20),wconc2(20,100),
     1wconc(20,100),pot(20,100)
      common/tprop/df(821),cd(821),tm(821),
     1ddf(821),dcd(821),dtm(821),dfu(821),d2fu(821)
      common/mat/ b,d
      common/bnd/ a,c,g,x,y
      dimension b(10,10),d(10,21)
      dimension a(10,10),c(10,821),g(10),x(10,10),y(10,10)
c
   99 format (1h ,//5x,'this run did not converge'//)
      nx=n
      li=1
c
      if (li.eq.1) then
      do 20 j=1,nj
      do 20 i=1,n
         c(i,j)=xt(i,j,kk-1)
   20      xx(i,j)=xt(i,j,kk-1)
c     sets first guess to last time step values
      else
  666 do 81 j=1,nj
      do 81 i=1,n
```

```
   81       c(i,j)=xx(i,j)
            endif
c           sets first guess to last iteration values
            jcount=0
            do 4 i=1,n
    4       xp(i)=0.0d0
c           initialize variables to begin each iteration
c           (jcount is iteration #)
    8       j=0
            jcount=jcount+1
            call prop(nj,lk)
c           obtains physical properties at this specific point
            do 9 i=1,n
            do 9 k=1,n
                 x(i,k)=0.0d0
    9            y(i,k)=0.0d0
c
c           store previous iteration of  (xp in xp0)  &  (xx in xx0)
            do 6 i=1,n
                 xp0(i)=xp(i)
    6            xx0(i,nj-5)=xx(i,nj-5)
c
            if (kk.eq.2.and.jcount.eq.1) then
            term(1)=cur/fc-cur*(tm(1)+tm(2))/fc/2.
            term(nj)=-cur/fc+cur*(tm(nj)+tm(nj-1))/fc/2.
            do jj=2,nj-1
            term(jj)=cur*(tm(jj)+tm(jj-1))/fc/2.-
           1cur*(tm(jj)+tm(jj+1))/fc/2.
            end do
            end if
c
c           for a given iteration, set up governing equations and bc's
c           start at the left interface and move across polymer
c
   10       j=j+1
c
            do 11 i=1,n
                 g(i)=0.0d0
                 xx(i,j)=c(i,j)
            do 11 k=1,n
                 a(i,k)=0.0d0
                 b(i,k)=0.0d0
   11            d(i,k)=0.0d0
c           clears all arrays before use
            if(j.ne.1) go to 13
c
```

```
c     ------------------------------------------------------
c
c     specify boundary conditions at left interface (j=1)
c     boundary conditions at negative electrode
c
c     equation 1:  flux specified by current
c
      dcf=(xx(1,j+1)-xx(1,j))/h
      b(1,1)=3.*eps*h/8./rr+(df(j)+df(j+1))/4./h-ddf(j)*dcf/4.
     1+cur*dtm(j)/4./fc
      d(1,1)=eps*h/8./rr-(df(j)+df(j+1))/4./h-ddf(j+1)*dcf/4.
     1+cur*dtm(j+1)/4./fc
      g(1)=-eps*h/rr*(0.375*(xx(1,j)-xt(1,j,kk-1))+0.125*
     1(xx(1,j+1)-xt(1,j+1,kk-1)))+(cur/fc+(df(j)+df(j+1))*dcf/2.-
     1cur*(tm(j)+tm(j+1))/2./fc)/2.+term(j)/2.
c
      dcf=(xx(1,j+1)-xx(1,j))/h
      r1=(xx(1,j+1)+xx(1,j))/2.0d0
      p1=(tm(j)+tm(j+1))/2.0d0
      p2=(cd(j)+cd(j+1))/2.0d0
      p3=(dtm(j)+dtm(j+1))/2.0d0
      p4=(dfu(j)+dfu(j+1))/2.0d0
      p5=(dcd(j)+dcd(j+1))/2.0d0
      p6=(d2fu(j)+d2fu(j+1))/2.0d0
      thermf=0.5*(1.+r1*p4)
      d(2,1)=(1.0d0-p1)*(1.0d0/r1+p4)/h
      b(2,1)=-d(2,1)+((1.0d0-p1)*(p6-1.0d0/r1/r1)*dcf
     1        -(1.0d0/r1+p4)*dcf*p3)/2.0d0
      d(2,1)=d(2,1)+((1.0d0-p1)*(p6-1.0d0/r1/r1)*dcf
     1        -(1.0d0/r1+p4)*dcf*p3)/2.0d0
      d(2,2)=-frt/h
      b(2,2)=frt/h
      g(2)=frt*cur/p2
     1-(2.*(1.0d0-p1)*thermf/h/r1)*(c(1,j+1)-c(1,j))
     1+frt/h*(c(2,j+1)-c(2,j))
c
      call band(j)
      go to 10
c
c     ------------------------------------------------------
c     specify governing equations in polymer separator
  13  if (j .ge. nj) go to 110
c
      dcf=(xx(1,j+1)-xx(1,j))/h
      dcb=(xx(1,j)-xx(1,j-1))/h
      b(1,1)=3.*eps*h/4./rr+(df(j-1)+2.*df(j)+df(j+1))/4./h
```

```
     1-ddf(j)*(xx(1,j+1)-2.*xx(1,j)+xx(1,j-1))/h/4.
     1+cur*dtm(j)/2./fc
      a(1,1)=eps*h/8./rr-(df(j)+df(j-1))/4./h+ddf(j-1)*dcb/4.
     1-cur*dtm(j-1)/4./fc
      d(1,1)=eps*h/8./rr-(df(j)+df(j+1))/4./h-ddf(j+1)*dcf/4.
     1+cur*dtm(j+1)/4./fc
      g(1)=-eps*h/rr*(0.75*(xx(1,j)-xt(1,j,kk-1))+0.125*(xx(1,j+1)-
     1xt(1,j+1,kk-1))+0.125*(xx(1,j-1)-xt(1,j-1,kk-1)))
     1+((df(j)+df(j+1))*dcf/2.-cur*(tm(j)+tm(j+1))/2./fc-
     1(df(j-1)+df(j))*dcb/2.+cur*(tm(j-1)+tm(j))/2./fc)/2.
     1+term(j)/2.
c
c
      dcf=(xx(1,j+1)-xx(1,j))/h
      r1=(xx(1,j+1)+xx(1,j))/2.0d0
      p1=(tm(j)+tm(j+1))/2.0d0
      p2=(cd(j)+cd(j+1))/2.0d0
      p3=(dtm(j)+dtm(j+1))/2.0d0
      p4=(dfu(j)+dfu(j+1))/2.0d0
      p5=(dcd(j)+dcd(j+1))/2.0d0
      p6=(d2fu(j)+d2fu(j+1))/2.0d0
      thermf=0.5*(1.+r1*p4)
      d(2,1)=(1.0d0-p1)*(1.0d0/r1+p4)/h
      b(2,1)=-d(2,1)+((1.0d0-p1)*(p6-1.0d0/r1/r1)*dcf
     1       -(1.0d0/r1+p4)*dcf*p3)/2.0d0
      d(2,1)=d(2,1)+((1.0d0-p1)*(p6-1.0d0/r1/r1)*dcf
     1       -(1.0d0/r1+p4)*dcf*p3)/2.0d0
      d(2,2)=-frt/h
      b(2,2)=frt/h
      g(2)=frt*cur/p2
     1-(2.*(1.0d0-p1)*thermf/h/r1)*(c(1,j+1)-c(1,j))
     1+frt/h*(c(2,j+1)-c(2,j))
c
c     g(2)=-c(4,j)
c     b(2,4)=1.0
c
      call band(j)
      go to 10
c     ------------------------------------------------------
  110 continue
c     specify boundary conditions at right interface(j=nj)
c
      dcb=(xx(1,j)-xx(1,j-1))/h
      b(1,1)=3.*eps*h/8./rr+(df(j)+df(j-1))/4./h+ddf(j)*dcb/4.
     1-cur*dtm(j)/4./fc
      a(1,1)=eps*h/8./rr-(df(j)+df(j-1))/4./h+ddf(j-1)*dcb/4.
```

```
     1-cur*dtm(j-1)/4./fc
      g(1)=-eps*h/rr*(0.375*(xx(1,j)-xt(1,j,kk-1))+0.125*
     1(xx(1,j-1)-xt(1,j-1,kk-1)))+(-cur/fc-(df(j)+df(j-1))*dcb/2.+
     1cur*(tm(j)+tm(j-1))/2./fc)/2.+term(j)/2.
c
c
      g(2)=-c(2,j)
      b(2,2)=1.0
c
      call band(j)
      do 605 jj=1,nj
      do 605 i=1,n
  605 c(i,jj)=xx(i,jj)+c(i,jj)
c     ------------------------------------------------
c
c     begin check for ss convergence
c
      do i=1,n
      xp(i)=(4.0d0*c(i,2)-3.0d0*c(i,1)-c(i,3))/2.0d0/h
      end do
      do 25 j=1,nj
      if(c(1,j).lt.xx(1,j)/1.0d02) c(1,j)=xx(1,j)/1.0d02
      if(c(2,j).lt.xx(2,j)-0.3d0) c(2,j)=xx(2,j)-0.3d00
      if(c(2,j).gt.xx(2,j)+0.3d0) c(2,j)=xx(2,j)+0.3d00
      if(c(1,j).lt.1.0d-10) c(1,j)=1.0d-10
c     if(c(1,j).ge.cmax) c(1,j)=0.999d0*cmax
      do 25 i=1,n
 25   xx(i,j)=c(i,j)
c
      if (jcount .gt. lim ) then
      rr=rr/2.0d0
      lim=lim+1
      ts(kk)=ts(kk-1)+rr
c     print*,' time step reduced to ', rr
      if (rr .lt. 1.0d-06) then
      print*,kk-1, ' this time step did not converge'
      print99
      call nucamb (lk,n,il2,0,il1)
      stop
      else
      go to 666
      end if
c
      else
          do 55 ii=1,n
                dxp=dabs( xp(ii)-xp0(ii) )
```

```
                dxx=dabs( xx(ii,nj-5)-xx0(ii,nj-5) )
              if (dxx.gt.1.0d-10*dabs(xx(ii,nj-5)))  go to 8
              if (dxp.gt.1.0d-09*dabs(xp(ii))) go to 8
c
   55     continue
c
c      print*,jcount,' iterations required'
c      Increasing time steps:
       if (jcount .lt. 5 .and. kk.gt.10) then
       if (ncue2.eq.0) then
       if (rr.lt.2.0d00) then
       rr=rr*3.5d0
c      print*,'time step increased to ',rr
       else
       go to 222
       end if
       else
       if (rr.lt.1.0d01.and.ncue2.eq.0) then
       rr=rr*2.0d0
c      print*,'time step increased to ',rr
       else
       continue
       end if
       end if
       else
       continue
       end if
  222 continue
c
c      The new termj section:
       j=1
       dcb=(xx(1,j)-xx(1,j-1))/h
       dcf=(xx(1,j+1)-xx(1,j))/h
       term(1)=cur/fc+(df(1)+df(2))*dcf/2.-
      1cur*(tm(1)+tm(2))/fc/2.
       j=nj
       dcb=(xx(1,j)-xx(1,j-1))/h
       dcf=(xx(1,j+1)-xx(1,j))/h
       term(nj)=-cur/fc-(df(nj)+df(nj-1))*dcb/2.+
      1cur*(tm(nj)+tm(nj-1))/fc/2.
       do j=2,nj-1
       dcb=(xx(1,j)-xx(1,j-1))/h
       dcf=(xx(1,j+1)-xx(1,j))/h
       term(j)=-(df(j)+df(j-1))*dcb/2.+cur*(tm(j)+tm(j-1))/fc/2.
      1+(df(j)+df(j+1))*dcf/2.-cur*(tm(j)+tm(j+1))/fc/2.
       end do
```

```
c
      end if
c
      return
      end
c
c*********************************************************************
      subroutine band(j)
      implicit real*8(a-h,o-z)
      common /n/ nx,nt,nj
      common/mat/ b,d
      common/bnd/ a,c,g,x,y
      dimension b(10,10),d(10,21)
      dimension a(10,10),c(10,821),g(10),x(10,10),y(10,10)
      dimension e(10,11,821)
  101 format (15h determ=0 at j=,i4)
      n=nx
      if (j-2)  1,6,8
    1 np1= n + 1
      do 2 i=1,n
      d(i,2*n+1)= g(i)
      do 2 l=1,n
      lpn= l + n
    2 d(i,lpn)= x(i,l)
      call matinv(n,2*n+1,determ)
      if (determ)  4,3,4
    3 print 101, j
    4 do 5 k=1,n
      e(k,np1,1)= d(k,2*n+1)
      do 5 l=1,n
      e(k,l,1)= - d(k,l)
      lpn= l + n
    5 x(k,l)= - d(k,lpn)
      return
    6 do 7 i=1,n
      do 7 k=1,n
      do 7 l=1,n
    7 d(i,k)= d(i,k) + a(i,l)*x(l,k)
    8 if (j-nj)  11,9,9
    9 do 10 i=1,n
      do 10 l=1,n
      g(i)= g(i) - y(i,l)*e(l,np1,j-2)
      do 10 m=1,n
   10 a(i,l)= a(i,l) + y(i,m)*e(m,l,j-2)
   11 do 12 i=1,n
      d(i,np1)= - g(i)
```

```
      do 12 l=1,n
      d(i,np1)= d(i,np1) + a(i,l)*e(l,np1,j-1)
      do 12 k=1,n
   12 b(i,k)= b(i,k) + a(i,l)*e(l,k,j-1)
      call matinv(n,np1,determ)
      if (determ)  14,13,14
   13 print 101, j
   14 do 15 k=1,n
      do 15 m=1,np1
   15 e(k,m,j)= - d(k,m)
      if (j-nj)  20,16,16
   16 do 17 k=1,n
   17 c(k,j)= e(k,np1,j)
      do 18 jj=2,nj
      m= nj - jj + 1
      do 18 k=1,n
      c(k,m)= e(k,np1,m)
      do 18 l=1,n
   18 c(k,m)= c(k,m) + e(k,l,m)*c(l,m+1)
      do 19 l=1,n
      do 19 k=1,n
   19 c(k,1)= c(k,1) + x(k,l)*c(l,3)
   20 return
      end
c*************************************************************************
      subroutine matinv(n,m,determ)
      implicit real*8(a-h,o-z)
      common/mat/ b,d
      dimension b(10,10),d(10,21)
      dimension id(10)
      determ=1.0
      do 1 i=1,n
    1 id(i)=0
      do 18 nn=1,n
      bmax=1.1
      do 6 i=1,n
      if(id(i).ne.0) go to 6
      bnext=0.0
      btry=0.0
      do 5 j=1,n
      if(id(j).ne.0) go to 5
      if(dabs(b(i,j)).le.bnext) go to 5
      bnext=dabs(b(i,j))
      if(bnext.le.btry) go to 5
      bnext=btry
      btry=dabs(b(i,j))
```

```
      jc=j
    5 continue
      if(bnext.ge.bmax*btry) go to 6
      bmax=bnext/btry
      irow=i
      jcol=jc
    6 continue
      if(id(jc).eq.0) go to 8
      determ=0.0
      return
    8 id(jcol)=1
      if(jcol.eq.irow) go to 12
      do 10 j=1,n
      save=b(irow,j)
      b(irow,j)=b(jcol,j)
   10 b(jcol,j)=save
      do 11 k=1,m
      save=d(irow,k)
      d(irow,k)=d(jcol,k)
   11 d(jcol,k)=save
   12 f=1.0/b(jcol,jcol)
      do 13 j=1,n
   13 b(jcol,j)=b(jcol,j)*f
      do 14 k=1,m
   14 d(jcol,k)=d(jcol,k)*f
      do 18 i=1,n
      if(i.eq.jcol) go to 18
      f=b(i,jcol)
      do 16 j=1,n
   16 b(i,j)=b(i,j)-f*b(jcol,j)
      do 17 k=1,m
   17 d(i,k)=d(i,k)-f*d(jcol,k)
   18 continue
      return
      end
c*********************************************************************
      subroutine nucamb(lk,n,il2,il3,il1)
      implicit real*8(a-h,o-z)
      common /n/ nx,nt,nj
      common /calc/ u(822,1600),ts(1600),h
      common/const/ fc,r,t,frt,cur,eps,pi
      common/var/ xp(10),xx(2,821),xi(2,821),xt(2,821,1600)
      common/cprop/ cmax,rka,rkc,hs,rr
      common/results/ fact,nmax,mmax,xc(20),wconc2(20,100),
     1wconc(20,100),pot(20,100)
      common/tprop/df(821),cd(821),tm(821),
```

```
     1ddf(821),dcd(821),dtm(821),dfu(821),d2fu(821)
      dimension zz(821)
c
  109 format(f7.1,', ',f7.2,' ,',f10.7)
  209 format(f10.5,', ',f8.2,', ',f8.2 ,', ',f10.7)
  309 format(f8.5,', ',f8.5)
   44 format('t = ',f7.2,' min')
c
      if (il3.eq.1) go to 13
      print*,' '
      print*,'bulk conc is ',xc(lk)
      print*,' '
      print*,'   It^1/2    -   wall concs   -  potential'
      do 11 j=1,mmax
  11  print209,0.1d0*cur*(fact*j*60.0d0)**0.5d0,wconc2(lk,j),
     1wconc(lk,j),pot(lk,j)
      if (il3.eq.0) go to 14
c
  13  continue
      if (il1.eq.1) then
      do 5 i=1,nj
   5  zz(i) =(i-1)*hs*1.0d06/(nj-1)
c
      do 10 l=1,nt+1,il2
      print*,' '
      print*,'distance  concen  potential'
      print*,'microns  (mol/m3)    (V) '
      print*,'time is  ',ts(l)
      do 10 j=1,nj,il2
c 10  print309,zz(j),u(j,l)
  10  print109,zz(j),xt(1,j,l),xt(2,j,l)
c
      end if
  14  continue
      return
      end
c*********************************************************************
      subroutine guess(n)
      implicit real*8(a-h,o-z)
      common /n/ nx,nt,nj
      common /calc/ u(822,1600),ts(1600),h
      common/const/ fc,r,t,frt,cur,eps,pi
      common/var/ xp(10),xx(2,821),xi(2,821),xt(2,821,1600)
      common/cprop/ cmax,rka,rkc,hs,rr
      common/results/ fact,nmax,mmax,xc(20),wconc2(20,100),
     1wconc(20,100),pot(20,100)
```

```
      common/tprop/df(821),cd(821),tm(821),
     1ddf(821),dcd(821),dtm(821),dfu(821),d2fu(821)
      dimension del(2)
c
c     del(1)=(xi(1,nj)-xi(1,1))/(nj-1)
      del(1)=0.0d0
      del(2)=cur*hs/4.0d00
c
      do 15 i=1,nj
      xi(2,i)=xi(2,1)+del(2)*(i-1)
      xt(2,i,1)=xi(2,i)
      xi(1,i)=xi(1,1)+del(1)*(i-1)
   15 xt(1,i,1)=xi(1,i)
c
      return
      end
c*********************************************************************
      subroutine cellpot(kk,il4,v)
      implicit real*8(a-h,o-z)
      common /n/ nx,nt,nj
      common /calc/ u(822,1600),ts(1600),h
      common/const/ fc,r,t,frt,cur,eps,pi
      common/var/ xp(10),xx(2,821),xi(2,821),xt(2,821,1600)
      common/cprop/ cmax,rka,rkc,hs,rr
c
  309 format(f8.5,', ',f8.5,',  ',f9.3)
c 309 format(f8.5,', ',f8.5,', ',f7.3,', ',f7.2)
      lim=20
c
      if (il4 .eq. 1 ) then
c     For polymer PEO elyte:
      vr=cmax-xt(1,1,kk)
c     if (vr .lt. 1.0d01) vr=1.0d01
      x0=rkc*(dsqrt((vr)*xt(1,1,kk)))
c     x0=7.375d-03*(dsqrt((cmax-xt(1,1,kk))*xt(1,1,kk)))
c
      else
c
c     For liquid PC elyte:
      x0=rkc*(dsqrt(xt(1,1,kk)))
c     x0=3.0d-01*(dsqrt(xt(1,1,kk)))
      end if
c
      p20=-0.01d0
      etasa=p20
      jcount=0
```

```
c
    8  jcount = jcount +1
       p20=etasa
       a1=0.33d0*frt
       c1=0.67d0*frt
c
       etasa=-cur/x0+(1.0d0+p20*a1)*dexp(-p20*a1)
      1-(1.0d0-p20*c1)*dexp(p20*c1)
       etasa=etasa/(a1*dexp(-a1*p20)+c1*dexp(c1*p20))
       etasc=etasa
c      print*,'stuff',xt(2,1,kk),kk,cur,etasa
       v=etasa + etasc + xt(2,1,kk)
c
       if(jcount .gt. lim) then
c      print*,jcount
       stop
       else
       dx=dabs(etasa-p20)
       if(dx .gt. dabs(1.0d-09*etasa)) go to 8
       end if
c
c      Material balance criteria:
       sum=0.0d0
       do j=2,nj-1
       sum=sum+xt(1,j,kk)*hs*eps
       end do
       sum=sum+(xt(1,1,kk)+xt(1,nj,kk))*hs*eps/2.0d0
       w=xt(1,1,1)*((nj-1)*hs*eps)
       ca=sum/w
c
       print309,v,ca,ts(kk)/60.
       return
       end
c**********************************************************************
       subroutine prop(nj,lk)
       implicit real*8(a-h,o-z)
       common/const/ fc,r,t,frt,cur,eps,pi
       common/var/ xp(10),xx(2,821),xi(2,821),xt(2,821,1600)
       common/results/ fact,nmax,mmax,xc(20),wconc2(20,100),
      1wconc(20,100),pot(20,100)
       common/tprop/df(821),cd(821),tm(821),
      1ddf(821),dcd(821),dtm(821),dfu(821),d2fu(821)
c
       do j=1,nj
       ee=eps
c
```

```
c  &&&&&&&&&&&&&&&&&&&&&&&&&&&&&&&&&&&&
c
c     Sodium Triflate in PEO
c
      r0=1.3041d-07
      r1=4.4978d-07
      r2=-3.1248d-07
      r3=-2.2383d-07
      r4=8.9264d-09
c
c     diffusion coefficient of the salt (m2/s)
      df(j)=0.0001d0*(ee**1.5d0)*(r0+r1*xx(1,j)/1000+
     1r2*((xx(1,j)/1000)**0.5d0) + r3*((xx(1,j)/1000)**1.5d0)
     1+ r4*((xx(1,j)/1000)**3.0d0))
      ddf(j)=0.0001d0*(ee**1.5d0)*(r1/1000d0 +
     10.5d0*r2*(xx(1,j)**(-0.5d0))/(1000.0d0**0.5d0)
     1+ 1.5d0*r3*(xx(1,j)**0.5d0)/1000d0**1.5d0 +
     13.0d0*r4*(xx(1,j)**2.0d0)/1000d0**3.0d0)
      if (xx(1,j).ge.3.0d03) then
      df(j)=(ee**1.5d0)*1.6477d-12
      ddf(j)=0.0d0
      end if
c     conductivity of the salt (S/m)
      r7=4.32d-05
      r8=0.00017d0
      r9=0.000153d0
      r10=3.73d-05
c
      cd(j)=100*(ee**(1.5d0))*(r7+r8*xx(1,j)/1000+r9*xx(1,j)
     1*xx(1,j)/1000000+r10*xx(1,j)*xx(1,j)*xx(1,j)/1000000000)
      dcd(j)=100*(ee**(1.5d0))*(r8/1000+2.0*r9*xx(1,j)/1000000
     1+3.0*r10*xx(1,j)*xx(1,j)/1000000000)
c
c     transference number of lithium
c
      if(xx(1,j).lt.0.3d03) then
      r5=0.32141d0
      r6=2.5768d0
      r11=71.369d0
      r12=643.63d0
      r13=1983.7d0
      r14=2008.d0
      r15=287.46d0
      tm(j)=r5-r6*xx(1,j)/1000.+r11*xx(1,j)*xx(1,j)/1000000.
     1-r12*((xx(1,j)/1000.)**(3.0d0))+r13*((xx(1,j)/1000.)**4.0d0)
     1-r14*((xx(1,j)/1000.)**(5.0d0))+r15*((xx(1,j)/1000.)**6.0d0)
```

```
      dtm(j)=-r6/1000.+2.0d0*r11*xx(1,j)/1000000.-
     13.0d0*r12*(xx(1,j)**2.0d0)/(1000.**3.0d0) +
     14.0d0*r13*(xx(1,j)**3.0d0)/(1000.**4.0d0) -
     15.0d0*r14*(xx(1,j)**4.0d0)/(1000.**5.0d0) +
     16.0d0*r15*(xx(1,j)**5.0d0)/(1000.**6.0d0)
      else
      tm(j)=0.0d0
      dtm(j)=0.0d0
      end if
c
      if(xx(1,j).ge.0.70d03) then
      r5=4.5679d0
      r6=4.506d0
      r11=0.60173d0
      r12=1.0698d0
      tm(j)=-r5+r6*dexp(-((xx(1,j)/1000.-r11)/r12)**2.)
      dtm(j)=-r6*(xx(1,j)/1000.-r11)*2.
     1*dexp(-((xx(1,j)/1000.-r11)/r12)**2.)/r12/r12/1000.
      end if
      if(xx(1,j).ge.2.58d03) then
      tm(j)=-4.4204d0
      dtm(j)=0.0d0
      end if
c
c     activity factor for the salt:  (dlnf/dc) and (d2lnf/dc2)
c
      if(xx(1,j).gt.0.45d03) then
      r17=0.98249d0
      r18=1.3527d0
      r19=0.71498d0
      r20=0.16715d0
      r21=0.014511d0
      thermf=r17-r18*xx(1,j)/1000.+r19*xx(1,j)*xx(1,j)/1000000.-
     1r20*xx(1,j)*xx(1,j)*xx(1,j)/1000000000.+r21*xx(1,j)*xx(1,j)
     1*xx(1,j)*xx(1,j)/1000000000000.
      dthermf=-r18/1000.+2.*r19*xx(1,j)/1000000.-
     13.*r20*xx(1,j)*xx(1,j)/1000000000.+4.*r21*xx(1,j)*xx(1,j)
     1*xx(1,j)/1000000000000.
      end if
c
      if(xx(1,j).le.0.45d03) then
      r23=0.99161d0
      r24=0.17804d0
      r25=55.653d0
      r26=303.57d0
      r27=590.97d0
```

```
       r28=400.21d0
       thermf=r23-r24*xx(1,j)/1000.-r25*xx(1,j)*xx(1,j)/1000000.+
      1r26*xx(1,j)*xx(1,j)*xx(1,j)/1000000000.-r27*xx(1,j)*xx(1,j)
      1*xx(1,j)*xx(1,j)/1000000000000.+r28*xx(1,j)*xx(1,j)*xx(1,j)
      1*xx(1,j)*xx(1,j)/1000000000000000.
       dthermf=-r24/1000.-2.*r25*xx(1,j)/1000000.+
      13.*r26*xx(1,j)*xx(1,j)/1000000000.-4.*r27*xx(1,j)
      1*xx(1,j)*xx(1,j)/1000000000000.+5.*r28*xx(1,j)*xx(1,j)
      1*xx(1,j)*xx(1,j)/1000000000000000.
       end if
c
       dfu(j)=(-1.+2.*thermf)/xx(1,j)
       d2fu(j)=1./xx(1,j)/xx(1,j)-2.*thermf/xx(1,j)/xx(1,j)+
      12.*dthermf/xx(1,j)
c
       if(xx(1,j).ge.3.00d03) then
       dfu(j)=-0.9520/xx(1,j)
       d2fu(j)=0.9520/xx(1,j)/xx(1,j)
       end if
c  &&&&&&&&&&&&&&&&&&&&&&&&&&&&&&&&
c
       end do
c
       return
       end
c*********************************************************************
```

## List of Symbols

| | |
|---|---|
| $a$ | microelectrode disk radius, cm |
| $A$ | parameter defined in equation 4-44 |
| $c$ | concentration of electrolyte, mol/dm$^3$ |
| $c_0$ | concentration of solvent, mol/dm$^3$ |
| $c_T$ | total concentration of solution, mol/dm$^3$ |
| $D$ | diffusion coefficient of electrolyte, cm$^2$/s |
| $\mathcal{D}_{ij}$ | pairwise interaction parameter between species $i$ and $j$, cm$^2$/s |
| $f_{\pm}$ | mean molar activity coefficient |
| $f_{max}$ | frequency maximum on Nyquist plot, s$^{-1}$ |
| $F$ | Faraday's constant, 96,487 C/eq |
| $\mathbf{i}$ | current density, mA/cm$^2$ |
| $I$ | cell current density, mA/cm$^2$ |
| $L$ | separator thickness, cm |
| $m$ | slope of polarization plot, $\Omega \cdot$cm$^2$/s$^{1/2}$ |
| $M_e$ | molar mass of the salt, g/mol |
| $M_i$ | chemical formula for species $i$ |
| $n$ | number of electrons involved in electrode reaction |
| $R$ | universal gas constant, 8.3143 J/mol·K |

| | |
|---|---|
| $R_b$ | bulk resistance, $\Omega \cdot cm^2$ |
| $R_{eff}$ | effective resistance of interface, $\Omega \cdot cm^2$ |
| $R_f$ | film resistance at interface, $\Omega \cdot cm^2$ |
| $s$ | Laplace-space variable |
| $t$ | time, s |
| $t_i^0$ | transference number of species $i$ |
| $t_i$ | time passed before interruption of current, s |
| $t_*$ | dimensionless time variable defined in equation 4-36 |
| $T$ | temperature, K |
| $u_i$ | mobility of species $i$, $cm^2 \cdot mol/J \cdot s$ |
| $U_{mn}$ | potential of concentration cell, V |
| $\mathbf{v}^{\square}$ | volume-average velocity, cm/s |
| $V$ | potential measured with reference electrode, V |
| $\overline{V}_i$ | partial molar volume of species $i$, $dm^3/mol$ |
| $\Delta V$ | potential impressed across full cell, V |
| $x$ | distance from the negative electrode, cm |
| $Y$ | dimensionless volume-average velocity defined in equation 4-17 |
| $z_i$ | charge number of species $i$ |
| $Z$ | dimensionless distance defined in equation 4-40 |
| $Z_\omega(0)$ | width of Warburg loop on Nyquist plot, $\Omega \cdot cm^2$ |

| | |
|---|---|
| $\alpha$ | transfer coefficient for electrochemical reaction |
| $\delta$ | quantity defined in equation 4-77 |
| $\zeta$ | perturbation parameter defined in equation 4-50 |
| $\eta$ | similarity transform variable defined in equation 4-13 |
| $\eta_s$ | surface overpotential, V |
| $\theta$ | dimensionless concentration variable defined in equation 4-37 |
| $\Theta$ | dimensionless concentration variable defined in equation 4-17 |
| $\kappa$ | conductivity of the electrolyte, S/cm |
| $\nu$ | fitting parameters used in equation 4-29 |
| $\rho$ | density of solution, $g/cm^3$ |
| $\tau$ | dimensionless time defined in equation 4-14 |
| $\Phi$ | electrical potential, V |
| $\omega_i$ | mass fraction of species *i* |

Subscripts

| | |
|---|---|
| 0 | solvent or initial condition |
| + | cation |
| - | anion |
| *a* | anode |
| *c* | cathode |

| | |
|---|---|
| *e* | electrolyte |
| *ss* | steady-state value |
| ∞ | infinity |

Superscripts

| | |
|---|---|
| 0 | with respect to the solvent |

## References

[1] M. A. Ratner, "Aspects of the Theoretical Treatment of Polymer Solid Electrolytes: Transport Theory and Models," in *Polymer Electrolyte Reviews-1,* Eds., J. R. MacCallum and C. A. Vincent, Elsevier Applied Science, London, pp. 173-236 (1987).

[2] A. Bouridah, F. Dalard, D. Deroo, and M. B. Armand, "Potentiometric Measurements of Ionic Transport Parameters in Poly(Ethylene Oxide)-LiX Electrolytes," *J. Appl. Electrochem.,* **17**, 625-634 (1987).

[3] C. D. Robitaille and D. Fauteux, "Phase Diagrams and Conductivity Characterization of Some PEO-LiX Electrolytes," *J. Electrochem. Soc.,* **133**, 315-325 (1986).

[4] P. G. Bruce and C. A. Vincent, "Effect of Ion Association on Transport in Polymer Electrolytes," *Faraday Disc. Chem. Soc.,* **88**, 43-54 (1989).

[5] M. Armand, "Polymer Solid Electrolytes - An Overview," *Solid State Ionics,* **9&10**, 745-754 (1983).

[6] F. M. Gray, *Solid Polymer Electrolytes,* VCH, New York, NY, p. 97 (1991).

[7] F. L. Tanzella, W. Bailey, D. Frydrych, G. C. Farrington, and H. S. Story, "Ion Transport in PEO-Alkali Salt Complex Polymeric Electrolytes," *Solid State Ionics,* **5**, 681-684 (1981).

[8] J. J. Fontanella, M. C. Wintersgill, J. P. Calame, F. P. Pursel, D. R. Figueroa, and C. G. Andeen, "Effect of Pressure on Conductivity in Poly(ethylene Oxide) Complexed with Alkali Metal Salts," *Solid State Ionics,* **9&10**, 1139-1146 (1983).

[9] K. Kakihana, S. Schantz, L. M. Torell, and J. R. Stevens, "Dissociated Ions and Ion-Ion Interactions in Poly(ethylene Oxide) Based $NaCF_3SO_3$ Complexes," *Solid State Ionics,* **40/41**, 641-644 (1990).

[10] D. Baril, Y. Chabre, and M. B. Armand, "Zinc Conducting Polymer Electrolytes Based on a Vehicular Process," *J. Electrochem. Soc.,* **140**, 2687-2690 (1993).

[11] L. Dominey, "Current State of the Art in Lithium Battery Electrolytes," in *Lithium Batteries: New Materials and New Perspectives,* vol. 5, Ed., G. Pistoia, Elsevier Applied Science, North Holland, pp. 137-165 (1994).

[12] J. Newman, *Electrochemical Systems,* Prentice-Hall, Englewood Cliffs, New Jersey (1991).

[13] P. R. Sorensen and T. Jacobsen, "Phase Diagram and Conductivity of the Polymer Electrolyte: $PEO_RLiCF_3SO_3$," *Polymer Bull.,* **9**, 47-51 (1983).

[14] J. Newman and T. W. Chapman, "Restricted Diffusion in Binary Solutions," *AIChE J.,* **19**, 343-348 (1973).

[15] S. D. Thompson and J. Newman, "Differential Diffusion Coefficients of Sodium Polysulfide Melts," *J. Electrochem. Soc.,* **136**, 3362-3369 (1989).

[16] M. Armand, personal communication, 1992.

[17] F. Alloin, J.-Y. Sanchez, and M. Armand, "Electrochemical Behavior of Lithium Electrolytes Based on New Polyether Networks," *J. Electrochem. Soc.*, **141**, 1915-1920 (1994).

[18] R. Pollard and J. Newman, "Mathematical Modeling of the Lithium-Aluminum, Iron Sulfide Battery," *J. Electrochem. Soc.*, **128**, 491-502 (1981).

[19] R. Pollard, *Mathematical Modeling of the Lithium-Aluminum, Iron Sulfide Battery,* Dissertation, University of California, Berkeley (1979).

[20] H. S. Carslaw and J. C. Jaeger, *Conduction of Heat in Solids,* Clarendon Press, Oxford, p. 75 (1959).

[21] D. Fauteux, J. Prud'homme, and P. E. Harvey, "Electrochemical Stability and Ionic Conductivity of Some Polymer-LiX Based Electrolytes," *S. S. Ionics,* **28-30**, 923-928 (1988).

[22] R. A. Robinson and R. H. Stokes, *Electrolyte Solutions,* p. 161, Butterworths, London, 2nd. Ed. (1959).

[23] M. Doyle, T. F. Fuller, and J. Newman, "The Importance of the Lithium Ion Transference Number in Lithium/Polymer Cells," *Electrochim. Acta,* **39**, 2073-2081 (1994).

[24] M. Doyle, T. F. Fuller, and J. Newman, "Modeling of Galvanostatic Charge and Discharge of the Lithium/Polymer/Insertion Cell," *J. Electrochem. Soc.*, **140**, 1526-1533 (1993).

[25] Y. Ma, M. M. Doeff, S. J. Visco, and L. C. De Jonghe, "Rechargeable Na/$Na_xCoO_2$ and $Na_{15}Pb_4$/$Na_xCoO_2$ Polymer Electrolyte Cells," *J. Electrochem. Soc.*, **140**, 2726-2733 (1993).

[26] M. Watanabe, M. Rikukawa, K. Sanui, and N. Ogata, "Evaluation of Ionic Mobility and Transference Number in a Polymeric Solid Electrolyte by Isothermal Transient Ionic Current Method," *J. Appl. Phys.*, **58**, 736-740 (1985).

[27] P. M. Blonsky, D. F. Shriver, P. Austin, and H. R. Allcock, "Complex Formation and Ionic Conductivity of Polyphosphazene Solid Electrolytes," *S. S. Ionics,* **18/19**, 258-264 (1986).

[28] P. G. Bruce and C. A. Vincent, "Steady State Current Flow in Solid Binary Electrolyte Cells," *J. Electroanal. Chem.*, **225**, 1-17 (1987).

[29] J. Evans, C. A. Vincent, and P. G. Bruce, "Electrochemical Measurement of Transference Numbers in Polymer Electrolytes," *Polymer,* **28**, 2324-2328 (1987).

[30] P. G. Bruce, J. Evans, and C. A. Vincent, "Conductivity and Transference Number Measurements on Polymer Electrolytes," *S. S. Ionics,* **28-30**, 918-922 (1988).

[31] P. G. Bruce and C. A. Vincent, "Effect of Ion Association on Transport in Polymer Electrolytes," *Faraday Discuss. Chem. Soc.*, **88**, 43-54 (1989).

[32] P. G. Bruce and C. A. Vincent, "Transport in Associated Polymer Electrolytes," *S. S. Ionics,* **40/41**, 607-611 (1990).

[33] P. G. Bruce, M. T. Hardgrave, and C. A. Vincent, "Dc Polarization of Polymer Electrolytes," *Electrochim. Acta,* Proceedings of the 3rd International Symposium on Polymer Electrolytes, **37**, 1517-1520 (1992).

[34] F. Croce, R. Curini, S. Pantaloni, S. Passerini, A. Selvaggi, and B. Scrosati, "Characteristics of a Poly(ethylene Oxide)-$LiBF_4$ Polymer Electrolyte," *J. Appl. Electrochem.*, **18**, 401-404 (1988).

[35] M. Watanabe, S. Nagano, K. Sanui, and N. Ogata, "Estimation of $Li^+$ Transport Number in Polymer Electrolytes by the Combination of Complex Impedance and Potentiostatic Polarization Measurements," *S. S. Ionics,* **28-30**, 911-917 (1988).

[36] G. G. Cameron, J. L. Harvie, and M. D. Ingram, "The Steady State Current and Transference Number Measurements in Polymer Electrolytes," *S. S. Ionics,* **34**, 65-68 (1989).

[37] G. G. Cameron, M. D. Ingram, and J. L. Harvie, "Ion Transport in Polymer Electrolytes," *Faraday Discuss. Chem. Soc.,* **88**, 55-63 (1989).

[38] H. P. Fritz and A. Kuhn, "Comparative Determination of Effective Transport Numbers in Solid Lithium Electrolytes," *J. Power Sources,* **41**, 253-261 (1993).

[39] R. D. Armstrong and H. Wang, "Steady State Currents in Electrolytic Cells Containing Divalent Cations," *Electrochim. Acta,* **39**, 1-5 (1994).

[40] Y. Ma, M. Doyle, T. F. Fuller, M. M. Doeff, L. C. De Jonghe, and J. Newman, "The Measurement of a Complete Set of Transport Properties for a Concentrated Solid Polymer Electrolyte Solution," *J. Electrochem. Soc.,* **142**, 1859-1868 (1995).

[41] R. Pollard and T. Comte, "Determination of Transport Properties for Solid Electrolytes from the Impedance of Thin Layer Cells," *J. Electrochem. Soc.,* **136**, 3734-3748 (1989).

[42] J. R. Macdonald, "Theory of Space-Charge Polarization and Electrode-Discharge Effects," *J. Chem. Phys.,* **58**, 4982-5001 (1973).

[43] J. R. Macdonald, "Simplified Impedance/frequency-Response Results for Intrinsically Conducting Solids and Liquids," *J. Chem. Phys.,* **61**, 3977-3996 (1974).

[44] J. R. Macdonald and D. R. Franceschetti, "Theory of Small-signal AC Response of Solids and Liquids with Recombining Mobile Charge," *J. Chem. Phys.*, **68**, 1614-1637 (1978).

[45] P. R. Sorensen and T. Jacobsen, "Conductivity, Charge Transfer and Transport Number - An A.C.-Investigation of the Polymer Electrolyte LiSCN-Poly(Ethylene Oxide)," *Electrochim. Acta,* **27**, 161 (1982).

[46] J. E. Weston and B. C. H. Steele, "Effects of Preparation Method on Properties of Lithium Salt-Poly(Ethylene Oxide) Polymer Electrolytes," *S. S. Ionics,* **7**, 81-88 (1982).

[47] P. R. Sorensen and T. Jacobsen, "Limiting Currents in the Polymer Electrolyte: $PEO_xLiCF_3SO_3$," *S. S. Ionics,* **9&10**, 1147 (1983).

[48] J. Newman and L. Hsueh, "The Effect of Variable Transport Properties on Mass Transfer to a Rotating Disk," *Electrochim. Acta,* **12**, 417-427 (1967).

[49] J. Xu and G. C. Farrington, "Microelectrode Studies of the $Li/Li^+$ Couple in Low Molecular Weight Liquid Polyether Electrolytes," work in progress, July 1994.

[50] M. Leveque, J. F. Le Nest, A. Gandini, and H. Cheradame, "Ionic Transport Numbers in Polyether Networks Containing Different Metal Salts," *Makromol. Chem., Rapid Commun.*, **4**, 497-502 (1983).

[51] P. G. Bruce, M. T. Hardgrave, and C. A. Vincent, "The Determination of Transference Numbers in Solid Polymer Electrolytes Using the Hittorf Method," *S. S. Ionics,* **53-56**, 1087 (1992).

[52] J. Shi, P. G. Bruce, and C. A. Vincent, "A Zinc Trifluoromethane Sulfonate Polymer Electrolyte," *Electrochim. Acta,* **37**, 1707-1710 (1992).

[53] C. Vincent, personal communication, June 1994.

LAWRENCE BERKELEY LABORATORY
UNIVERSITY OF CALIFORNIA
TECHNICAL AND ELECTRONIC
INFORMATION DEPARTMENT
BERKELEY, CALIFORNIA 94720